European Commission

technical steel research

Steel products and applications for building, construction and industry

Design rules for cold-formed structural hollow sections

P. Salmi, J. Kouhi (1), R. Puthli, S. Herion, O. Fleischer (2), F. Espiga (3), P. Croce (4), E. Bayo, R. Goñi (5), T. Björk (6), R. Ilvonen (7), W. Suppan (8)

(1) **VTT Technical Research Centre of Finland** — P.O. BOX 1800, FIN-02044 VTT
(2) **University of Karlsruhe** — Kaiserstraße 12, D-76128 Karlsruhe
(3) **LABEIN** — Parque Tecnológico de Biskaia, Edificio 101, E- 48170 Zamudio
(4) **University of Pisa** — Via Diotisalvi 2, I-56126 Pisa
(5) **University of Navarra** — Carretera del Sadar s/n, E- 31009 Pamplona
(6) **Lappeenranta University of Technology** — P.O. Box 20, FIN-53851 Lappeenranta
(7) **Ruukki** — Harvialantie 420, FIN-13300 Hämeenlinna
(8) **voestalpine Krems** — P.O.Box 43, A-3500 Krems

Contract No 7210-PR/253
1 July 2001 to 31 December 2003

Final report

Directorate-General for Research

2006 EUR 21973 EN

Europe Direct is a service to help you find answers to your questions about the European Union

Freephone number (*)**:**

00 800 6 7 8 9 10 11

(*) Certain mobile telephone operators do not allow access to 00 800 numbers or these calls may be billed.

A great deal of additional information on the European Union is available on the Internet. It can be accessed through the Europa server (http://europa.eu.int).

Cataloguing data can be found at the end of this publication.

Luxembourg: Office for Official Publications of the European Communities, 2006

ISBN 92-79-01088-3

Printed in Luxembourg

PRINTED ON WHITE CHLORINE-FREE PAPER

Abstract

Structural hollow sections on the market are classified into three groups based on the manufacturing method: hot formed, hot finished and cold formed. Common arguments against the safe use of cold-formed hollow sections are that mechanical properties of cold-formed hollow sections are inhomogeneous around perimeter due to difference in strain hardening during cold forming. Cold forming reduces impact toughness of cold-formed hollow sections, which restricts the use of them at low temperatures. The tensile plastic elongation of a cold formed hollow section is lower and depends on the location in the sections. This may restrain the use of plastic design methods, which require adequate amount of ductility. There may be microcracks in the corners of cold-formed hollow sections, which will reduce safety of the structure and fatigue properties.

The overall objective of *Design rules for cold formed structural hollow sections* project is to validate whether these argument are meaningful in the design of welded connection from cold formed structural hollow sections.

This overall objective is divided to following more detailed objectives:

- Determine mechanical properties of finished cold formed structural hollow section (CFSHS) (WP1).
- Determine rotation capacity and limits for cross-section classification required in plastic analysis for CFSHS (WP2).
- Determine reliable design rules for welded tubular connections using CFSHS (WP3A).
- Extend applicability of design rules for welded tubular connections for CFSHS having $b/t > 35$ (WP3B).
- Determine requirements for reliable welding of CFSHS connections (WP4).

The research work was divided into four work packages. Summary of the work done in these is presented in following paragraphs:

WP1 MECHANICAL AND TOUGHNESS PROPERTIES OF CFSHS (CHAPTER 2)

Characteristic properties of cold-formed hollow section differ from hot-formed and hot-finished hollow sections. In cold-formed structural hollow section (CFSHS) mechanical and ductility properties vary around the section, while cold forming rate differs in different parts of the section. The strength and deformation capacities are decreased at least in the cold-formed corner areas.

Extensive test programme has been executed to determine mechanical and toughness properties of CFSHS. Aim of this work has been to show the actual characteristics of CFSHS at European market and verify requirements set in product standard EN 10219 and in Eurocode 3, Part 1.1 for the steel material.

The test programme was composed of cold-formed structural hollow sections from five different manufacturers of cold-formed sections in Europe. Requested steel grade for most of sections was S355. For comparison three hot-formed hollow sections and four cold formed from higher strength steel grade S460 were included in the test programme. The whole test programme contained 51 sections and 15 different section sizes.

For each section following measurements and tests were carried out:

- Cross-sectional dimensions of each CFSHS were measured.
- Chemical analysis was made to determine chemical content of base material.

- Tensile test coupons were manufactured from five different locations around perimeter: from the weld positions, from both faces and from two corners having either minimum or maximum corner radius.

- For three sections, which were used to determine deviation of properties around perimeter, altogether 13 coupons were manufactured around half of the perimeter.

- The toughness properties of hollow sections were determined by defining transition curve with Charpy V Notch (CVN) impact tests.

In addition also influence of welding to brittle fracture possibility at low temperatures was studied experimentally with test programme that is composed of coupon and whole section tension tests for welded and non welded specimen in room and at low temperatures. Altogether 14 whole section tension tests for five different section sizes were done at room and low temperature (-60^{o}C) for non welded and welded sections. Some welded sections contained transverse weld pass in the mid-length of section done with TIG process to simulate heat input. Tensile test coupons from same sections were manufactured and tested. Both welded and non welded coupon from flat face and corner was tested in the room temperature and at -60^{o}C temperature.

WP2 APPLICABILITY OF PLASTIC DESIGN FOR CFSHS MEMBERS AND STRUCTURES (CHAPTER 3)

Some recent research work has raised doubts about applicability present cross section classification requirement for CFSHS in plastic design arguing that they do not satisfy the material ductility requirements of Eurocode 3, Part 1.1 or that they have not enough geometric ductility (ability to develop the needed large rotations keeping the plastic moment capacity). Applicability of present section classification limits for CFSHS in Eurocode 3, Part 1.1 are studied.

In this research project, the ductility of hollow sections in general and CFSHS in particular has been studied both numerically and experimentally. Test programme has been executed and extensive amount of numerical analyses have been done to extend the experimental results. The objective has been to find understanding of the parameters, which influence the rotation behaviour of hollow sections.

Ductility requirement for plastic design is proposed to be characterised by available inelastic rotation instead of rotation capacity even though there is connection between these two definitions. Experimental and numerical analyses has been carried out to describe different phenomena that have an effect on the ductility and rotation capacity.

Modifications are proposed to current cross-section classification of hollow sections of Eurocode 3. A more demanding limit for cross-section class 1 is proposed, which includes interaction between the flange and web slenderness.

Alternative design procedure for cross-section classification is given where the available rotation requirement is analysed structurally and compared to available inelastic rotation of members. Advanced approach, which is based on the concept of available inelastic rotation, φ_{av}, is proposed for the global plastic design. The member performance may be analysed determined with experimentally verified analytical methods or numerically using calibrated FE simulation. Required and available inelastic rotations φ at plastic hinge location are compared directly. The required rotation has been studied with FE simulation for beams and portal frames. The available rotation for CFSHS is verified using different methods: calculation models, FE simulations and experimentally. Test results from literature are collected as test database, which has been extended with set of 20 bending tests.

WP3A APPLICABILITY OF DESIGN RULES FOR TUBULAR CONNECTION FROM CFSHS (CHAPTER 4)

The design models for structural hollow section joints proposed in design provision are developed from tests with hot-formed structural sections (HFSHS) at room temperatures. Relatively few test results are available for cold-formed structural hollow sections (CFSHS) at low temperatures.

High degree of cold forming may decrease the ductility in the corner areas for CFSHS. Due to this higher degree of cold forming, the yield strength of the corner is typically higher than that of the adjacent flat faces, where degree of cold forming is lower and consequently the yield strength is lower but ductility better.

When the applicability of cold-formed structural hollow sections are considered, the ultimate loading carrying capacity shall not be the critical for the use of present design methods but the deformation capacity. The possible decrease in deformation capacity may not occur in room temperatures but in lower temperatures.

The deformation capacity of the joint can be restricted by preventing the plastic deformation to take place. This will happened partly due to the gap geometry itself, where the free deformation of the chord face in transverse direction is prevented by adjacent brace members. The pretension of the chord member will decrease the deformation capacity of the joint as well. Thus pretension of the chord member was included in K- and X-joint tests series. Behaviour of CFSHS in welded connections is studied with K-joint and X-joint test in normal and at low temperatures. The test programme comprised of altogether 41 K-joint test and 32 X-joint tests.

WP3B EXTENSION OF APPLICABILITY OF DESIGN RULES FOR TUBULAR CONNECTIONS (CHAPTER 5)

Eurocode 3, Part 1.8 provides design guidelines for rectangular hollow sections joints made of members having b/t ratios smaller than 35. In practice, there is an increasing demand to use more slender sections. These sections are already regulated in technical delivery conditions such as EN 10210 or EN 10219. The present product ranges of the manufacturers are however much wider, especially for cold formed sections.

Design rules backed by experimental tests for K-Joints with gap made out of rectangular hollow sections (RHS) are given, for example, in Eurocode 3. Here, the allowable width-thickness ratio of welded RHS K-Joints with gap is limited to 35. In addition to the slenderness limits, Eurocode 3 gives a restriction for the gap size.

In the framework of this research project 47, tests on K-joints with gap and with slenderness as well as gap sizes outside the range given in Eurocode 3 are carried out. The ultimate load and the load deformation behaviour had been determined.

For high slenderness 2γ and high width ratios β, buckling of the chord webs could be observed from the tests in case of gap sizes permissible in Eurocode 3. Because this failure mode has not to be considered for K-joints, the formula for T- and Y-joints for chord web failure is used for the design load prediction. For very small gap sizes, down to the minimum requirements for welding, either punching shear failure or brace effective width failure can be observed. For both failure modes, the influence of a reduced effective length could be observed in the tests. Another failure mode observed in the tests is the buckling of the compression brace, which appears if the width ratio $\tau < 1.00$.

WP4 EFFECT OF WELDING IN COLD FORMED AREAS (CHAPTER 6)

According to DIN 17014, Part 1, Edition 1988, ageing is a change of the properties of a material at or close to room temperature by movement of interstitial dissolved elements. In relation to welding in cold-formed areas, strain ageing is relevant. In addition to the preceding cold-forming,

strain ageing causes an increase in the yield strength, tensile strength and hardness, together with a decrease of strain, the reduction of area and the Charpy V notch impact energy. In the last few decades such restrictions have been formulated against "*dangerous strain ageing*" in different design provisions.

In this project only the influence of strain ageing adjacent to the weld seam is to be investigated. Notch effects and geometrical influences such as single-layer welding are to be excluded or minimised in order to prevent any dominating influence of such conditions on the test process. A multi-layer weld would e.g. cause a normalising effect that would cover the ageing. On this basis, the bead-on-plate weld has been removed afterwards, so that only the influence of the thermal effect of the weld bead in the cold-formed area of the specimen - the strain ageing caused by welding - remains as an influencing parameter. The bead-on-plate weld is only regarded as an "expedient" for the generation of the ageing area typical for a weld seam.

The shift of the transition temperature caused by welding (ageing effects) is investigated using Charpy V notch test (CVN tests) and cold-formed structural hollow sections.

For the evaluation of brittle fracture, the notch was prepared in the zone reheated by welding. It was to be investigated, whether this reheating (ageing) influences the brittle fracture temperature. An extensive material analysis was carried out, in which transition temperatures at 27 J of the following material conditions were to be determined: base material (sampling location in flat area), base material (sampling location in curved area) and base material (sampling location in curved area, artificially aged). For each material condition, about 18 tests are carried out to obtain sufficient data for statistical analysis.

Welding in cold-formed areas is also an open question for for dynamically loaded structures (fatigue resistance). Especially for structural joints made of hollow sections with large width-ratios b_1/b_0, it is often necessary to weld in the areas close to the edges. A lot of these structures are subjected to dynamic loading. Therefore the fatigue behaviour of welded (notched) and non-welded (un-notched) test specimens made of different steel grades and wall thicknesses are compared directly with each other to determine, whether a weld notch influences the fatigue behaviour in cold-formed regions of hollow sections and if so, to what extent. The intention of all tests was to find out, whether there is a difference in the fatigue behaviour of artificial aged specimens and non-aged specimens. It was not the intention to get an absolutely correct fatigue curve for square hollow sections under unusual loading conditions as they have been used during the tests. The fatigue tests were carried out as 4-point-bending-tests, both on welded and un-welded specimens for comparison. The weld seam was removed before the tests by grinding.

Contents

Abstract 3

Contents 7

1 Introduction 9

1.1 Structural hollow sections 9
1.1.1 Hot formed hollow sections 9

1.2 Project 10

2 Mechanical and toughness properties of CFSHS 13

2.1 Introduction 13

2.2 Test programme 13
2.2.1 Chemical composition 16
2.2.2 Geometrical dimensions 17

2.3 Mechanical properties 19
2.3.1 Testing 19
2.3.2 Effect of cold forming on mechanical properties 21
2.3.3 Effect of welding and low temperature 24
2.3.3 Requirements of product standard EN 10219 27
2.3.4 Ductility requirements for steel material in Eurocode 3 30

2.4 Toughness properties 36
2.4.1 Testing and evaluation 36
2.4.2 Analysis of results 36

3 Applicability of plastic design for CFSHS members and structures 39

3.1 Introduction 39

3.2 Ductility of hollow sections 39
3.2.1 Ductility of cross section defined by available inelastic rotation 39
3.2.3 Influence of load type and moment gradient 42
3.2.4 Influence of plate slenderness and aspect ratio – Experimental and numerical verification 44
3.2.5 Influence of manufacturing method 55
3.2.6 Required inelastic rotation at the structural level 55
3.2.2 Influence of lateral restraints 57

3.3 Recommendation for cross-section classification 59
3.3.1 Current cross-section classification 59
3.3.2 Modified proposal for classification limit in class 1 60

3.4 Guidance for plastic design 62
3.4.1 Alternative approach based on available and required rotation checking 62
3.4.2 Numerical evaluation of available inelastic rotation 63
3.4.3 Design models for available inelastic rotation 67

3.5 Conclusions 73

4 Applicability of design rules for tubular connection from CFSHS 75

4.1 Introduction 75

4.2 Methods and materials 76
4.2.1 Analysing methods 76
4.2.2 Materials 76

4.3 Experimental tests 76
4.3.1 Test specimen 76
4.3.2 Test set up 80

4.4 Test Results 82
4.5 Evaluation of test results 86
4.7 Conclusions and recommendation 91
5 Extension of applicability of design rules for tubular connections ***93***
5.1 Aim of the investigation 93
5.1.1 Test programme 94
5.2 Test set-up 96
5.2.1 Test rig, measuring equipment and test set-up 96
5.2.2 Load introduction 98
5.3 Measuring arrangement and measuring methods 98
5.4 Fabrication and geometry of test specimens 99
5.5 Material properties 100
5.6 General observations and results from test 100
5.6.1 Influence of the gap size parameter g' and the width ratio β on the load carrying behaviour 100
5.6.2 Influence of the thickness ratio τ on the load carrying behaviour 103
5.6.3 Influence of brace inclination Θ on the load carrying behaviour 103
5.6.4 Influence of material properties on the load carrying behaviour 106
5.6.5 Influence of imperfections 107
5.6.6 Annotation to some test results 108
5.7 Calculation of welded connections between rectangular hollow sections according to prEN1993-1-8 109
5.7.1 Modified analytical model for (reduced) punching shear failure 110
5.8 Comparison of test results with calculation results according to prEN1993-1-8 111
5.9 Conclusions 113
5.10 Numerical investigations 114
6 Effect of welding in cold formed areas ***115***
6.1 Introduction and aims 115
6.2 Test specimens 117
6.2.1 Hollow sections 117
6.2.2 Mechanical-technological data 118
6.2.3 Chemical analysis 119
6.2.4 Welding 119
6.2.5 Metallography 121
6.3 Charpy V notch impact (CVN) tests 122
6.4 Fatigue tests 125
6.5 Recommendations and Future work 136
7 General conclusions ***139***
Technical Annex ***145***
References ***147***

1 Introduction

1.1 Structural hollow sections

Structural hollow sections on the market are classified into three groups based on their manufacturing method: hot formed, hot finished and cold formed. Hot formed sections are extruded from continuously cast rounds and the final section is longitudinally seamless. Both hot finished and cold formed are roll formed from the steel strip into circular or directly rectangular shape and weld edges of strip longitudinally together. The external weld is usually cleaned off mechanically to improve the external appearance of the tube. In hot finished hollow sections the mother pipe is reheated to rolling temperature before shaping into final circular, square or rectangular shape. For cold formed hollow sections sizing and shaping is done without reheating.

The hot-formed and hot finished are considered similar from the material characteristics of final product, even though form of initial billet and the whole manufacturing are different. Still the product standard EN 10210 [1-1] covers them both. Product standard for cold-formed structural hollow sections is EN 10219 [1-2].

Soininen [1-3, 1-4] has stated that the most common arguments against the safe use of cold-formed hollow sections are:

- The mechanical properties of cold-formed hollow sections are inhomogeneous around perimeter due to difference in strain hardening during cold forming.

- The tensile plastic elongation of a cold-formed hollow section is lower and depends on the location in the sections.

In hot formed and hot finished sections mechanical properties are homogenous over the whole cross section.

- There may be microcracks in the corners of cold-formed hollow sections, which will reduce safety of the structure and fatigue properties. Therefore allowance of welding on cold-formed corner region is limited in design rules.

- Cold forming reduces impact toughness of cold-formed hollow sections, which restricts the use of them at low temperatures.

These arguments are used also in promotions of hot formed and hot finished hollow sections against cold-formed sections.

Cold formed hollow sections have some advantage, which have made them competitive against hot formed and hot finished hollow sections. The manufacturing method needs less energy and manufacturing lines are more compact and less expensive. Cold formed hollow section can be produced with tighter tolerances and they have better surface quality.

1.1.1 Hot formed hollow sections

Thus there exist different processes in production of hot formed hollow sections in principle hot formed hollow sections are manufactured in following manner:

- Continuously cast heated rounds are shaped into hollows in press or rolling mill. The temperature of round is between 1150 and 1300 ^{o}C.

- A piercing mandrel is inserted into shell to shape the hollow in required diameter and thickness.

- These circular shells are reheated before forming into the final dimensions and circular, square or rectangular tube shape.

Cold forming of hollow sections

The cold forming process of hollow section may be divided into following phases:

Pre-mill Preparation - The strip is uncoiled and fed through another set of levelling rollers and a guillotine trims the ends of the strip. Welding joins the strips, the edges are trimmed and they are recoiled as the raw material for the forming mill.

Cold Forming and Welding - Two alternative possibilities exists for cold-forming. The final shape is reached through circular mother pipe or direct cold forming into square or rectangular shape. Series of forming rolls forms the flat steel into mother tube. The steel is not heated and this gradual cold forming process enhances the strength of the steel and allows for very tight dimensional tolerances.

The strip edges are heated by either high frequency (HF) induction or electric resistance welding and then forged together by weld rolls to create a continuous longitudinal weld without the addition of filler metal. The most common welding process is the electric resistance welding, where the edges of the strip are heated normally by high frequency electrical current.

The weld seam is then cooled and processed. Special scarping tools remove the external weld flash and the pipe is cooled uniformly in a cooling trough. Because weld quality is absolutely vital to the quality of the end products, its integrity is checked and any tube that does not measure up is registered as reject material. The weld seam of thicker section may be heat treated, normalised just after welding by inductive heating. This heat treatment is normally covers an area about 10 mm on the both sides of the weld.

In direct forming in square or rectangular shape forming dies progressively shape the flat strip by forming the top two corners of the square or rectangular tube. Subsequent stations form the bottom two corners. No cold working of the sides of the shape is performed, and the shape's seam is welded by high-frequency contacts when the tube is near its final shape and size. The welded tube is cooled and then driven through a series of sizing rolls.

Sizing and Shaping - The tube then enters the sizing and shaping stations where rolls turn it into products such as square and rectangular hollow sections. These sections are then cleaned and degreased before entering the in-line painting process.

Hot finished hollow sections

The manufacturing process for hot finished sections is similar to cold-formed hollow sections. The steel strip is shaped into either open pipe or directly rectangular section in multi stand cold forming process. The longitudinal edges of strip are connected to each other with welding. In high frequency induction (HFI) welding short distance of edges is heated in welding temperature and pushed together using pressure rolls. The external weld reinforcement is removed using special grinders. Internal weld reinforcement may be removed also. Before hot finished hollow section is shaped into final circular, square or rectangular shape, the mother pipe is reheated inductively to rolling temperature.

1.2 Project

In the design recommendations such as Eurocode 3 Design of steel structures (EN 1993-1-1) (1-3) requirements are set for mechanical properties of steel material to ensure adequate deformation capacity needed in plastic design. Requirements cover minimum values for tensile strength to yield strength ratio f_u/f_y, elongation at fracture A_5 and uniform elongation at maximum force $\varepsilon_u/\varepsilon_y$. Numerical values for these requirements differ in different provisions.

Tests on welded joints of cold formed and hot formed hollow section show that the observations from the tests do not correlated with these requirements. Welded connections from cold-formed hollow sections [1-3] have shown to have sufficient resistance and deformation capacity even at low temperatures. Thus the requirements set for the base material are not fulfilled in the corner areas due to cold forming.

These tests also have shown that chemical composition and welding parameters seems to have significant influence on the ductile behaviour of the joint independent on fulfilment of requirements for base material.

Therefore the objective of *Design rules for cold formed structural hollow sections* project is to validate whether these requirements set for mechanical properties of the base material are meaningful in the design of welded connection from cold formed structural hollow sections. Utilisation of plastic design for both structures such as beams and welded connections is trusses are considered. Restriction to welding in the cold-formed area is studied separately.

Eurocode 3, Part 1.8 Design of joints (EN 1993-1-8) [1-4] provides design guidelines for rectangular hollow sections joints made of members having b/t ratios smaller than 35. In practice, there is an increasing demand to use more slender sections. The present product ranges of the manufacturers are however much wider, especially for cold-formed sections. Therefore extension of this b/t ratio is of interest.

In general the overall objective of Design *rules for cold formed structural hollow sections* project can be stated in the form:

- to obtain reliable and economical design rules for cold formed structural hollow sections (CFSHS)

This is obtained by verifying available design rules given in Eurocode 3 and developing new design rules for these European design provisions.

The study subjects set for the project this general objective is divided to following more detailed objectives:

1. Determine mechanical properties of finished cold formed structural hollow section (CFSHS) (WP1).

2. Determine rotation capacity and limits for cross-section classification required in plastic analysis for CFSHS (WP2).

3. Determine reliable design rules for welded tubular connections using CFSHS (WP3A).

4. Extend applicability of design rules for welded tubular connections for CFSHS having $b/t>35$ (WP3B).

5. Determine requirements for reliable welding of CFSHS connections (WP4).

Research work in the project was divided into four main work packages (WP) to obtain their detailed objectives (Figure 1-1). Work package WP3 considering tubular connections is divided into two parts WP3A and WP3B depending on the objective set for research.

Collaborating partners in each work packages are shown in Table 1-1. The first partner in each is responsible one for the work in that specific work package.

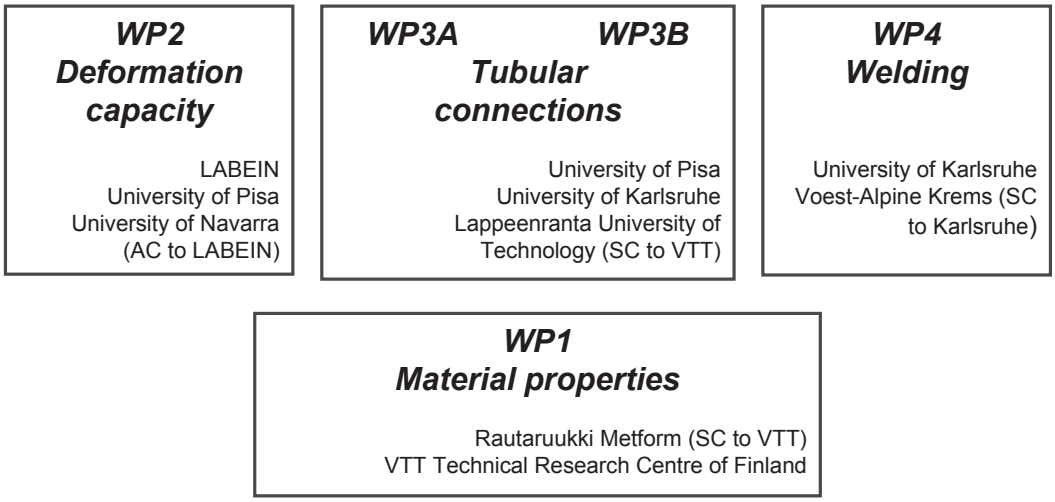

Figure 1-1. Division of project into Work Packages and partners involved in the research work in each Work Package.

Table 1-1. Work packages and partners involved in research.

Work package	Partners
WP1 Material properties	**Rautaruukki Metform** (SC to VTT) VTT Technical Research Centre of Finland
WP2 Deformation capacity	**LABEIN** University of Navarra (AC to LABEIN) University of Pisa
WP3 Tubular connections WP3A Applicability of design rules WP3B Extension of applicability	 **Lappeenranta University of Technology** (SC to VTT) University of Pisa **University of Karlsruhe** University of Pisa Voest-Alpine Krems (SC to Karlsruhe)
WP4 Welding	**University of Karlsruhe** VTT Building and Transport Voest-Alpine Krems (SC to Karlsruhe)
WP5 Management and co-ordination	**VTT Technical Research Centre of Finland**

SC - Subcontractor
AC - Associated contractor

2 Mechanical and toughness properties of CFSHS

2.1 Introduction

Characteristic properties of cold-formed hollow section differ from hot-formed and hot-finished hollow sections. In cold-formed structural hollow section (CFSHS) mechanical and ductility properties vary around the section, while cold forming rate differs in different parts of the section. The strength and deformation capacities are decreased at least in the cold-formed corner areas.

Extensive test programme has been executed to determine mechanical and toughness properties of CFSHS. Aim of this work has been to show the actual characteristics of CFSHS at European market and verify requirements set in product standard EN 10219 (2-1) and in Eurocode 3, Part 1.1 (prEN1993-1-1)(2-2) for the steel material.

The test programme was composed of cold-formed structural hollow sections from five different manufacturers of cold-formed sections in Europe. Requested steel grade for most of sections was S355. For comparison three hot-formed hollow sections and four cold formed from higher strength steel grade S460 were included in the test programme. The whole test programme contained 51 sections and 15 different section sizes. Mechanical properties around section and toughness properties from flat face were determined.

2.2 Test programme

The whole test programme and sections are shown in Table 2-1. For each section size slenderness rations are given. Section sizes from different manufacturers A, B, C, D and E are shown in different columns. Also hot-formed (HF) section and high strength steel (S460) section sizes are included. Section sizes in the additional test programme are given in the column AD. Altogether 51 sections were enclosed to the programme containing 15 different section sizes.

The tests reported in this report are also collected to Table 2-2 showing also the section number used to identify different sections. As an example cross-sections of test series B and AD are shown in Figure 2-1.

Figure 2-2 division into different slenderness ranges according to non-dimensional parameter (H+B)/2T, which is used to describe cross-sectional size.

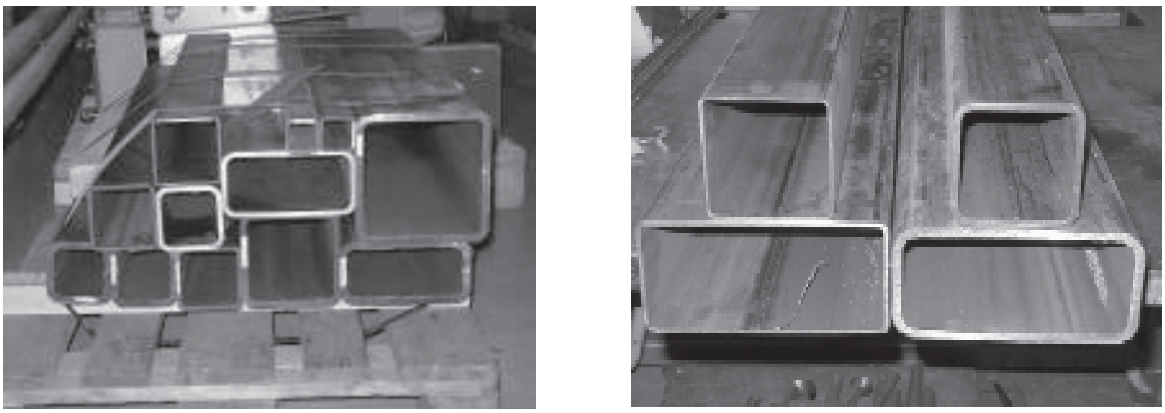

B AD

Figure 2-1. Sections in test series B and AD are shown.

Table 2-1. The whole test programme is given containing section sizes and different manufacturers for test specimen in WP1.

Section name	Section size HxBxT	H/T	B/T	H/B	Test series [1]							
					A	B	C	D	E	HF	460	AD
RHS1	50x50x3	16.67	16.67	1.00		T			T			
RHS1	50x50x5	10.00	10.00	1.00		TC			TC	TC		
RHS2	100x100x3	33.33	33.33	1.00	T	T			T		T	T
RHS2	100x100x5	20.00	20.00	1.00	TC	TC	TC				TC	
RHS2	100x100x6	16.67	16.67	1.00	TC	TC			TC		TC	T13
RHS2	100x100x8	12.50	12.50	1.00	TC[2]	TC		TC		TC	TC	
RHS2	100x100x10	10.00	10.00	1.00	TC	TC		TC	TC			
RHS3	150x150x8	18.75	18.75	1.00	TC	TC		TC		TC		
RHS4	200x200x10	20.00	20.00	1.00	TC	TC						
RHS5	300x300x6	50.00	50.00	1.00	TC							
RHS5	300x300x12.5	24.00	24.00	1.00	TC							
RHS6	200x100x4	50.00	25.00	0.50								T13
RHS6	200x100x8	25.00	12.50	0.50	TC	TC	TC	TC				T13
RHS6	200x100x10	20.00	10.00	0.50	TC	TC						
RHS7	160x160x6	26.67	26.67	1.00			TC		TC			

T five tensile coupons around perimeter
C Transition curve with Charpy V notch specimen
T13 Detailed tensile property distribution. 13 coupons around half of the perimeter.
[1] Manufacturers A/B/C/D/E, hot-formed HF, S460 steel grade S460, additional tests AD
[2] Deviation of results in the same specimen and effect of testing speed (Four additional sections)

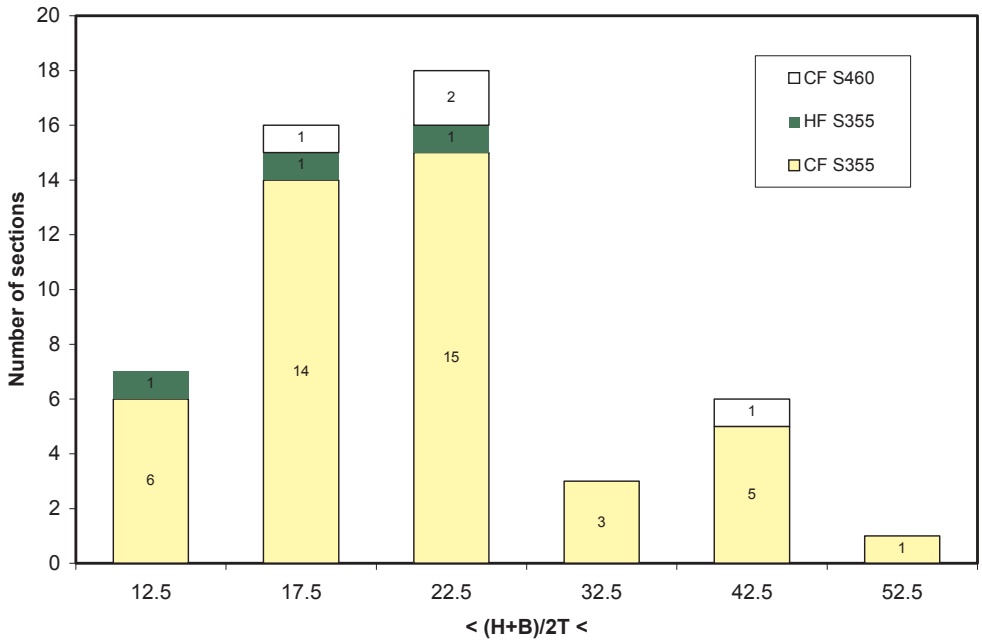

Figure 2-2. Number of specimen with different slenderness ratio in the test programme is shown. Slenderness is depicted with non-dimension ratio (B+H)/2T.

Table 2-2. Identification of test sections is given for the whole test programme.

Section code	Manu-facturer A, B, C, D, E	Size of specimen HxBxT	Informed Steel grade	Tensile coupon test	Toughness with impact tests
S01	A	100x100x3	S355J2H	1 W, 2 H, 3 B, 4 Rmax, 5 Rmin	
S02	A	100x100x5	S355J2H	1 W, 2 H, 3 B, 4 Rmax, 5 Rmin	Charpy V Notch
S04	A	100x100x6	S355J2H	1 W, 2 H, 3 B, 4 Rmax, 5 Rmin	Charpy V Notch
S05	A	100x100x8	S355J2H	Test speed 1.	
S06	A	100x100x8	S355J2H	Test speed 2.	
S07	A	100x100x8	S355J2H	Test speed 3.	
S08	A	100x100x8	S355J2H	1 W, 2 H, 3 B, 4 Rmax, 5 Rmin	Charpy V Notch
S09	A	100x100x8	S355J2H	Test speed 4.	
S10	A	100x100x8	S355J2H	Test speed 5.	
S14	A	100x100x10	S355J2H	1 W, 2 H, 3 B, 4 Rmax, 5 Rmin	Charpy V Notch
S15	A	150x150x8	S355J2H	1 W, 2 H, 3 B, 4 Rmax, 5 Rmin	Charpy V Notch
S16	A	200x200x10	S355J2H	1 W, 2 H, 3 B, 4 Rmax, 5 Rmin	Charpy V Notch
S17	A	300x300x6	S355J2H	1 W, 2 H, 3 B, 4 Rmax, 5 Rmin	Charpy V Notch
S18	A	300x300x12.5	S355J2H	1 W, 2 H, 3 B, 4 Rmax, 5 Rmin	Charpy V Notch
S19	A	200x100x8	S355J2H	1 W, 2 H, 3 B, 4 Rmax, 5 Rmin	Charpy V Notch
S20	A	200x100x10	S355J2H	1 W, 2 H, 3 B, 4 Rmax, 5 Rmin	Charpy V Notch
S21	B	50x50x3	S355J2H	1 W, 2 H, 3 B, 4 Rmax, 5 Rmin	
S22	B	50x50x5	S355J2H	1 W, 2 H, 3 B, 4 Rmax, 5 Rmin	Charpy V Notch
S23	B[1]	100x100x3	S355J2H	1 W, 2 H, 3 B, 4 Rmax, 5 Rmin	
S24	B[1]	100x100x5	S355J2H	1 W, 2 H, 3 B, 4 Rmax, 5 Rmin	Charpy V Notch
S25	B	100x100x6	S355J2H	1 W, 2 H, 3 B, 4 Rmax, 5 Rmin	Charpy V Notch
S26	B	100x100x8	S355J2H	1 W, 2 H, 3 B, 4 Rmax, 5 Rmin	Charpy V Notch
S28	B	100x100x10	S355J2H	1 W, 2 H, 3 B, 4 Rmax, 5 Rmin	Charpy V Notch
S29	B	150x150x8	S355J2H	1 W, 2 H, 3 B, 4 Rmax, 5 Rmin	Charpy V Notch
S30	B	200x200x10	S355J2H	1 W, 2 H, 3 B, 4 Rmax, 5 Rmin	Charpy V Notch
S31	B	200x100x8	S355J2H	1 W, 2 H, 3 B, 4 Rmax, 5 Rmin	Charpy V Notch
S32	B	200x100x10	S355J2H	1 W, 2 H, 3 B, 4 Rmax, 5 Rmin	Charpy V Notch
S33	C	100x100x5	S355J2H	1 W, 2 H, 3 B, 4 Rmax, 5 Rmin	Charpy V Notch
S34	C	200x100x8	S355J2H	1 W, 2 H, 3 B, 4 Rmax, 5 Rmin	Charpy V Notch
S35	C	160x160x6	S355J2H	1 W, 2 H, 3 B, 4 Rmax, 5 Rmin	Charpy V Notch
S36	D	100x100x8	S355J0H	1 W, 2 H, 3 B, 4 Rmax, 5 Rmin	Charpy V Notch
S37	D	100x100x10	S355J0H	1 W, 2 H, 3 B, 4 Rmax, 5 Rmin	Charpy V Notch
S38	D	150x150x8	S355J0H	1 W, 2 H, 3 B, 4 Rmax, 5 Rmin	Charpy V Notch
S39	D	200x100x8	S355J0H	1 W, 2 H, 3 B, 4 Rmax, 5 Rmin	Charpy V Notch
S40	E	50x50x3	S355J2H	1 W, 2 H, 3 B, 4 Rmax, 5 Rmin	
S41	E	50x50x5	S355J2H	1 W, 2 H, 3 B, 4 Rmax, 5 Rmin	Charpy V Notch
S42	E	100x100x3	S355J2H	1 W, 2 H, 3 B, 4 Rmax, 5 Rmin	
S43	E	100x100x6	S355J2H	1 W, 2 H, 3 B, 4 Rmax, 5 Rmin	Charpy V Notch
S44	E	100x100x10	S355J2H	1 W, 2 H, 3 B, 4 Rmax, 5 Rmin	Charpy V Notch
S45	E	160x160x6	S355J2H	1 W, 2 H, 3 B, 4 Rmax, 5 Rmin	Charpy V Notch
S46	B [1]	100x100x3	S460	1 W, 2 H, 3 B, 4 Rmax, 5 Rmin	
S47	B [1]	100x100x5	S460	1 W, 2 H, 3 B, 4 Rmax, 5 Rmin	Charpy V Notch
S48	B	100x100x6	S460	1 W, 2 H, 3 B, 4 Rmax, 5 Rmin	Charpy V Notch
S49	B	100x100x8	S460	1 W, 2 H, 3 B, 4 Rmax, 5 Rmin	Charpy V Notch
S50	HF	50x50x5	S355J2H	1 W, 2 H, 3 B, 4 Rmax, 5 Rmin	Charpy V Notch
S51	HF	100x100x8	S355J2H	1 W, 2 H, 3 B, 4 Rmax, 5 Rmin	Charpy V Notch
S52	HF	150x150x8	S355J2H	1 W, 2 H, 3 B, 4 Rmax, 5 Rmin	Charpy V Notch
S53	A	100x100x3	S355J2H	1 W, 2 H, 3 B, 4 Rmax, 5 Rmin	
S54	A	100x100x6	S355J2H	13+1 coupons	Charpy V Notch
S55	A	200x100x8	S355J2H	13+1 coupons	
S56	A	200x100x4	S355J2H	13+1 coupons	

[1] Sections were directly cold formed into rectangular shape from the strip.

For each section following measurements and tests were carried out:

- Cross-sectional dimensions of each CFSHS were measured.
- Chemical analysis was made to determine chemical content of base material.
- Tensile test coupons were manufactured from five different locations around perimeter: from the weld positions, from both faces and from two corners having either minimum or maximum corner radius.
- For three sections, which were used to determine deviation of properties around perimeter, altogether 13 coupons were manufactured around half of the perimeter.
- The toughness of hollow sections was determined with Charpy V Notch (CVN) impact tests. The transition curve was determined with three specimen in single temperature for sections having material thickness larger or equal than 5 mm.

2.2.1 Chemical composition

Carbon equivalents *CEV* and P_{CM} (Figure 2-3) are calculated to describe characteristic of base material and weldability of steels based on chemical composition of steels.

CEV is calculated with equation

$$CEV = C + \frac{Mn}{6} + \frac{Cr + Mo + V}{5} + \frac{Cu + Ni}{15} \tag{2-1}$$

P_{CM} is calculated with equation.

$$P_{CM} = C + \frac{Si}{30} + \frac{Mn + Cu + Cr}{20} + \frac{Ni}{60} + \frac{Mo}{15} + \frac{V}{10} + 5B \tag{2-2}$$

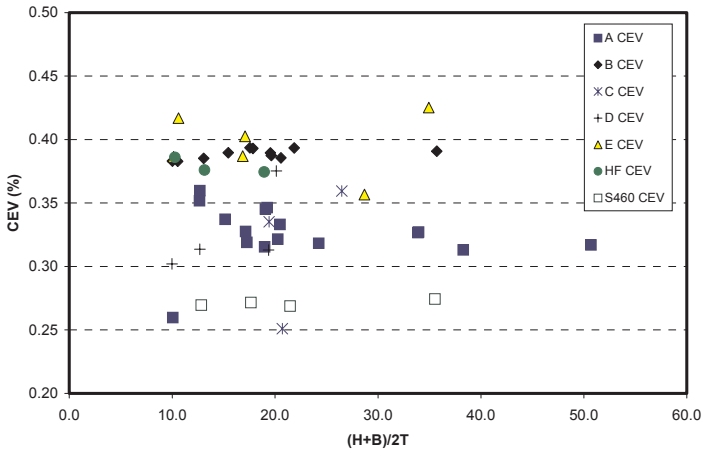

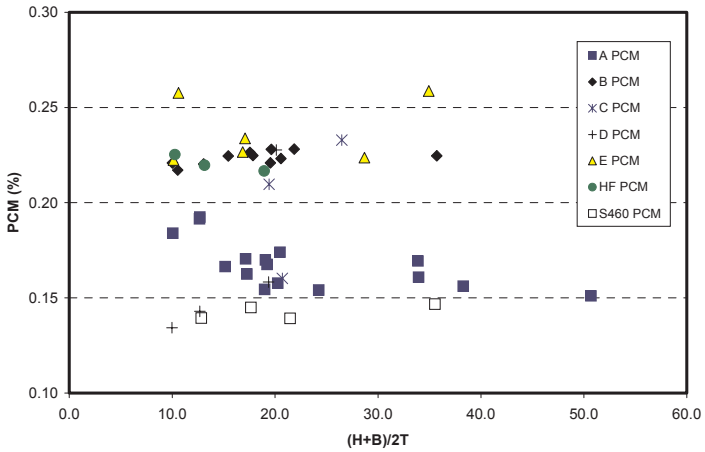

Figure 2-3. Carbon equivalent CEV and P_{CM} values for hollow sections in the test programme given as function of section slenderness.

2.2.2 Geometrical dimensions

Cross-sectional dimensions were measured from each section according to instruction given in EN 10219-2. The measurement of width, height and thickness is quite obvious. Instead corner region widths are measured according to instruction in EN 10219. Then the external corner radius R is calculated as the average value from the corner measurements a_i, b_i, c_i and d_i. Therefore the true internal and external corner radius were measured with radius templates. Also thickness of corner area is measured from corner coupons.

Following conclusion can be drawn from the measurement of overall geometrical dimensions:

- The overall dimensions of sections fulfilled tolerance in the product standard EN 10219.

- The thickness of sections depends on the coil thickness used to produce the section. The normalised thickness measurements are compared to tolerances of EN 10219 in Figure 2-4. The average values are well within requirements set in EN 10219. The value that falls below minimum tolerance is for hot-formed section.

- Judgement of corner radius is more challenging, while in practise the widths of corner area are measured not the radius and there is large deviation in the widths. Figure 2-5 shows normalised corner width values as function of thickness that can be compared to the EN 10219 tolerances. The average of all corner width measurement from section is used as base value. The error bars show the minimum and maximum corner width value from the respective section. The deviation of widths within single section can be very large. Some of the values fall clearly below the tolerance set in EN 10219.

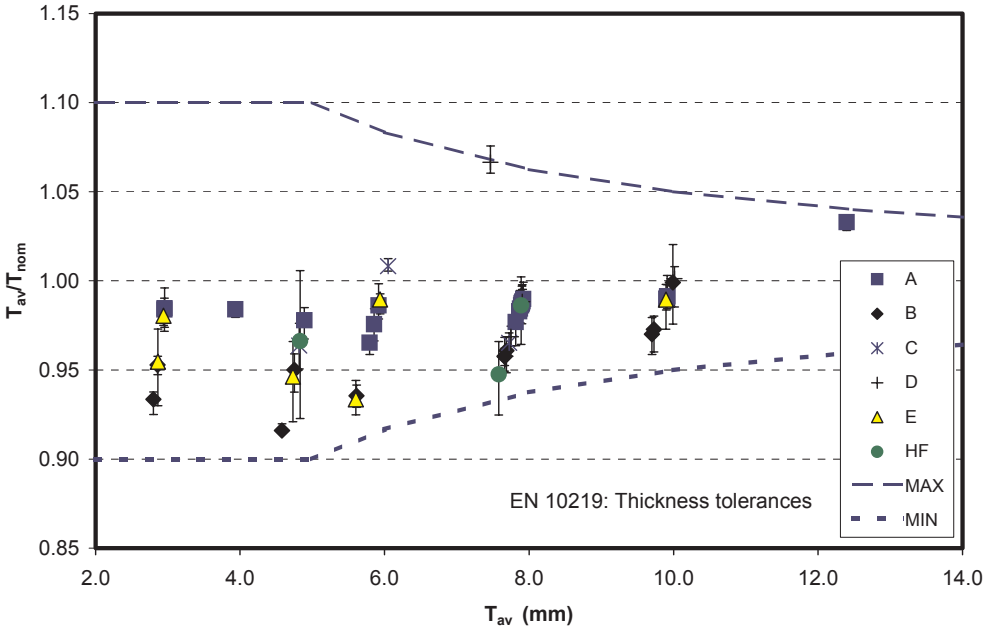

Figure 2-4. Comparison of measured thickness to tolerances set in EN 10219 for thickness. Thickness is average of eight measurements from flat faces of hollow section. Error bars show maximum and minimum values within these measurements.

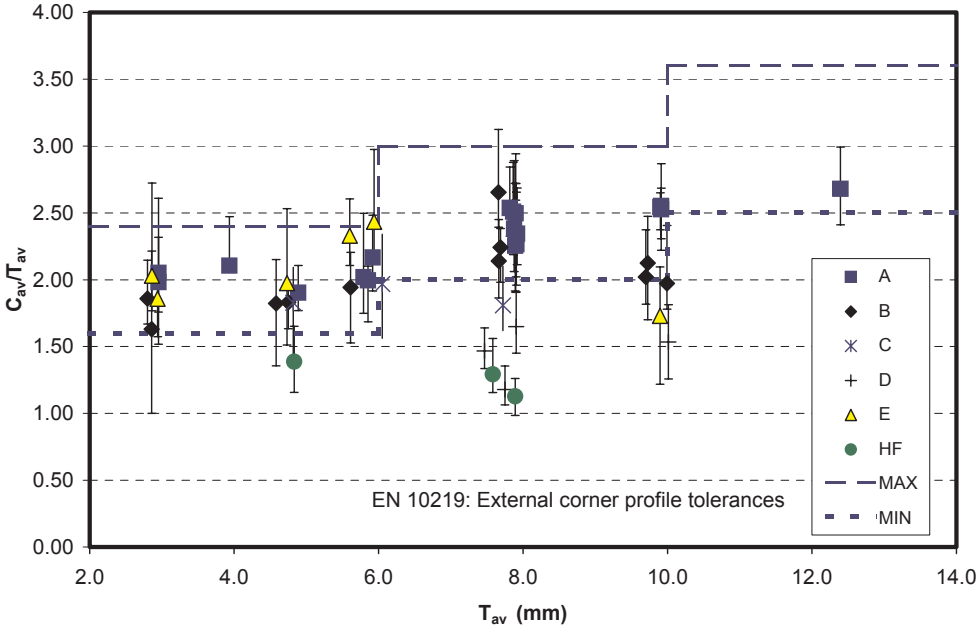

Figure 2-5. Average of measured corner area widths compared to tolerances set in EN 10219. Average value is calculated from two widths available for each corner. The error bars show minimum and maximum values within corner area widths from one section. The green dots show values for hot-formed sections.

Dimensions of corner region and corner radius relate to condition in Eurocode 3, Part 1.8 (prEN 1993-1-8:2003) for welding in the cold formed zones or adjacent to them. According to clause 4.14 (1) welding may be carried out within a length *5t* either side of the cold formed zone provided that the cold formed zones are normalised after cold forming but before welding or the *r/t* ratios satisfy requirements set in given Table 4.2. These conditions are compared against measured internal corners to material values thickness in Figure 2-6.

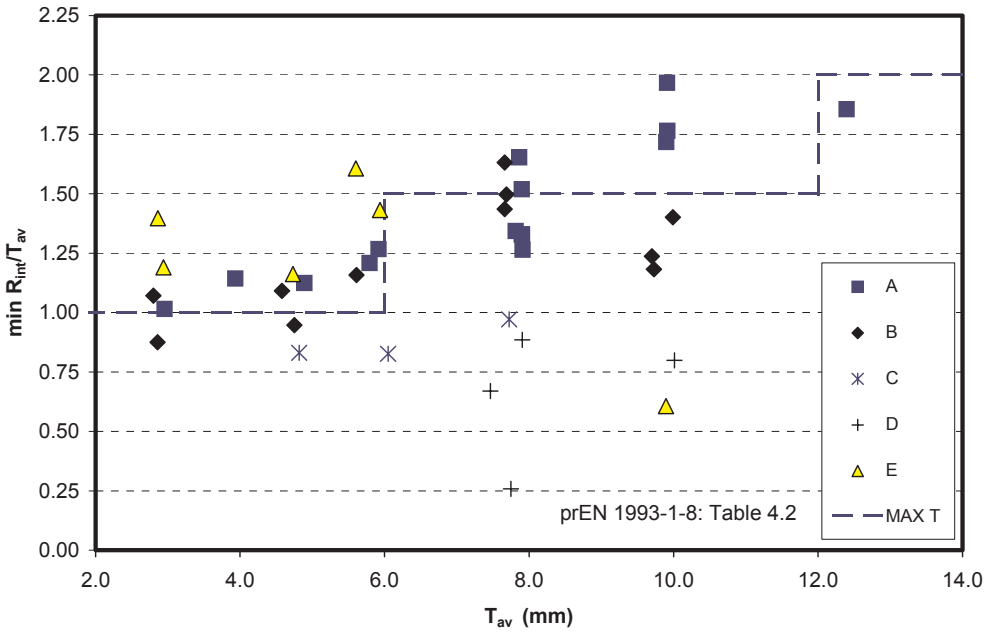

Figure 2-6. Evaluation of measured corner radius dimensions against limitation to welding in the cold-formed zone according to prEN 1993-1-8. The ***minimum of actual internal corner radius measured with corner gauges*** *is used in the comparison. T_{av} is the average thickness from all thickness measurements around section.*

2.3 Mechanical properties

2.3.1 Testing

Mechanical properties are determined from tensile coupon tests according to EN 10002-1. Three sections were enclosed to test programme to determine the deviation of properties around perimeter of section in more detail. Deviation was determined with altogether 14 coupons; one from the location of weld seam and thirteen around the half of the perimeter of the section (Figure 2-7 S54 and S56). These coupon are located in following positions:

- Centres of three faces: one in the face of seam weld (Coupon 11), one opposite to that (Coupon 23) and one perpendicular to these (Coupon 17) and
- Both corners (Coupon 14 and 20).
- Coupons located to both sides of the corner in the way that the other edge of the coupon is located in position where the corner area starts (Coupons 13 and 15 for corner 14 and Coupons 19 and 21 for corner 20).
- Coupon located in the faces 1/3 or 1/4 of width from the corner seam weld face (Coupon 12), face next to that (Coupons 16 and 18) and face opposite to that (Coupon 22).

From section of the main test programme tensile test coupons were manufactured from five positions around the perimeter of CFSHS (Figure 2-7 right).

- The seam weld is located in the middle of the W coupon (Coupon 1 W).
- The coupons from flat elements H (Coupon 2 H) and B (Coupon 3 B) are positioned in the middle of the side of specimen.

- The corner coupons are manufactured from two corners: Rmax from the corner where the largest corner radius was measured (Coupon 4 Rmax) and Rmin from the corner where smallest corner radius was measured (Coupon 5 Rmin).

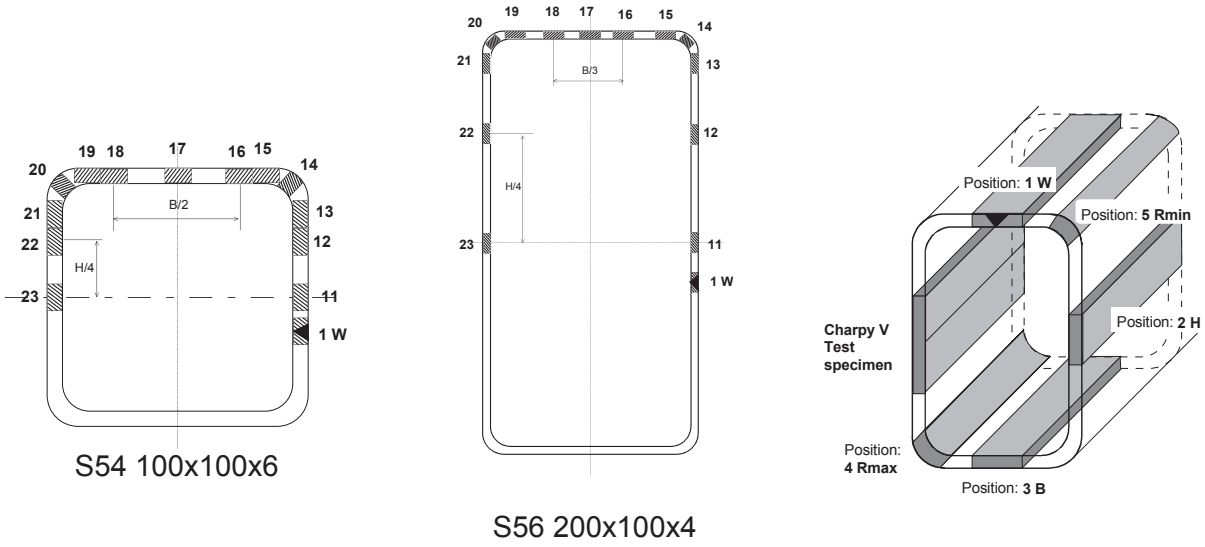

Figure 2-7. Location and designation of coupon test specimen in the sections S54 and S56 to determine detailed distribution and in the section of the main test programme. Note: the location of weld in reality is usually in the H face of section. H coupon is chosen opposite to longitudinal weld.

The coupons were dimensioned according to instruction given in testing standard EN 10002. The width of the corner coupons was equal to the average value of internal radius for the section but not less than 5 mm. The internal radius was calculated from external radius obtained with the widths of the corner area and average thickness of the section. The width was rounded to full millimetre value. The corner coupon is positioned in the middle of the corner area.

The billets for coupons machined directly from the section. The ends of the corner coupons and weld coupon were machined before testing to avoid eccentricity in the testing.

The tensile tests were carried out according to standard EN 10002 at displacement control. The test speed was 50% of the allowable maximum specified by EN 10002. In the elastic range up to strain level 1.0% used straining rate (mm/min) corresponding to stressing rate was 15 N/mm^2 s^{-1} and after the corresponded that straining rate 0.004 1/s.

The force-elongation values recorded during loading were transferred to engineering stress strain curve. The force is divided with nominal coupon area and strain is calculated from proportional elongation. Mechanical properties are determined from these stress-strain curves according to EN 10002-1. Following notes are on the determination of values:

- $R_{p0.2}$ proof strength corresponding to 0.2% permanent extension is determined with nominal elastic modulus E = 210 000 N/mm^2. This has an effect on the proof stress value depending on the true elastic modulus; when it is higher the proof stress is overestimated using nominal elastic modulus and when it is lower the proof stress is underestimated.

- In the determination of A_{gt} percentage of total elongation at maximum force the shape of engineering stress strain curves influences the results. Especially the coupons from flat faces do not exhibit clear elongation when the necking initiates. The range of elongation around maximum force can be large. The shifting in measurement system makes determination of absolute maximum difficult.

- The location of fracture in the coupon may have an effect on the value of A_5 percentage of elongation after fracture determined from coupon. When the fracture is not located in the middle of

the coupon the measurement length for A_5 has to be chosen in the way that the extension is measured from the narrow part of coupon non centric to fracture position.

- In weld coupon (1 W) the area of seam weld is not taken in to consideration in the area of coupon. Stress is determined dividing the force with area obtained with thickness and width of the coupon has been measured. Therefore the stress value may be larger than in reality.

2.3.2 Effect of cold forming on mechanical properties

The cold forming of steel strip as hollow section has an influence of the mechanical properties of hollow cross-section. In principle cold forming increases the stress level and decreases elongation values. The cold forming rate varies in different part of the cross section. The cold forming into circular mother tube has about the same influence through the perimeter of the shell. Some variation may occur near the edges.

Most of the cold work is done in shaping the section from circular mother tube into rectangular shape. The largest cold forming rates are found in the corners of the section. Also welding of the longitudinal seam influences mechanical properties.

The distribution of mechanical properties around section was studied with three section sizes having different slenderness ratios: b/t = 12.7, 16.7 and 25. As described in Chapter 2.3.1 13 tensile test coupons were manufactured from different positions around half of the perimeter of section. Engineering stress-strain -curves from tests is shown in Figure 2-8 to characterise changes in stress strain relationship due to cold forming.

The changes in characteristics of stress strain relationship due cold forming can be seen from the curves:

- Strength is increased. This influences both proof stress $R_{p0.2}$ and tensile strength R_m.

- Elongation values are decreased. Uniform elongation before reaching the maximum force, where necking localises, is significantly lower in cold formed corners. Elongation at fracture are also lower, thus the localised elongation at necking before fracture seems be of same order.

The cold forming has significant effect on the stress-strain relationship in the actual corner, where the cold forming rate is highest. Cold forming has influence on the properties of the flat face near the corner, but this region is equal to 1-2 times material thickness.

2.3.2.1 Strength properties

The amount of increase in strength values is shown in Figure 2-9 for proof stress $R_{p0.2}$ and in Figure 2-10 for tensile strength R_m. The ratio between minimum strength values found from the face to respective value from corners is drawn as function of section slenderness (B+H)/2T. Similar pattern is found from both figures; the lower the slenderness ratio is the smaller is increase in strength due to cold forming. The amount of cold forming to circular tube increases strength levels in low slenderness ration. Therefore difference between values from flat face and corners is smaller in lower slenderness.

Respective comparison against material thickness T, corner radius R and corner radius to thickness ratio R/T, which depend on each other, shows, that the higher these value are the lower is increase in strength values due to cold forming.

Some thinner section from manufacturer B having quite high slenderness was manufactured directly into rectangular shape, but these cases cannot be deviated from results.

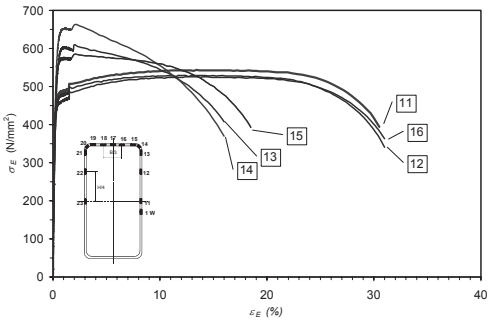

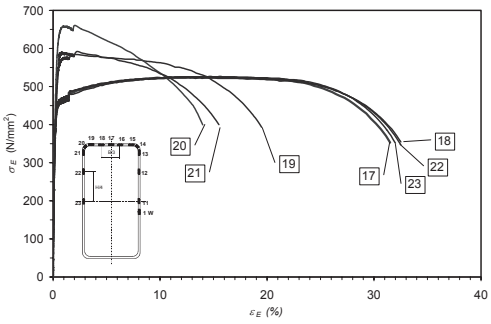

S56 200x100x4 A S355J2H **B/T = 25**

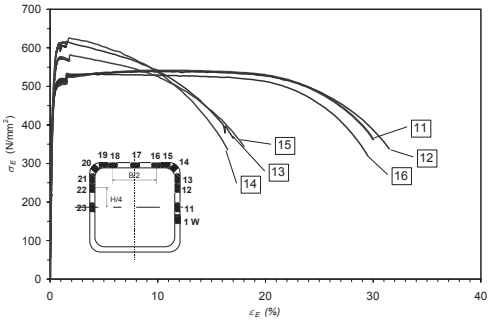

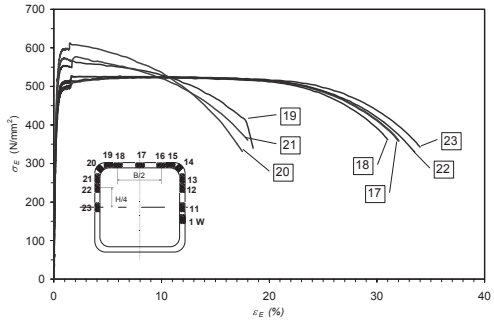

S54 100x100x6 A S355J2H **B/T = 16.7**

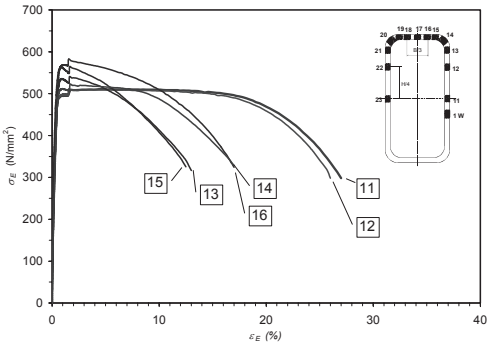

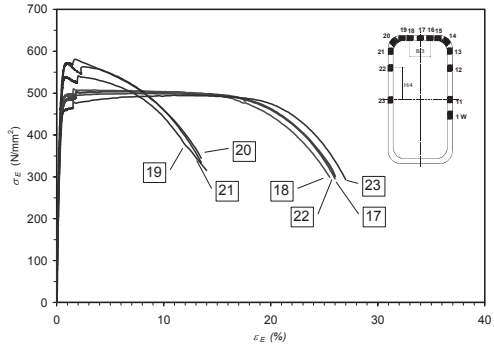

S55 200x100x8 A S355J2H **B/T = 12.5**

Figure 2-8. Influence of cold forming rate to engineering stress strain curves.

2.3.2.2 Elongation properties

The cold forming has significant effect on the uniform elongation, before necking localises. Figure 2-11 shows the rations between elongation values at maximum force from flat faces compared to corners as function of section slenderness (B+H)/2T. Respectively effect of cold forming rate to elongation after fracture values is shown in Figure 2-12.

Figure 2-9. Effect of cold forming in proof stress $R_{p0.2}$ around section as function of section slenderness (B+H)/2T. The proof stress in the corners is compared with minimum proof stress found from face of the section.

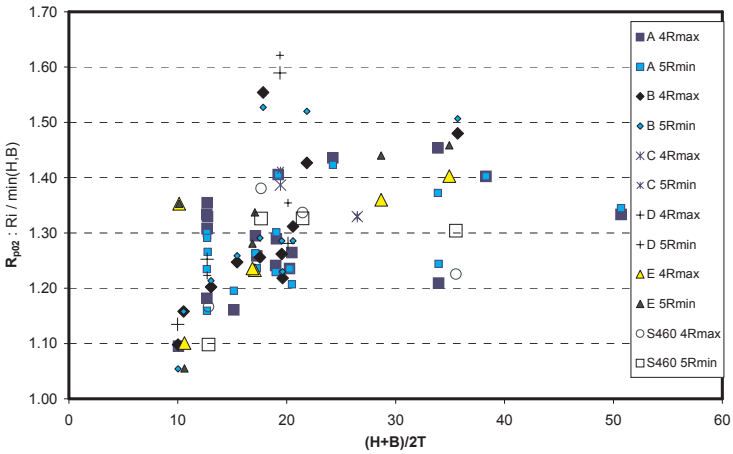

Figure 2-10. Effect of cold forming in tensile strength R_m around section as function of section slenderness (B+H)/2T. The tensile strength in the corners is compared with minimum tensile strength found from face of the section.

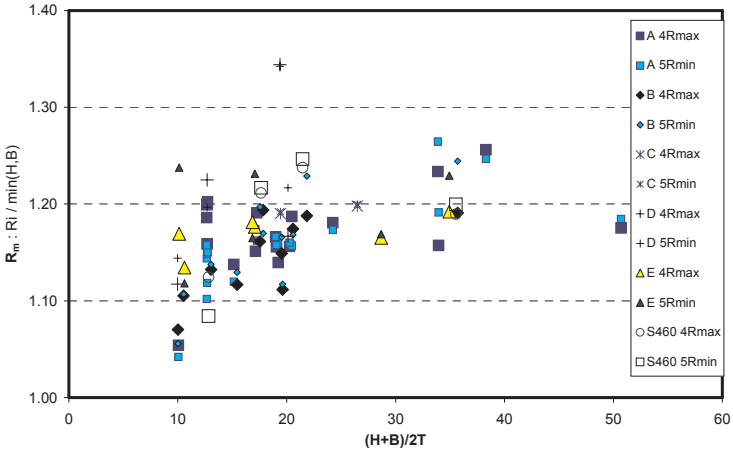

Figure 2-11. Effect of cold forming in elongation at maximum force A_{gt} as function of section slenderness (B+H)/2T. The elongation at maximum force in the corners is compared with maximum elongation at maximum force found from face of the section.

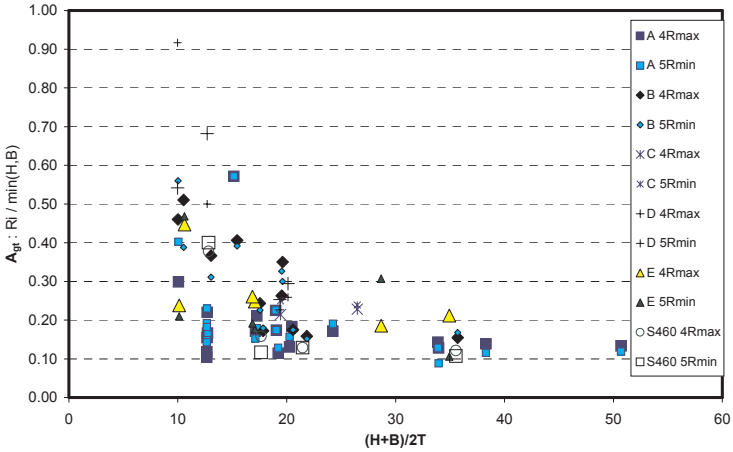

Figure 2-12. Effect of cold forming in elongation after fracture A_5 as function of section slenderness (B+H)/2T. The elongation after fracture in the corners is compared with maximum elongation after fracture found from face of the section.

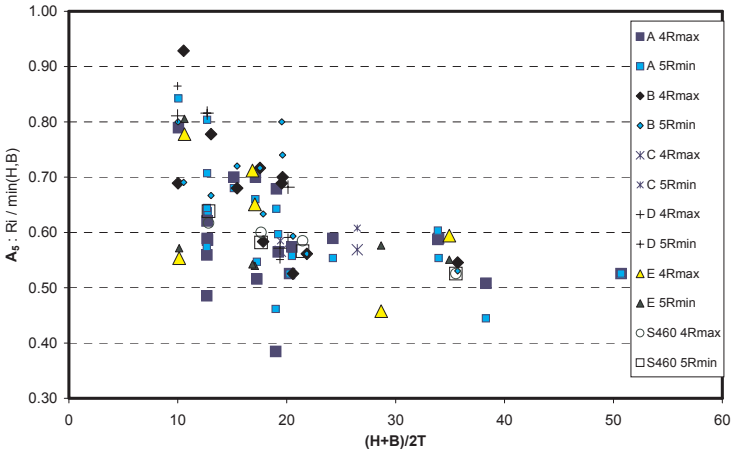

2.3.3 Effect of welding and low temperature

The heat input of welding affects mechanical properties, when CFSHS members are welded. Welding causes avoidable flaws, which may initiate brittle crack growth. Combined with low temperature the possibilities of brittle fracture or in general decreased ductility are to be considered also is welded connections.

In cold-formed structural hollow section (CFSHS) mechanical and ductility properties vary around the section, while cold forming rate is different in different parts of the section. The strength is increased and deformation capacity is decreased in the corner areas due to work hardening during cold forming. The coupon test shows that the properties around section are different. Therefore whole section tension tests are used to evaluate the redistribution around section.

2.3.3.1 Test programme

To determine effect of welding on mechanical properties on cold-formed material and to consider possibility of brittle fracture test programme presented in Table 2-3 was defined. The test programme contained following tests:

- Tensile tests are done for coupons made from sections with transverse weld. Whole section tension tests are made with specimen with similar transverse weld. These results are compared to similar tests for non-welded specimen.

- These tensile coupon tests and whole section tension tests for welded and non-welded specimen are done at both normal (+20^{o}C) and low temperature (-60^{o}C).

- Coupon tests to verify effect of welding and effect of low temperature are done with two coupons - one from flat face and one from corner area (2 H and 4 Rmin).

- Effect of low temperature on the mechanical properties of CFSHS is studied with two different section from different manufacturer to verify effect of steel strip content.

- Some whole section tension tests are carried out in normal temperature to verify average distribution of mechanical properties around the cross-section. For these sections detailed distribution around section is determined with 13 coupons located around half of the perimeter of section.

Table 2-3. Contents of the additional test programme. The number in each cell shows amount of tests done for this section.

No of test	Non welded specimen				Welded specimen			
Test type	Coupon test		Whole section tension test		Coupon test		Whole section tension test	
Test temperature	+20	-60	+20	-60	+20	-60	+20	-60
100x100x3	2	2	1	1	2	2	1	1
100x100x6	2+2 [1]	2+2 [1]	1 [2]	1	2	2	1	1
100x100x10	2+2 [1]	2+2 [1]	1 [2]	1	2	2	1	1

[1] From two manufacturer A and B to study effect of base material.
[2] Same whole section tension test results are used for both comparison.

2.3.3.2 Welding

In the welding of transverse pass around hollow section specimen MAG (135) process was replaced by TIG (14) process in order to avoid the need for surface machining after welding. In TIG-welding the adjustable parameters are travel speed and current. If the heat input in TIG-process is the same as in MAG-process, the throat thickness *a* of fillet weld in MAG-welding can be estimated by the following simple semi empirical formula

$$a \approx \sqrt{\frac{\eta \cdot U \cdot I}{50000 \cdot v}} \tag{2-3}$$

The measured welding process parameters and calculated values are seen in Table 2-4. Thermo couples measured the maximum root side temperature during the weld process. The passes are welded without consumables except the case of tube with wall thickness of 10 mm, where additional filler material was used in order to avoid the decreasing of the wall thickness caused by TIG process.

Table 2-4. The welding parameter.

Tube	U_{TIG} [V]	I_{TIG} [A]	v_{TIG} [m/s]	Q [kJ/mm]	a_{fillet} [mm]	$T_{max,root}$ [°C]
100x100x10	13.6	270	0.0015	1.47	5.5	804
100x100x6	12.9	250	0.0026	0.74	4	984
100x100x3	9.3	85	0.0022	0.22	2	-

2.3.3.3 Testing

Principle of test set-up for whole section tests is seen in Figure 2-13. The end plates were connected to testing machine with pinned connections in one plane. During testing both overall extension over the testing length and local extension within specimen at varied length was measured. The local extension measurement length was increased because necking localised outside measurement length. Section was equipped with strain gauge in location of transverse weld. In the low temperature test also temperature of the specimen was controlled: the coolant liquid was circulating in the section long enough before testing.

Figure 2-14 shows stress displacement curves from whole section tensile tests for section 100x100x10.

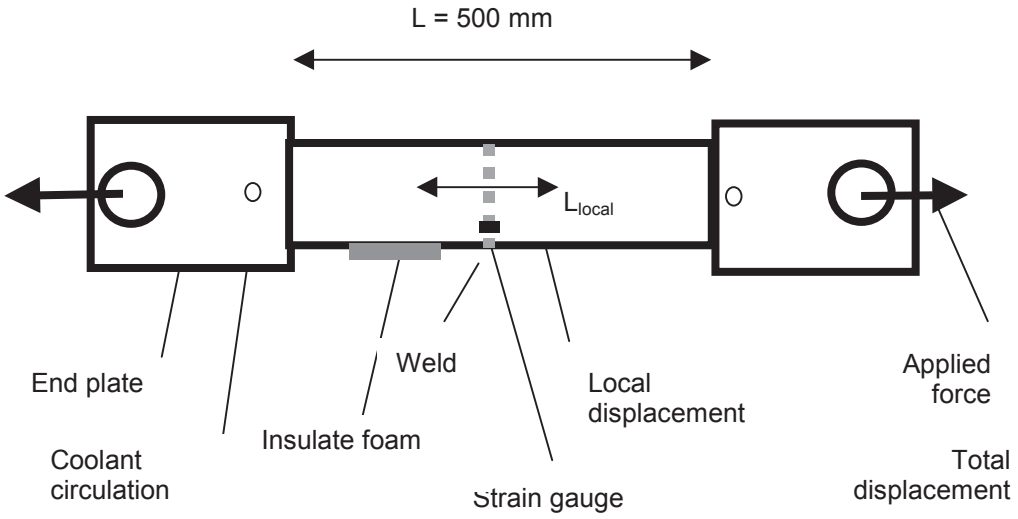

Figure 2-13. Principle of test and measurement arrangement in whole section tensile test.

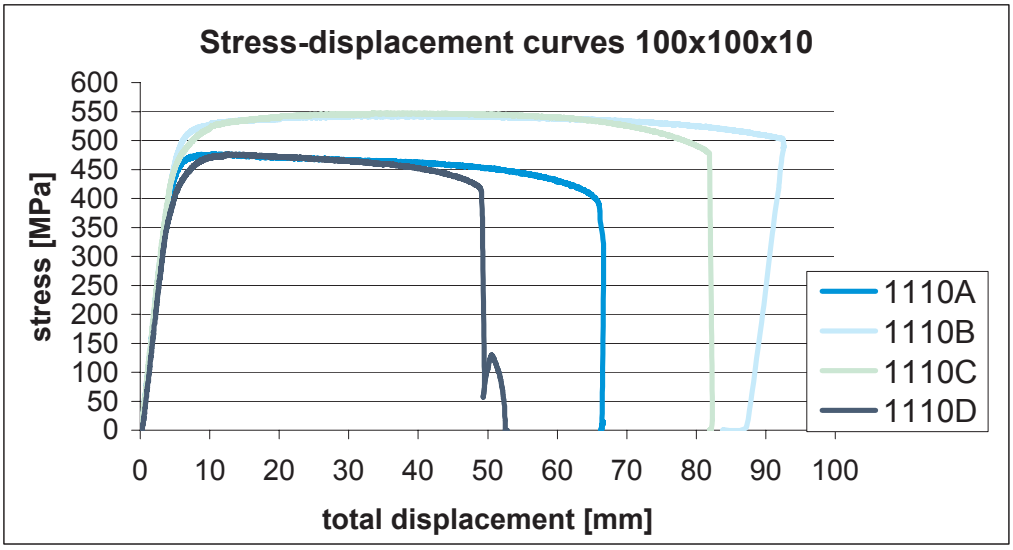

Figure 2-14. Stress displacement curves from tests for section 100x100x10: A - is room temperature with no weld; B - low temperature with no weld; D - room temperature with transverse weld and C - low temperature with transverse weld.

The low temperature testing for tensile coupons was done with testing equipment having cooling chamber. To ensure equal testing conditions for normal temperature testing all tensile tests for welded coupons and comparative test at normal temperature for non-welded coupons were done with the same testing equipment.

The welding of sections for coupon tests was done in the same time as the section for whole section tension tests were welded. The marking of the positions for manufacturing was made clear to ensure that tensile test coupons are from the same corner and face. The bar of each section size was cut and marked to guarantee that the direction of sections was same.

2.3.3.4 Conclusions

Whole section tensile tests and coupon tests are evaluated separately. The effect of low temperature and effect of welding are analysed from results.

In the whole section tensile tests strength comparison is done from the maximum force. Thus also the stress corresponding to 0.2% proof stress is given. Ductility verification is done with total extension at fracture divided by the whole section length. In the coupon tests evaluation is based on mechanical properties: proof stress $R_{p0.2}$, tensile strength R_m and uniform elongation at maximum force A_{gt} and elongation at fracture A_5. Following conclusions can be drawn from the results:

Effect of low temperature on mechanical properties:

- Tensile strength is higher in low temperature (-60°C) than in room temperature (+20°C) for both section without and with transverse weld. In whole section tensile tests decrease of temperature increases tensile strength in both welded and non-welded sections about 10%. In coupon tests tensile strength R_m is increased about 10-20% depending on the section size.

- Proof stress $R_{p0.2}$ is increasing about in the same ratio as the tensile strength in both whole section tensile and coupon tests.

- Decrease of temperature increases also deformation capacity independent of existence of transverse weld. In the whole section tension test plastic elongation is 14-89 % higher. In coupon test elongation at fracture A_5 seems to be increasing in most of the comparison, thus two comparison from the face of section show decrease.

- Elongations at maximum force A_{gt} show large deviation in the comparison with no clear dependence with temperature or section size. The characteristics of stress strain curve having shallow shape may have an influence on the value defined.

- In room temperature whole section test stress-displacement curve has similar shape than corners in coupon test especially in thick sections. Maximum force occurs at relative low elongation value. In low temperature tests the shape is shallower like in faces of the hollow section.

Effect of welding on the mechanical properties:

- Welding does not have significant an effect on the tensile strength in room or at low temperature. In the whole section tests the transverse weld is not the weakest position in the section. Also sections with transverse weld fail from the non-welded part of specimen in whole section tension test. In coupon tests at room temperature welding does not change the tensile strength R_m values in the face of section but seems to decrease it in corners about 10%. At low temperature welding does not influence the tensile strength values.

- Transverse weld seems to decrease the deformation capacity in both room and at low temperatures. In coupon tests at room temperature welding decreases total elongation values 25% in faces and also in corners, except in corner of section 100x100x6. At low temperature welding decreases total elongation after fracture A_5 values 20% in faces but in the corners reduction is lower, except in corner of section 100x100x3. Thus in whole section tests this may be due to used long measurement length of extension, which is used to calculate elongation. In the coupon tests the elongation along the length of section is not uniform in welded section.

- Fractures of specimen did not occur in the weld zone. In the whole section tests fracture initiated from the longitudinal seam weld.

2.3.3 Requirements of product standard EN 10219

Requirements according to EN 10219 for strength properties are shown in Table 2-5. The tensile test results are evaluated against these requirements. According to this product standard verification of properties is done with tensile test from the flat face. Figures 2-16 - 2-19 show main mechanical properties from coupons B and H drawn as functions of section slenderness. In addition to value given in Table 2-5 also uniform elongation A_{gt} is drawn.

Table 2-5. Requirements according to EN 10219 for strength and impact properties.

	Tensile test - EN 10002			Charpy V Notch - EN 10045	
	Minimum yield strength R_{eH} N/mm^2	Minimum tensile strength R_m N/mm^2	Minimum elongation A % $L_0 = 5.65\sqrt{S_0}$	Test temperature ^oC	Minimum impact energy KV (J/cm^2)
S355J0H	355	490	20	0	35
S355J2H	355	490	20	-20	35
S460MH	460	550	17	-20	50
S460MLH	460	550	17	-50	35

Statistical evaluation of results in test database is based on 38 sections from steel grade S355. Single section S33 was excluded while it did not fulfil the tensile strength requirement for S355 and is assumed to be of steel grade S275. Also sections S05-S07 and S09-S10 of 100x100x8 from manufacturer A are excluded, while their testing condition were not similar to other and their results would have caused too large influence on this single sections size on the deviation.

Results from the statistical evaluation of strength properties are collected to Table 2-6, where mean value, standard deviation and coefficient of variation are given each coupon separately. In addition minimum and maximum values are given. Also results from evaluation, where the coupons from both faces and from both corners have been considered as one test group, are given. Respectively analysis of elongation values is presented in Table 2-7.

Properties determined from faces of sections fulfilled strength requirements according to EN 10219 except in single case. This exception seems to be of steel grade S275. One other section had single tensile strength value 1% below the requirement, but the tensile strength from other face was above 490 N/mm^2. The elongation requirement was fulfilled in all cases.

Results from statistical evaluation of strength properties in Table 2-6 shows that also strength properties at longitudinal seam weld and in the corners fulfil requirement of EN 10219.

Instead the elongation values at fracture are fulfilled neither in the seam weld nor at corners. Thus the average is close to the requirement. The properties of weld depend on the treatment after welding: normalising is needed to achieve adequate ductility. Thus it should be considered that the requirements are set for the tensile test made from face of section.

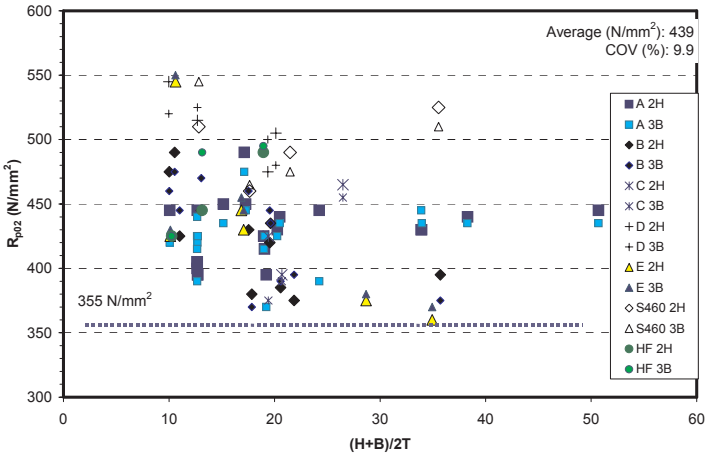

Figure 2-15. Proof stress $R_{p0.2}$ values for coupons 2 B and 3 H from faces of the section. In the lower picture the same results are shown in more detail.

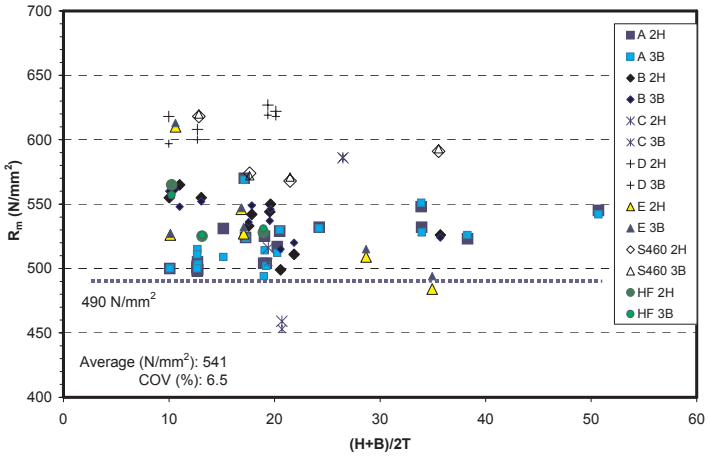

Figure 2-16. Tensile strength R_m values for coupons 2 B and 3 H from faces of the section. In the lower picture the same results are shown in more detail. Note that results for section S33 of steel grade S275 are included in the pictures.

Figure 2-17. Elongation values at maximum force A_{gt} for coupons 2 B and 3 H from faces of the section.

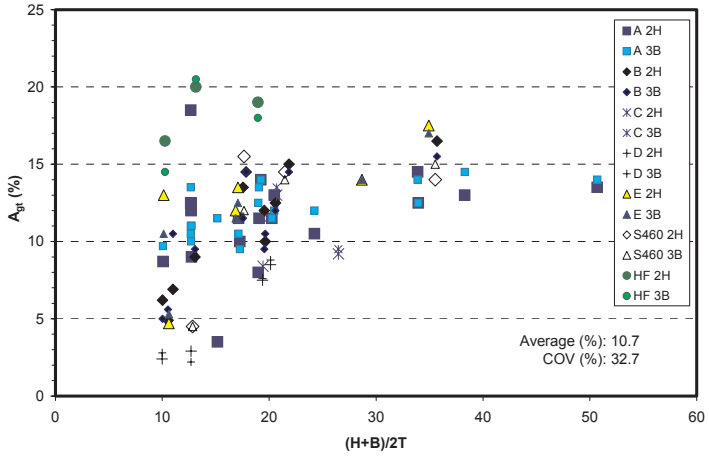

Figure 2-18. Elongation values at fracture A_5 for coupons 2 B and 3 H from faces of the section.

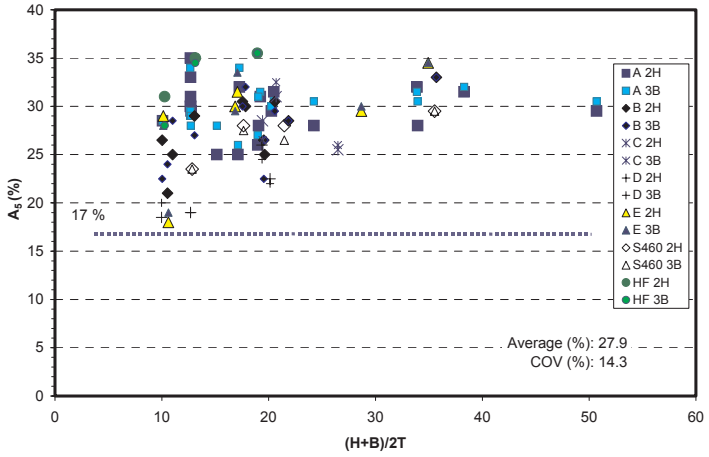

Table 2-6. Statistical evaluation of proportional limit $R_{p0.2}$ and tensile strength R_m.

N/mm^2	$R_{p0.2}$					R_m				
	W	H	B	Rmax	Rmin	W	H	B	Rmax	Rmin
AVER.	579	441	438	555	558	670	542	541	629	633
STDEV	78.7	43.0	43.8	52.7	52.5	82.0	36.6	34.3	54.1	55.8
COV(%)	13.5	9.8	10.1	9.5	9.3	12.3	7.1	6.8	8.8	8.7
AVER.		439		556			541		631	
STDEV	-	43.1		52.3		-	35.2		55	
COV (%)		9.9		9.4			6.5		8.8	
MIN	455	360	370	460	460	520	484	494	527	521
MAX	745	545	550	755	770	802	627	619	832	831

Table 2-7. Statistical evaluations of elongation at maximum force A_{gt} and after fracture A_5.

(%)	A_{gt}					A_5				
	W	H	B	Rmax	Rmin	W	H	B	Rmax	Rmin
AVER.	5.1	10.6	10.9	2.2	2.2	16.1	27.8	28.1	16.9	16.8
STDEV	3.1	3.8	3.4	0.6	0.6	7.0	4.0	4.1	2.5	2.3
COV(%)	61.2	35.1	30.4	26.0	28.3	42.7	14.2	14.4	15.2	13.6
AVER.		10.7		2.2			27.9		16.9	
STDEV		3.5		0.6			4.0		2.4	
COV(%)		32.7		27.0			14.3		14.2	
MIN	1.3	2.4	2.2	1.3	1.1	4.9	18.0	19.0	10.0	12.0
MAX	11.0	17.5	17.0	3.6	4.3	31.0	34.5	34.5	22.5	24.0

Assessment of the strength results available for the sections is carried out according to guidelines given in EN 1990 Eurocode: Basis of structural design (2002). The characteristic strength properties determined from the test results are collected to Table 2-8. The factor k=1.64 which with in this case provides characteristic values corresponding to 5% fractile at 75% confidence level. The evaluation is done using both normal and lognormal distribution. According to *Probabilistic Model Code* (2001) prepared by *Joint Committee of Structural Safety (JCSS)* log normal distribution should be used for strength properties of steel. The JCSS proposes 7% as coefficient of variation for yield strength and tensile strength of structural steel.

Table 2-8. Characteristic values for proportional limit $R_{p0.2}$ and tensile strength R_m according to EN 1990 using normal and log-normal distribution: char = mean – 1.64 stdev.

N/mm^2	$R_{p0.2}$					R_m				
	W	H	B	Rmax	Rmin	W	H	B	Rmax	Rmin
Normal	450	370	366	469	471	536	482	484	541	542
		368		471			484		542	
Log. N	460	375	370	477	480	543	486	488	549	549
		373		479			487		549	

The characteristic proof strength $R_{p0.2}$ values are above the limit set in EN 10219 for stress used as yield strength f_y=355 N/mm^2. The characteristic value for tensile strength R_m instead falls 1% below the required value (f_u=490 N/mm^2) even though all the tests results are above as in case of B face.

2.3.4 Ductility requirements for steel material in Eurocode 3

Eurocode 3, Part 1.1 (prEN 1993-1-1) sets following requirements for the ductility of structural steel in section 3.2.2 *Ductility requirements*. When minimum ductility is required, it will be expressed in terms of limits for:

1. The ratio f_u/f_y of the specified minimum ultimate tensile strength f_u top specified minimum yield strength f_y;

2. The elongation at failure on a gauge length $5.65\sqrt{A_0}$ (where A_0 is the original cross-sectional area);

3. The ultimate strain ε_u, where ε_u corresponds to the ultimate strength f_u.

According to note given the limiting values of the ratio f_u/f_y, elongation at failure A_5 and the ultimate strain ε_u may be defined in the National Annex. Thus some values were given as recommendations:

1. $f_u / f_y \geq 1.10$; (2-4)

2. Elongation at failure not less than $A_5 \geq 15\%$; (2-5)

3. $\varepsilon_u \geq 15\,\varepsilon_y$, where ε_y is the yield strain ($\varepsilon_y = f_y / E$). (2-6)

The requirements were modified from prestandard ENV 1993-1-1 during the conversion to EN standard.

These requirements are transferred to mechanical properties from tensile test:

1. $f_u / f_y = R_m / R_{p0.2} \geq 1.10$
   Statistical evaluation of test results is shown in Table 2-9.

2. $A_5 \geq 15\%$
   The statistical evaluation of elongation at fracture values are collected to Table 2-7.

3. $\varepsilon_u \geq 15\,\varepsilon_y$
   When the true proof stress level is considered while the use of nominal does not give safe sided evaluation of this requirement. Following conversion is made
   $$A_{gt} \geq 15\frac{f_y}{E} = 15\frac{f_{y,n}}{E}\frac{R_{p0.2}}{f_{y,n}} \Leftrightarrow \frac{1}{R_{p0.2}/f_{y,n}} A_{gt} \geq 15\frac{355}{210000} = 2.5\%$$
   Statistical evaluation of this parameter is shown in Table 2-10.

The tensile test results are presented against these requirements. Each requirement is considered separately for properties from the longitudinal weld position, faces of the section and corners. Test database for coupon test from CFSHS of steel grade S355 is analysed against these requirements.

2.3.4.1 Tensile strength to yield strength ratio

Table 2-9 shows results for tensile strength to yield strength ratio in different position sections: in the weld, in both faces of section and in two corners of section. For coupons from each position average value, standard deviation and coefficient of variation are given. Characteristic value is calculated according to EN 1990 Basis of structural design. To show maximum deviation smaller and largest value is given separately. The results are also presented graphically in Figure 2-19 as function of section slenderness (B+H)/2T for longitudinal weld position, for flat faces and for corners of section.

2.3.4.2 Elongation after fracture

Statistical evaluation of elongation after fracture A_5 is done at Table 2-7. Figure 2-20 shows elongation at fracture results for longitudinal seam weld, both faces and both corners as function of section slenderness.

Table 2-9. Statistical evaluation of $R_m/R_{p0.2}$ ratio is given. The characteristic value is calculated according to EN 1990 using equation given in the footnote.

	$R_m / R_{p0.2}$				
	W	B	H	Rmax	Rmin
AVERAGE	1.16	1.24	1.24	1.14	1.14
STDEV	0.06	0.07	0.08	0.03	0.03
COV (%)	5.42	5.99	6.51	2.69	2.80
Character. [1]	1.06	1.11	1.11	1.09	1.08
MAX	1.33	1.43	1.48	1.18	1.21
MIN	1.05	1.12	1.11	1.07	1.07

[1] *c = m -1.64 s*

2.3.4.3 Uniform elongation at maximum force

Table 2-10 shows results for elongation at maximum force values in different position sections: in the weld, in both faces of section and in two corners of section. For coupons from each position average value, standard deviation and coefficient of variation are given. Characteristic value is calculated according to EN 1990 Basis of structural design. To show maximum deviation smaller and largest value is given separately. The results are also presented graphically in Figure 2-21 as function of section slenderness (B+H)/2T.

Table 2-10. Statistical evaluation of elongation at maximum force A_{gt} related requirement ratio where the effect of true proof stress has been considered.

	$\frac{1}{R_{p0.2}/f_{y,n}} A_{gt}$				
	W	B	H	Rmax	Rmin
AVERAGE	3.43	8.83	9.14	1.45	1.42
STDEV	2.50	3.68	3.38	0.43	0.46
COV (%)	72.84	41.71	36.93	29.71	32.78
Character. [1]	-	2.79	3.60	0.74	0.65
MAX	8.40	17.26	16.31	2.53	2.83
MIN	0.62	1.56	1.49	0.78	0.62

[1] *c = m -1.64 s*

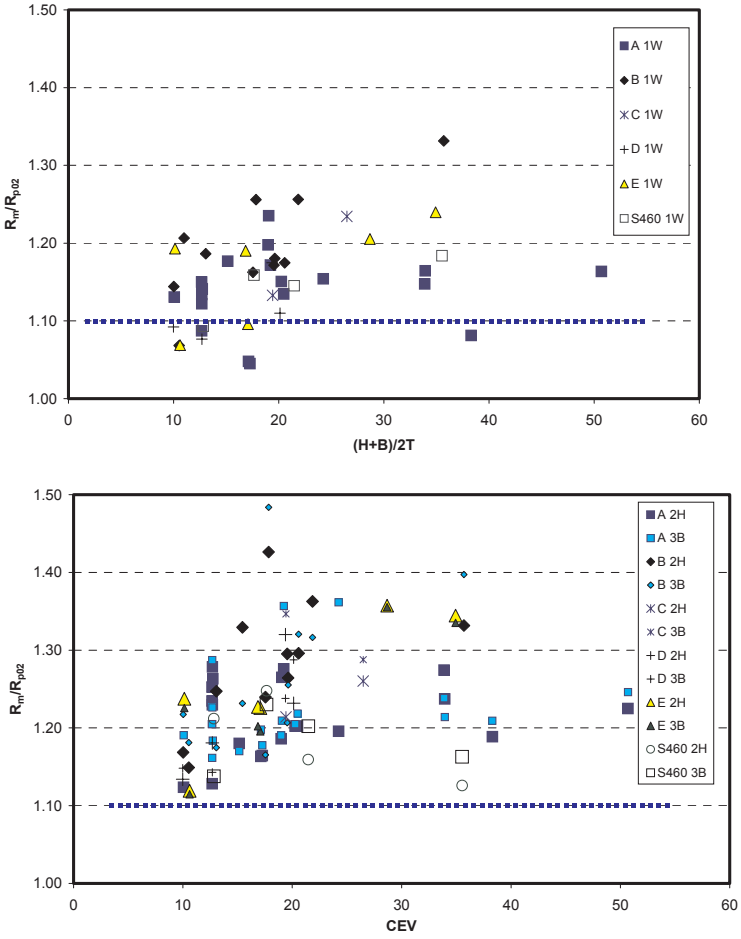

Figure 2-19. Values for $R_m/R_{p0.2}$ ratios drawn as function of slenderness (B+H)/2T for longitudinal weld above, flat faces at centre and corners below.

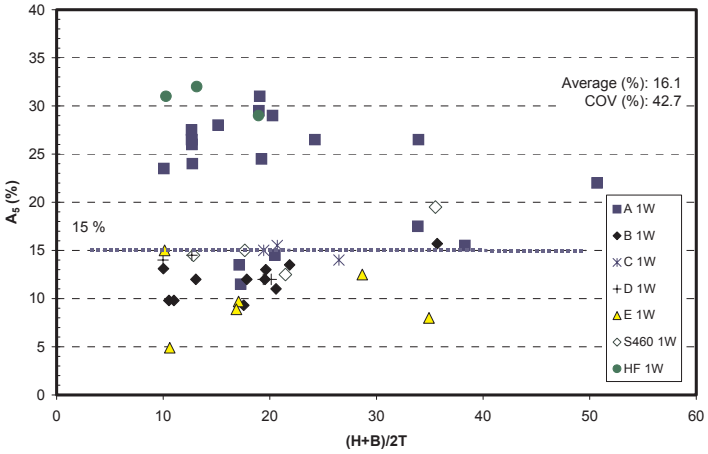

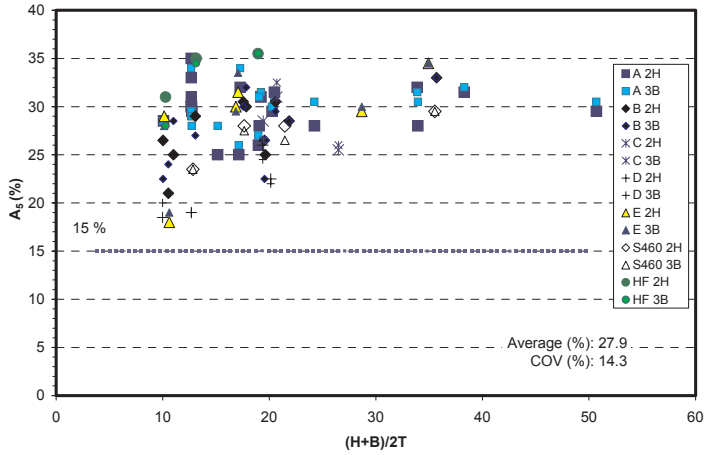

Figure 2-20. Values for elongation after fracture drawn as function of slenderness (B+H)/2T for longitudinal weld above, flat faces at centre and corners below.

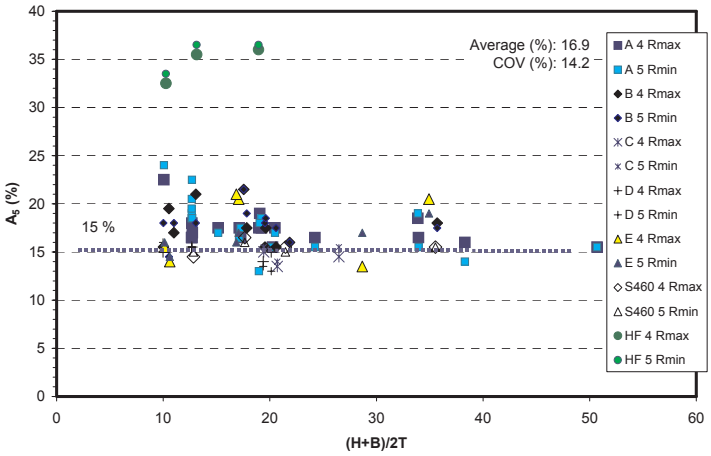

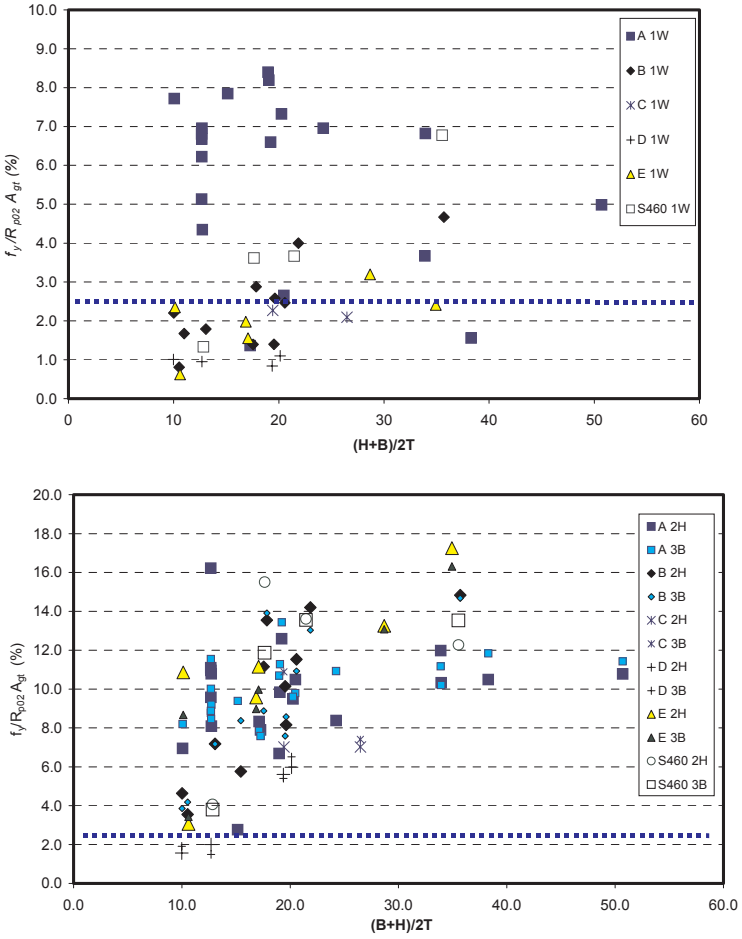

Figure 2-21. Values for $f_y/R_{p0.2}\,A_{gt}$ ratios drawn as function of slenderness (B+H)/2T for longitudinal weld above, flat faces at centre and corners below.

2.3.4.3 Conclusions

Following conclusions are drawn from evaluation of ductility requirements for steel material against tensile test results for section in test programme:

- The properties from flat faces B and H of section fulfil all three ductility requirements. Characteristic value for the tensile strength to yield stress ratio is 1.11. Values for elongation after fracture are clearly larger than required 15%. Some individual sections do not fulfil requirement for uniform elongation at maximum force.

- The longitudinal seam weld has to be normalised after welding to fulfil elongation requirements in ductility. Thus even some individual sections don't satisfy the tensile strength to yield stress ratio.

- The requirement for uniform elongation at maximum for corners of section is not fulfilled. Most of the sections do not satisfy this requirement. Some sections fail also in elongation after fracture and tensile strength to yield stress ratio requirement. The changes in characteristic of stress-strain relationship due to high cold forming rate decrease the uniform elongation dramatically. The influence of this has to be considered in the K- and X-joint tests. The safety of design provision has to be considered while design models are based on the plastic hinge mechanism.

2.4 Toughness properties

Brittle fracture is characteristic for normally ductile steel material at certain low temperatures. Toughness of a material is its ability to absorb energy in the plastic range. Safe use of steel structures requires that at service temperature chosen steel material does not exhibit brittle behaviour. This toughness is defined as materials ability of absorb energy either in presence of notch under dynamic loading or using unnotched specimen which may be loaded in principle statically under loading conditions where critical member is in tension.

2.4.1 Testing and evaluation

The toughness of steel material is measured with Charpy V Notch (CVN) specimen, which is standardised in testing standard EN 10045. The rectangular test specimen with a machined notch of specified geometry is used. Dynamic testing is done in pendulum testing machine where the amount of energy absorbed by the test specimen is measured. The test specimens are cooled at desired testing temperature in cooling chambers or using liquid hydrogen before testing.

Test specimen for Charpy V Notch (CVN) impact tests were taken from the flat face of the section opposite to H coupon (Figure 2-7). The billet for test specimen was sawn or machined from the section. Through thickness notch position was used in the specimen.

The dimension of test specimen was 10 x W x 55 according to EN 10045-1, which means that the height of test piece was 10 mm and length was 55 mm. The width varied with different wall thickness of the section; about 0.5 mm was machined from both surfaces of the section except with 12.5 mm material thickness, which was machined to 10 mm width. The width values for each section thickness are given in Table 2-11. The cross-sectional dimensions and notch depth were measured before testing to determine true area.

Table 2-11. Width of the impact test specimen corresponding to section thickness.

Nominal material thickness of section (mm)	5	6	8	10	12.5
Width of the impact test specimen (mm)	4	5	7	9	10

2.4.2 Analysis of results

When independent absorbed energy KV values are plotted against respective testing temperature values, a transition curve is formed showing the change from ductile (shear) behaviour to brittle (cleavage) behaviour. Ductile region of toughness curve is called "upper shelf" and brittle region as "lower shelf". Between them is transition region. The classification of material properties is different design for steel structures, pressure vessels and bridges and also requirement is product standards are based on certain amount of absorbed energy at specified temperature.

In addition to absorbed energy values also the amount of ductile area may be used to define the transition curve. The percentage of shear fracture from cross-sectional area at notch position, than can

be considered to be ductile, is used in vertical y-axis. This ductile-to-brittle transition temperature (DBTT) is defined at temperature when the amount of ductile behaviour of cross-sectional area is 50%.

In addition to temperature and loading rate (static or dynamic) the constraint depending on material thickness which affect on the stress state in the crack tip. Plane strain state, which provided best constraint, occurs at very thick specimen. Plane stress condition is found in very thin specimen with lowest constraint. The change in specimen dimensions influences constraint and stress state, which have different impact of absorbed energy level. Therefore general correlation between energy values obtained with CVN specimen of different size or shape are not feasible.

The results are presented in a graph where the impact strength is in the y-axis and testing temperature in x-axis. Line is drawn through average impact strength values determined for set of tests in the same test temperature. The amount of ductile area of fracture surface is presented in the same way.

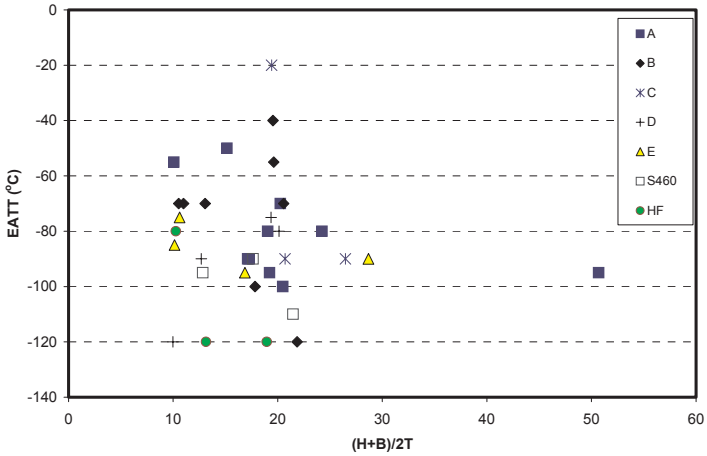

Figure 2-22. Transition temperatures corresponding 35 J/cm^2 fracture toughness requirement EATT (Energy Absorption Transition Temperature) as function of section slenderness (B+H)/2T.

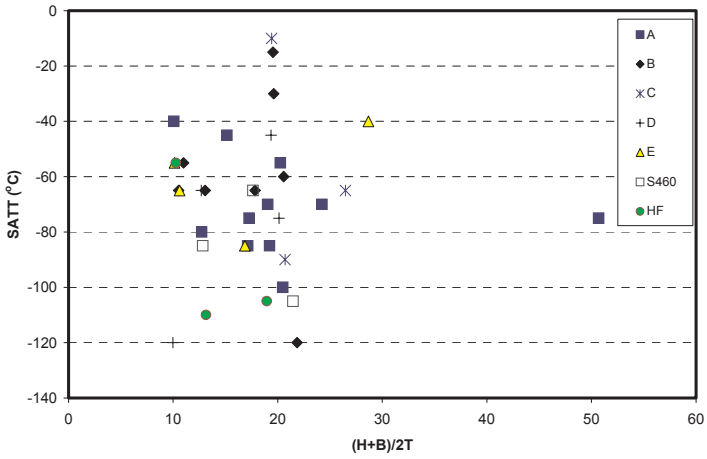

Figure 2-23. Transition temperatures corresponding 50% ductile area criteria SATT (Shear Appearance Transition Temperature) as function of section slenderness (B+H)/2T.

Conclusion drawn from the results:

- Requirement set in product standard EN 10219 is for 35 J/cm^2 for J0 at 0 ^{o}C temperature and for J2 at -20 ^{o}C temperature. EATT transition temperature fulfils these criteria clearly, when the CVN specimen are chosen from plane element with though thickness crack position.

3 Applicability of plastic design for CFSHS members and structures

3.1 Introduction

If the plastic design is utilised, it has to be ensured that the structure possesses enough deformation capacity. Thus, section ductility of members becomes an important requirement to ensure stability of the members at plastic hinge locations enabling the structure be able to carry further load through redistribution of internal forces.

Plastic design rests on the following assumptions:

- Each member section is able to reach the plastic moment level through plastic yielding of the entire cross section.
- The material possesses enough ductility so that large plastic strains can be accommodated without fracture.
- The section has sufficient ductility allowing rotation at relatively constant moment will occur through a considerable rotation.

Previous research has raised doubts about applicability of present plastic design rules for cold formed structural hollow sections (CFSHS). The argument has been that they do not satisfy the material ductility requirements of Eurocode 3, Part 1.1 (prEN 1993-1-1) or that they have not enough geometric ductility (ability to develop the needed large rotations keeping the plastic moment capacity). Recent studies published by Wilkinson and Wilkinson&Hancock [3-2, 3-3] support the latter conclusion. They found that a large number of sections currently classified in the cross-section class 1 did not meet rotation requirements for plastic design.

In this research project, the ductility of hollow sections in general and CFSHS in particular has been studied both numerically and experimentally. Test programme has been executed and extensive amount of numerical analyses have been done to extend the experimental results. The objective has been to find understanding of the parameters, which influence the rotation behaviour of hollow sections.

In chapter 3.2 ductility requirement for plastic design is proposed to be characterised by available inelastic rotation instead of rotation capacity even though there is connection between these two definitions. Experimental and numerical analyses has been carried out to describe different phenomena that have an effect on the ductility and rotation capacity.

In chapter 3.3 modifications are proposed to current cross-section classification of hollow sections of Eurocode 3, which considers the finding in chapter 3.2. In chapter 3.4 alternative design procedure for cross-section classification is given where the available rotation requirement is analysed structurally and compared to available inelastic rotation of members. The member performance may be analysed determined with experimentally verified analytical methods or numerically using calibrated FE simulation.

3.2 Ductility of hollow sections

3.2.1 Ductility of cross section defined by available inelastic rotation

The behaviour of a real beam is quite different from the assumption made in the plastic hinge theory. The moment-rotation diagram presents not only a curve shapes between the elastic and the plastic moment, but it also goes over the value of the plastic moment because of the strain hardening of steel.

The curve reaches a maximum, which corresponds to the maximum bearing capacity of the beam, and then, the moment must decrease because of local instability phenomena. Local buckling of compressed part of the section is the mechanism responsible for a change in the stress distribution giving rise to the resistance loss at that part. The fact of reaching the plastic moment corresponds to the full plastification of a cross-section, the formation of the plastic hinge. When the moment continues to increase, the plastic hinge rotates inelastically (Figure 3-1).

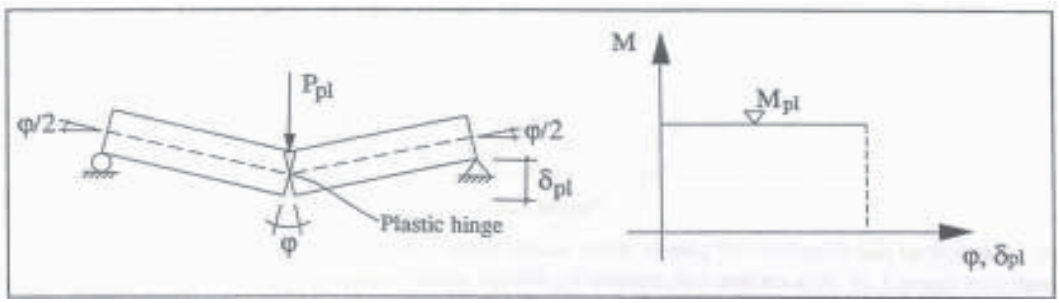

Figure 3-1. Idealised moment-rotation behaviour at plastic hinge.

Inelastic rotation, φ, can be defined as the parameter necessary to allow redistribution of bending moments M. Ductility of a cross section can be measured in terms of inelastic rotation at the moment of ultimate strength or inelastic rotation at the instant of falling below theoretical plastic moment resistance.

Available inelastic rotation, φ_{av}, is typically derived from the moment-rotation curve measured in the 3-point or 4-point bending tests and it is obtained from the descending branch of the curve at the moment of crossing down the plastic moment level (Figure 3-2).

The available inelastic rotation φ_{av} of the plastic hinge is clearly defined in the figure which presents a typical M-φ curve for a 3-point bending beam and can be expressed by the following formula:

$$\varphi_{av} = \varphi_{rot} - \varphi_{pl} \tag{3-1}$$

where:

φ_{rot} is the rotation corresponding to the bending moment as it reaches the plastic moment value (M_{pl}) in the descending part of the moment-rotation curve, expressed in radians and

φ_{pl} is the elastic rotation corresponding to the theoretical plastic bending moment (M_{pl}) of the beam, expressed in radians.

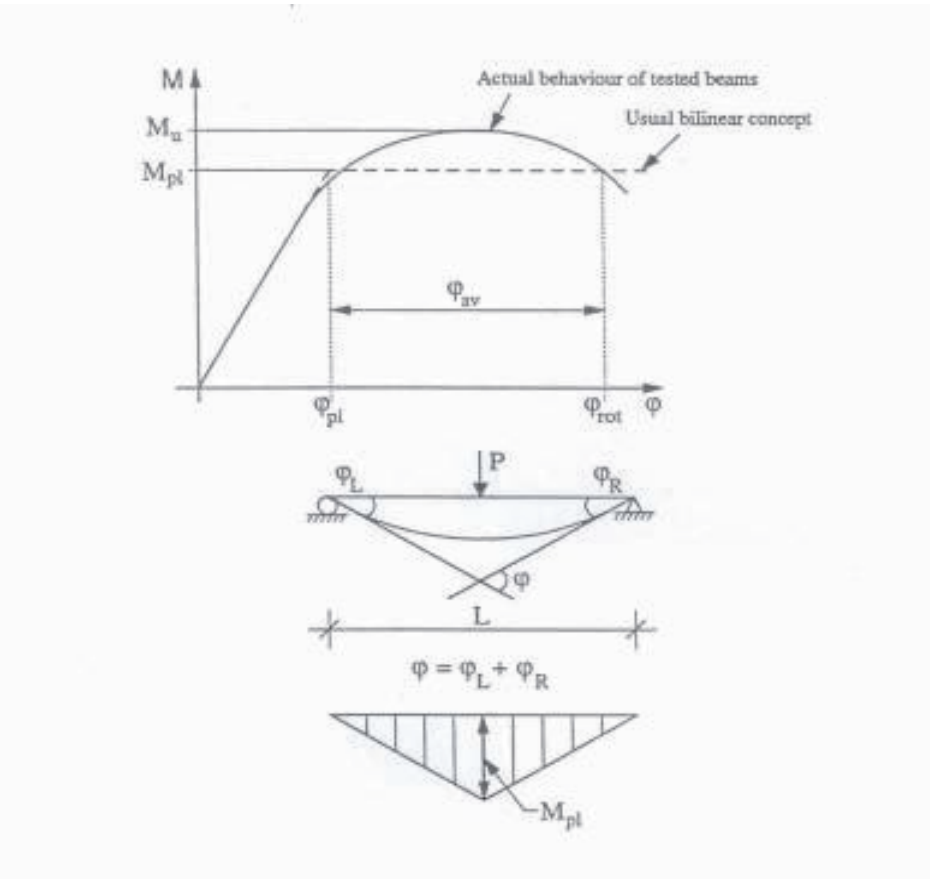

Figure 3-2. Concept of available rotation.

Rotation capacity, R, can be used as a ductility parameter. Available rotation capacity (R_{av}) is defined as the ratio between the available plastic rotation, φ_{av}, and a theoretical rotation, φ_{pl}, calculated at the plastic moment level.

$$R_{av} = \varphi_{av} / \varphi_{pl} \qquad (3\text{-}2)$$

with $\varphi_{pl} = M_{pl}\, L / 2\, E\, I$ (3-point bending test) or $\varphi_{pl} = M_{pl}\, (L+l) / 2\, E\, I$ (4-point bending test with a length l between loads).

In the same way, required rotation capacity, R_{req}, is defined as the ratio between the required inelastic rotation, φ_{req}, and the theoretical rotation, φ_{pl}.

"Rotation capacity" can be used instead of "inelastic rotation" to make the parameter dimensionless. The validity of plastic analysis can also be checked in the cross-sections by comparing rotation capacities although it is essential to compute both available and required rotation capacities with the same reference length to keep consistency.

The concept of rotation capacity introduces a supplementary parameter length L of a reference beam which describes structural parameter and not cross-sectional as also observed in previous ECSC funded project *Promotion of plastic design for steel and composite cross-sections* [3-4]. Available rotation capacity relates to a particular length while φ_{pl} depends also on the length of the beam, which may be difficult to identify.

Wilkinsson calculates a particular rotation capacity, R-value, in terms of curvatures instead of rotations by dividing inelastic curvature with the elastic one. Curvature (M_{pl} / EI) does not depend on any reference length thus leading to R values which can be considered as a cross-section property.

The simplest way to check ductility of plastic hinges is to compare directly structurally required and cross-sectionally available inelastic rotations φ instead of transforming rotations in rotation capacities R values. Design programmes may directly compute rotations instead of R parameters. The inelastic rotations are depends mainly on the dimensions of the cross-sections and the material properties of webs and flanges. In general, they do not depend on the span length except in those cases where insufficient lateral restraints may cause lateral or lateral-torsional buckling coupled with local buckling. In the rotation capacity R the span length is also included, while it is a function of φ_{pl}. ($\varphi_{pl}=M_{pl}(L+l)/2EI$, for 4 point bending beam with span length L and distance between loads l).

This approach is proposed also in "Background document 5.09 for chapter 5 of EN 1993-1-1 on b/t ratios" by Sedlacek and Feldmann [3-5]. The paragraph (14) states: "*..The conclusions for the present EN 1993-1-1 rules are as follows: the presentation of the available rotation capacities terms of angles ("phi-values") gives more information on the actual inelastic behaviour rather than the presentation in terms of nondimensional "R-values" which is the comparison of the rotation of inelastic deformation of the plastic hinge and the elastic deformation of the beam*".

In conclusion:

- The available inelastic rotation describes with φ_{av} is a proper parameter to characterise the deformation capacity of a cross-section under bending. φ_{av} can be considered as a cross-section property while it depends on the yielding and local buckling which are determined by geometrical and material properties of the section.

- Available rotation capacity defined as the ratio between the available inelastic rotation, φ_{av}, and a theoretical rotation, φ_{pl}, is a function of the total span length of the beam. Also the total rotation φ_{rot} is function of the total length since the elastic part of rotation is included in it which is distributed along all the member length.

- Available inelastic rotation (φ_{av}), as measured in a 4-point bending test, comprises a component distributed along the constant-moment central region of the beam and a component concentrated at the plastic hinge zone. Only this second component of the available inelastic rotation can be considered to be a characteristic cross-sectional parameter. The distributed part depends on the distance between loads so it cannot be considered as a cross-section parameter.

3.2.3 Influence of load type and moment gradient

The influence of the type of loading on the available rotation was assessed with FE simulation. Four point bending tests are mostly used for evaluating rotation capacity of hollow sections. Once bending progresses beyond the elastic region, inelastic deformation concentrates in the plastic hinge appearing at the constant moment central region of the beam. Available rotation at the hinges is measured by monitoring rotation values at both ends. In this study, the distance between loads for the 4-point bending test was the key parameter to investigate.

When the rotation is expressed, in the usual way, by the sum of angles measured at both support ends a general trend is observed: the larger the distance between loads is the higher inelastic rotations and lower maximum moments are obtained.

The observation of the deformation patterns obtained for every case provides additional insight on the apparent reduction of deformation capacity when increasing the length of the constant-moment region. The analysis of the deformed shapes allows differentiating three kind of deformation for every case:

1. Elastic deformation: it is distributed along the full span length of the beam.

2. Distributed plastic deformation: it develops in a uniformly distributed manner along the constant-moment region.

3. Localised plastic deformation: it is concentrated in the plastic hinge.

Thus, the available inelastic rotation can be divided in two components depending on the origin of the deformation: the first one, the distributed inelastic rotation, distributed along the constant-moment region and a second part, the concentrated inelastic rotation, which is developed in the plastic hinge itself. This latter part of inelastic rotation does depend on either the total span length or the length between loads. This concentrated part of the inelastic rotation is the responsible for the decreasing of the moment below the plastic moment level due to local buckling developing in the plastic hinge area.

However, the distributed part of inelastic rotation depends on the distance between loads, where the bending moment is constant. The longer this region is the higher distributed component of inelastic rotation appears. Therefore the total inelastic rotation depends clearly on the distance between loads.

The deformation patterns in Figure 3-3 show very clearly an increasing role of the distributed component of inelastic rotation when increasing the distance between loads. The case with larger length between loads (upper picture in Figure 3-3) shows a fully distributed inelastic rotation: the plastic hinge has not appearing. However, the case with shorter length between loads (lower picture in Figure 3-3) presents an inelastic deformation almost completely dominated by the concentrated rotation at the plastic hinge area.

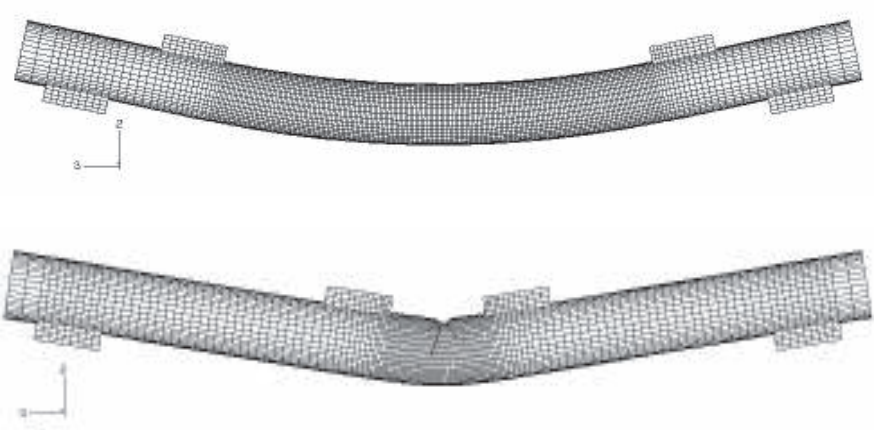

Figure 3-3. Effect of distance between loading point to the deformation pattern.

Figure 3-4 shows the plastic buckling deformation at the hinge location after the maximum of the bending moment for two cases with different distances between loads, l=1000 mm and l=400 mm.

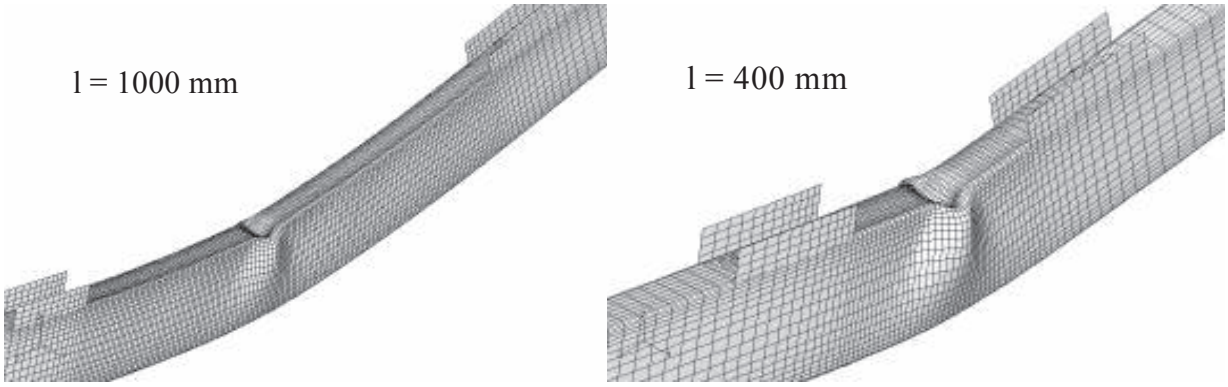

Figure 3-4. Plastic buckling deformation at hinge locations when length between loading point is varied.

Figure 3-5 shows how the distance between loads alters the moment-rotation curve. On the left are moment rotation curves where the rotation is from the ends of the beam and on the right the rotation is at the plastic hinge. The moment-rotation curve on the right shows that the concentrated component of available inelastic rotation is not significantly affected by the length between loads.

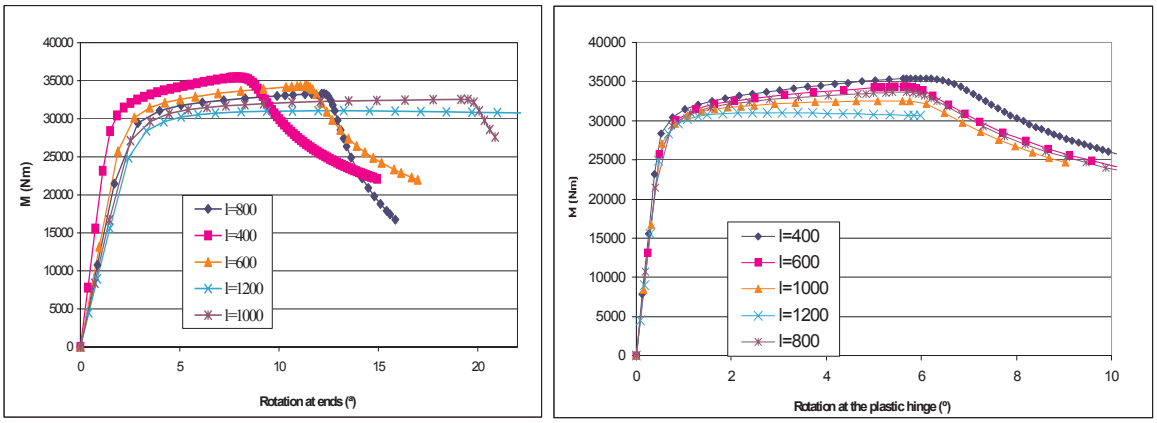

Figure 3-5. Effect of distance between loading points to different rotations: on the left at ends and on the right at the plastic hinge.

Thus, the following conclusions may be drawn:

- Available rotation capacity defined as the ratio between the available inelastic rotation, φ_{av}, and a theoretical elastic rotation, φ_{pl}, depends on the total span length of the beam. Also the total rotation φ_{rot} is dependent on the total length since it includes the elastic part of rotation which is distributed along the member length.

- Available inelastic rotation (φ_{av}), as measured in a 4-point bending test, comprises a component distributed along the constant-moment central region of the beam and a component concentrated at the plastic hinge zone. Only this second component of the available inelastic rotation can be considered to be a characteristic cross-sectional parameter. The distributed part depends on the distance between loads.

- As a consequence, the 4-point bending test must be designed so that the distance between loads is not much larger than the expected size for the plastic hinge. Then the contribution of the distributed part of deformation to the inelastic rotation is minimised.

3.2.4 Influence of plate slenderness and aspect ratio – Experimental and numerical verification

3.2.4.2 Experimental verification

Test programme (Table 3-1) was executed to verify performance of hollow sections. Most of the sections chosen to it were cold formed but some hot formed were included as reference to compared differences caused by manufacturing methods.

The bending tests provided also insight about the influence of web and flange slenderness on the section ductility. Some of specimens were selected to fall in the surroundings of boundary between cross-section class 1 and 2.

Table 3-1. Section sizes in the test programme.

	Section	Material	H (mm)	B (mm)	T (mm)	R (mm)	Flat f_y (N/mm^2)	Corn f_y (N/mm^2)	length (mm)
1	**200x100x12.5**	S355J2H	200	100	12.5	37.5	364	474	2800
2	**100x100x10**	S355J2H	100	100	10	25	357	447	2500
3	**120x60x6**	S355J0H	120	60	6	12	408	472	2800
4	**100x100x8**	S355J0H	100	100	8	16	360	414	2800
5	**200x200x8**	S355J2H	200	200	8	20	361	414	2800
6	**300x200x8**	S355J2H	300	200	8	20	361	414	2800
7	**400x200x8**	S355J2H	400	200	8	20	361	414	2800
8	**120x80x3**	S355J2H	120	80	3	6	371	474	2800
9	**200x200x7**	S355J0H	200	200	7	14	408	472	1800
10	**150x150x5**	S355J2H	150	150	5	10	352	448	2800
11	**250x150x5**	S355J2H	250	150	5	10	404	515	2800
12	**100x100x6**	S355J2H	100	100	6	12	398	472	2800
13	**200x100x4**	S355J2H	200	100	4	8	385	442	2800
14	**200x100x8**	S355J2H	200	100	8	16	361	414	2800
15	**100x150x3**	S355J2H	100	150	3	6	371	474	2800
16	**150x100x4**	S355J2H	150	100	4	8	378	438	2800
17	**100x200x4**	S355J2H	100	200	4	8	385	442	1800
18	**70x70x3**	S355J2H	70	70	3	6	371	474	1800
19	**70x70x5**	S355J2H	70	70	5	10	357	458	1800
20	**100x100x5**	S355J2H	100	100	5	10	360	448	1800
21	**HF 100x100x8**	S355J0H	100	100	8	16	383	479	1800
22	**HF 150x150x5**	S355J2H	150	150	5	10	404	515	2800
23	**HF 250x150x5**	S355J2H	250	150	5	10	431	515	2800

Four-point bending loading arrangement has been adopted, where the load is transferred to the web through suitable web reinforcement, as much as possible independent on the upper flange of the section. A system of hinges and sliding plates, where the friction is minimised using couples of teflon sheets, allowed fulfilling at the best the theoretical conditions. The tests were carried out under displacement control. Displacements were measured using inductive transducers from in the seven sections, while the loads were measured through a load cell (Figure 3-6).

Plastic hinge rotations are evaluated as sum of the rotations of sections No. 3 and No. 5, deduced considering differences in measured displacements in sections No. 3 / No. 2 and No. 5 / No. 6, (Figure 3-7). Of course, as actual rotations in sections No. 3 and No. 5 are smaller than actual rotations in sections No. 2 and No. 6, this method overestimates rotations in the elastic range, but the errors becomes smaller as plastic hinge develops.

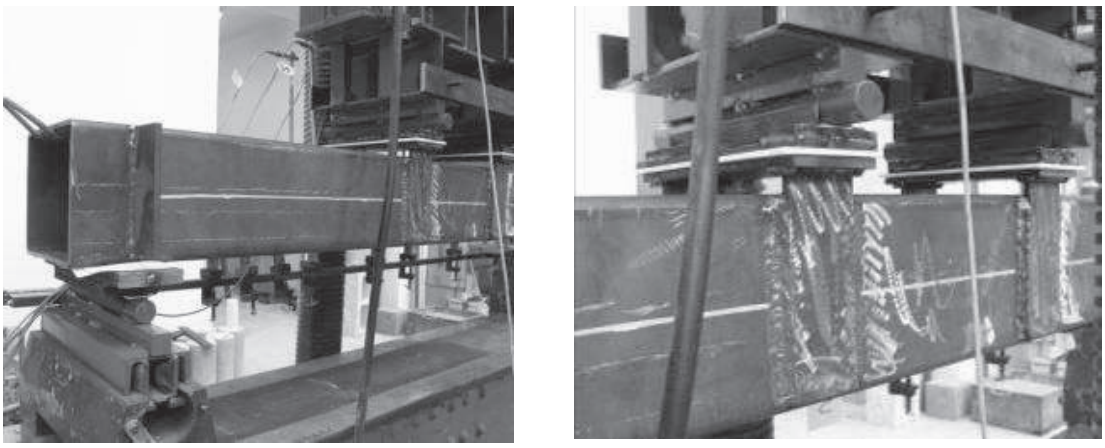

Figure 3-6. Test arrangement detail at the support and on the loading position.

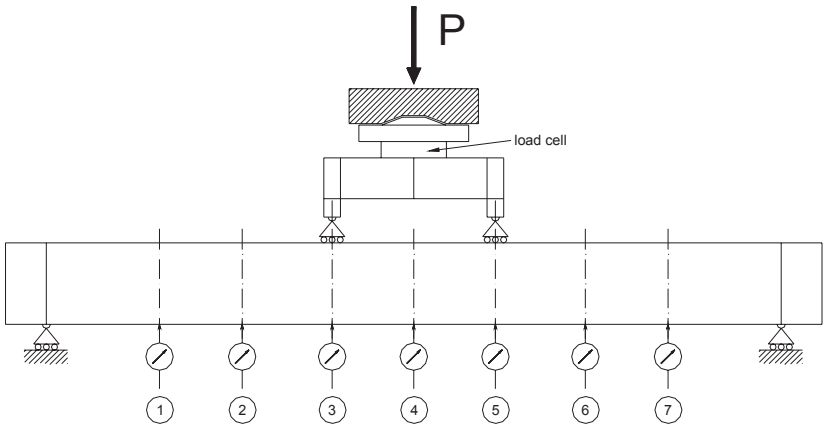

Figure 3-7. Location of displacement transducers in bending tests.

Table 3-2 summarises the results for tested specimen. The available inelastic rotation and maximum moment obtained from the measured moment-rotation curves are given. Figure 3-8 shows the measured available rotations as a function of slenderness ratios. Figure 3-9 show example of moment rotation curves for section size 150x150x5.

In Table 3-2 following values are given:

$\varphi_{av,nom}$ represents the available inelastic rotation at nominal M_p value (M_p is determined with f_y=355 MPa);

$\varphi_{avflange}$ represents the available inelastic rotation at the M_{pfl} value (M_{pfl} is determined with the actual f_y values for the flange);

$\varphi_{av,true}$ represents the available inelastic rotation at the M_{ptrue} value (M_{ptrue} is determined with the actual f_y values for flanges and corner areas);

R represents the rotation capacity at nominal M_p value (M_p is determined with f_y=355 MPa);

R_{flange} represents the rotation capacity at the M_{pfl} value (M_{pfl} is determined with the actual f_y values for the flange);

R_{true} represents the rotation capacity at the M_{ptrue} value (M_{ptrue} is determined with the actual f_y values for flanges and corner areas).

Table 3-2. Actual slenderness rations of tested sections. Maximum bending moment and available rotation obtained from the tests.

	SECTION	λ_{web}	λ_{flange}	M_{max} [kNm]	$\varphi_{av,nom}$ [deg]	$\varphi_{av,flange}$ [deg]	$\varphi_{av,true}$ [deg]	R_{nom}	R_{flange}	R_{true}
1	200x200x7	32.58	32.54	205	5.1	4.1	4.0	11.2	6.6	6.3
2	100x100x8 (HF)	10.94	10.97	40	> 15	> 15	> 15	>20	>20	>20
3	100x100x8	10.62	10.61	59	> 15	> 15	> 15	>20	>20	>20
4	200x100x12.5	12.14	2.27	215	>15	> 15	> 15	>20	>20	>20
5	100x100x10	7.00	6.97	56	>15	> 15	> 15	19.3	>15	>15
6	300x200x8	41.53	25.95	398	4.1	4.0	3.8	7.9	7.5	6.8
7	300x200x8	41.31	25.82	385	3.4	3.3	3.2	9.3	9.9	9.1
8	400x200x8	57.49	26.10	575	2.3	2.1	2.0	7.0	6.4	5.9
9	200x100x4	58.77	26.83	75	3.1	2.8	2.3	5.4	4.5	3.3
21	200x100x4	58.26	26.86	70	2.1	1.5	1.4	4.2	2.6	2.4
10	120x60x6	22.29	8.37	47	> 15	> 15	> 15	>20	>20	>20
11	120x80x3	45.05	28.28	20.5	2.2	2.0	1.9	1.9	1.6	1.5
12	120x80x3	45.00	28.20	22	3.1	2.8	2.6	3.1	2.7	2.4
13	120x80x3	45.05	28.20	21.5	2.6	2.2	1.9	3.0	2.4	2.0
14	150x150x5	33.09	33.09	75	5.8	5.9	5.5	6.3	6.8	6.0
15	150x150x5 (HF)	33.79	33.82	67	5.2	2.6	2.1	8.4	3.1	2.4
16	150x150x5 (HF)	34.56	34.51	67	3.8	1.6	1.2	4.4	1.6	1.2
17	200x200x8	25.68	25.65	210	6.2	6.0	5.9	12.1	11.5	11.0
18	100x100x6	14.76	14.74	42	> 15	> 15	> 15	>20	>20	>20
19	250x150x5	61.15	34.35	147	2.0	1.2	1.1	3.2	1.5	1.3
20	250x150x5 (HF)	59.44	33.43	156	2.5	1.2	1.1	6.6	2.4	2.4
22	200x100x8	27.82	12.36	175	>10	>10	>10	18.4	>15	>15
23	100x150x3	35.94	56.14	21	0.9	0.0	-	0.6	-	-
24	150x100x4	41.39	26.20	40	2.4	1.9	1.6	1.8	1.3	0.9
25	100x200x4	26.57	58.33	35	1.4	-.	-	0.8	-	-
26	70x70x3	23.81	23.86	10	8.6	8.1	7.3	5.9	5.4	4.8
27	100x100x5	25.93	26.04	27	6.9	6.7	5.5	6.0	5.7	4.0
28	70x70x5	12.36	12.32	16	>10	>10	>10	>9	>9	>9

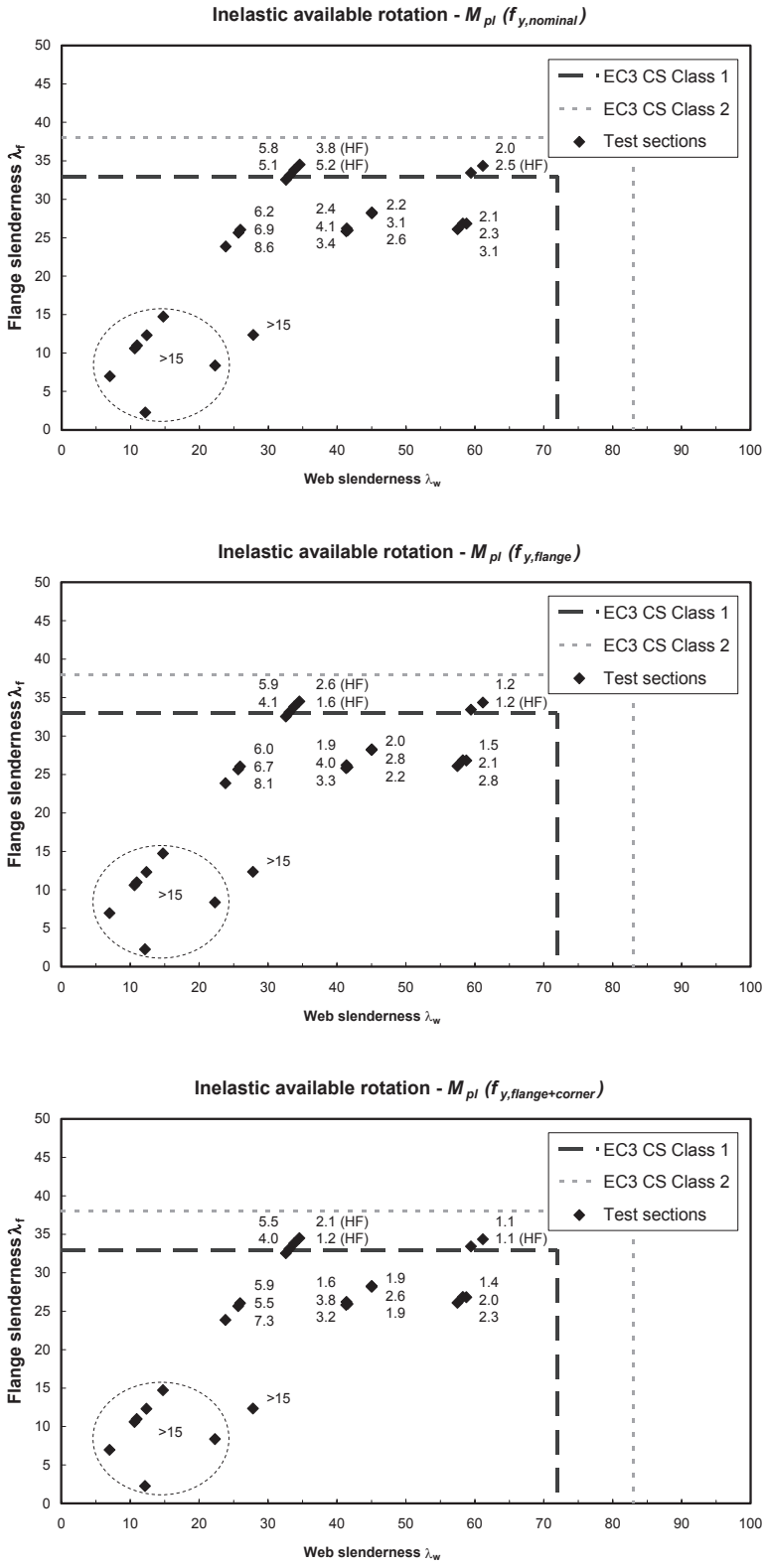

Figure 3-8. Experimentally determined available inelastic rotation (degrees) in flange/web slenderness charts. Sections are classified using actual flange and web slenderness calculated with true cross-sectional dimensions and flange material strengths. The available rotations are determined corresponding plastic moment level based on nominal yield strength, measured yield strength from flange and actual where increased yield strength on corners in included.

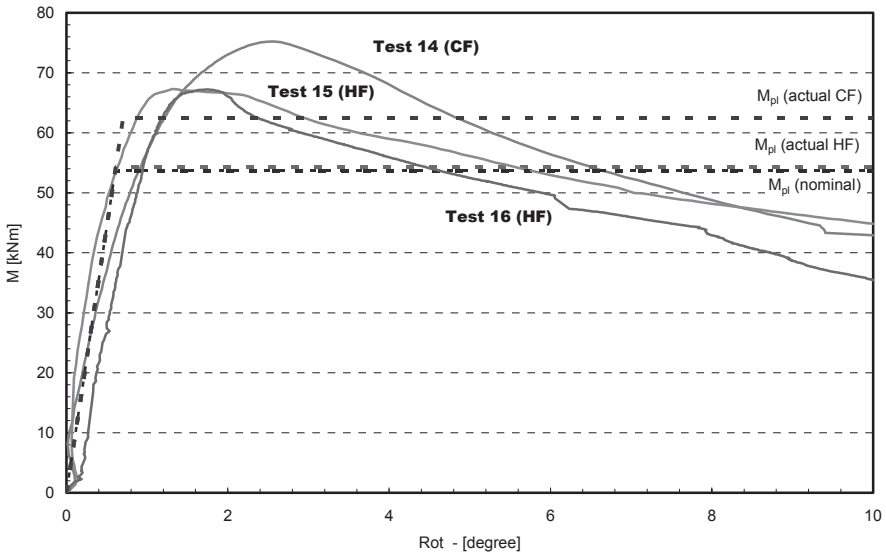

Figure 3-9. Moment rotation curves for section size 150x150x5. Three sections were tested – cold-formed and two hot-formed.

3.2.4.1 Numerical analysis

The influence of web and flange slenderness on the ductility of hollow sections was evaluated using FE simulations. The simulation programme comprises 24 section sizes selected in a slenderness range corresponding to the limit between cross section class 1 and class 2 (Figure 3-10) since this is the relevant area regarding usability of hollow sections for plastic analysis. To obtain moment-rotation curve each case was analysed numerically using nonlinear FE analyses where both geometrical and material non-linearities were included. The characteristics of CFSHS were considered by using different material properties for flat and corner part of hollow sections in the models.

The geometrical non-linearity was initiated with initial imperfection. Three types of initial imperfections were considered for each section:

a) Local buckling: maximum magnitude of 0.1% of the flange width;

b) Local buckling: maximum magnitude of 1% of the flange width and

c) web bow-out and flange bow-in: maximum magnitude of 1/500 the plate width.

Thus, a total number of 72 numerical tests were performed. Table 3-3 summarizes the results in terms of calculated available inelastic rotations.

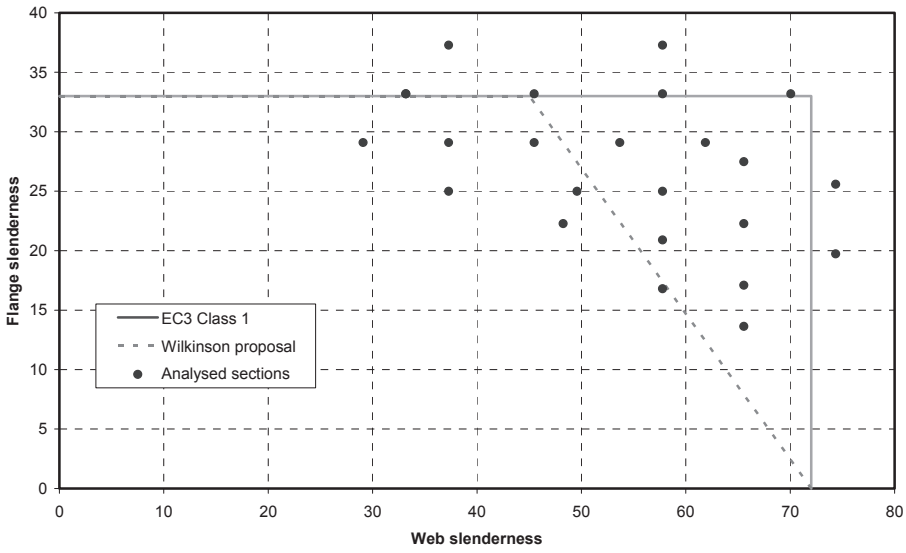

Figure 3-10. Sections chosen for the numerical simulations. EC3 Class 1 line shows current slenderness limit for cross section class 1. Wilkinson proposal as updated limit for cross-section class 1 is obtained from [3-3, 3-4].

Table 3-3. Available rotation values obtained from numerically determined moment rotation curves. For comparison analysed cases are calculated with two calculation models: Kecman and Kubo.

	φ_{AV} (deg)				
	FEM			Kecman model	Kubo model
Section	i.i. 1%b	i.i. 0.1%b	i.i. bow		
80x80x3	1.26	2.32	3.54	2.56	2.78
100x80x3	1.02	2.13	4.33	1.86	2.06
120x80x3	0.74	1.83	3.42	1.40	1.53
140x80x3	0.43	1.45	3.01	1.06	1.12
160x80x3	0.00	1.20	2.40	0.79	0.79
150x150x 5	0.74	1.56	2.40	1.62	2.03
200x150x5	0.42	1.19	2.39	0.91	1.22
250x150x5	0.00	1.01	2.03	0.48	0.67
300x150x5	0.00	0.73	1.49	0.18	0.26
400x100x7.1	0.98	2.31	4.15	3.21	2.42
400x120x7.1	0.82	2.02	4.00	2.57	1.86
400x150x7.1	0.52	1.58	2.92	1.65	1.24
400x180x7.1	0.00	1.14	2.36	0.92	0.78
300x100x6	1.08	2.81	5.64	2.98	2.26
300x 120x6	0.73	2.38	4.38	2.15	1.72
100x100x3	0.00	0.95	1.52	0.96	1.42
150x100x3	0.00	0.62	1.40	0.23	0.43
150x70x3	0.49	1.80	3.61	1.46	1.29
100x70x3	1.33	3.13	6.22	2.55	2.48
400x120x6.3	0.39	1.18	2.28	1.72	1.20
400x150x6.3	0.00	1.00	1.84	0.90	0.65
300x300x10	0.63	1.37	1.90	1.70	2.03
260x140x6	0.72	2.30	4.63	1.81	1.68
300x150x7.1	0.96	2.98	5.67	2.46	2.05

The rotation values predicted by simplified calculation models of Kecman [3-11, 3-12] and Kubo-type [3-13] are also included for comparison purposes (see section 3.4.3 of this report where these models are described and their accuracy verified against test database). A reasonably satisfactory correlation is obtained for the imperfection level equal to 0.1% of the flange width, as it is shown in Figure 3-11 for both models.

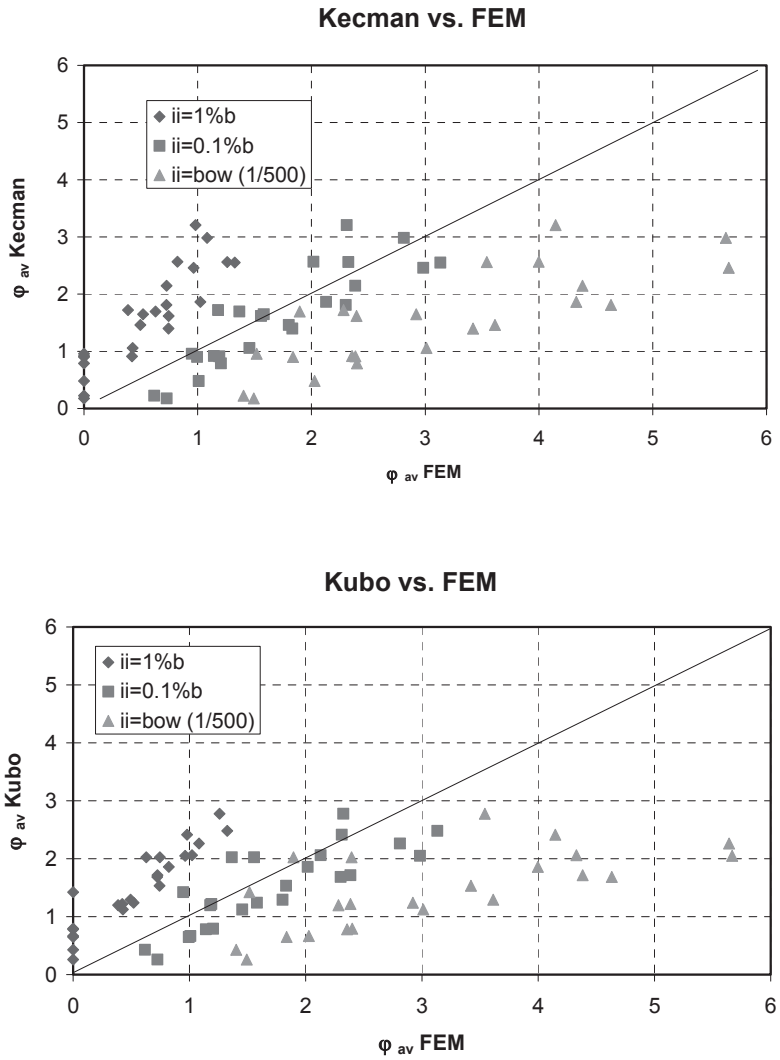

Figure 3-11. Comparison between results from numerical FE analyses and simplified calculation models: On the top Kecman-model and on the bottom Kubo–model. In the vertical axis are the values from simplified models and in the horizontal axis values from FE analyses.

Following conclusions can be drawn:

- Available inelastic rotation seems to depend on both web and flange slenderness ratios. Interaction between web and flange slenderness can be noted.

- The maximum moment and the inelastic rotation up to the maximum moment depend essentially on the flange slenderness. Figure 3-12, upper case, shows the resulting moment-rotation curves for a series of five sections with the same web slenderness. It is observed that flange slenderness determines how far the curve goes before reaching the maximum load. However, slope of descendent part of the curve does not seem to be substantially affected by the change in flange slenderness. The lower case of Figure 3-12 shows the resulting moment-rotation curves for a series of five sections with the same flange slenderness: in this case the curves are very similar up to the maximum moment. Afterwards, and in contrast to the preceding behaviour, the slope of descending part appears to depend heavily on the web slenderness.

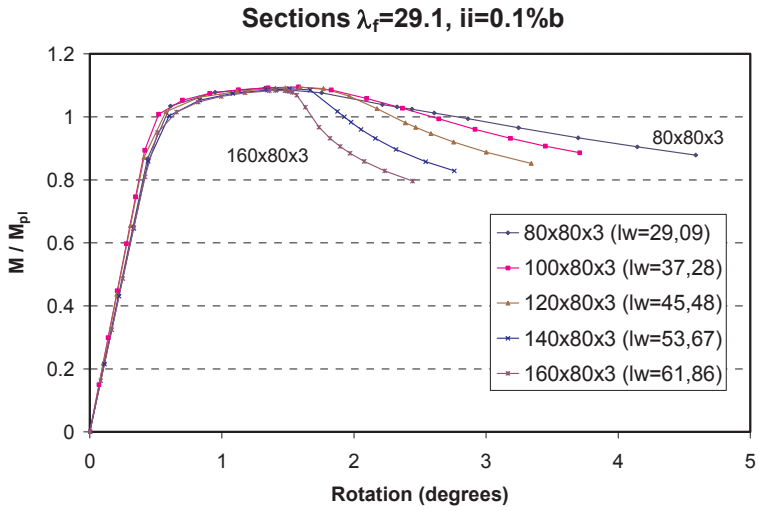

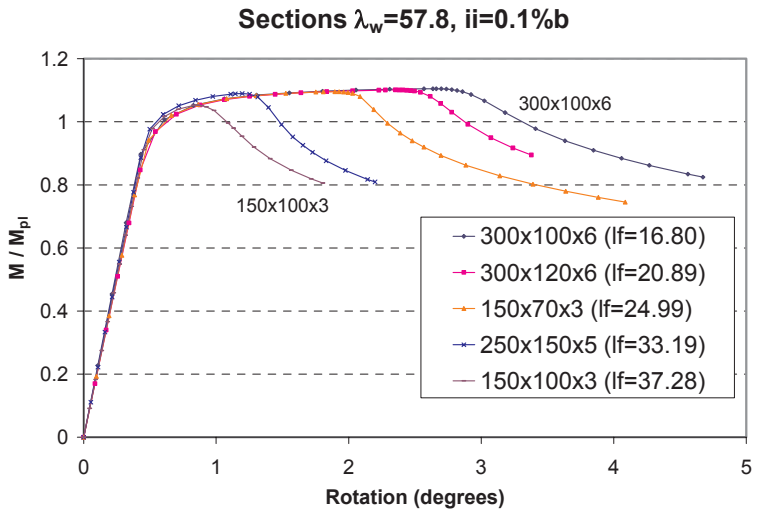

Figure 3-12. On the top, effect of web slenderness on the moment rotation behaviour with constant flange slenderness. On the bottom, effect of flange slenderness with constant web slenderness.

The reason behind that is that behaviour up to the maximum of the moment seems to be determined by the initiation of local flange buckling so that flange slenderness is the key parameter influencing the moment rotation curve before it reaches the maximum load. A very limited influence of web slenderness is observed provided that flange slenderness is in the range next to cross-section class 2 limit.

Descendent slope of moment rotation curve after the maximum of the moment depends mainly on the web slenderness with a limited influence of flange slenderness when next or above cross-section class 2 limit. However, behaviour after the maximum load seems to be determined by the interactive coupling of local web buckling accompanying the primer flange buckling.

Figure 3-13 shows the resulting inelastic rotation as function of the web slenderness with constant flange slenderness (the upper case) and as function of flange slenderness with constant web slenderness (the lower case). In both graphs, results for the three imperfection levels considered in the study are included.

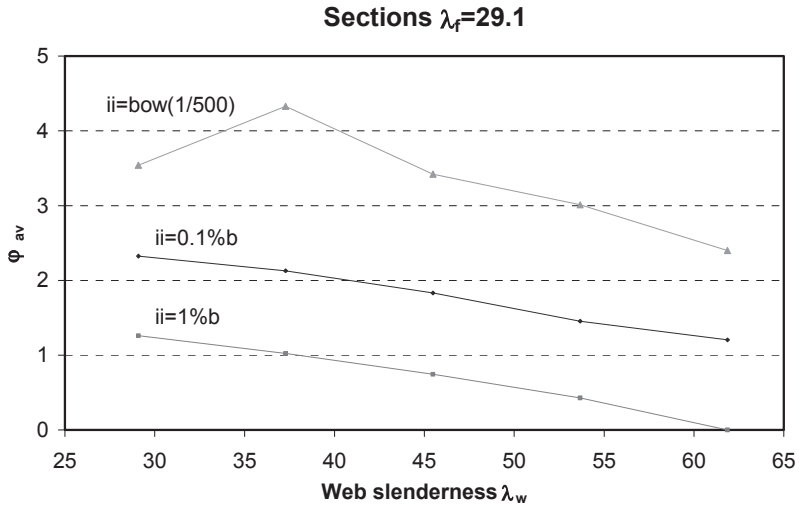

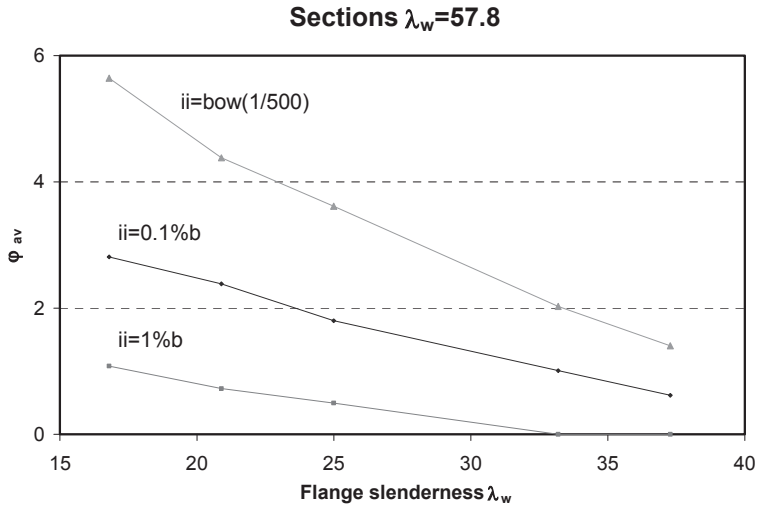

Figure 3-13. Available inelastic rotation values obtained from parametric analysis programme. On the top the flange slenderness is constant and on the bottom the web slenderness.

Aiming at assessing the interactive influence of flange and web slenderness (λ_f and λ_w) on the ductility, results from the parametrical study have been processed to provide the shape of iso-rotation curves when representing the available rotation values in terms of both, flange and web slenderness. These iso-rotation curves indicate combinations of λ_f and λ_w giving the same available rotation. Parabolic polynomial regression over the results of numerical experimentation is used to find iso-rotation curves (Figures 3-14, 3-15 and 3-16). The current limit for cross section class 1 and modification proposal by Wilkinson are shown in the figures.

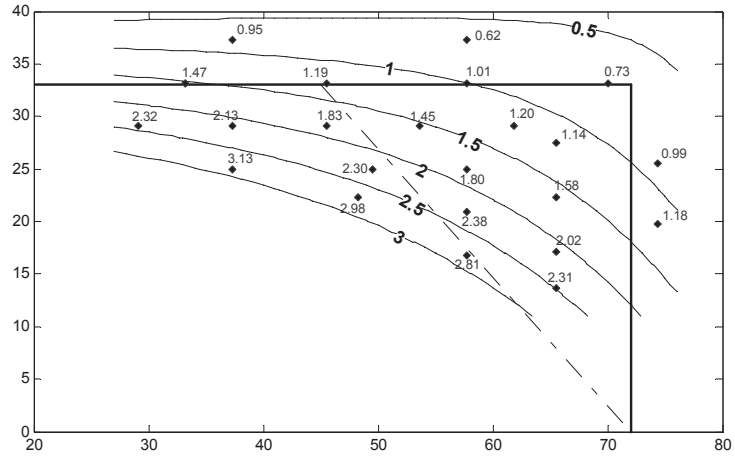

Figure 3-14. Initial imperfection in analysis local buckling: maximum magnitude of 0.1% of the flange width.

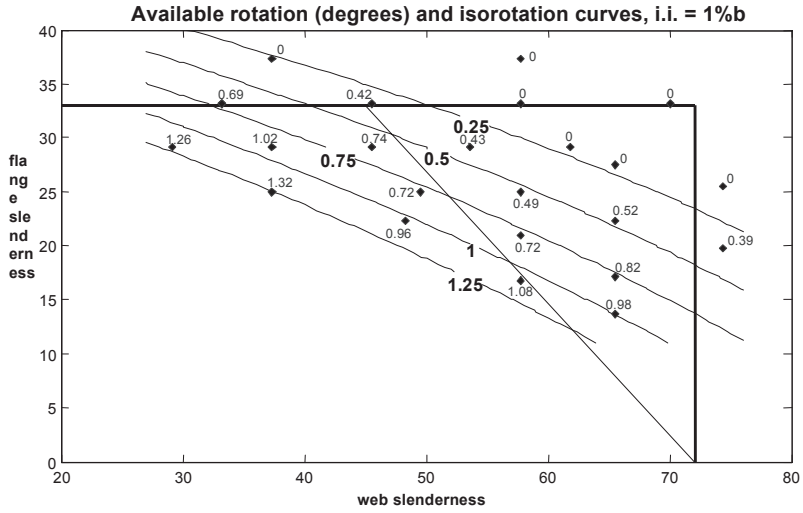

Figure 3-15. Initial imperfection in analysis local buckling: maximum magnitude of 1% of the flange width.

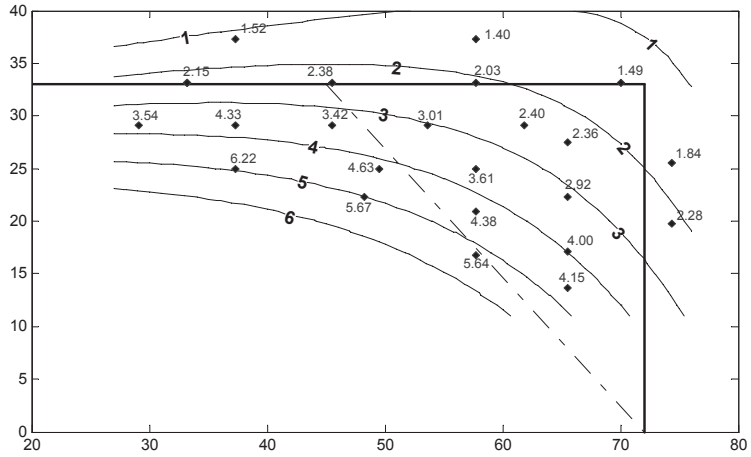

Figure 3-16. Initial imperfection in analysis web bow-out and flange bow-in: maximum magnitude of 1/500 the plate width.

3.2.5 Influence of manufacturing method

Figures 3-9 for section size 150x150x5 and Figure 3-17 for section 250x150x5 show comparison of moment rotation curves from tests to cold formed and hot formed section of same size. The characteristics in the shape of curves are similar thus the level of maximum moment deviates while the material strengths are different. The level of available inelastic rotation is also of same magnitude. It seems, that manufacturing method does not have major influence on the performance of sections, when plastic buckling occurs.

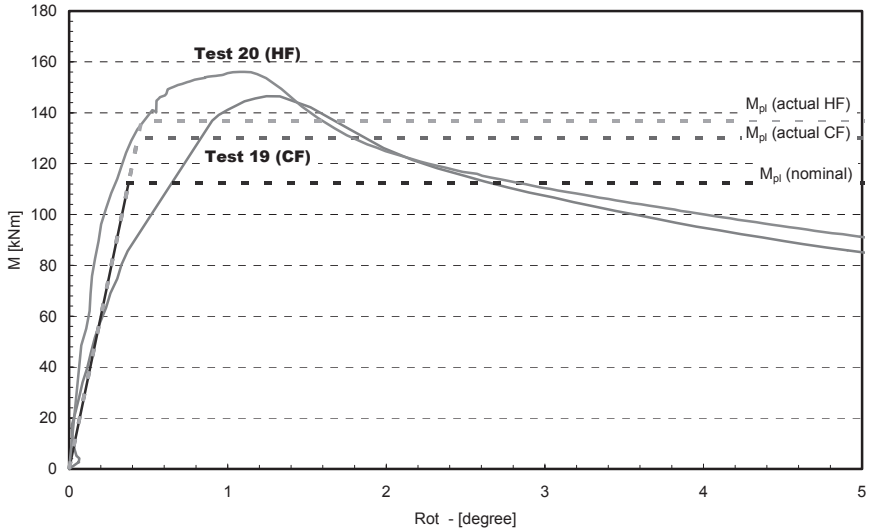

Figure 3-17. Comparison of moment-rotation curves for hot-formed and cold-formed hollow sections of same section size 250x150x5.

3.2.6 Required inelastic rotation at the structural level

A parametrical study has been carried out to assess the required inelastic rotations at the structural level. The evaluation has been performed by virtual testing carried out by both, matrix structural analysis and finite element analysis on structural systems composed of continuous beams (2 and 3 span) and portal frames.

Two types of analyses are dealt with in this study: elastic-perfectly plastic (EP), and plastic-zone analysis (PZ). The elastic-perfectly-plastic analyses are performed using the matrix structural analysis program, MASTAN that allows for plastic analysis including second order effects. The plastic-zone analysis is performed via finite element analysis using COSMOS program.

For the continuous beams under the Ultimate Limit State a vertical uniform load is applied incrementally until the collapse mechanism is reached. The Serviceability Limit State is also checked to consider the worst possible scenario. The deflection limits are set equal to L/200 for the vertical displacement and H/150 for the horizontal displacement.

In the case of portal frames also Limit States, Ultimate and Serviceability, are considered. The types of actions taken into account are a uniform vertical load, to account for the dead load and snow, and a horizontal load that accounts for the wind effect. Again, these loads are applied incrementally and proportionally until the collapse mechanism is reached. The deflection limits are set equal to L/200 for the vertical displacement and H/150 for the horizontal displacement.

For the two and three span continuous beams uniformly, the first plastic hinges are formed at the internal supports; the subsequent ones are formed within the external spans, thus yielding the collapse mechanism. Consequently, the first hinge undergoes the largest inelastic rotation, which will reach a

maximum at the time of collapse. For long spans the vertical deflections become large enough for the Serviceability Limit State to control the performance of the structure. If a plastic hinge is already formed then the rotation is measured at the time when the allowable displacement is reached.

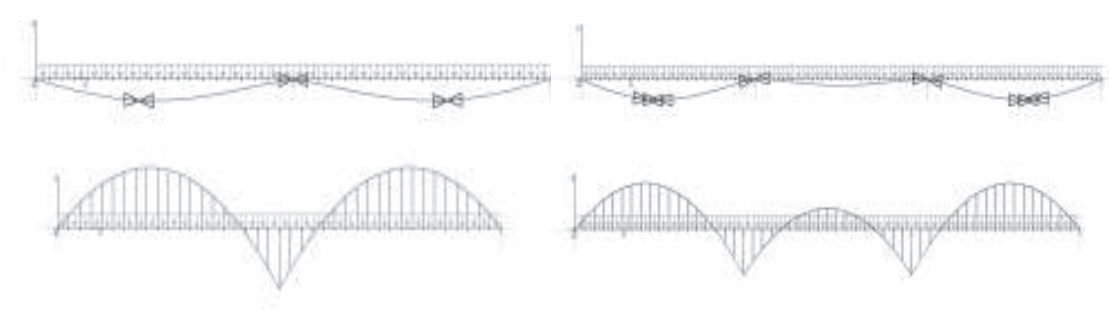

Figure 3-18. Two and three span continuous beam. Collapse mechanisms and bending moments.

Table 3-4 below illustrates the results obtained using the EP analysis for different lengths of two and three span continuous beams. The darker shaded area indicates that Ultimate Limit State is limiting the performance of the structure. The lighter shaded area indicates that Serviceability Limit State is controlling the performance. The non-shaded area corresponds to the cases when the allowable displacement is reached before any plastic hinge is formed. Maximum rotation demand predicted by the elastic-plastic (EP) and plastic-zone (PZ) methods have shown to be quite similar, although the more accurate PZ method predicts a larger ultimate load.

Table 3-4. Rotations corresponding to plastic hinges are given. Darker shaded are cases where ULS is limiting and lighter shaded were SLS.

	2 Span			
Section Type	3 m	4 m	5 m	6 m
#100.5	1.449	0.103	0.000	0.000
#120.6	1.822	1.065	0.000	0.000
#160.5	1.335	1.781	1.581	0.338
#200.8	1.082	1.443	1.776	1.724

	3 Span			
Section Type	3 m	3.6 m	4 m	5 m
#100.5	0.000	0.000	0.000	0.000
#120.6	0.000	0.000	0.000	0.000
#160.5	0.607	0.509	0.022	0.000
#200.8	0.492	0.578	0.647	0.080

The maximum rotation required for plastic analysis is below 2 for two span beams. Three span beams require rotations below 1 degree. A similar trend is expected for four and five span continuous beams.

A typical portal frame built with structural hollow sections has also been considered. The first plastic hinge is formed at the intersection between the girder and the column and consequently will undergo the largest rotation, which will reach a maximum at the time of collapse. For long spans the vertical deflections and for high frames the horizontal deflections become large enough for the Serviceability Limit State to limit the rotations. If plastic hinges are already formed then the rotation is measured at the time when the allowable displacement is reached.

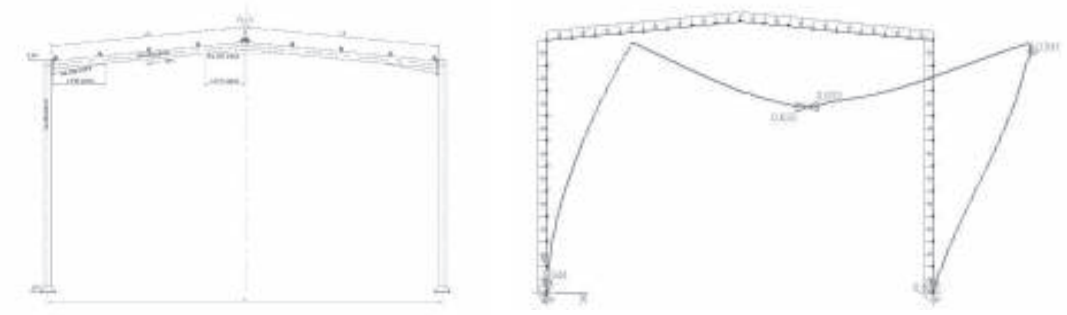

Figure 3-19. Portal frame. Collapse mechanism.

In the same way as before, Table 3-5 below illustrates the results obtained using EP method for different lengths and heights of portal frames. The notation (r) means that the limiting factor is the plastic rotation under U.L.S.; (v) and (h) mean that the limiting factor has been the vertical or horizontal displacement, respectively, under S.L.S. The plastic zone method tends to predict slightly larger inelastic rotations and ultimate loads than the elastic-plastic method.

Table 3-5. Rotations corresponding to plastic hinges are given. Darker shaded are cases where ULS is limiting and lighter shaded were SLS.

Height	Section Type	Span				
		10 m	12 m	15 m	18 m	20 m
6 m	#300.200.8	0.74 (h)	0.83 (v)	0.00 (v)	0.00 (v)	0.00 (v)
	#400.200.8	2.46 (r)	2.35 (r)	1.07 (v)	0.86 (v)	0.67 (v)
8 m	#300.200.8	0.00 (h)	0.00 (h)	0.00 (v)	0.00 (v)	0.00 (v)
	#400.200.8	0.00 (h)	0.44 (h)	0.76 (v)	0.63 (v)	0.00 (v)
10 m	#300.200.8	0.00 (h)	0.00 (h)	0.00 (h)	0.00 (h)	0.00 (v)
	#400.200.8	0.00 (h)	0.00 (h)	0.00 (h)	0.00 (v)	0.00 (v)

Conclusions regarding the required inelastic rotation in standard structural systems, derived from this study are the following:

- Although the structural systems may undertake substantial plastic deformation prior to the collapse mechanism, in practice the Serviceability Limit State, which imposes limitations on the displacements, limits the required plastic rotations.

- The maximum rotation angle measured in continuous beams is of the order of 2º (0.035 radians). In cases of large spans the deflections imposed by the Serviceability Limit State constitute the limiting factor, and no plastic hinges are formed.

- In the case of portal frames the plastic hinges may undergo rotations of up to 3º (0.05 radians).

3.2.2 Influence of lateral restraints

The influence of lateral restraints in the deformation capacity of hollow sections has been assessed from conclusions derived in a parametrical study by numerical experimentation. The criteria set forth in Eurocode 3, Part 1.1 (ENV 1993-1-1) (3-6) is used to induce lateral instability. The initial bow imperfection e_o prescribed by ENV 1993-1-1 is modelled by means of the equivalent lateral force applied at the compression flange and defined as (Clause 5.3.3):

$$q = \frac{8M_{pl}e_o}{hL^2} \qquad (3\text{-}3)$$

where, M_{pl} is the plastic moment, h is the height of the section, L is the length of the beam, and $e_o=\alpha_m L/500$. α_m=1 in this case.

According to ENV 1993-1-1 Clause 5.4.3, lateral restraint at the compression flange should be provided at all plastic hinge and plastic zone locations within a distance from the plastic hinge not exceeding 1.5 times the width of the flange. The parametric study is performed considering 2 and 4 times this distance, in order to assess its influence in the rotation capacity and plastic moment as show in Figure 3-3. In addition, the beam is analysed with lateral restraints at the supports only.

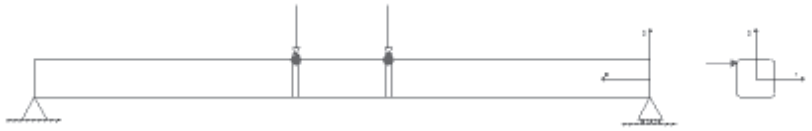

Lateral Restraints according to ENV 1993-1-1 (EC3)

Lateral Restraints at 4 times the ENV 1993-1-1 (EC3) limit

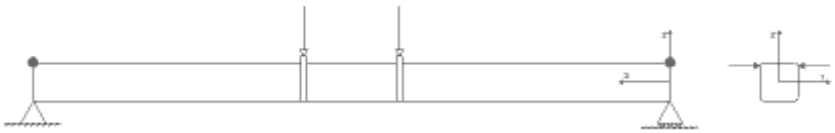

Lateral Restraints at supports.

Figure 3-20. Different lateral restraint locations used in the analyses.

The results obtained for the different sections are illustrated in the following tables. The three parameters that are used as means of comparison are, the plastic moment M_{pl}, the total inelastic rotation φ_{av}, and the non-dimensional rotation R_{av}. The distances that have been considered for lateral restraints have been the distance imposed by the ENV 1993-1-1, two and four times this distance, and the restraints at the supports only.

It is important to mention that no lateral buckling instability has been detected and as shown in the tables both the plastic moment and rotation capacity do not vary significantly with the restraint distance.

Table 3-6. Results for the section 100x100x3.

Distance for lateral restraint	M_{pl} (kNm)	φ_{av} (º)	R_{av}
EC3	14.5 kN m	2.12	1.12
2 EC3	14.5 kN m	2.12	1.12
4 EC3	14.5 kN m	2.12	1.12
At Supports	14.5 kN m	2.12	1.12

.

Table 3-7. Results for the section 160x80x3.

Distance for lateral restraint	M_{pl} (kNm)	φ_{av} (º)	R_{av}
EC3	25.1 kN m	1.13	0.9
2 EC3	25.1 kN m	1.13	0.9
4 EC3	25.1 kN m	1.13	0.9
At Supports	25.1 kN m	0.91	0.73

The main conclusions are the following:

1. Cold formed structural hollow sections have a large torsional capacity and, as a consequence, a large lateral stability as well.

2. The distance of lateral restraint in the neighbourhood of the plastic hinge and plastic zone can be much larger than that for open sections. The rotation capacity does not appreciably change even for four times the distance prescribed by Eurocode 3.

Consequently the limits to prevent lateral torsional buckling set forth by Eurocode 3, although valid for open sections, are over conservative for rectangular structural hollow sections.

3.3 Recommendation for cross-section classification

3.3.1 Current cross-section classification

Following assumptions are made for members when plastic design may be used:

- Each member section is able to reach the plastic moment level through plastic yielding of the entire cross section.

- The material possesses enough ductility so that large plastic strains can be accommodated without fracture.

- The section has sufficient ductility to allow for a considerable rotation at a relatively constant moment.

Concerning material ductility specifications, EN 1993-1-1 defines a key number of requirements to ensure that the material is able to sustain all the deformation required by the plastic hinge.

In fact, all the available test evidence, including tests made in this project, confirm *that the limiting factor determining the failure mode is not material ductility but geometrical ductility*. Local buckling affects the bending behaviour of hollow sections. As a consequence, steel design specifications define different classes of cross sections depending on how sensitive they are to the occurrence of local buckling during bending. In EN 1993-1-1, sections are classified as Class 1, 2, 3 or 4 based on the point at which local buckling occurs and the consequent capability of the section to maintain the plastic moment level for sufficiently large rotations which are needed to allow for moment redistribution in plastic design:

Class 1: Sections, which are able to form a plastic hinge with sufficient rotation capacity, required for plastic analysis.

Class 2: Sections, which can develop their plastic moment resistance but have limited rotation capacity due to local buckling.

Class 3: Sections in which local buckling is liable to prevent development of plastic moment resistance.

Class 4: Sections in which local buckling is liable to prevent development of elastic moment resistance.

The rules for classification consider the combination of cross-sectional dimensions (*b/t* slenderness ratios for the web and flange), the yield strength and the type of applied loading (separate or combined axial and/or bending moments).

Clause 5.3.3 (4) of Eurocode 3 (ENV 1993-1-1) states cross section requirements for plastic global analysis: "*For building structures in which the required rotations are not calculated, all members containing plastic hinges shall have class 1 cross-sections at the plastic hinge location*".

Doubts have been presented about applicability of CFSHS for plastic design arguing that they do not satisfy the material ductility requirements of ENV 1993-1-1 or that they have not enough geometric ductility (ability to develop the needed large rotations keeping the plastic moment capacity). Recent studies by Wilkinsson [3-3, 3-4] support the latter conclusion based on interpretation of test results performed for the purpose. They found that a large number of sections currently classified as Class 1 demonstrated insufficient rotation for plastic design making the above clause unsafe in certain cases.

Based on the results of the study on hollow section ductility (Chapter 2.2), it has also been concluded that current limits of classification in ENV 1993-1-1 may be nonconservative for hollow sections when used to ensure ability of a class 1 section to exhibit sufficient rotation capacity for every structure. Therefore following studies have been made to alter cross-section classification limits of ENV 1993-1-1 for hollow sections especially cold-formed structural hollow sections.

3.3.2 Modified proposal for classification limit in class 1

In "Background document 5.09 for chapter 5 of EN 1993-1-1 on b/t ratios" [3-5] has been stated available rotation capacity R_{av} which would identify sections which fulfil requirements for the use of plastic design, should be $R_{av} \geq 3.0$. In continuous beams required available rotation for before SLS become limiting is of the order of two degrees and respectively in portal frame up to three degrees. Figure 3-21 shows rotation capacities determined for tested sections. Respective inelastic available rotation values are shown in Figure 3-8 (c. low).

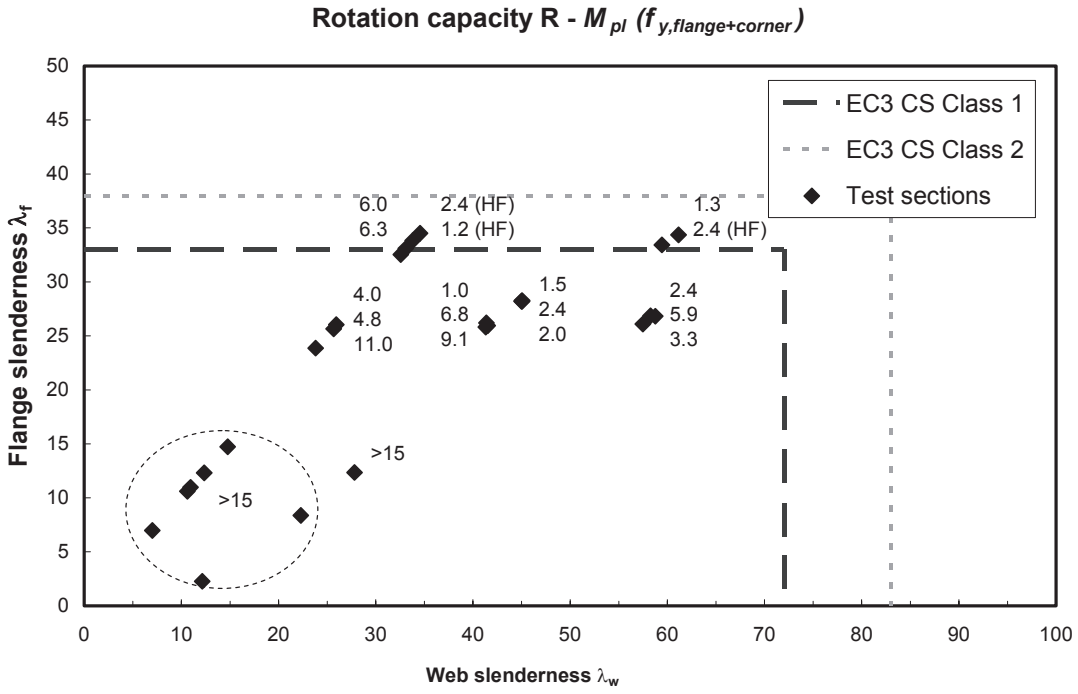

Figure 3-21. Rotation capacities R determined for tested specimen. The available rotation is determined using plastic bending moment resistance level calculated with actual flange and corner yield strengths.

Figure 3-22 shows inelastic available rotation values and rotation capacity values for all the cases in the test database (Table 3-9). Both values determined using yield strength from the flange of section. Increased yield strength of corners is not considered. The values between hot-formed and cold formed sections are comparable.

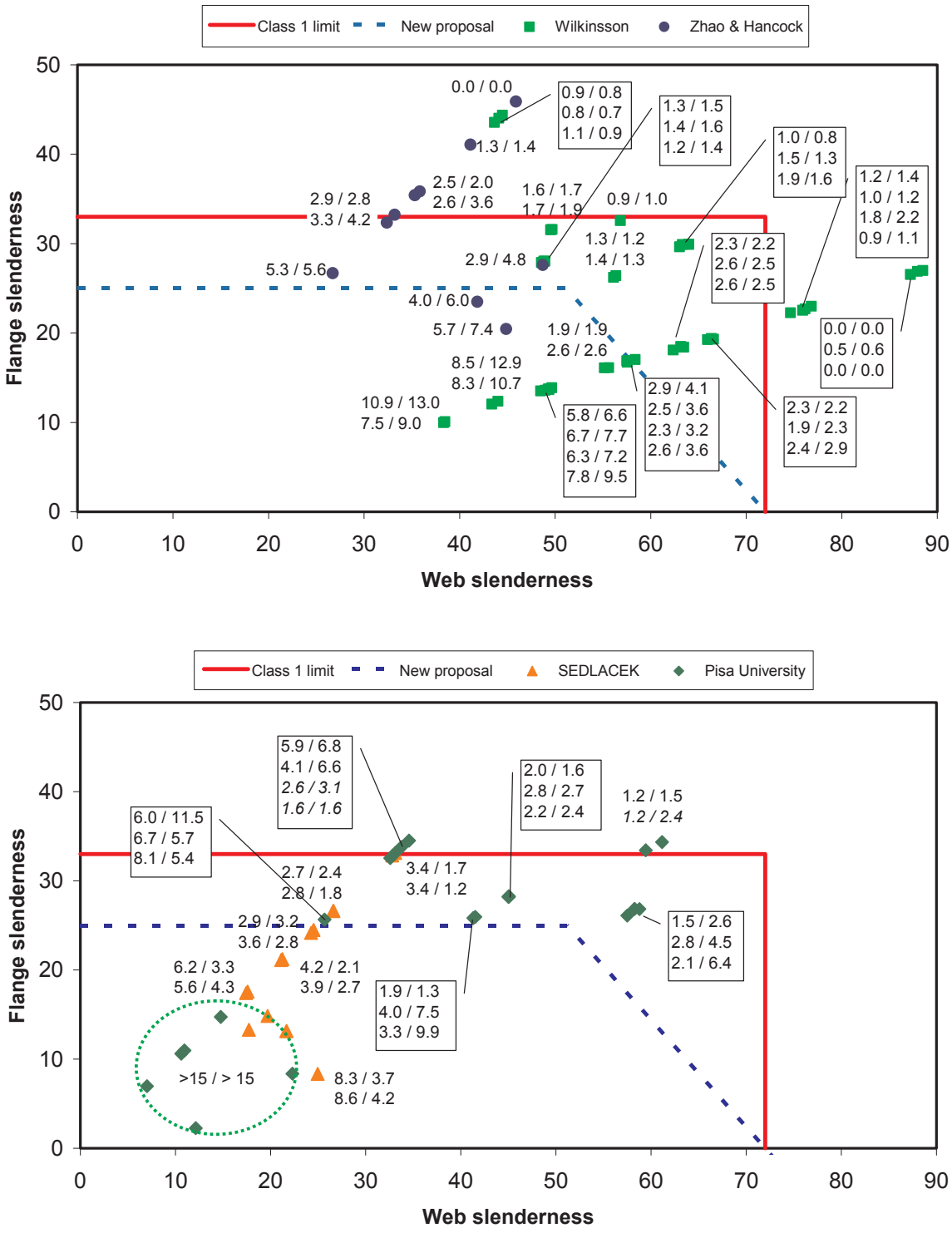

Figure 3-22. Inelastic rotation φ_{av} and rotation capacity R_{av} values are shown for each case in test database (φ_{av} / R_{av}). The values are determined using actual yield strength from the flange of the section. The influence of corners is not included.

The current rules for classification consider the combination of cross-sectional dimensions, *b/t* slenderness ratios for the web and flange in an independent way. As concluded in Chapter 3.2.4, ductility is dominated by flange slenderness when the section is in the region of lower web slenderness ratios (λ_w<≈ 60) and only global patterns (constant along the length) of initial imperfections are considered. However, the influence of interaction with web slenderness becomes relevant in region

between Class 1 and Class 2. When considering local patterns of initial imperfections the interactive influence of web slenderness happens to be more intense even for sections in the lower range of web slenderness (see iso-rotation curves represented in Chapter 3.2.4). Previous work from Wilkinsson& Hancock reached similar conclusions.

This proposal is made on the basis of keeping straightforward and simple rules but incorporating the findings of this research in terms of providing a safer approach to classify a hollow section to Class 1 for the plastic design. Thus, interaction between both, web and flange slenderness, should be considered to account for the interacting influence of both parameters particularly in the region of the border between Class 1 and Class 2.

This proposal is based on the information from iso-rotation curves, which are fitted to calibrated numerical simulation results and test results. Previous findings reported by Wilkinsson have also been taken into consideration to confirm reached conclusions. Thus, at present state, following changes in the present classification limit are proposed:

- A global limit for flange slenderness should be lowered though the test results are deviating. In Figure 3-22 lower limit down to $\lambda_f = 25$ is proposed instead with current limit of λ_f=33. Detailed statistical analysis is required to adjust the level of safety.

- A linear interaction between flange and web slenderness should be considered in the region where web slenderness approaches current limit of Class 1 ($\lambda_w = 72$). Wilkinson's proposal as relationship is adopted but modified to be limited to proposed global limit of $\lambda_f = 25$:

$$\lambda_w \leq 72 - (5/6)\,\lambda_f \qquad \text{with } \lambda_f \leq 25 \qquad (3\text{-}4)$$

According to the results from calibrated numerical simulations – which have shown to be conservative in comparison to tests– this proposal would guarantee a minimum available inelastic rotation around 5-6 degrees (Figure 3-16) when considering global imperfections patterns and around 3 degrees when accounting for more unfavourable case of local imperfections (Figures 3-14 and 3-15). The proposal is also in reasonable agreement with test results collected in test database (Figure 3-22) though there are large deviations in the test results.

This proposal is also in line with the one proposed by Wilkinson and Hancock [3-4], which is also indicated in Figure 3-10. More recently, Wilkinson [3-5] has proposed a simplified alternative ignoring the effect of flange-web interaction by setting an absolute limit on the web slenderness equal to 55 instead of 72.

More detailed statistical analyses should be carried to adjust the slenderness limits in the way that safety level corresponds to other sections geometries.

3.4 Guidance for plastic design

3.4.1 Alternative approach based on available and required rotation checking

A more rigorous approach is also proposed based on the concept of available inelastic rotation as a measure of section geometrical ductility. The method which compares required and available inelastic rotations for each formed plastic hinges is an alternative to the use of section classification rules existing in ENV 1993-1-1, for the verification of sufficient ductility of plastic hinges.

ENV 1993-1-1 provides general rules concerning rotation requirements of plastic hinges (Clause 5.3.3): "(*3) At plastic hinges locations, the cross-section of the member which contains the plastic hinge shall have a rotation capacity of not less than the required rotation at that plastic hinge location. (4) To satisfy the above requirement, the required rotations should be determined from a rotation analysis*"

Thus, the application of the rotation capacity concept to plastic design as a global analysis method involves checking that the required inelastic rotation (φ_{req}) does not exceed the available inelastic rotation (φ_{av}) for each plastic hinge appeared in a structure submitted to design loads:

$$\varphi_{req,d} \leq \varphi_{av,d} \quad \text{or} \quad \varphi_{req,d} \leq \varphi_{av} / \gamma_{M\varphi} \tag{3-5}$$

where:

$\varphi_{req,d}$ is the design value of required inelastic rotation at the plastic hinge location (calculated from plastic global analysis of the structure submitted to design loads).

$\varphi_{av,d}$ is the design value of available inelastic rotation

φ_{av} is the characteristic value of available inelastic rotation. In the context of this research new tools in the form of simple models are proposed to evaluate available inelastic rotation.

$\gamma_{M\varphi}$ is partial safety factor.

The values of partial safety factor should be determined from statistical evaluation of a sufficient number of available test results on the scope of the design model used to evaluate available rotations. At the present time a value $\gamma_{M\varphi} = 1.5$ is suggested on the basis of previous studies for open cross-sections since test data base is still insufficient to state definite values.

Three different methods can be used for evaluation of available inelastic rotations: tests, numerical simulation (Finite Element Analysis) and approximate predictive models. Guidelines and recommendations are given in the following sections for evaluation by FEA (section 3.4.2). In addition to this, two predictive simplified models are proposed for the same purpose in section 3.4.3.

Preliminary estimates of the required inelastic rotations for standard structural systems that make common use of CFSHS, have been provided in section 3.2.8.

3.4.2 Numerical evaluation of available inelastic rotation

Numerical simulation by finite elements provides an adequate way of modelling the inelastic behaviour involved in the collapse response of the cross-section. Detailed finite element modelling including effects of plasticity, strain hardening, geometrical nonlinearities and residual stresses is proposed for evaluating deformation capacities of individual members (section characterisation). Appropriate modelling alternatives are proposed for shape and magnitude of initial imperfections, material, residual stresses, and boundary conditions and meshing.

A set of simulations to model the tests were performed to confirm the FE modelling strategy. The correlation analysis with the test results gives rises to the following conclusions:

1. Maximum load capacities (in terms of maximum moment) measured in tests are always well above the values predicted by FE models (Figure 3-23). This is very likely caused by the fact that real yielding stress of the material in test specimens is above the nominal values used in the FE models. Discrepancy caused by this "over-strength" effect can be overcome by updating the yielding and ultimate stresses assumed in FE models. M-φ curves derived from updated FE models are shown in the next figures also indicating the used factor.

2. The general shape of the M–φ curves, particularly in the descending part, is reproduced by the FE models in a satisfactory way. Quantitative estimation of this agreement is done by comparing the parameters, which characterise the post-buckling descending slope of the curve ($\varphi_{90\%}$ and $\varphi_{95\%}$). FEM seems to provide generally safer values of post buckling slopes for the three available cases (Table 3-8).

3. FEM curves appear to be shifted in the rotation axis when compared to the test ones, in such a way that rotations from tests are higher that in the simulations. Explanation for this discrepancy has been elaborated based on detailed modelling of the section 200x100x4.

   Standard modelling strategy was developed to provide simple and safe assumptions allowing safe predictions of available inelastic rotation be made. Some of these assumptions are revised using more realistic hypothesis with regard to both material data and imperfections:

   - Actual stress strain curves from material tests.

   - Measurements of imperfections for the test specimen showed that the imperfections are sensibly uniform along the specimens where the magnitude of local imperfection (with wave lengths in the order of flange width) is far from reaching the level proposed in standard modelling strategy (0,1% of flange width in the first local eigenmode). Based on the case was modelled without using any initial imperfections (Figure 3-24).

   The results show how the calculated curve approaches closer to the experimental one although it remains still far from reaching the experimental rotation levels.

Table 3-8. Comparison of the available ration results at level of 90% and 95% of the moment resistance.

	Tests		**FEM**	
	φ 95%	**φ 90%**	**φ 95%**	**φ 90%**
300x200x8	0.31	0.68	0.29	0.71
400x200x8	0.39	0.80	0.17	0.39
200x100x4	0.30	0.61	0.19	0.30

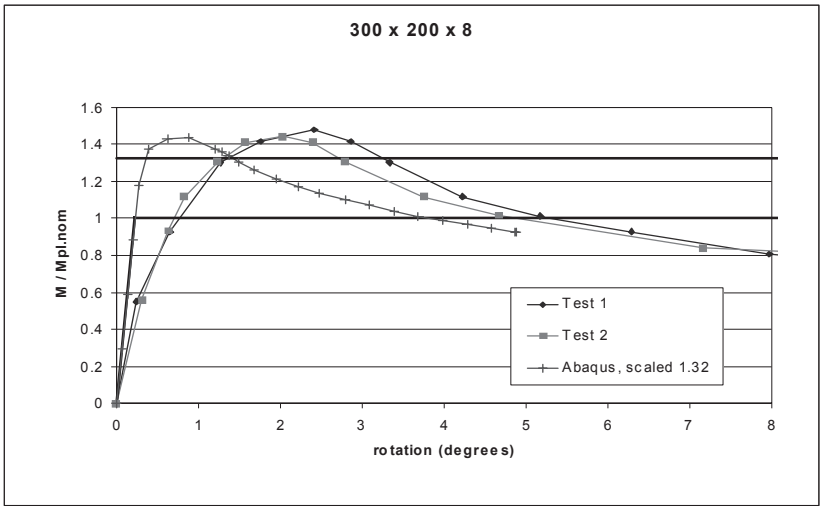

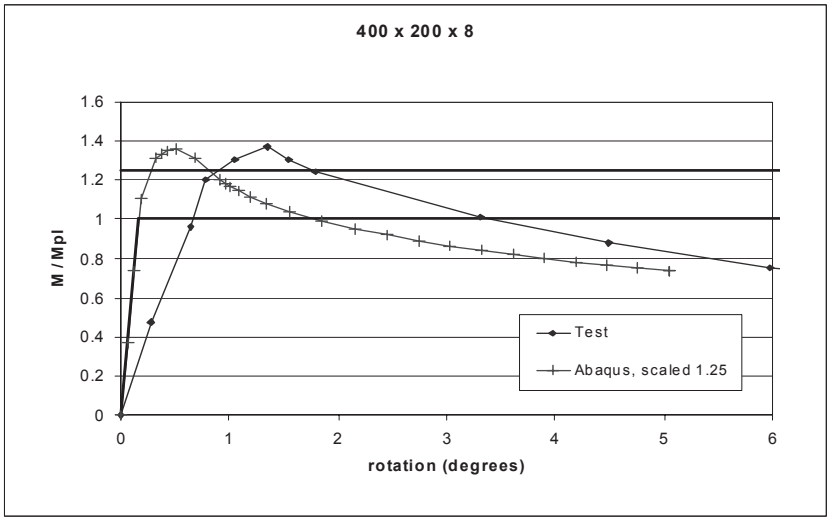

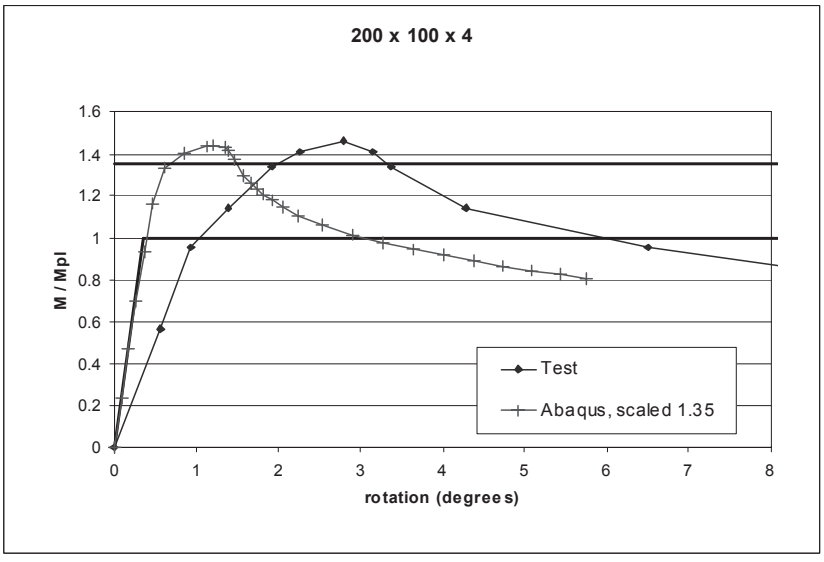

Figure 3-23. Comparison of moment-rotation curves from tests and FE simulations for section sizes300x200x8, 400x200x8 and 200x100x4. FE results are analysed with nominal material properties and then scaled to reach experimental moment resistance. M_{pl} is calculated with nominal yield strength.

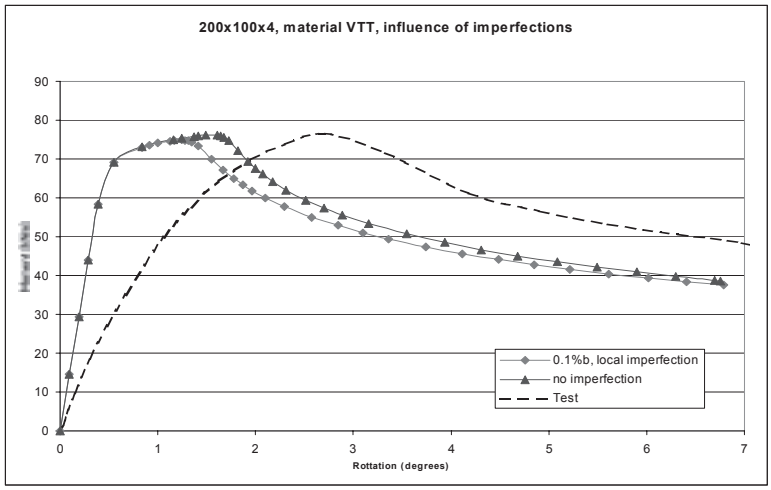

Figure 3-24. Effect of imperfection on the moment –rotation curve for section 200x100x4.

It can also be observed a very relevant lack of agreement between the numerical and test curves regarding the starting slope in elastic part. This is an indication that rotations could not be measured in the same way. Measurements of rotations in tests are done by using vertical displacements of locations 2 and 3, on the one hand and 5 and 6 on the other one (Figure 3-7).

Due to the elastic part of rotations, this measure overestimates the actual rotation of the plastic hinge. The following figure shows the difference between the M-φ curve obtained by directly monitoring rotations at both ends of the plastic hinge (as proposed in standard strategy) and the one obtained from the test (deduced from displacements at a given distance of both loading ends). It can also be appreciated how the initial slope of elastic part of the curve fits now much better to the experimental one although rotations are still lower compared to test (Figure 3-25).

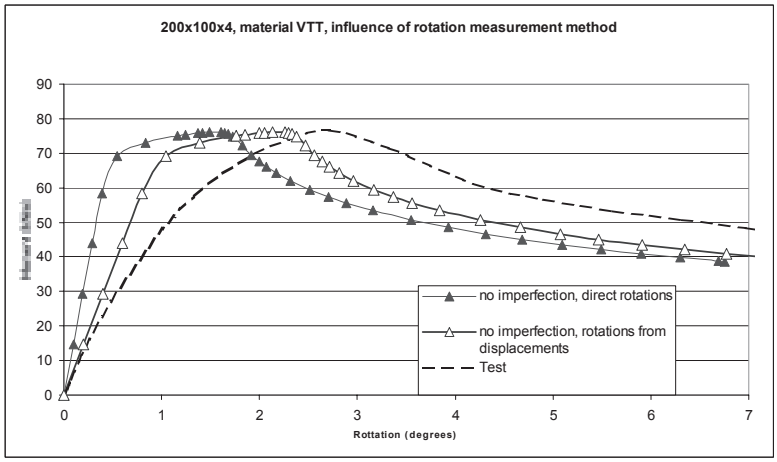

Figure 3-25. Effect of different ways of determining rotation to moment –rotation curves.

Detailed observations of the respective deforming shapes (FE model and test) give also some differences. The general mode is the same but deformation in the test tends to concentrate very close to one of the loading plates. Numerical deformation is also shifted from the midspan but in a less evident manner.

Residual stresses that can be expected to arise in the areas where loading plates are welded are very likely to be responsible for this effect as well as for the shifting of the curve towards regions of higher rotations as observed in test curve. Preliminary numerical studies proved the strong influence of residual stresses on the shape of the moment-rotation curve before reaching the maximum moment. Figure 3-26 shows how the introduction of a given pattern of residual stresses (uniform along the beam) makes the ascending part of the moment-rotation curve to lie closer to the experimental one.

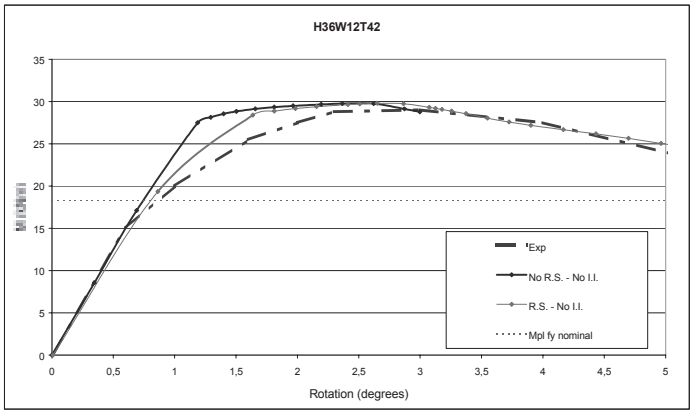

Figure 3-26. Effect of residual stresses on the moment rotation curve.

3.4.3 Design models for available inelastic rotation

3.4.3.1 Types of models

A review of predictive simplified models for evaluation of available inelastic rotation of CFSHS is done on the basis of their theoretical basis, scope, limitations and application guidelines. A test database collecting test data and results from different sources has been used for the purpose of performing a reliability analysis of the different models by correlation with the test results.

Approximate models, however, conform to practical demands although they are valid in limited ranges and scope. Important physical effects to consider are:

- Membrane stress rearrangement-giving rise to a post critical load capacity reserve.
- Occurrence of yielding at plate edge and loss of capacity resulting from this kind of yielding.
- Bending moments developing in a buckled plate and determining the basic mechanism responsible for the loss of capacity of the plate to carry membrane stresses.
- Yielding mechanisms of plastic deformations of plates in post buckling range.

Relevant additional factors to take account of their effects in models are strain hardening, residual stresses and initial geometrical imperfections.

The following models are distinguished considering their purpose and physical basis:

I. Models aimed to obtain the maximum bending moment capacity of the member

Most of them are based on the Effective Width concept. Attention is focused on predicting the response up to the maximum moment. These models do not try to simulate the behaviour after the maximum moment so post buckling modelling is not of concern for them. They provide estimation of ultimate resistance of a member under bending moment or bending moment combined with axial force as well as deformation of the member (rotation) when ultimate moment is reached. The difficulties associated to the calculation of the falling branch of the moment-rotation curve is avoided by assuming that the total inelastic rotation available prior to the moment falling below the plastic moment is directly related to the rotation at maximum moment.

These kinds of methods are more suitable for slender sections made up with webs and flanges of thin plate. Buckling of webs or flanges is then likely to occur in elastic region. This local buckling does not

lead immediately to the loss of resistance in the member appearing a post critical reserve of load bearing capacity.

Thus, models based on effective widths take into account membrane stress rearrangement and occurrence of yielding at plate edge derived from local buckling. Conversely, they do not consider the loss of capacity to carry membrane stresses due to bending moments arising in a buckled plate. This limits its applicability for stocky sections.

Nevertheless, effective width approach has been extended into the inelastic range to account for plasticity effects actually taking place for plates in the intermediate range of slenderness. Alternative models to the ones based on Effective Width concept to evaluate moment-rotation response of moderately thick plate members are based on tracking the stress-strain path at each plate of the section.

II. Models aimed to obtain the falling branch of moment-rotation curve

The physical base behind most of these models is some approach of yield line kinematics mechanisms.

Local buckling causes the stress distribution to change suddenly: a flanged which is assumed to carry only membrane stresses before buckling will have to absorb bending moments once local buckling appears, reducing considerably its capacity to keep carrying membrane stresses. The models belonging to the previous group ignore the bending moments which begin to develop once local buckling has appeared so that they do not make any provision to account for the reduction caused to membrane strength. The behaviour of the member after the maximum of the load, in the post buckling range, is assumed to be dominated by this effect.

In this respect, the models based on yield line kinematics mechanisms try to represent the post buckling response and particularly the descending part of the load-displacement or moment-rotation curves.

These methods are suitable to deal with stocky sections made of relatively thick plates where local buckling comes into being with yielding practically at the same time. No relevant post critical reserve is considered to develop.

III. Models based on statistical fitting

These models have their applicability limited by the range of test results used for the fitting. Different forms of slenderness ratios are used as basic parameters. Complex and interacting phenomena involved in the real behaviour that determines the rotation capacity of a member are in this way integrated in very simple equations.

3.4.3.2 Test Data Base

Three sets of experimental data, all of them corresponding to 4-point bending tests, have been found and used for correlation and validation of predictive models: Wilkinsson & Hancock (3-2), Sedlacek (3-7) and Zhao & Hancock (3-8) (Table 3-9).

Table 3-9. Test series in test database that have been used to evaluate behaviour CFSHS in bending.

Type of test	No. tests	Sections	Mate-rial	d/b range	b/t range	Charac-teristics	Reference
4 point bending test	44	14 CF d=75-150 b=25-100 t=1,54-4,92	2 C350 C450	1-3	10-33	3 different loading methods	Tests to examine compact web slenderness of CF RHS T.Wilkinson, GJ Hancock J.Struct.Eng. Vol 124 No10, Oct. 1998
4 point bending test	28	4 CF-SHS 3 CF-RHS 4 HR-SHS d=50-200 b=40-200 t=3-8	3 Fe360 FeE460 Fe510	1	20-30 25-32 8-13	2 span lengths (2 moment gradients)	Investigation of the rotation behaviour of hollow section beams. Report EUR 17994 EN. 1998 G.Sedlacek et all.
4 point bending test	10	10 CF: - SHS from 100x100x3,8 to 65x65x2,3 - RHS from 125x75x3,8 to 100x50x2,8	1 (C450)	1-2	15,9 – 33,7		Tests to determine plate slenderness limits for cold formed RHS of grade C450 XL Zhao, GJ Hancock, Steel Constr. Vol.25 No4, 1991
4 point bending test	28	13 CF 3 HF d=100-400 b=100-200 t=3-12.5	S355	1-2	8-30		Tests done in this project at University of Pisa.

The test results have been re-evaluated in terms of available inelastic rotations (φ_{av}) to make them homogeneous and comparable since different definitions of rotation capacities were originally used. Sedlacek tests are reported in form of standard definition of rotation capacity so a simple multiplying operation by φ_{pl} allows obtaining the desired available inelastic rotations (φ_{av}). This is not the case for both sets of test results, Wilkinson&Hancock (3-3) and Zhao&Hancock (3-8), which give rotation capacities defined in terms of curvatures instead of usual definition in terms of rotations. In these cases available inelastic rotations (φ_{av}) values are recalculated values of providing, thus, a homogeneous measurement for all the tests.

3.4.3.3 Proposed simplified methods based on Kecman model and Kubo model

a) Method based on Kecman model:

The Kecman model (3-9, 3-10) has been evaluated by comparing experimental results in test database to assess reliability of the model.

The maximum moment M_{max} is obtained through the following formulas:

$$(1)\ M_{\max} = M'_m = \sigma_p t b^2 \left[\frac{2a + b + a_e + \left(3\frac{a}{b} + 2 \right)}{3(a+b)} \right] \quad \text{when } \sigma_{cr} \le \sigma_p \tag{3-6}$$

$$(2)\ M_{\max} = M'_p + \left(M_p - M'_p \right) \frac{\sigma_{cr} - \sigma_p}{2\sigma_p} \quad \text{when } \sigma_p < \sigma_{cr} \le 3\sigma_p \tag{3-7}$$

$$(3)\ M_{\max} = M_p = \sigma_p t \left[a(b-t) + 0.5(b-2t)^2 \right] \text{ when } \sigma_{cr} > 3\sigma_p \tag{3-8}$$

where

$$\sigma_{cr} = 0.9E \left(5.23 + 0.16\frac{a}{b} \right) \left(\frac{t}{a} \right)^2 \tag{3-9}$$

$$M'_p = \sigma_p t b \left(a + \frac{b}{3} \right) \tag{3-10}$$

$$a_e = a \left(0.7\frac{\sigma_{cr}}{\sigma_p} + 0.3 \right) \quad with \cdot a_e = a \cdot if \cdot \sigma_{cr} \ge \sigma_p \tag{3-11}$$

.

The comparison of maximum moment values calculated from the Kecman model and those from the test presents a satisfactory correlation as shown in Table 3-10 and Figure 3-27.

Table 3-10. Statistical analysis of comparison between experimental moment resistance and analytical determined with Kecman model.

Maximum moment		
TESTS	Correlation coefficient	Average error
All	99.7%	6.8%
Wilkinsson-Hancock	99.1%	7.8%
Sedlacek	99.9%	3.6%
Zhao-Hancock	98.5%	12.2%
University of Pisa	99.5%	7.3%

The available rotation is calculated by numerical derivation of the formula giving the energy, *W (θ)*, absorbed by the yielding line mechanism postulated by Kecman:

$$M_D(\theta_D) = \frac{\Delta W(\theta_D)}{\Delta \theta_D} \tag{3-12}$$

where

$$W(\theta_D) = 0.5\sigma_{pu}t^2\left[a(\pi - 2\beta) + 2b \cdot arc \cdot \tan\left(\frac{z_A}{\sqrt{(h - x_{A''})^2 + (y_{A''} - y_A)^2}}\right) + \right.$$

$$\left. + h\left(\pi + 2 \cdot arc \cdot \tan\left(\frac{z_A}{y_A}\right)\right) + 2\frac{z_A}{r}\left(h + \frac{2}{3}\sqrt{h^2 + y_A^2 + z_A^2}\right)\right] \quad (3\text{-}13)$$

$$h = \frac{b}{2} \cdot if \cdot a \geq b \text{ or } h = \frac{a}{2} \cdot if \cdot a \leq b$$

$$\theta_J = 2\,arc \cdot \sin\left(\frac{h - 0.5t}{b}\right) \quad (3\text{-}14)$$

$$\rho = \frac{\theta_D}{2} \quad (3\text{-}15)$$

$$x_{A''} = y_{A''} \times \tan \cdot \rho \quad (3\text{-}16)$$

$$r = \left(0.07 - \frac{\theta_D}{70}\right)h = \left(0.07 - \frac{\rho}{35}\right)h \quad (3\text{-}17)$$

$$y_{A''} = \frac{h \cdot \tan \cdot \rho + b \cdot \cos \cdot \rho - \sqrt{b \cdot \sin \cdot \rho(2h - b \cdot \sin \cdot \rho)}}{1 + \tan^2 \rho} \quad (3\text{-}18)$$

From the $M(\theta)$ curve obtained with these equations, a rotation value can be derived by intersecting the curve with a given plastic moment level (M_{pl}). The calculated rotation value has been assumed to represent the inelastic available rotation according to the definition given in the introduction ($\varphi_{av} = \varphi_{rot} - \varphi_{pl}$). A reasonably satisfactory correlation has been obtained by comparison with test data although the rotations given by the model have been modified by a constant value to minimise the error.

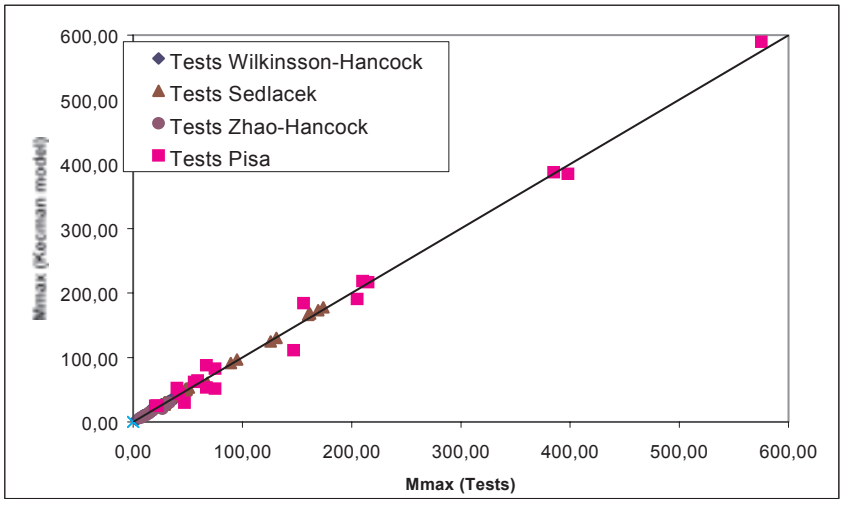

Figure 3-27. Correlation between experimentally determined moment resistance and calculation with Kecman model.

Table 3-11. Statistical analysis of comparison between experimentally determined inelastic available rotation and analytical determined with Kecman model.

Available inelastic rotation		
TESTS	Correlation coefficient	Average error
All	95.2%	22.2%
Wilkinsson-Hancock	93.9%	26.7%
Sedlacek	92.4%	18.8%
Zhao-Hancock	98.3%	17.8%
University of Pisa	97.5%	21%

Figure 3-28 represents the comparison between the results given by the modified Kecman model (corrected by subtracting a constant rotation value equal to 2.72º) and the test results. The Kecman model provides a better agreement with test results of Zhao&Hancock and test from this project than with Sedlacek et all. and Wilkinsson&Hancock tests.

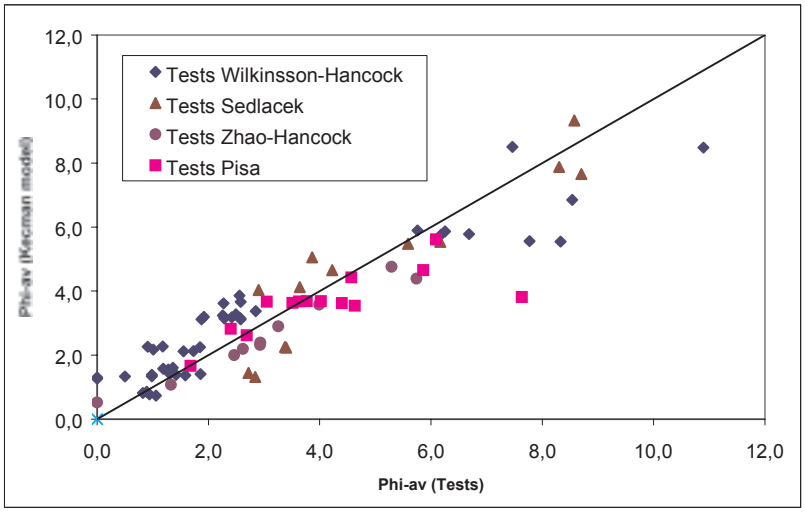

Figure 3-28. Correlation between experimentally determined available inelastic rotation and calculation with Kecman model.

b) Method based on Kubo model

Kubo (3-11) proposes a statistical formula using a combined flange/web slenderness ratio as basic parameter:

$$\lambda_s = \sqrt{\lambda_{pf}\lambda_{pw}} \tag{3-19}$$

where λ_{pf} and λ_{pw} are calculated from:

$$\lambda_p = \frac{b}{t}\sqrt{\frac{12(1-\nu^2)}{\pi^2 k}}\sqrt{\frac{\sigma_y}{E}} \tag{3-20}$$

Kubo used data of I-sections to fit a simple formula for the rotation capacity R as follows:

$$R_\theta = \frac{0.24}{\lambda_s - 0.44} \leq 12 \tag{3-21}$$

An equivalent model has been derived using a similar equation and re-evaluating the value of the coefficients by fitting with the test data base of hollow sections. The following formula has been obtained under the criterion of providing a conservative value for the available inelastic rotation:

$$\varphi_{av} = \frac{2.5}{\lambda_S} - 4 \qquad (3\text{-}22)$$

This model has been implemented and evaluated by contrasting its results with the experimental data base with the aim of assess its reliability.

Table 3-12. Statistical analysis of comparison between experimentally determined inelastic available rotation and analytical determined with Kubo model.

Available inelastic rotation		
TESTS	Correlation coefficient	Average error
All	86,6%	53,5%
Wilkinsson-Hancock	95,4%	49,7%
Sedlacek	85,8%	37,8%
Zhao-Hancock	94,6%	49,1%
University of Pisa	96,2%	66,5%

Figure 3-29 shows the comparison between the results given by the fitted Kubo-type model and the test results.

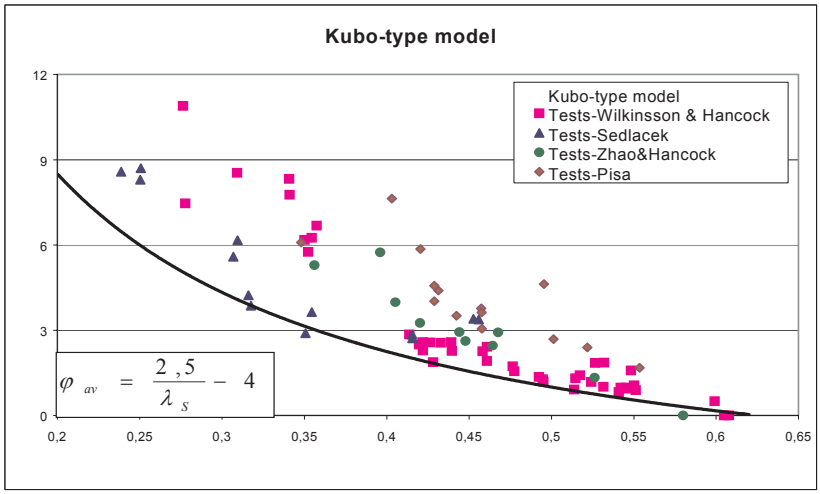

Figure 3-29. Comparison with experimentally determined inelastic available rotations to Kubo model.

The method based on Kubo model provides a better agreement with test results of Wilkinsson&Hancock and Zhao&Hancock tests than with Sedlacek et all. tests. The large values of average error are motivated by the criterion used to provide safe values of available inelastic rotations.

3.5 Conclusions

Following conclusions are drawn

- The available inelastic rotation marked φ_{av} should be used to model the deformation capacity of a cross-section in bending, while it can be considered as a cross-section property that is limited by

material property related yielding and geometric dimension related local buckling. Traditionally rotation capacity $R = (\varphi_{rov} - \varphi_{pl})/ \varphi_{pl}$. is used to describe deformation capacity.

- The inelastic rotation capacity of hollow sections depends on the shape of descending part of the moment rotation curve, which is limited by plastic local buckling as failure mode. Material ductility is not the limiting phenomena on the deformation capacity of hollow sections.

- When moment rotation performance of hollow sections is considered the moment resistance and the inelastic rotation up to the moment resistance seems depends essentially on the flange slenderness. The web slenderness seems to have an influence on the descending part of moment rotation curve after maximum moment has been reached. Available inelastic rotation depends on both web and flange slenderness ratios. There is interaction between web and flange.

- Cold formed and hot-formed sections behave similarly in four point bending tests. The moment resistance level depends on the material strength, which may be larger in cold formed sections due increased strength of corners. The moment-rotation curves have similar shape and available rotation values are of same magnitude though numerical differences may be found. There are no clear differences in moment rotation characteristic that reflect the manufacturing method.

- The current cross-section classification in EN 1993-1-1 seems to be non conservative for hollow sections. The interaction of web and flange in bending is not considered when slenderness limit are given separately. Also the rotation capacity required to form necessary plastic hinge should be clarified. A more demanding proposal for slenderness limits in class 1 is presented though statistical analyses is still required to set the safety level respective to other section shapes.

- Instead of cross-section classification more advanced analysis of structurally required rotation compared to available rotation of hollow section members should be used. The available rotation of structural member may be determined experimentally, numerically with calibrated FE simulation or using verified empirical design provision such as Kecman or Kubo model.

4 Applicability of design rules for tubular connection from CFSHS

4.1 Introduction

The joints are typically the most critical points of any constructions. This statement is valid of course for structures made of structural hollow sections. The overall strength of the whole structure is in many cases depends on the load carrying and deformation capacities of the joints. On the other hand, from the fabrication costs point of view, the joints have again the most important role. Therefore special attention should be focused on the design of the joint.

The design rules for structural hollow section joints obtained in design codes are developed based on the experimental verification of failure modes and safety level adjusted to experimental resistances. Most of these results, however, are based on tests of hot-formed structural sections (HFSHS) at room temperatures. Relatively few test results are available for cold-formed structural hollow sections (CFSHS) at low temperatures.

Characteristic for CFSHS is that high degree of cold forming may decrease the ductility in the corner areas for CFSHS. Due to this higher degree of cold forming, the yield strength of the corner is typically higher than that of the adjacent flat faces, where degree of cold forming is lower and consequently the yield strength is lower but ductility better. This may have influence on the behaviour of hollow section joints.

Under external service loads of the joints, the deformations will concentrate in the corners of the section. However, the higher yield strength of the corner area, which restrains the plastic deformation to take place, may direct plastic deformations to the areas adjacent to corners. Thus, even when the ductility would be decreased locally in the corner areas of sections, it will not decrease the overall deformation capacity of the joint. This mismatching effect is applicable as long the flat faces have smaller yield strength than the corners. This assumption is valid if the degree of cold forming in flat face is moderately small.

The degree of cold forming in the corner area is more or less independent on the wall slenderness of the section. However, in the flat face the degree of cold forming depends on the b_o/t_0-ratio (if the section has a round shape in the previous fabrication state). Therefore the b_o/t_0-ratio should correlate to the general degree of the cold forming of the cross section. In order to study the most critical joint configurations with respect to deformation capacity, the section sizes are chosen in the way that the degree of cold forming is chosen to be high level. Thus the sections with small b_o/t_0-ratio are chosen for test specimens.

It is obvious, that the ultimate loading carrying capacity may not become critical but the deformation capacity, when the applicability of cold–formed structural hollow sections for structural use is considered. The potentially decreased deformation capacity may not occur in room temperatures but in lower temperatures. Thus the tests are carried out in low test temperatures as well.

Therefore the main objective is to validate the applicability of current design rules in Eurocode 3, Part 1.8 for cold-formed structural section joints, when the degree of the cold forming is high and the service temperature is low. Secondary objective is to define the critical parameters, which correlate to the capacity of the joint.

The deformation capacity of the joint can be restricted by preventing the plastic deformation to take place. This will happened partly due to the gap geometry itself, where the free deformation of the chord face in transverse direction is prevented by adjacent brace members. The pretension of the chord member will decrease the deformation capacity of the joint as well. Thus pretension of the chord member was included in K- and X-joint tests series. Behaviour of CFSHS in welded connections is

studied with K-joint and X-joint test in normal and at low temperatures. The test programme comprised of altogether 41 K-joint test and 32 X-joint tests (20 executed at LUT and 12 at University of Pisa).

4.2 Methods and materials

4.2.1 Analysing methods

The ductility of the joint is depending on many parameters. The geometrical parameters can be taking into account in a theoretical model, but the other parameters like chemical composition, heat input and metallurgical phenomena are still impossible to include in any theoretical model. Therefore, the validation of design rules must be done with experimentally. Considering K- and X-joints, the deformation capacities are restricted in those joints by quite different mechanisms. Therefore both type of joints are included in this investigation. The results from experimental test will be compared to capacities defined by theoretical models given in current design code Eurocode 3, Part 1.8 [4-1]. For the deformation capacity of the joint, the reference value is a "generally accepted" limit for plastic deformation $\geq 0.01*b_0$ for $\beta= b_1/b_0<1$ and $\geq 0.005*b_0$ for $\beta=1$, where b_1 is width of the brace member and b_0 with of the chord, respectively.

4.2.2 Materials

There are different kinds of cold-formed section depending for example on the chemical composition and fabrication method. Therefore CFSHS from two different manufacturers (A and B) are chosen for the test specimen. Also some hot-formed sections (HF) are tested form comparison. Taking into account the availability of different type hollow section tubes the S355 steel grade was chosen for the base material of the tubes. The tests seen in Table 4-1 for the material used in experimental tests are carried out. The results of these analysis are seen in test reports [4-2] and [4-3].

Table 4-1.Material characteristics determined from test specimen.

Test	test temperature	parameters
chemical compositions	room	carbon contents C equivalent carbon contents C_{equ}
coupon test	same as joint temperature +20…-60 °C	yield strength f_y tensile strength $f_{u,}$ ultimate elongation A5
Charpy V- tests	+20…-100 °C	- 50 % - ductile area of fractured surface

4.3 Experimental tests

4.3.1 Test specimen

In K-joints the sections of brace members are typically smaller than the section of chord member ($\beta=b_1/b_0<1$). The gap type joints are preferred to lap type joints from fabrication point of view. In this type of K-joints the gap is critical area of the joint.

The deformation capacity of the joint is highly depend on the deformation capacity of the gap. The deformation capacity of the gap is depend on the ductility of the flat face of the section and the geometry. The smaller the b_o/t_0-ratio, the higher is the degree of cold forming. In addition, the smaller the gap size is compared to width of the chord (g/b_0 –ratio), the bigger are plastic strain concentrations. In order to find lower limit for deformation capacity, the test specimens are chosen to have gap sizes

near the lower limits allowed in the design code. In order to keep the geometry of the joint as simply as possible, the joints are designed to be symmetrical.

The schematic picture of tested K-joint is seen in Figure 4-1. The geometrical parameters are seen in Table 4-2, where L_1 and b_1* are distances from weld toe to weld of the tension brace, L_1 in longitudinal direction of chord member and b_1* in transverse direction, respectively

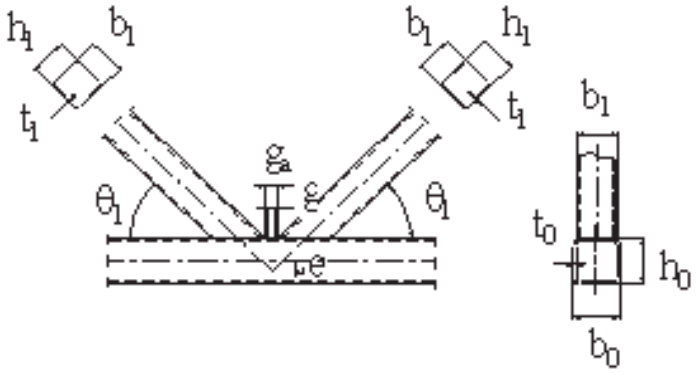

Figure 4-1. Joint geometry for K-joints.

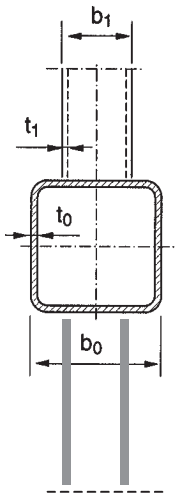

Figure 4-2. Joint geometry for X-joints.

In X-joints the corners of the chord member are the critical areas. If the width of the brace members is smaller than that of the chord member ($\beta<1$), the transverse ligaments between the corner of the chord and the fixing weld of the brace member are the critical areas. If the width of the brace and chord members are equal ($\beta=1$), either the web side of the chord member or the parallel flat face of the brace member is critical.

In both X-joint types the degree of cold forming of the flat faces will be the critical parameter when the deformation capacity of the joint is considered. In principle the X-joint will be even more critical than the K-joint concerning the degree of cold forming, while the transverse direction of the section is the critical direction, which is the major direction of cold forming as well.

In K-joint only the transverse component of the brace load is actually critical. On the other hand the joint area is bigger in K-joint when compared to the cross section of the brace member thus decreasing the nominal stress level of joint. In spite of this, the K-joint area can be the critical part of the structure, if the gap size is small and the ductility of the flat face is reduced.

The schematic picture of tested X-joints is seen in Figure 4-2 and the geometrical parameters are seen in Tables 4-3 and 4-4.

Table 4-2. Dimensions for K-joints.

Specimen id	Chord		Brace		Joint							
	b_0 x h_0 x t_0 [mm]	b_0/t_0	b_1 x h_1 x t_1 [mm]	b_1/t_1	$\beta = b_1/b_0$	g [mm]	R_0 [mm]	R_i [mm]	θ_1 [°]	θ_2 [°]	b_1^* [mm]	L_1 [mm]
K1	100.1 x 100.8 x 5.90	17.0	80.4 x 80.4 x 4.90	16.4	0.8	5	13	11	44.5	44.4	91	127
K2	100.5 x 100.2 x 7.90	12.7	49.9 x 50.0 x 4.94	10.1	0.5	8	19	11	49.6	49.6	60	79
K3	99.6 x 100.2 x 7.90	12.6	50.0 x 50.1 x 4.94	10.1	0.5	8	18	10	49.5	49.7	64	80
K4	100.2 x 100.7 x 7.90	12.7	50.0 x 50.0 x 4.94	10.1	0.5	7	21	10	49.6	49.3	63	79
K5	100.1 x 100.9 x 7.90	12.7	70.1 x 70.1 x 4.94	14.1	0.7	9	22	9	44.4	44.7	80	112
K6	100.1 x 100.7 x 7.90	12.7	100.5 x 100.2 x 5.90	17.0	1.0	14	22	12	44.3	44.5	100	154
K7	100.1 x 100.7 x 5.90	17.0	50.1 x 50.0 x 4.94	10.1	0.5	8	11	9	49.6	49.7	65	79
K8	100.4 x 100.2 x 5.87	17.1	50.1 x 50.0 x 4.94	10.1	0.5	7	11	9	49.4	49.5	65	79
K9	100.0 x 100.1 x 7.82	12.8	50.0 x 50.0 x 4.94	10.1	0.5	6	17	9	49.7	49.6	64	81
K10	100.4 x 100.2 x 5.90	17.0	50.0 x 50.0 x 4.94	10.1	0.5	8	12	9	50.5	50.5	65	80
K11	100.3 x 100.2 x 5.96	16.8	50.0 x 50.0 x 4.94	10.1	0.5	20	12	10	50.5	50.6	65	80
K12	100.3 x 100.2 x 5.86	17.0	50.0 x 50.0 x 4.94	10.1	0.5	20	12	10	50.5	50.6	64	81
K13	99.9 x 100.2 x 6.00	16.7	50.1 x 50.0 x 4.94	10.1	0.5	7	12	9	49.7	49.5	65	80
K14	99.9 x 100.1 x 5.82	17.2	50.1 x 50.1x 4.95	10.1	0.5	20	12	11	49.4	49.5	65	81
K15	99.9 x 100.4 x 5.60	17.8	50.2 x 50.2 x 4.85	10.4	0.5	5	11	9	49.5	49.5	65	81
K16	100.2 x 100.1 x 5.60	17.9	50.1 x 50.1 x 4.90	10.2	0.5	18	11	9	49.4	49.6	64	80
K17	100.1 x 100.3 x 7.73	12.9	50.2 x 50.1 x 4.70	10.7	0.5	6	16	10	49.7	49.6	64	80
K18	100.1x 100.2 x 5.76	17.4	50.2 x 50.2 x 4.70	10.7	0.5	1	13.5	11.5	50.0	50.3	66	81
K19	100.1 x 99.8 x 5.75	17.4	50.1 x 50.1 x 4.65	10.7	0.5	18	13.5	11.5	499	50.2	66	80
K20	100.2 x 100.4 x 5.93	16.9	49.7 x 50.1 x 4.80	10.6	0.5	5	10	7.5	50.5	50.1	66	78
K21	100.1 x 99.9 x 5.75	17.4	50. 1x 49.9 x 4.90	10.2	0.5	9	13.5	11.5	50.5	50.4	65	79
K22	99.9 x 100.3 x 5.97	16.7	49.7 x 50.1 x 5.00	9.9	0.5	9	10	7.5	50.4	50.7	67	81
K23	100.1 x 100.2 x 5.95	16.8	49.6 x 50.2 x 4.90	10.1	0.5	8	10	7.5	50.6	50.4	66	80
K24	100.3 x 100.3 x 6.09	16.5	49.8 x 50.2 x 4.80	10.4	0.5	3.5	10	7.5	50.4	50.3	66	81
K25	99.9 x 100.2 x 7.50	13.3	49.6 x 50.4 x 5.00	9.9	0.5	7	15.5	7.5	50.6	50.1	66	80
K26	149.8 x 150.3 x 9.85	15.2	80.1 x 80.1 x 5.83	13.7	0.53	9	25	15	50.3	49.7	110	125
K27	149.9 x 150.2 x 9.86	15.2	80.2 x 80.2 x 5.93	13.5	0.53	10	25	15	50.0	50.0	100	120
K28	149.7 x 150.4 x 9.84	15.2	79.9 x 80.1 x 5.85	13.7	0.53	8	25	15	50.2	49.8	101	123
K29	150.1 x 150.3 x 9.90	15.2	80.1 x 80.2 x 5.82	13.7	0.53	33	25	15	50.0	50.0	100	120
K30	149.9 x 150.2 x 9.83	15.2	80.2 x 80.1 x 5.92	13.6	0.53	34	25	15	50.2	50.6	100	120
K31	149.9 x 150.1 x 9.84	15.2	79.8 x 79.9 x 5.90	13.5	0.53	12	25	15	50.0	50.5	99	117
K32	149.9 x 150.0 x 9.85	15.2	79.9 x 79.8 x 5.90	13.5	0.53	9	25	15	50.2	50.0	99	118
K33	149.9 x 150.1 x 7.87	19.1	80.2 x 80.1 x 5.90	13.7	0.53	34	20	15	50.4	50.3	99	115
K34	150.2 x 150.4 x 7.84	19.1	80.3 x 80.2 x 5.87	13.0	0.53	8	20	15	50.6	50.2	102	121
K35	150.3 x 150.3 x 7.94	18.9	80.4 x 80.4 x 5.93	13.6	0.53	8	20	15	50.3	50.5	101	123
K36	100.2 x 100.3 x 6.04	16.6	49.9 x 50.1 x 4.90	10.2	0.5	18	10	7.5	50.2	50.3	66	81
K37	150.1 x 150.3 x 5.94	25.3	80.2 x 80.3 x 5.90	13.6	0.53	35	14	15	50.5	50.4	96	120
K38	150.1 x 150.1 x 5.90	24.4	80.3 x 80.2 x 5.90	13.6	0.53	9	14	15	50.4	50.2	97	122
K39	150.3 x 150.4 x 5.90	25.5	80.3 x 80.2 x 5.90	13.6	0.53	10	14	15	50.6	50.3	98	123
K40	150.2 x 150.2 x 5.92	25.4	100.3 x 100.1 x 5.85	17.2	0.67	12	14	15.5	44.0	44.5	118	155
K41	150.3 x 150.2 x 7.86	19.1	100.3 x 100.2 x 5.81	17.3	0.67	14	20	15.5	44.2	45.0	120	154

Table 4-3. Dimensions for X-joints tested at LUT.

Specimen Id	Chord			Braces			Joint	
	b_0 x h_0 [mm]	R_0 [mm]	r_0 [mm]	b_1 x h_1 [mm]	R_1 [mm]	r_1 [mm]	b_w*) [mm]	h_w *) [mm]
X3A	100.2x100.3x7.82	21.5	13.9	100.2x100.3x7.82	21.5	13.9	-	120.5
X3B	100.2x100.3x7.82	21.5	13.9	100.2x100.3x7.82	21.5	13.9	-	124.7
X4	100.2x100.3x7.82	21.5	13.9	100.2x100.3x7.82	21.5	13.9	-	125.2
X6	99.8x99.8x7.66	10.4	5.3	99.8x99.8x7.66	10.4	5.3	-	122.5
X8	99.8x99.9x7.65	17.0	11.6	99.8x99.9x7.65	17.0	11.6	-	122.5
X13	99.8x99.9x10.06	26.2	19.0	99.8x99.9x10.06	26.2	13.9	-	124.7
X18	99.8x99.9x9.93	26.2	19.0	99.8x99.9x9.93	26.2	19.0	-	123.5
X19	99.8x99.9x9.97	26.2	19.0	99.8x99.9x9.97	26.2	19.0	-	124.7
X20	99.8x99.9x9.97	26.2	19.0	50.0 x50.3x4.90	9.6	6.3	63.3	67.5
X21	99.8x99.9x9.97	26.2	19.0	50.0 x50.3x4.91	9.6	6.3	63.5	66.5
X22	99.9x99.8x9.51	10.5	4.8	99.9x99.8x9.51	10.5	4.8	-	118.7
X23	99.9x99.8x9.49	10.5	4.8	50.5 x50.3x4.84	5.7	3.1	66.0	65.5
X24	99.8x100.1x9.85	18.6	12.7	99.8 x100.1x9.85	18.6	12.7	-	127.7
X25	99.8x100.1x9.77	18.6	12.7	50.1 x50.2x4.76	9.3	6.3	66.5	70.0
X26	100.2x100.3x7.81	21.5	13.9	100.2x100.3x7.81	21.5	13.9	-	125.5
X27	100.2x100.3x7.81	21.5	13.9	50.0 x50.3x4.90	9.6	6.3	68.2	70.7
X28	100.5x100.3x5.83	12.0	8.3	100.5 x100.3x5.83	12.0	8.3	-	117.5
X29	100.5x100.3x5.83	12.0	8.3	50.0 x50.3x4.90	9.6	6.3	65.0	69.0.
X30	150.1x150.0x12.63	32.8	25.5	80.1 x80.2x5.82	12.3	8.5	98.7	102.7
X32	149.9.1x150.4x9.79	24.3	18.0	80.4 x80.4x5.82	12.3	8.5	99.5	103.7

*) b_w and h_W are distances between from weld toe to weld toe relating to width and length of the joint area.

Table 4-4. Dimensions X-joint tests tested at University of Pisa.

Test	Main parameters					Special variables				Failure (EC3)	Notes
	Chord		Braces		Joint	Conditions		Materials			
	b_0xh_0xt_0	b_0/t_0	b_1xh_1xt_1	b_1/t_1	$\beta=b_1/b_0$	T	F_{chord}	Type	C_{eqv}	W=Web F=Flange B = brace	
1	100.2×100.0×7.9	12.5	50.0×50.1×4.9	10	0.5	+20	No	CFSHS	<0.4	F	
2	99.9×100.1×8.0	12.5	70.2×70.1×4.8	14	0.7	+20	No	CFSHS	<0.4	F	
5	100.0×100.3×8.1	12.5	49.9×50.0×5.0	10	0.5	+20	No	HFSHS	<0.4	F	
7	100.1×100.0×7.9	12.5	50.1×50.0×5.1	10	0.5	+20	No	CFSHS	>0.4	F	
9	100.1×100.3×5.9	16.7	50.0×49.8×5.0	10	0.5	+20	No	CFSHS	<0.4	F	K-joint chord
10	100.0×100.3×5.9	16.7	100.1×100.2×5.9	16.7	1.0	+20	No	CFSHS	<0.4	W	F_u= 860 kN
11	100.2×100.0×10.0	10	50.1×50.0×4.9	10	0.5	+20	No	CFSHS	<0.4	F	
12	100.0×100.1×10.2	10	49.8×50.1×4.8	10	0.5	+20	No	HFSHS	<0.4	F	
14	100.0×100.1×5.9	20	70.2×70.1×2.9	23.3	0.7	+20	No	CFSHS	<0.4	F	F_u= 240 kN
15	100.2×100.1×5.8	20	100.1×100.1×4.0	25	1.0	+20	No	CFSHS	<0.4	B	
16	100.0×99.9×5.8	20	100.1×100.2×4.9	20	1.0	+20	No	CFSHS	<0.4	B/W?	F_u= 800 kN
17	100.1×100.3×6.2	20	100.0×100.2×6.2	16.7	1.0	+20	No	HFSHS	<0.4	W	See X10

4.3.2 Test set up

The statically illustration of test arrangement for K- and X-joints are seen in Figure 4-3. The special test parameters are seen in Table 4-5 and Table 4-6. The test arrangement for K- and X-joint can be seen in Figure 4-4 for LUT tests and in Figure 4-5 for University of Pisa tests.

In both cases the low temperatures are arranged by circulating a coolant inside the test specimens. The test specimen is isolated by a mat made of plastic foam. This makes the installation of measuring devices rather difficult as well the observation of the joint behaviour during the test. The test specimens are instrumented by strain gauges and by local and global displacement transducers.

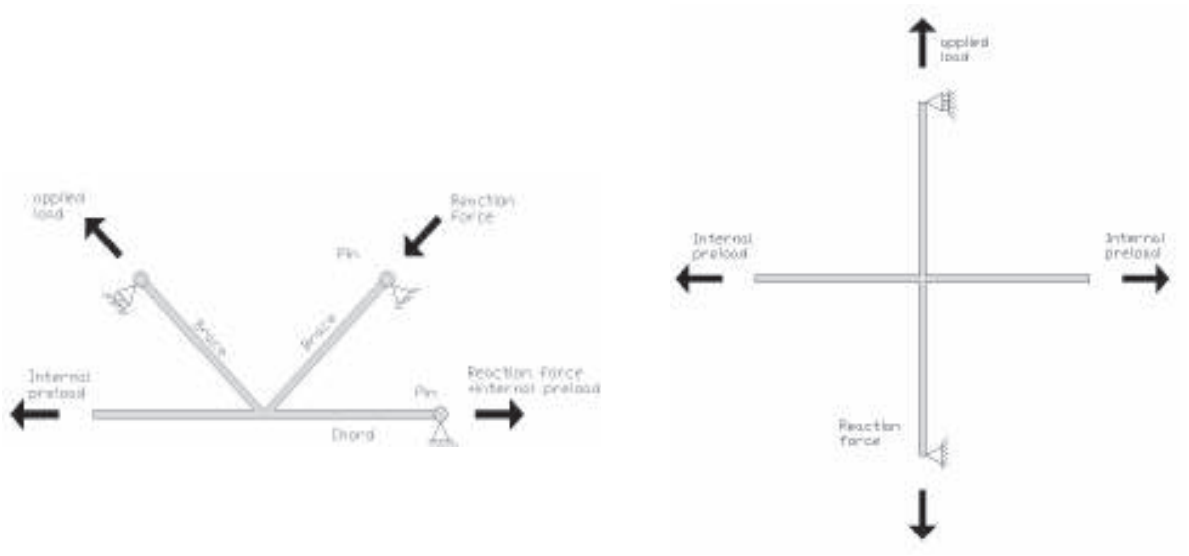

Figure 4-3. Statical description of test set up in K-joint and X-joint test.

Table 4-5. The special test parameters for X-joints tested at LUT.

#	b_o x h_0 x t_0	b_1 x h_1 x t_1	type	Manufac-turer	F_{chord}	T
X3A	100x100x8	100x100x8	CFSHS	A	580/60	+20
X3B	100x100x8	100x100x8	CFSHS	A	580/60	+20
X4	100x100x8	100x100x8	CFSHS	A	0/0	+20
X6	100x100x8	100x100x8	HFSHS	HF	580/60	+20
X8	100x100x8	100x100x8	CFSHS	B	580/60	+20
X13	100x100x10	100x100x10	CFSHS	A	690/60	+20
X18	100x100x10	100 x100x10	CFSHS	A	690/60	-40
X19	100x100x10	100 x100x10	CFSHS	A	690/60	-60
X20	100x100x10	50 x50x5	CFSHS	A	690/60	-40
X21	100x100x10	50 x50x5	CFSHS	A	690/60	-60
X22	100x100x10	100 x100x10	HFSHS	HF	690/60	-40
X23	100x100x10	50 x50x5	HFSHS	HF	690/60	-40
X24	100x100x10	100 x100x10	CFSHS	B	690/60	-40
X25	100x100x10	50 x50x5	CFSHS	B	690/60	-40
X26	100x100x8	100 x100x8	CFSHS	A	580/60	-40
X27	100x100x8	50 x50x5	CFSHS	A	580/60	-40
X28	100x100x6	100 x100x6	CFSHS	A	461/60	-40
X29	100x100x6	50 x50x5	CFSHS	A	461/60	-40
X30	150x150x12.5	80 x80x6	CFSHS	A	1320/60	-40
X32	150x150x10	80 x80x6	CFSHS	A	1120/60	-40

Table 4-6. The special test parameters for K-joints.

#	b_o x h_0 x t_0	b_1 x h_1 x t_1	type	Manufac-turer	F_{chord}	T
K1	100 x 100 x 6	80 x 80 x 5	CFSHS	A	0	+20
K2	100 x 100 x 8	50 x 50 x 5	CFSHS	A	580	-40
K3	100 x 100 x 8	50 x 50 x 5	CFSHS	A	580	-40
K4	100 x 100 x 8	50 x 50 x 5	CFSHS	A	580	-40
K5	100 x 100 x 8	70 x 70 x 5	CFSHS	A	580	-40
K6	100 x 100 x 8	100 x100 x 6	CFSHS	A	0	-40
K7	100 x 100 x 6	50 x 50 x 5	CFSHS	A	460	-40
K8	100 x 100 x 6	50 x 50 x 5	CFSHS	A	460	-60
K9	100 x 100 x 8	50 x 50 x 5	CFSHS	A	580	-60
K10	100 x 100 x 6	50 x 50 x 5	CFSHS	A	0	-60
K11	100 x 100 x 6	50 x 50 x 5	CFSHS	A	460	-60
K12	100 x 100 x 6	50 x 50 x 5	CFSHS	A	460	-40
K13	100 x 100 x 6	50 x 50 x 5	CFSHS	A	460	+20
K14	100 x 100 x 6	50 x 50 x 5	CFSHS	A	460	+20
K15	100 x 100 x 6	50 x 50 x 5	CFSHS	A	460	-40
K16	100 x 100 x 6	50 x 50 x 5	CFSHS	B	460	-40
K17	100 x 100 x 8	50 x 50 x 5	CFSHS	B	580	-60
K18	100 x 100 x 6	50 x 50 x 5	CFSHS	B	460	-20
K19	100 x 100 x 6	50 x 50 x 5	CFSHS	B	460	-20
K20	100 x 100 x 6	50 x 50 x 5	HFSHS	HF	460	-60
K21	100 x 100 x 6	50 x 50 x 5	CFSHS	B	460	+20
K22	100 x 100 x 6	50 x 50 x 5	HFSHS	HF	460	-40
K23	100 x 100 x 6	50 x 50 x 5	HFSHS	HF	460	+20
K24	100 x 100 x 6	50 x 50 x 5	HFSHS	HF	460	-60
K25	100 x 100 x 8	50 x 50 x 5	HFSHS	HF	580	-60
K26	150 x 150 x 10	80 x 80 x 6	CFSHS	A	1100	-60
K27	150 x 150 x 10	80 x 80 x 6	CFSHS	A	1100	+20
K28	150 x 150 x 10	80 x 80 x 6	CFSHS	A	1100	-40
K29	150 x 150 x 10	80 x 80 x 6	CFSHS	A	1100	-60
K30	150 x 150 x 10	80 x 80 x 6	CFSHS	A	1100	+20
K31	150 x 150 x 10	80 x 80 x 6	HFSHS	HF	1100	-60
K32	150 x 150 x 10	80 x 80 x 6	HFSHS	HF	1100	+20
K33	150 x 150 x 8	80 x 80 x 6	CFSHS	A	920	-60
K34	150 x 150 x 8	80 x 80 x 6	CFSHS	A	920	-60
K35	150 x 150 x 8	80 x 80 x 6	CFSHS	A	920	+20
K36	100 x 100 x 6	50 x 50 x 5	HFSHS	HF	460	-60
K37	150 x 150 x 6	80 x 80 x 6	CFSHS	A	720	-60
K38	150 x 150 x 6	80 x 80 x 6	CFSHS	A	720	-60
K39	150 x 150 x 6	80 x 80 x 6	CFSHS	A	720	+20
K40	150 x 150 x 6	100 x 100 x 6	CFSHS	A	720	-40
K41	150 x 150 x 8	100 x 100 x 6	CFSHS	A	920	-40

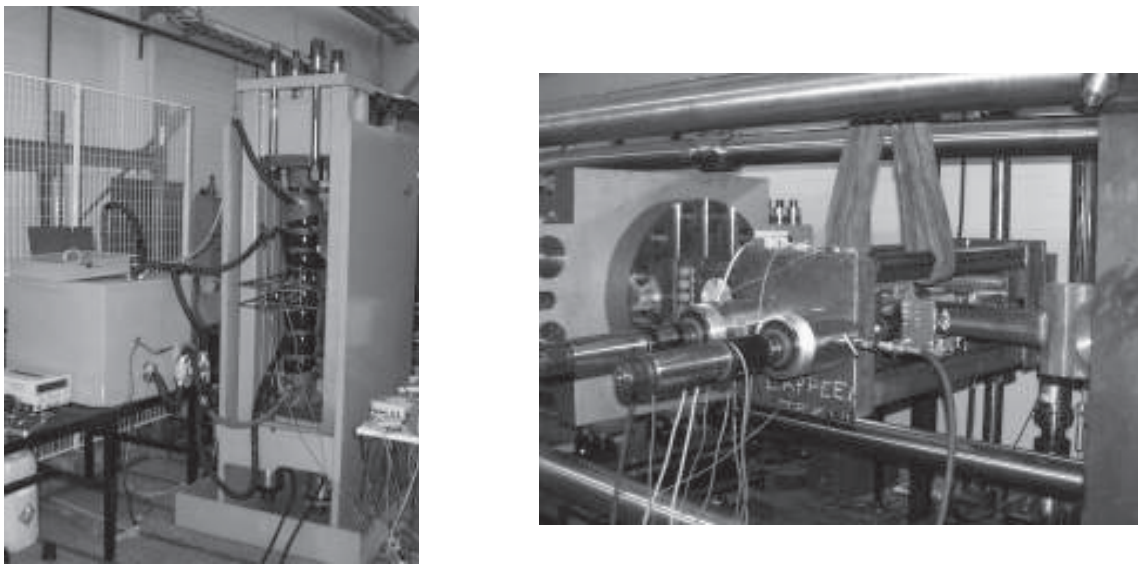

Figure 4-4. Test set up for K- and X-joint tests executed in LUT.

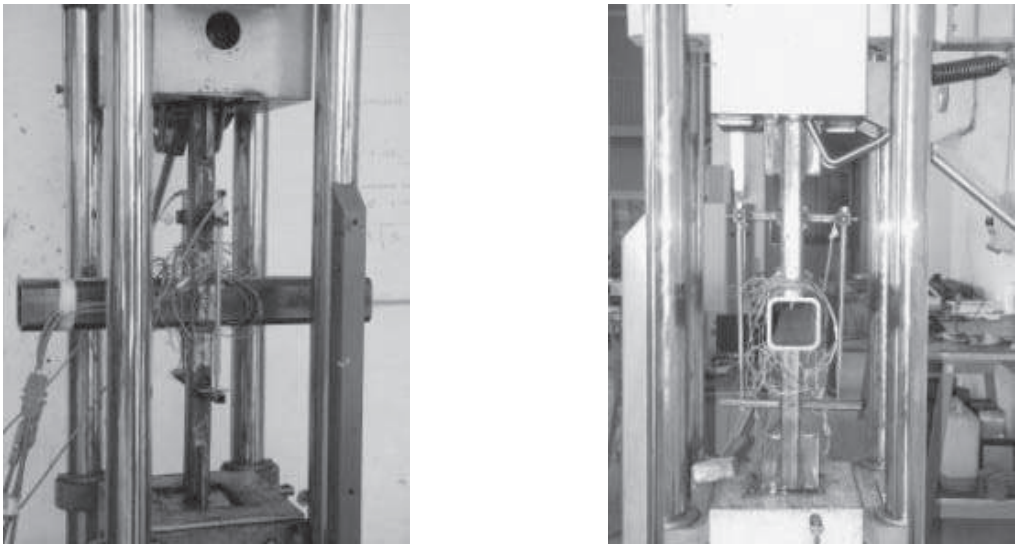

X-joint test arrangement *. Mounting of inductive transducers*

Figure 4-5. Connection details and test set up for X-joint tests executed at University of Pisa.

4.4 Test Results

A typical test result for K-joint (22) is seen in Figure 4-6, where the displacements perpendicular to the chord and the displacement in the end of tension brace versus the applied load are illustrated. Based on the simple drawing method the ultimate load F_u and the plastic deformation δ_p are presented as well. In Figure 4-7 is illustrated the same diagram for a X-joint X6. The three common failure mode are seen in Figure 4-8 for K- and X-joints.

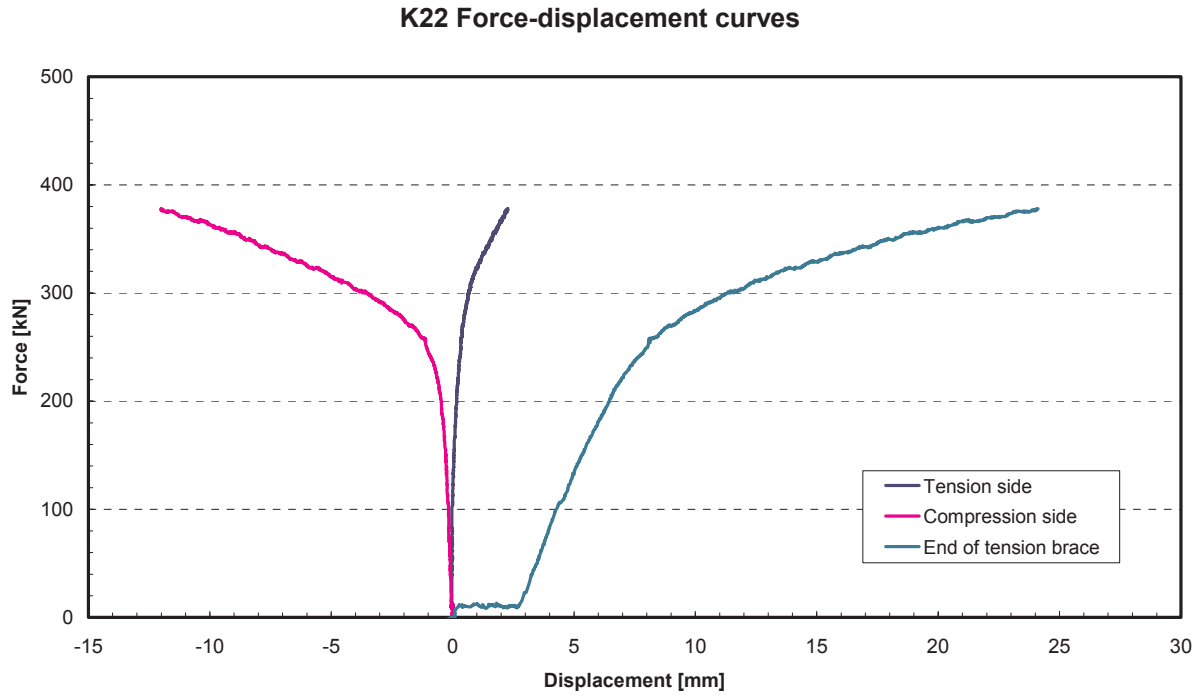

Figure 4-6. Force-displacement curves for a K-joint K22.

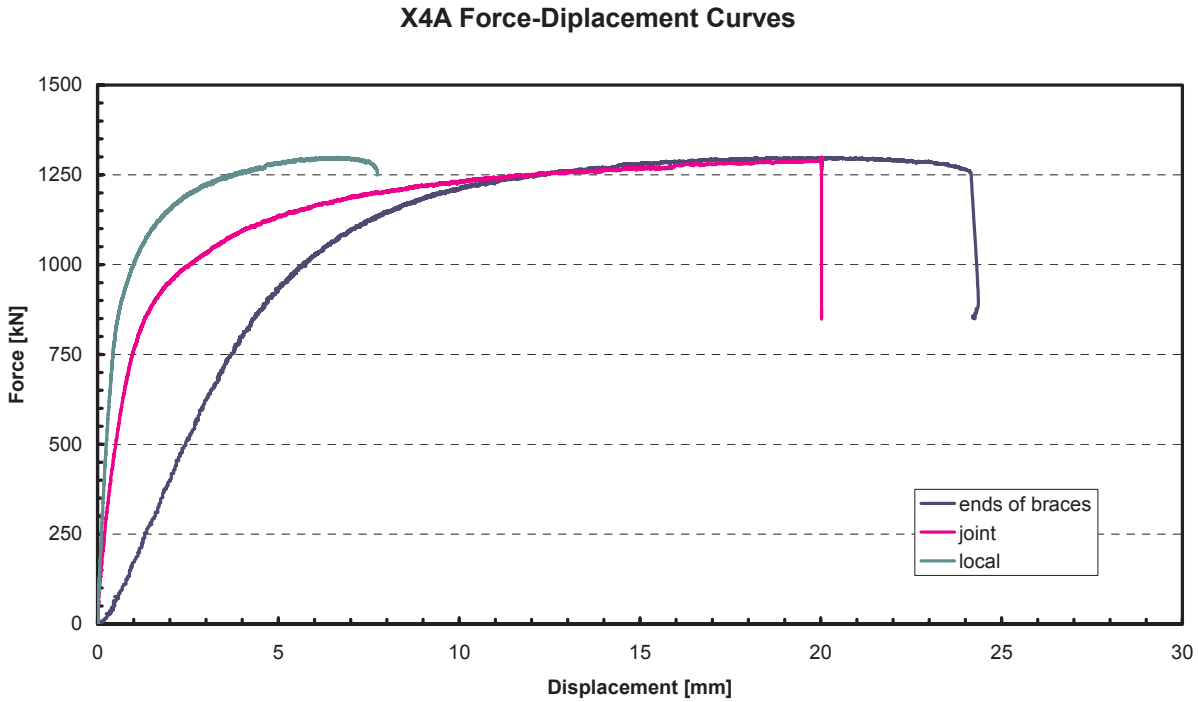

Figure 4-7. Force-displacement curves for X –joints X4A.

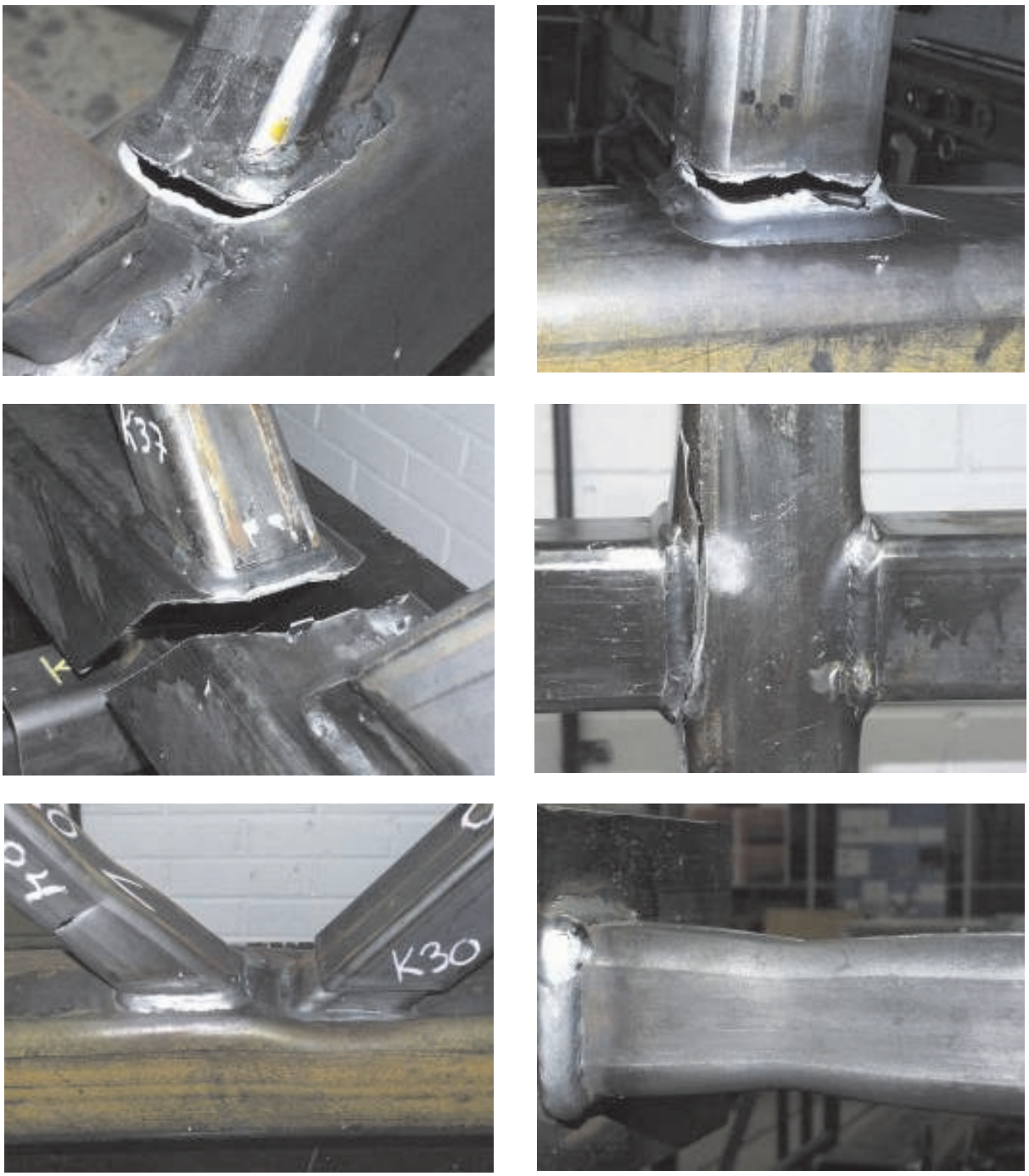

Figure 4-8. Typical failures for K- (left) and X-joint (right side). Failure mode can be ductile or partly brittle.

In the following Tables 4-7 and 4-8 different tests are compared to each other to highlight some relationships or influences of effect of low temperature and differences between cold formed and hot-formed sections.

Table 4-7. Influence of low temperature on the load resistances.

Test	$b_0 \times h_0 \times t_0$ *[mm]*	$b_1 \times h_1 \times t_1$ *[mm]*	b_0/t_0	b_1/t_1	$\beta = b_1/b_0$	*Type*	*T [°C]*	F_{chord} *[kN]*	N_1 *[kN]*	δ_p/b_o [%]	*Failure mode*
1	100×100×8	50×50×5	12.5	10.0	0.5	CF	+20	0.00	447	6	B
27							-40	580	373	3	B
3-B	100×100×8	100×100×8	12.5	12.5	1.0	CF	+20	580	1368	4.5	B
4							+20	0.0	1295	9	C
26							-40	580	1516	8	C [1]
11	100×100×10	50×50×5	10.0	10.0	0.5	CF	+20	0.0	400	1.5	B
20							-40	690	455	1.5*	B
21							-60	690	468	1.5*	B
12	100×100×10	50×50×5	10.0	10.0	0.5	HF	+20	0.0	415	7*	B
23							-40	690	400	3.5	B
13	100×100×10	100×100×10	10.0	10.0	1.0	CF	+20	690	1602	2*	B
18							-40	690	1750	2.5*	B
19							-60	690	1844	3*	B
10	100×100×6	100×100×6	16.7	16.7	1.0	CF	+20	0.0	840	2	C
28							-40	461	1140	4.5	C
9	100×100×6	50×50×5	16.7	10.0	0.5	CF	+20	0.0	212	3.5	C
29							-40	461	271	5	C

[1] 45° crack in chord web.

* marked sections did not fail from joint but from members. B is brace failure and C chord failure.

Table 4-8. Influence of manufacturing method on the load resistances.

Test	$b_0 \times h_0 \times t_0$ *[mm]*	$b_1 \times h_1 \times t_1$ *[mm]*	b_0/t_0	b_1/t_1	$\beta = b_1/b_0$	*T [°C]*	*Type*	F_{chord} *[kN]*	N_1 *[kN]*	δ_p/b_o [%]	*Failure mode*
1	100×100×8	50×50×5	12.5	10.0	0.5	+20	CF	0.0	447	6	B
5							HF	0.0	368	9	C flan
3-B	100×100×8	100×100×8	12.5	12.5	1.0	+20	CF	580	1368	4.5	B
4							CF	0.0	1295	9	C
6							HF	580	1306	6	C flan
11	100×100×10	50×50×5	10.0	10.0	0.5	+20	CF	0.0	400	1.5	B
12							HF	0.0	415	7*	
10	100×100×6	100×100×6	16.7	16.7	1.0	+20	CF	0.0	840	2	C flan
17							HF	0.0	978	3	B
18	100×100×10	100×100×10	10.0	10.0	1.0	-40	CF	690	1750	2.5*	B
22							HF	690	1720	6.5	B
20	100×100×10	50×50×5	10.0	10.0	0.5	-40	CF	690	455	1.5*	B
23							HF	690	400	3.5	B

* marked sections did not fail from joint but from members. B is brace failure and C chord failure.

Following conclusion may be drawn:

- Decrease of testing temperature seems to increase resistance of the X-joint but also in most of the cases the deformation capacity of X-joint.

- The resistance in the X-joint tests for hot formed and cold formed is of same magnitude thus some deviation may be seen from the results. The deformation capacity don't show clear tendency while some cold formed joints did not fail from the joint but form the member.

4.5 Evaluation of test results

The theoretical capacities for each joint are calculated according Eurocode 3, Part 1.8. Because the chord loading is tension, the tensile brace loading capacity can be find by the any of following formulas obtaining the lowest capacity for the K-joints:

$$F_y = \frac{8.9 \cdot f_{y,0} \cdot t_0^2}{\sin\theta_1}\left[\frac{b_1+b_2}{2b_0}\right] \cdot \sqrt{\frac{b_0}{2t_0}} \qquad \text{if flange of the chord is critical (F)} \qquad (4\text{-}1)$$

$$F_y = \frac{f_y \cdot t_0}{\sqrt{3} \cdot \sin\theta_1}\left[2h_0 + \sqrt{\frac{1}{1+\frac{4g^2}{3t_0^2}4}} \cdot b_0\right] \qquad \text{if the web of the chord is critical (W)} \qquad (4\text{-}2)$$

$$F_y = f_y \cdot t_1\left[2h_1 - 4t_1 + b_1 + b_{eff}\right] \qquad \text{if the brace is critical (B)} \qquad (4\text{-}3)$$

$$\text{where} \quad b_{eff} = \frac{10b_1 \cdot t_0^2 \cdot f_{y,0}}{b_0 \cdot t_1 \cdot f_{y,1}} \le b_1 \qquad (4\text{-}4)$$

And for X-joints, respectively:

$$F_y = \frac{f_y \cdot t_0^2}{(1-\beta)\sin\theta}\left[\frac{2\eta}{\sin\theta} + 4\sqrt{1-\beta}\right] \qquad \text{if flange of the chord is critical (F) and } \beta \le 0.85 \qquad (4\text{-}5)$$

$$F_y = \frac{f_y \cdot t_0}{\sin\theta}\left[\frac{2h_1}{\sin\theta} + 10t_0\right] \qquad \text{if the web of the chord is critical (W) and } \beta = 1.00 \qquad (4\text{-}6)$$

$$F_y = f_y \cdot t_0\left[2h_1 - 4t_1 + 2b_{eff}\right] \qquad \text{if the brace is critical (B) and } \beta > 0.85 \qquad (4\text{-}7)$$

$$\text{where} \quad b_{eff} = \frac{10b_1 \cdot t_0^2 \cdot f_{y,0}}{b_0 \cdot t_1 \cdot f_{y,1}} \le b_1 \qquad (4\text{-}8)$$

Failure of specimen can occur in four different places:

- Failure of a brace member (B);
- Failure in the flange of a chord (F);
- Failure of a chord member (C) and
- Failure in the web of a chord member (W).

In Table 4-9. are seen the test results for K-joint tests and the theoretical capacities based on measured joint geometry and nominal yield strength. The capacity based on real yield strength and an informal ultimate capacity based on ultimate strength is presented as well.

In the most tests the primary failure mode was ductile (d) except in one test K31 it was brittle (b). In several cases a ductile primary failure mode was followed by brittle (b) type secondary failure. This is presented by the symbol d→b in table 4-5. In some early tests the buckling (bc) of compression member (local or global) was the critical mode.

In Tables 4-10 and 4-11 are presented the results for X-joints, respectively.

Table 4-9. Test results for K-joints.

Id. number	Test				Eurocode 3, Part 1.8				Comparison		
	δ_p/bo [%]	F_u [kN]	Ftest 3 % kN]	failure mode	$F_{y,355}$ [kN]	$F_{y,02}$ [kN]	F_u [kN]	failure mode	$\frac{F_{u,test}}{F_{y,355}}$	$\frac{F_{u,test}}{F_{y,0.2}}$	$\frac{F_{u,test}}{F_{u,cal}}$
K1	0.5*	670		B, bc	365	504	589	F	1.83	1.33	1.14
K2	1.0*	465		B, d→b	293	418	453	F≈B	1.59	1.11	1.03
K3	1.5*	485		B, d	294	420	455	F≈B	1.65	1.15	1.07
K4	1.5*	490		B, d	325	420	455	F≈B	1.67	1.16	1.08
K5	0.1*	606		B, bc	434	-	-	B	1.39	-	-
K6	0.0*	999		W, d	573	838	981	W	1.74	1.19	1.02
K7	1.5	365		F, d	210	308	360	F	1.74	1.19	1.01
K8	1.5	388		C, d→b	208	332	366	F	1.86	1.17	1.06
K9	1.0	517		B, d	320	461	531	F	1.61	1.12	0.97
K10	2.8	426		F, d→b	207	330	364	F	2.06	1.29	1.17
K11	2.5	432		C, d→b	210	301	348	F	2.05	1.43	1.24
K12	3.0	424		F, d	205	283	327	F	2.07	1.50	1.30
K13	2.0	356		F, d	216	296	346	F	1.65	1.20	1.03
K14	3.0	408		F, d	207	270	299	F	1.97	1.51	1.37
K15	1.8	376		C, d→b	196	231	323	F	1.92	1.63	1.16
K16	1.8	344		C, d→b	195	231	323	F	1.76	1.49	1.06
K17	1.0*	540		B, d	316	501	548	F≈B	1.71	1.08	0.99
K18	4.0	455	426	B, d	202	307	370	F	2.11	1.39	1.15
K19	4.1	441	432	F, d	234	355	428	F	1.85	1.22	1.01
K20	1.5	367		F, d→b	209	302	364	F	1.76	1.21	1.01
K21	3.0	412		F, d	200	292	350	F	2.06	1.41	1.18
K22	2.0	378		F, d	211	290	350	F	1.79	1.30	1.08
K23	1.8	329		F, d	209	269	327	F	1.57	1.22	1.01
K24	1.4	349		F, d→b	218	316	380	F	1.60	1.11	0.92
K25	1.5	495		F, d	297	410	500	F≈B	1.67	1.21	0.99
K26	1.6	944		C, d→b	588	813	919	F	1.61	1.16	1.03
K27	0.9*	918		B, d	592	698	793	F	1.55	1.31	1.16
K28	3.3	1016	974	F, d	587	723	881	F	1.66	1.35	1.10
K29	2.7	1000		C, d→b	595	822	929	F	1.68	1.22	1.08
K30	2.7*	915		B, d	587	693	787	F	1.56	1.32	1.16
K31	0.2	564		C, b	587	710	920	F	0.96	0.79	0.61
K32	3.0	808		F, d	587	603	828	F	1.38	1.34	0.98
K33	0.7	503		C, d→b	419	613	707	F	1.20	0.82	0.71
K34	0.2	540		C, d→b	416	608	701	F	1.30	0.89	0.77
K35	3.3	733	723	B, d	426	558	632	F	1.70	1.29	1.14
K36	2.8	379		F, d	216	313	377	F	1.76	1.21	1.01
K37	2.0	534		C, d→b	275	432	484	F	1.94	1.24	1.10
K38	2.0	589		C, d→b	272	428	479	F	2.16	1.38	1.23
K39	1.7	508		F, d	271	378	424	F	1.87	1.35	1.20
K40	0.08	730		F, d	379	551	645	F	1.93	1.33	1.13
K41	0.05	965		C, d→b	578	823	921	F	1.67	1.17	1.05
								Average	1.72	1.24	1.06
								Stdev.	0.25	0.17	0.14

* The joint did not fail but the member in tension broke.

Table 4-10. Test results of X-joints tested at LUT.

Id. number	Test				Calculation F EC3				Comparison			
	$\frac{\delta_p}{bo}$ [%]	ultimate load F_u [kN]	load related to 3 % [kN]	failure mode W=web B= Brace F=Flange	$F_{y,355}$ [kN]	$F_{y,02}$ [kN]	F_u [kN]	failure mode W=web B=brace F=flange	$\frac{F_{u,test}}{F_{y,355}}$	$\frac{F_{u,test}}{F_{y,0.2}}$	$\frac{F_{u,test}}{F_u}$	$\frac{F_{u,test3\%}}{F_u}$ or $\frac{F_{u,test}}{F_u}$
X3A	1.5	1142		W/d	772	1027	1125	W	1.48	1.11	1.02	1.02
X3B	4.5	1368	1319	B/d	772	1027	1125	W	1.77	1.33	1.22	1.17
X4	9	1295	1164	W/d	772	1027	1125	W	1.68	1.26	1.15	1.04
X6	6	1306	1139	W/d	752	901	1131	W	1.74	1.45	1.15	1.01
X8	4	1388	1362	W/d	751	1020	1144	W	1.85	1.36	1.21	1.19
X13	2*	1602		B/d	1074	1340	1488	W	1.49	1.20	1.08	1.08
X18	2.5*	1750		B/d	1068	1408	1657	W	1.64	1.24	1.06	1.06
X19	3*	1844	1798	B/d	1061	1509	1733	W	1.74	1.22	1.06	1.04
X20	1.5*	455		B/d	273	360	423	F	1.67	1.26	1.08	1.08
X21	1.5*	468		B/d	270	384	441	F	1.73	1.22	1.06	1.06
X22	6.5	1720	1507	W/d→b	994	1187	1570	W	1.73	1.45	1.10	0.96
X23	3.5	400	392	B/d	245	293	387	W	1.63	1.37	1.03	1.01
X24	3.5*	2025	2003	B/d→b	1044	1467	1780	W	1.94	1.38	1.14	1.13
X25	2	495		B/d→b	264	370	449	F	1.88	1.34	1.10	1.10
X26	8	1516	1437	W/d→b	769	1089	1223	W	1.97	1.39	1.24	1.17
X27	3	373		B/d→b	165	233	263	F	2.26	1.60	1.42	1.42
X28	4.5	1140	1088	W/d→b	535	770	887	W	2.13	1.48	1.29	1.23
X29	5	271	220	F/d	92	133	153	F	2.95	2.04	1.77	1.44
X30	3.5	931		B/d→b	459	631	723	F	2.02	1.47	1.28	1.28
X32	5	728	587	B/d→b	275	339	413	F	2.63	2.13	1.75	1.42
								Average	**1.90**	**1.42**	**1.21**	**1.15**
								Stdev.	**0.37**	**0.26**	**0.21**	**0.15**

* The joint did not fail but the member in tension broke.

In Figure 4-9 the relative capacities (a test value divided by a theoretical value) for K- and X-joints are illustrated.

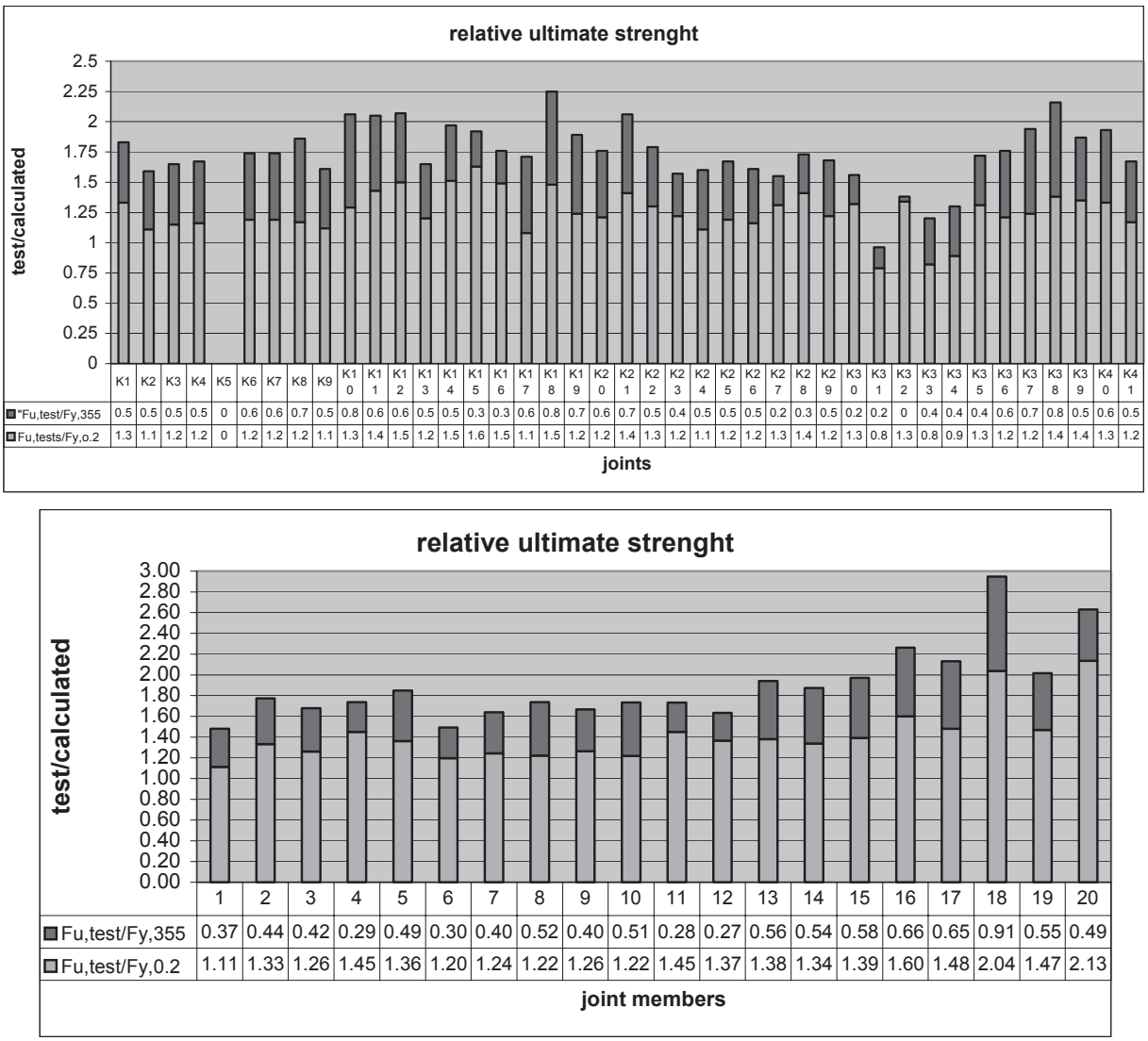

Figure 4-9. Relative strength (= $F_{test}/F_{calculated}$) of the K- (upper) and X-joints (lower).

Table 4-11. Comparison of experimental and theoretical resistances at the room temperature.

Test N.	Location of failure at test	EC3 Failure mode	δ_p/bo [%]	P_u [kN]	$N_{1,Rd}$ [kN]	$\frac{P_u}{N_{1,Rd}}$
1	brace	chord flange	6	447.0	174.0	2.57
2	brace	chord flange	3	561.2	320.2	1.75
5	chord flange	chord flange	9	368.1	174.0	2.12
7	brace+chord flange	chord flange	5	409.9	174.0	2.36
9	chord flange	chord flange	3.5	212.0	97.9	2.17
10	chord flange+brace	brace	2	840.2	630.0	1.33
11	brace	chord flange	1.5	399.5	271.8	1.45
12	brace	chord flange	7*	415.2	271.8	1.53
14	brace	chord flange	2.5	315.5	153.0	2.06
15	brace	brace	1.5	687.7	516.4	1.33
16	chord+brace	Brace	2	869.4	574.6	1.51
17	brace	Brace	3	977.6	630.0	1.55

The tests results were analyzed and correlation of different variables to analysis result was studied. Only the b_0/t_0-ratio seems to have clear correlation on the capacity. This correlation is seen in the Figure 4-10.

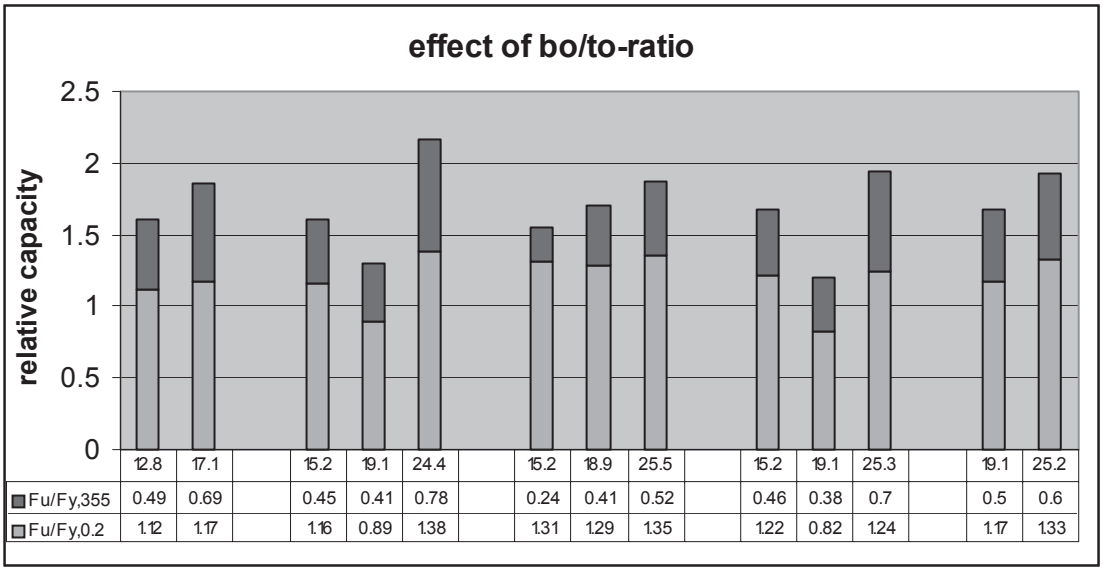

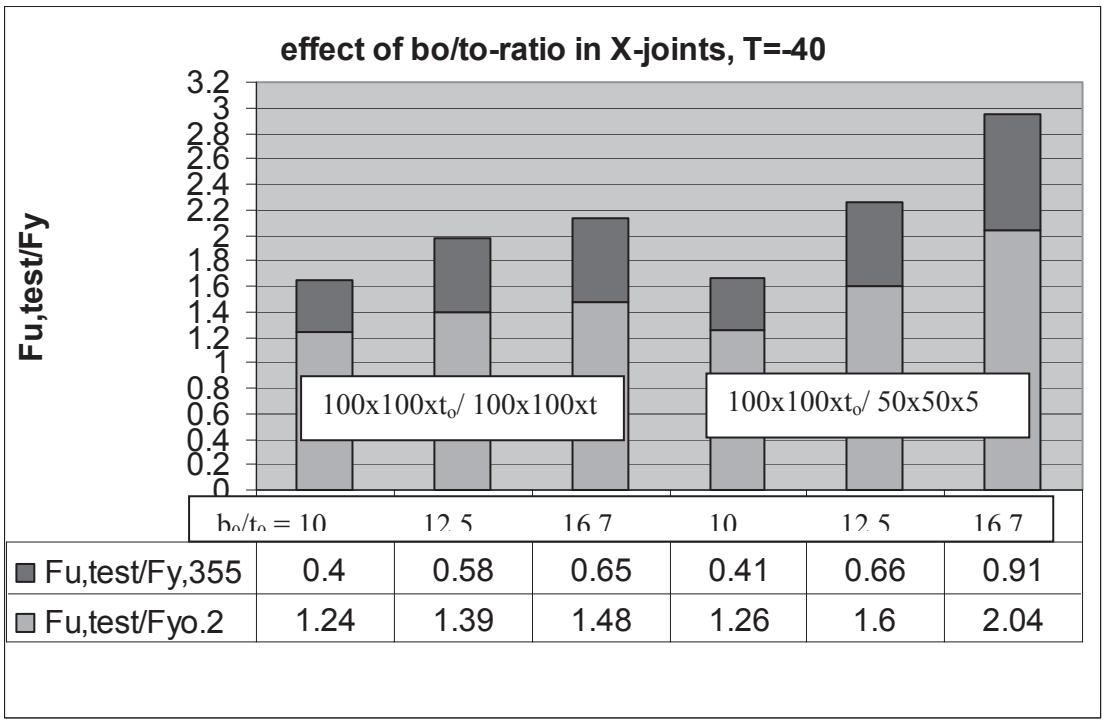

Figure 4-10. Effect of the chord flange slenderness on the load carrying capacity.

However, although the correlation between the flange slenderness and experimental resistance seems to be clear, the membrane effect increases load carrying resistance rather than the degree of cold forming of the chord section. In the K-joints the membrane effect are not so significant than in X-joints. This is due the gap effect, which is more important effect in the K-joints than the membrane effect and will take place independent on the b_0/t_0-ratio.

4.7 Conclusions and recommendation

Main conclusions drawn from tests and their analyses that are valid for both K- and X-joints are:

1. Tested K- and X-joints fulfilled the "generally accepted" requirements for deformation capacity down to –40°C temperatures and most test cases even down to –60°C.

2. Present design rules in Eurocode 3, Part 1.8 to estimate resistance of K- and X-joints are safe and may be used both cold formed and hot formed structural hollow sections.

3. Degree of cold forming defined by *b/t*-ratio seems to be insignificant on the deformation and load carrying capacity of the joints made from CFSHS.

4. The manufacturing method of hollow sections (cold- or hot-formed) does not show significant differences in behaviour down to –40°C test temperatures, when the performance of joints were compared.

Following secondary conclusion and recommendations can be draw from results:

- Good correlation between load carrying capacity of joints and parameters varied in the test programme (material properties and joint geometry) could not be found.

- The small gap size (much smaller than allowed in Eurocode 3, Part 1.8) did not have significant influence on the resistance of K-joints. The limitation could be altered..

- The calculation model predicted well the ultimate failure mode for K-joints (better than for X-joints). Some exceptions were found where two competing theoretical failure modes were close to each other.

- The resistance prediction calculated with the measured ultimate strength of base material matched well with the experimental resistance of tested joint. The results were even better, when the 3 % deformation limit was taken into account, when defined the ultimate capacity from test.

- The decrease of temperature seems to increase the load carrying capacity, when the temperature is decreased from room temperature to –40 C…-60 C, if no brittle failure takes place.

- The primary failure mode was ductile in almost all cases down to –40 C and in most cases down to –60 C followed either by secondary brittle or ductile failure. Only with one hot formed K-joint (K31) the failure mode was fully brittle at–60 C.

- The larger the b_0/t_0-ratio, the bigger the relative load carrying capacity. This is valid especially for X-joints. However, this seems not to be due to the degree of cold forming but rather due to the membrane effect, which takes place more prominent in chord with large slenderness.

- The chord pretension seems to decrease the deformation capacity of the joint.

- The eccentricities of joints were small and seem to have no influence on the joint capacity.

- The weld geometry on the corner area of the chord is important in the case of X-joints, when $\beta=1$. The additional weld passes with smooth surface and less eccentricity introduce considerable more load capacity.

- A good fusion of fillet weld in joint is a very important quality factor especially when wall thickness of chord is remarkable larger than wall thickness of brace member.

5 Extension of applicability of design rules for tubular connections

5.1 Aim of the investigation

Eurocode 3 (prEN1993-1-8: 2003) [5-1] provides design guidelines for rectangular hollow sections joints made of members having b/t ratios smaller than 35. In practice, there is an increasing demand to use more slender sections. These sections are already regulated in technical delivery conditions such as EN 10210 [5-2] or EN 10219 [5-3]. The present product ranges of the manufacturers are however much wider, especially for cold formed sections.

Hollow sections offer a number of favourable characteristics with respect to load carrying capacity and function. Because of its closed shape and the missing definitive strong axis, they possess high torsional stiffness, almost balanced flexural rigidity in all directions and almost equal buckling behaviour about both major axes. Therefore, they are optimally suited for resisting loads in varying directions, which occur for wind or wave loading. In addition to these functional advantages, hollow sections offer attractive scopes for design.

Design rules backed by experimental tests for K-Joints with gap made out of rectangular hollow sections (RHS) are given, for example, in Eurocode 3 [5-1]. Here, the allowable width-thickness ratios of welded RHS K-Joints with gap are limited to 35. In addition to the slenderness limits, Eurocode 3 [5-1] gives a restriction for the gap size.

Table 5-1. Range of validity for welded RHS K joints with gap according to prEN1993-1-8 [5-1].

Braces		**Chord**	**Chord and Braces**		**Gap size**	**Brace Angles**
Compression	Tension	b_0/t_0 and h_0/t_0	h_0/b_0 and $h_{1,2}/b_{1,2}$	$b_{1,2}/b_0$	g	$\Phi_{1.,2}$
$b_{1,2}/t_{1,2} \le 35$ and $h_{1,2}/t_{1,2} \le 35$ and Class 2	$b_{1,2}/t_{1,2} \le 35$ and $h_{1,2}/t_{1,2} \le 35$	≤ 35 and Class 2	≥ 0.5 but ≤ 2.0	≥ 0.35 and $\ge 0.1 + 0.01 \cdot \frac{b_0}{t_0}$	$\ge 0{,}5 \cdot (1-\beta) \cdot b_0$ $\le 1{,}5 \cdot (1-\beta) \cdot b_0$ [1] $\ge t_1 + t_2$	$\begin{cases} \le 60° \\ \ge 30° \end{cases}$
$0{,}6 \le \frac{b_1 + b_2}{2 \cdot b_1} \le 1.3$ [2)]						

Notes: [1] if $g/b_0 > (1-\beta)$ and $g/b_0 > t_1 + t_2$ treat the joint as two separate T or Y joints

Hot finished hollow sections, which were the basis of previous research work, mostly comply with this limiting value (up to 90 % of the sections in EN 10210-2 [5-2]). The cold formed hollow sections conforming to EN 10219-2 [5-3] however often reach values of h/t = 40, even for small sections such as 80 x 40 x 2.0mm.

In practice, there is an increasing demand to use more slender sections for trusses, lattice girders, conservatories, greenhouses and also masts and cranes. These slender sections are also standardised in EN 10219-2 [5-3], the stock lists of the manufacturers giving even more sections outside the allowable limits. The use of these sections is therefore only permissible in many countries (e.g. Germany) by experimental verifications and expert advice, followed by acceptance for individual cases.

5.1.1 Test programme

In Table 5-2, the geometrical dimensions and the geometrical parameters of the test specimens are shown in detail.

The test programme aims to determine the influence of varying parameters on the load carrying behaviour with b_0/t_0-ratios and gap sizes outside the range covered at present. All test specimens possess a symmetrical arrangement of the braces, so that $b_1 = b_{1,2}$; $h_1 = h_{1,2}$; $\Theta_1 = \Theta_{1,2}$ etc. The specimens KJ-01 to KJ-40 are made of steel grade S355, while the specimens KJ-41 to KJ-47 are made of S460.

In addition to the chord slenderness 2γ, Eurocode 3 [5-1] limits the non-dimensional gap size g'_{min} to a lower bound of

$$g' \geq \frac{1}{2} \cdot \left(1 - \frac{b_{1,2}}{b_0}\right) \cdot 2\gamma = g'_{min} \tag{5-1}$$

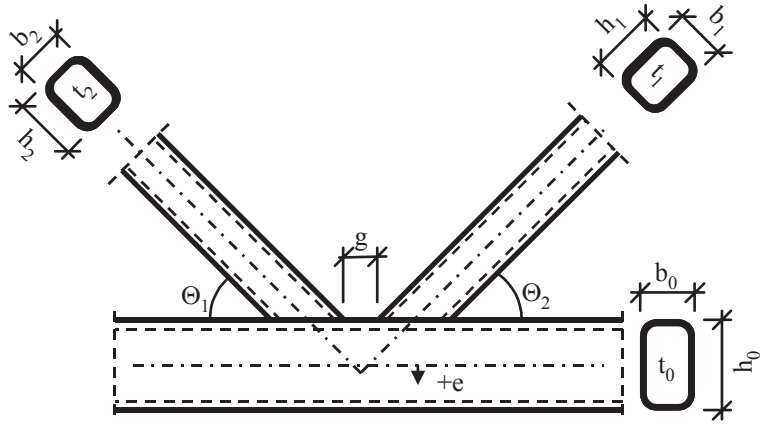

Figure 5-0-1. K -joint geometry.

The fabrication of the welded connections, however, requires a minimum non-dimensional gap size $g'_{min.w}$ of only

$$g' \geq \frac{t_1 + t_2}{t_0} = 2 \cdot \frac{t_{1,2}}{t_0} = 2 \cdot \tau = g'_{min,w} < g'_{min} \tag{6-2}$$

Table 5-2a. Test Programme – nominal dimensions. Specimen KJ01-KJ36.

Nos.	Mat.	Cross sections		Geometry parameters							
		Chord $b_0 \times h_0 \times t_0$ [mm]	Brace $b_{1,2} \times h_{1,2} \times t_{1,2}$ [mm]	β	τ	ξ	2γ	g'	g'_{min} (EC 3)	e/h_0 [mm]	Φ [°]
KJ-01	S355	300x200x6	100x100x6	0.33	1.00	0.24	50	9.76	16.7	0.00	45
KJ-02	S355	300x200x6	150x100x6	0.42	1.00	0.48	50	9.76	12.5	0.00	45
KJ-03	S355	300x200x6	200x100x6	0.50	1.00	0.72	50	9.76	8.33	0.00	45
KJ-04	S355	300x200x6	100x100x6	0.33	1.00	0.16	50	4.00	16.7	-0.09	45
KJ-05	S355	300x200x6	100x100x6	0.33	1.00	0.32	50	8.00	16.7	-0.03	45
KJ-06	S355	300x200x6	100x100x6	0.33	1.00	0.48	50	12.0	16.7	0.03	45
KJ-07	S355	300x200x6	150x100x6	0.42	1.00	0.12	50	4.00	12.5	-0.09	45
KJ-08	S355	300x200x6	150x100x6	0.42	1.00	0.24	50	8.00	12.5	-0.03	45
KJ-09	S355	300x200x6	150x100x6	0.42	1.00	0.36	50	12.0	12.5	0.03	45
KJ-10	S355	300x200x6	200x100x6	0.50	1.00	0.24	50	4.00	8.33	-0.09	45
KJ-11	S355	300x200x6	200x100x6	0.50	1.00	0.16	50	8.00	8.33	-0.03	45
KJ-12	S355	300x200x6	200x100x6	0.50	1.00	0.20	50	12.0	8.33	0.03	45
KJ-13	S355	200x300x6	100x100x6	0.50	1.00	0.20	33	4.00	8.33	-0.22	45
KJ-14	S355	200x300x6	150x100x6	0.63	1.00	0.25	33	4.00	4.17	-0.22	45
KJ-15[3]	*S355*	*200x100x4*	*80x80x3*	*0.40*	*0.75*	*0.30*	*50*	*4.00*	*15.0*	*0.15*	*45*
KJ-16	S355	200x100x4	80x80x4	0.40	1.00	0.20	50	4.00	15.0	0.15	45
KJ-17	S355	200x100x5	80x80x5	0.40	1.00	0.25	40	4.00	12.0	0.17	45
KJ-18	S355	200x100x6	80x80x6	0.40	1.00	0.30	33	4.00	10.0	0.19	45
KJ-19	S355	200x100x4	80x80x3	0.40	0.75	0.46	50	4.00	15.0	0.15	45
KJ-20	S355	200x100x5	80x80x3	0.40	0.60	0.46	40	4.00	12.0	0.17	45
KJ-21	S355	200x100x6	80x80x3	0.40	0.50	0.46	33	4.00	10.0	0.19	45
KJ-22	S355	150x150x4	80x80x3	0.53	0.75	0.15	38	9.22	8.75	0.00	45
KJ-23	S355	150x150x4	80x80x3	0.53	0.75	0.15	38	9.22	8.75	0.00	45
KJ-24[7]	*S355*	*150x150x4*	*80x80x3*	*0.53*	*0.75*	*0.15*	*38*	*9.22*	*8.75*	*0.00*	*45*
KJ-25	S355	120x120x3	80x80x3	0.67	1.00	0.15	40	4.00	6.67	0.02	45
KJ-26	S355	120x120x3	80x80x3	0.67	1.00	0.24	40	4.00	6.67	0.02	45
KJ-27	S355	120x120x3	80x80x3	0.67	1.00	0.48	40	4.00	6.67	0.02	45
KJ-28[4]	*S355*	*120x120x3*	*80x80x3*	*0.67*	*1.00*	*0.72*	*40*	*4.00*	*6.67*	*0.02*	*45*
KJ-29	S355	300x200x6	100x100x6	0.33	1.00	0.24	50	4.00	16.7	0.10	60
KJ-30	S355	300x200x6	100x100x6	0.33	1.00	0.48	50	8.00	16.7	0.21	60
KJ-31	S355	300x200x6	100x100x6	0.33	1.00	0.72	50	12.0	16.7	0.31	60
KJ-32	S355	300x200x6	100x100x6	0.33	1.00	0.16	50	4.00	16.7	-0.18	30
KJ-33	S355	300x200x6	100x100x6	0.33	1.00	0.32	50	8.00	16.7	-0.14	30
KJ-34	S355	300x200x6	100x100x6	0.33	1.00	0.48	50	12.0	16.7	-0.11	30
KJ-35	S355	300x200x6	150x100x6	0.42	1.00	0.24	50	4.00	12.5	0.10	60
KJ-36	S355	300x200x6	150x100x6	0.42	1.00	0.48	50	8.00	12.5	0.21	60

Table 5-2b. Test Programme – nominal dimensions. Specimen KJ37-KJ47.

Nos.	Mat.	Cross sections		Geometry parameters							
		Chord $b_0 \times h_0 \times t_0$ [mm]	Brace $b_{1,2} \times h_{1,2} \times t_{1,2}$ [mm]	β	τ	ξ	2γ	g'	g'_{min} (EC 3)	e/h_0 [mm]	Φ [°]
KJ-37	S355	300x200x6	150x100x6	0.42	1.00	0.72	50	12.0	12.5	0.31	60
KJ-38	S355	300x200x6	150x100x6	0.42	1.00	-0.18	50	4.00	12.5	-0.18	30
KJ-39	S355	300x200x6	150x100x6	0.42	1.00	-0.14	50	8.00	12.5	-0.14	30
KJ-40	S355	300x200x6	150x100x6	0.42	1.00	-0.11	50	12.0	12.5	-0.11	30
KJ-41	S460	200x100x4	80x80x3	0.40	0.75	0.20	50	4.00	15.0	0.15	45
KJ-42	S460	200x100x4	80x80x4	0.40	1.00	0.20	50	4.00	15.0	0.15	45
KJ-43	S460	200x100x5	80x80x5	0.40	1.00	0.25	40	4.00	12.0	0.17	45
KJ-44[5]	*S460*	*200x100x6*	*80x80x6*	*0.40*	*1.00*	*0.30*	*33*	*4.00*	*10.0*	*0.19*	*45*
KJ-45[3]	*S460*	*200x100x4*	*80x80x3*	*0.40*	*1.00*	*0.20*	*50*	*4.00*	*15.0*	*0.15*	*45*
KJ-46	S460	200x100x5	80x80x3	0.40	0.60	0.25	40	4.00	12.0	0.17	45
KJ-47[5]	*S460*	*200x100x6*	*80x80x3*	*0.40*	*0.50*	*0.30*	*33*	*4.00*	*10.0*	*0.19*	*45*

Notes:
1 test stopped before failure, failure mode assumed (see Appendix 3 for details)
2 only strain measurements made and tested only in elastic region
3 different steel grade for the compression brace (S460) and the tension brace (S355)
4 different steel grade for the compression brace (S355) and the tension brace (S460)
5 different wall thickness of compression brace (t_1 = 4 mm) and tension brace (t_2 = 3mm)
6 chord welded in mid of the gap
7 KJ-24 not tested until failure (strain measurement)
the radius specifies the outer corner radius according EN 10219-2

Except for the gap size and the b_0/t_0-ratio, which in Eurocode 3 [5-1] is limited to a maximum of 35, the parameters are within permissible limits.

The test programme provides new knowledge on the load carrying behaviour of slender chord members and small gap sizes. Additionally, these tests can be used to validate FE models to provide a basis for a parameter study. Based on the results of the experimental investigations and FE analyses, an extension of the existing design rules can be made, which include slender chord sections and small gap sizes.

5.2 Test set-up

5.2.1 Test rig, measuring equipment and test set-up

The test rig was designed to comply with the following requirements:

- Carrying capacity up to 100 tonnes (1000 kN).
- Large stiffness, so that the deformations do not significantly influence the measurements.
- Quick assembly, allowing easy transportation and storage.
- Good access to all important locations of the test specimens.
- Adjustable for the different chord- and brace lengths as well as for different brace inclinations.
- Adaptability to the statically system of the test specimen (pinned support of the tension brace and the chord, roller support at the load introduction support).

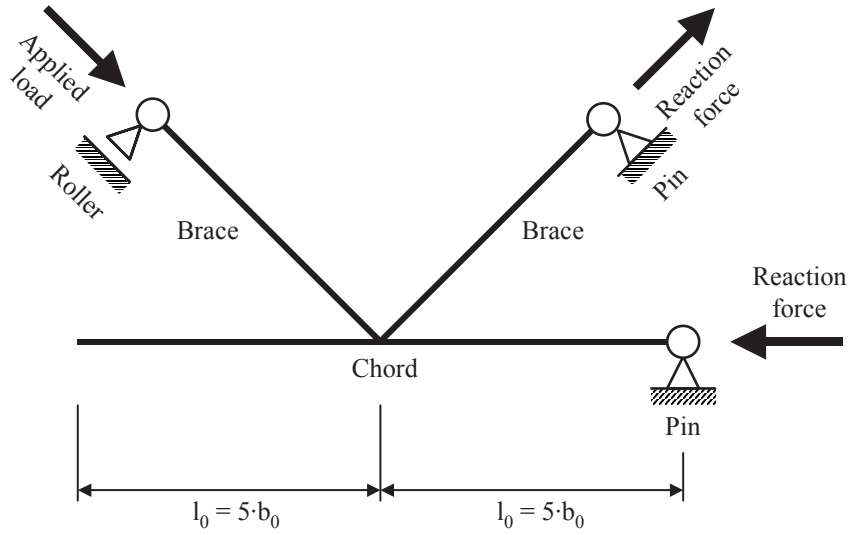

Figure 5-2. Statically system of the test set-up.

The test rig consists of a base (HE 450 M) to which a column (HE 450 M) is rigidly fixed. The load is introduced to the compression brace by a hydraulic jack (1000kN) placed on the base. The adjacent brace is subjected to tension due to reaction forces. The tension brace is attached to a hinge, which is connected by four threaded bolts (M20 – 10.9) and a plate (407x260x30 mm, S460) behind the column. The top of the column is supported by a strut (HE 300 A) with bolts. At the top and opposite side of the column, the chord support (eye bar) is welded on. For test specimens with small dimensions, an additional chord support can be bolted to the column at a lower level.

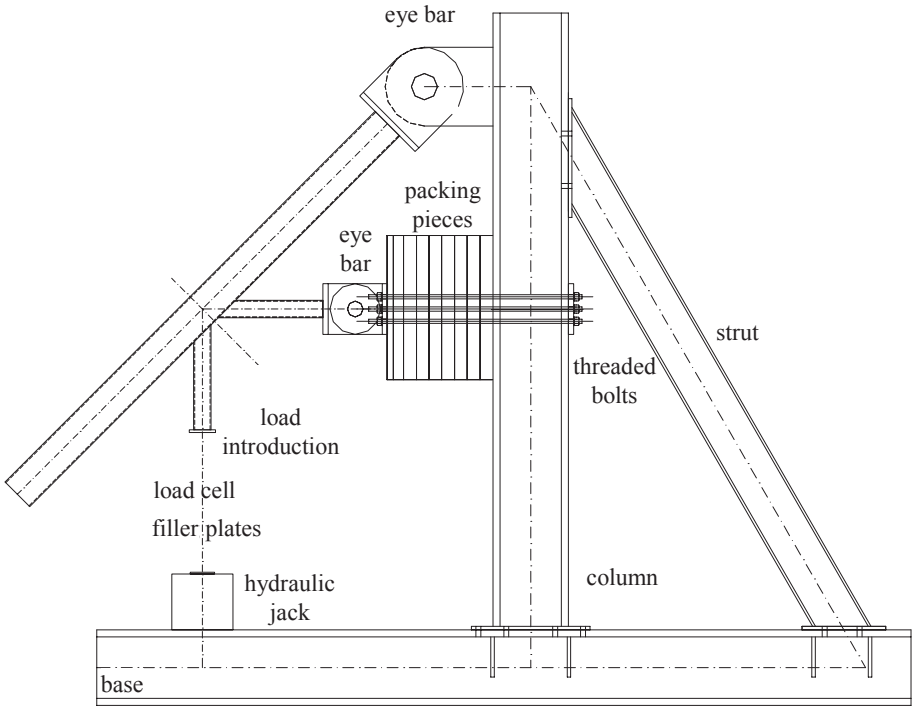

Figure 5-3. Test set-up for large K joints and a brace angle of 45°.

Since the geometrical dimensions of the test specimens are different, the test set-up must be able to accommodate different chord- and brace lengths and varying brace angles too. Therefore, adjustments are made with packing pieces and filler plates. Drawings of the test rig are shown in Appendix 7.

The load is manually introduced by a hydraulic jack (Lukas 1000 kN) as compression load on one brace, so that the other brace is reacted by tension and the chord by compression loading. Due to the height of the main jack in use, some tests (KJ-35 to KJ-40) have had to be carried out with a shorter

jack (Weber). This jack however offers a limited ultimate load (approx. 600 kN) as well as a limited gauge length (approx. 50 mm).

Below the support to the compression brace, a load cell (Hottinger Baldwin, 100 kN) is provided. To record the local displacements, linear voltage displacement transducers (LVDT - Hottinger Baldwin W50) are used. The data acquisition system and measuring amplifier is provided by a SPIDER 8 (Hottinger Baldwin) using CATMAN (Software) Version 3 and 4.

This testing arrangement was chosen because it gives lower (more conservative) ultimate loads than a test set-up with the loaded chord in tension. The supports are provided as hinges so that bending moments are only caused due to eccentricities at the joint and secondary effects.

5.2.2 Load introduction

The first test (KJ-16) was initially begun with a swivel bearing. Because this support allows an easy horizontal shift, it was replaced by a socket support for this specimen (KJ-16).

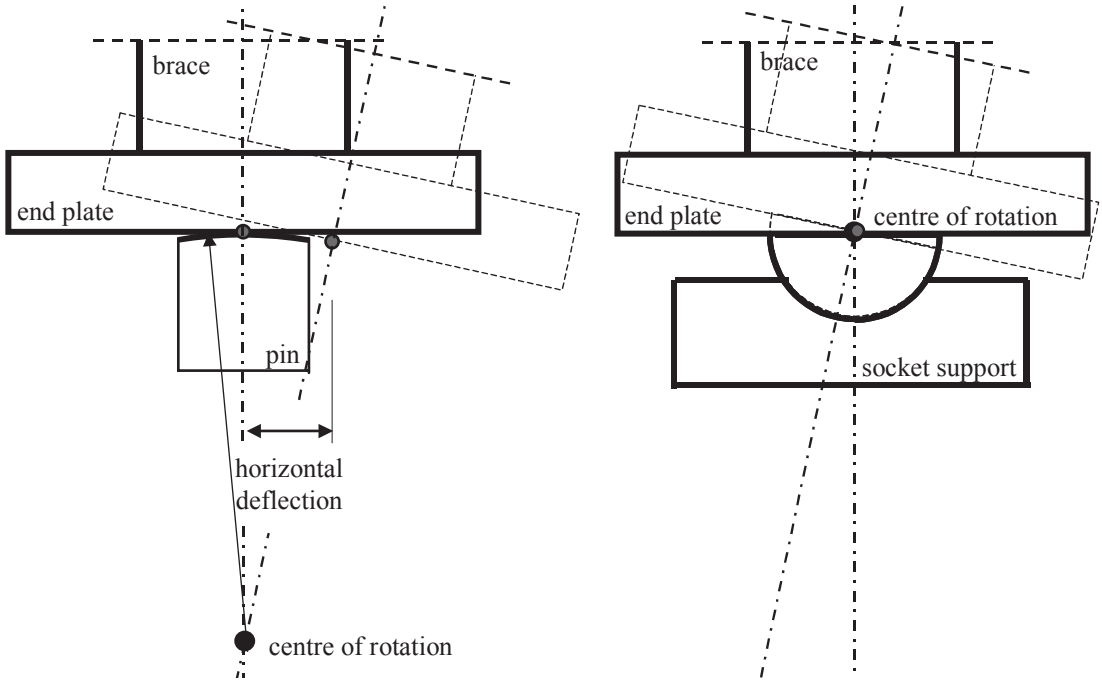

Figure 5-4. Different load introduction used.

The socket support was used for all tests except tests KJ-03, KJ-10, KJ-11 KJ-12 and KJ-14. For these tests, no bearing could be placed due to lack of space, so that the compression brace had to be loaded directly by the jack. An additionally carried out FE analysis were performed for these specimens, which show this does not have a significant influence on results.

5.3 Measuring arrangement and measuring methods

The number of measuring points is limited by the used measuring system (Spider 8), which offers 8 channels for a continuous recording of measurement.

The applied load is recorded using channel 0. Figure 5-5 shows the positions between which the measurements of deformation are taken for the experimental investigations and the algebraic sign defines the direction of the positive local displacement measurements. Furthermore, the relative deformations calculated from the measurements are defined.

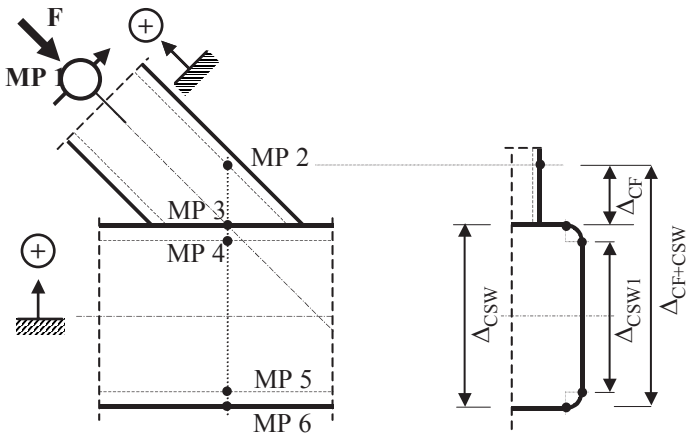

Figure 5-5. Position of the measured points.

The relative displacement Δ_{CF} refers to the chord face deformation. Δ_{CSW} refers to the in-plane deformation of the chord side-wall including any rotation of the corners, while Δ_{CSW1} refers to the chord side-wall in-plane deformation excluding the rotation of the corners and, hence, gives the actual in-plane deformation of the chord side-wall.

For the preliminary test KJ-16, plates at 90° offset to the measurement direction are glued to the measuring points. Because it is difficult to measure at the desired locations exactly, thin pins were glued into superficially drilled holes (∅ 2 mm) for the tests KJ-15 and KJ-17 to KJ-23. At the top of the pins, plates are fixed, to which the LVDTs are attached. This method provides a much more exact determination of the measurements but was changed again, because the measurement error due to a rotation of the measuring points should be minimised. Finally, eyelets were screwed into tapped holes and wires attached. At the end of the wires the LVDTs had been fixed. To optimise the measurements, a steel cored twine (fishing line) was used later.

For the strain measurements, a manual changeover switch was used, because it was sufficient to measure the strains at fixed load steps only.

5.4 Fabrication and geometry of test specimens

For the chord and brace sections, cold formed rectangular hollow sections from Rautaruukki Metform, Finland (manufacturer A) and Voest Alpine, Austria (manufacturer B) are used. The production of the specimens was carried out by Fa. Maurer Soehne, Munich, who have much experience in welding hollow structures.

To avoid end effects, the minimum brace length l_{brace} is fabricated with a length of five times the brace width. The distance to the pinned ends of the chord from the joint is also five times the chord width. Additionally, the brace angles (both braces simultaneously) are varied between 30° and 60°.

In Appendix 6, Figure A6-1 and Figure A6-2, parameterised shop drawings of the joints and the braces can be found. The parameters are listed in Table A6-1 and Table A6-2 and define the dimensions of all braces, the chords and the positions of the braces on the chord of each joint. The weld design and the welding procedure specifications are covered by the shop drawings as well.

The real dimensions of the delivered hollow sections were measured. The mean values of all measured dimensions are given in the Appendix 6, Table A6-3 and Table A6-4 (hollow sections produced by manufacturer A as well as manufacturer B). A check of the marginal deviations according to DIN EN 10219 [5-3] has also been carried out and the results are listed in these tables. The measurements were carried out for the width b and the height h at 5 positions over the length of each hollow section. The outer and inner corner radii r_o and r_i have been determined at both ends and all corners using a radius gage, so that 8 measured values for each hollow section are available in all. Finally, the thickness t has been measured at the ends and on all four side walls. On the side wall with

the seam weld, the thickness was measured on the two sides of the weld. In total, 10 measurements for every hollow section have been carried out.

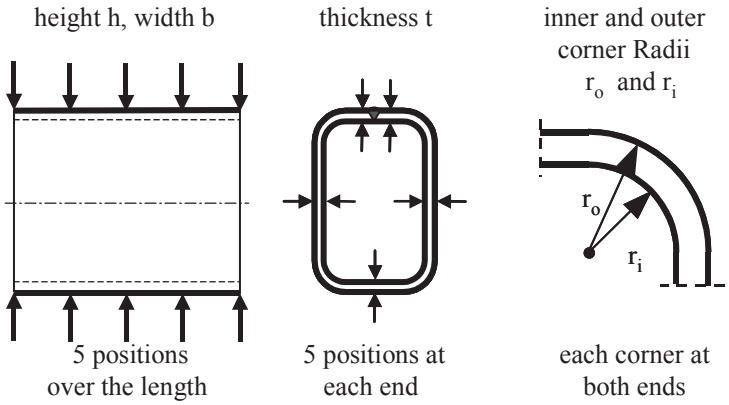

Figure 5-6. Position of measurement.

To identify every section used to fabricate a joint, all sections are labelled with an extended batch number, which is annotated on every part (chord and braces) of the joints after fabrication.

Due to the large dimensions and the huge number of test specimens, all possess a 30 µm thick corrosion protection, so that it is possible to store them outside. After welding, all joints had been sandblasted before painting.

5.5 Material properties

The material properties of the sections have been provided by the manufacturers according to the specifications of EN10204-3.1.B [5-4]. The characteristic values such as yield strength $R_{p0.2}$, ultimate strength R_m and the uniform strain A_5 are determined according to EN10002 [5-5] (tensile test), the toughness according to EN10045 [5-6] (Charpy V test). Additionally, the chemical composition is determined. The mechanical properties of each batch can be found in Appendix 5.

Because the sections of manufacturer B had been delivered without batch numbers, chemical analysis had been carried out from every part of the joints which was delivered by manufacturer B. With the detected chemical composition it was possible to reassign the batch numbers to the parts.

5.6 General observations and results from test

All measured dimensions, measurements of the LVDTs, calculated relative displacements, pictures of tests and annotations are shown for every test are documented in the test reports.

5.6.1 Influence of the gap size parameter g' and the width ratio β on the load carrying behaviour

For small gaps and low to medium β-ratios, the gap area is relatively too stiff compared to the other parts around the perimeter. This results in smaller effective widths and therefore smaller punching shear loads. Therefore, Eurocode 3 [5-1] and other standards do not allow the gap to be less than given below, when using the presented punching shear formulae in these standards.

$$g' \geq 0.5 \cdot \left(1 - \frac{b_{12}}{b_0}\right) \cdot 2\gamma \qquad (5\text{-}3)$$

For all tests with a very small gap size (g' = 4.00) punching shear failure can be observed. The crack runs from one transition radius of the brace to the other through the chord flange. Due to the increased stiffness of the gap region, the effective punching shear length decreases.

It can be seen in Figure 5-7 that, with increase of the width ratio β of the connection, buckling of the chord webs increasingly becomes the dominant failure mode. Regarding the ultimate loads, the gap size does not have a significant influence. The ultimate load is mainly influenced by the width ratio, increasing with the width ratio. Another observation of the tests is that the stiffness of the connection increases as the gap size decreases (Figure 5-7) and the width ratio increases (Figure 5-8).

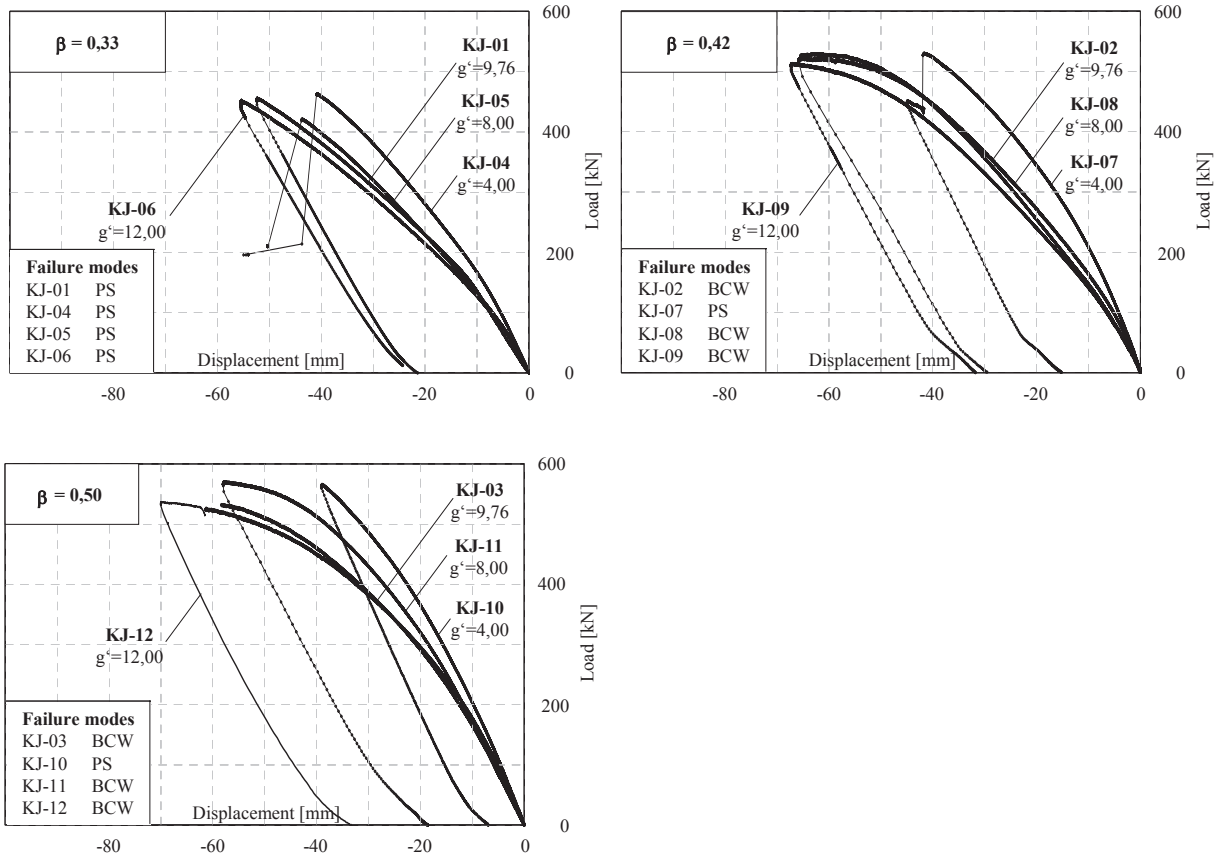

Figure 5-7. Influence of the gap size g' for varying width ratios β.

Failure Modes	
CF	*chord face failure*
PS	*punching shear failure*
BCW	*buckling of chord web failure*

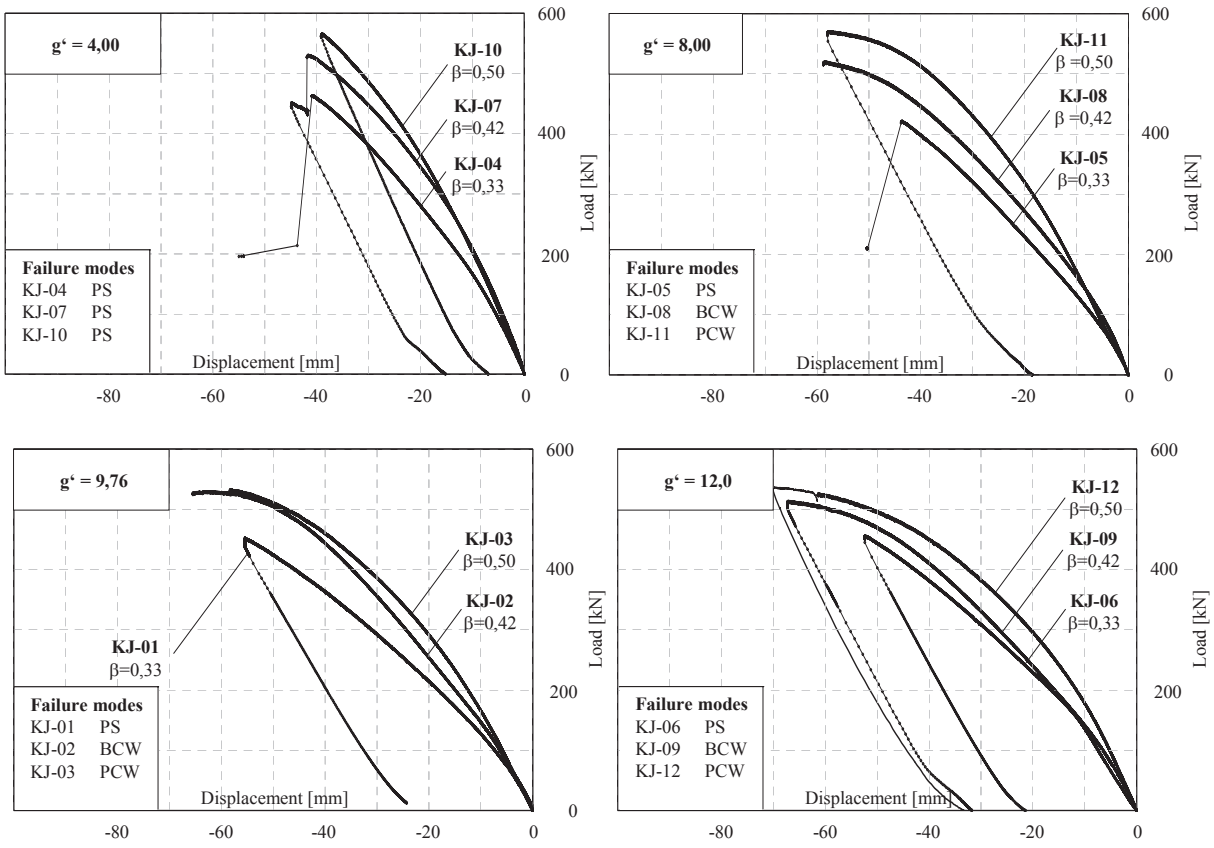

Figure 5-8. Influence of the width ratio for different gap sizes.

Failure Modes	
PS	punching shear failure
BCW	buckling of chord web failure

5.6.2 Influence of the thickness ratio τ on the load carrying behaviour

The following Table 5-3 show tests with a thickness ratio $0.5 \leq \tau \leq 0.75$.

Table 5-3. Tests with thickness ratios $\tau < 1.00$.

No.	Thickness ratio τ	Chord section $b_0 \times h_0 \times t_0$ [mm]	Brace sections $b_{1.2} \times h_{1.2} \times t_{1.2}$ [mm]	Gap size g'	Width ratio β	Slenderness ratio 2γ	Ult. load F_u [kN]	Failure mode
KJ-15[1]	0.75	200 x 100 x 4.0	80 x 80 x 3.0	4.00	0.40	50.0	236	EW
KJ-19	0.75	200 x 100 x 4.0	80 x 80 x 3.0	4.00	0.40	50.0	194	EW
KJ-20	0.60	200 x 100 x 5.0	80 x 80 x 3.0	4.00	0.40	40.0	241	BB
KJ-21	0.50	200 x 100 x 6.0	80 x 80 x 3.0	4.00	0.40	33.3	282	BB
KJ-22	0.75	150 x 150 x 4.0	80 x 80 x 3.0	9.22	0.53	37.5	222	BCW
KJ-23	0.75	150 x 150 x 4.0	80 x 80 x 3.0	9.22	0.53	37.5	212	BCW
KJ-41	0.75	200 x 100 x 4.0	80 x 80 x 3.0	4.00	0.40	50.0	265	BB
KJ-42	0.75	200 x 100 x 4.0	80 x 80 x 3.0	4.00	0.40	50.0	222	EW
KJ-45[2]	0.75	200 x 100 x 4.0	80 x 80 x 3.0/4.0	4.00	0.40	50.0	186	EW
KJ-46	0.60	200 x 100 x 5.0	80 x 80 x 3.0	4.00	0.40	40.0	265	BB
KJ-47[3]	0.50	200 x 100 x 6.0	80 x 80 x 3.0	4.00	0.40	33.3	207	CG

Notes:
[1] two different brace members (compression brace S460, tension Brace S355)
[2] two different brace thicknesses (compression brace $t_1 = 4.0$ mm, tension brace $t_2 = 3$ mm)
[3] incorrect weld execution – not considered for the evaluation
EW brace failure (effective width)
BB buckling of brace failure
BCW buckling of chord web failure
CG crack in the mid of the gap due welding of the chord

For thickness ratios $\tau < 1.00$, small gap sizes g' and low to medium width ratios β, buckling of the brace (KJ-20, KJ-21, KJ-41, KJ-46) or effective width failure (KJ-15, KJ-19, KJ-32, KJ-33, KJ-34, KJ-42, KJ-45) can be observed during the tests.

For effective width failure, the crack runs from one transition radius of the brace to the other through the brace width, next to the gap. As for punching shear failure mentioned before, the stiffness of the gap region is increased compared to the other parts around the perimeter. This result in a smaller effective width b_{eff} and smaller failure loads for brace failure.

As the width ratios and gap sizes both increase (KJ-22 and KJ-23), the load is transferred predominantly to the chord webs. Due to this, a change of the failure mode can be observed. For higher width ratios with higher gap sizes, buckling of the chord webs become the predominant failure mode.

5.6.3 Influence of brace inclination Θ on the load carrying behaviour

The effect of varying brace inclinations was determined from tests with different width ratios β ($\beta = 0.33$ and 0.50) and gap sizes g' (g' = 4, 8 and 12) at brace inclinations of 30, 45 and 60°. The comparison of the load displacement curves can seen in Figure 5-9 for $\beta = 0.33$ and in Figure 5-10 for $\beta = 0.50$.

The highest ultimate load is always reached at brace inclinations of 30°, the lowest at brace inclinations of 60°. When considering the component perpendicular to the chord ($F_u \cdot \sin \Theta$), it can be seen that there is only a little difference in the values for brace inclinations of 45° and 60° but in case of 30° this load component is significantly reduced (see Table 5-4). Because the load component perpendicular to the chord face is smaller for brace inclinations of 30° brace failure becomes more dominant in case of small gap sizes (reduced effective width). For higher gap sizes where effective length increases, bucking of

the chord webs becomes dominant instead of punching shear, because of the larger width ratios for higher gap sizes.

Table 5-4. Comparisons of test with varying brace inclinations

No.	Brace angle Θ [°]	Chord section b_0 x h_0 x t_0 [mm]	Brace sections $b_{1,2}$ x $h_{1,2}$ x $t_{1,2}$ [mm]	Gap size g'	Ult. load F_u [kN]	Ult. load $F_u \cdot \sin\Theta$ [kN]	Failure mode
KJ-32	30	300 x 200 x 6.0	100 x 100 x 6.0	4.00	550	275	EW[1]
KJ-04	45				463	327	PS
KJ-29	60				392	339	PS
KJ-33	30	300 x 200 x 6.0	100 x 100 x 6.0	8.00	550	275	EW[1]
KJ-05	45				421	298	PS
KJ-30	60				343	297	PS
KJ-34	30	300 x 200 x 6.0	100 x 100 x 6.0	12.00	519	260	EW
KJ-06	45				456	322	PS[1]
KJ-31	60				365	316	PS[4]
KJ-38	30	300 x 200 x 6.0	150 x 100 x 6.0	4.00	581	291	BCW[2]
KJ-07	45				530	375	PS
KJ-35	60				390	338	PS[2]
KJ-39	30	300 x 200 x 6.0	150 x 100 x 6.0	8.00	558	279	BCW[2]
KJ-08	45				522	369	BCW
KJ-36	60				414	359	PS[2,]
KJ-40	30	300 x 200 x 6.0	150 x 100 x 6.0	12.00	553	277	BCW[2]
KJ-09	45				513	367	BCW[5]
KJ-37	60				332	288	PS[2]

Notes:
[1] not identifiable by test, failure mode assumed (see evaluation of tests – Appendix A3)
[2] not identifiable by test, specimen loaded with shorter jack, failure mode assumed (see evaluation of tests - Appendix A3)
EW brace failure (effective width)
PS punching shear failure
BCW buckling of chord web failure

As seen before, the ultimate load is not influenced by the gap size significantly but the failure mode is.

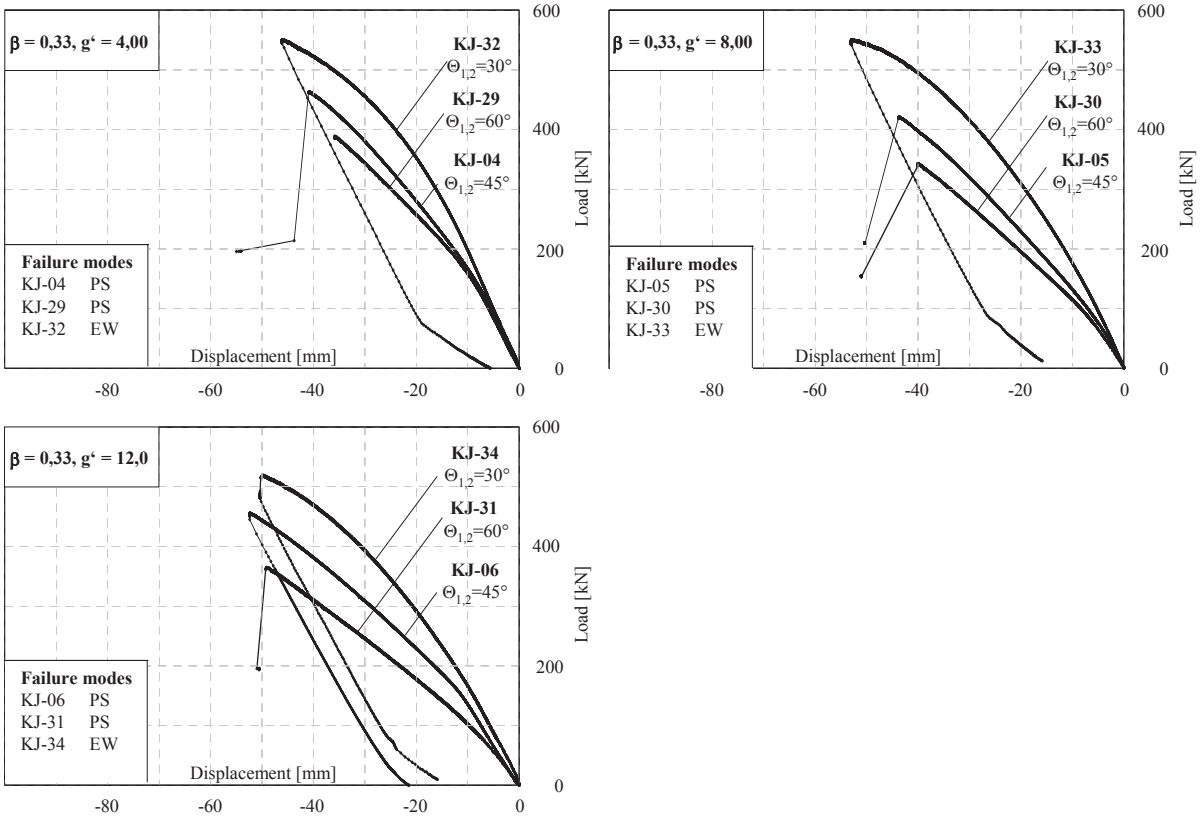

Figure 5-9. Influence of the brace inclinations for β = 0.33 and varying gap sizes g'.

Failure Modes

CF	chord face failure
EW	brace effective width failure
PS	punching shear failure

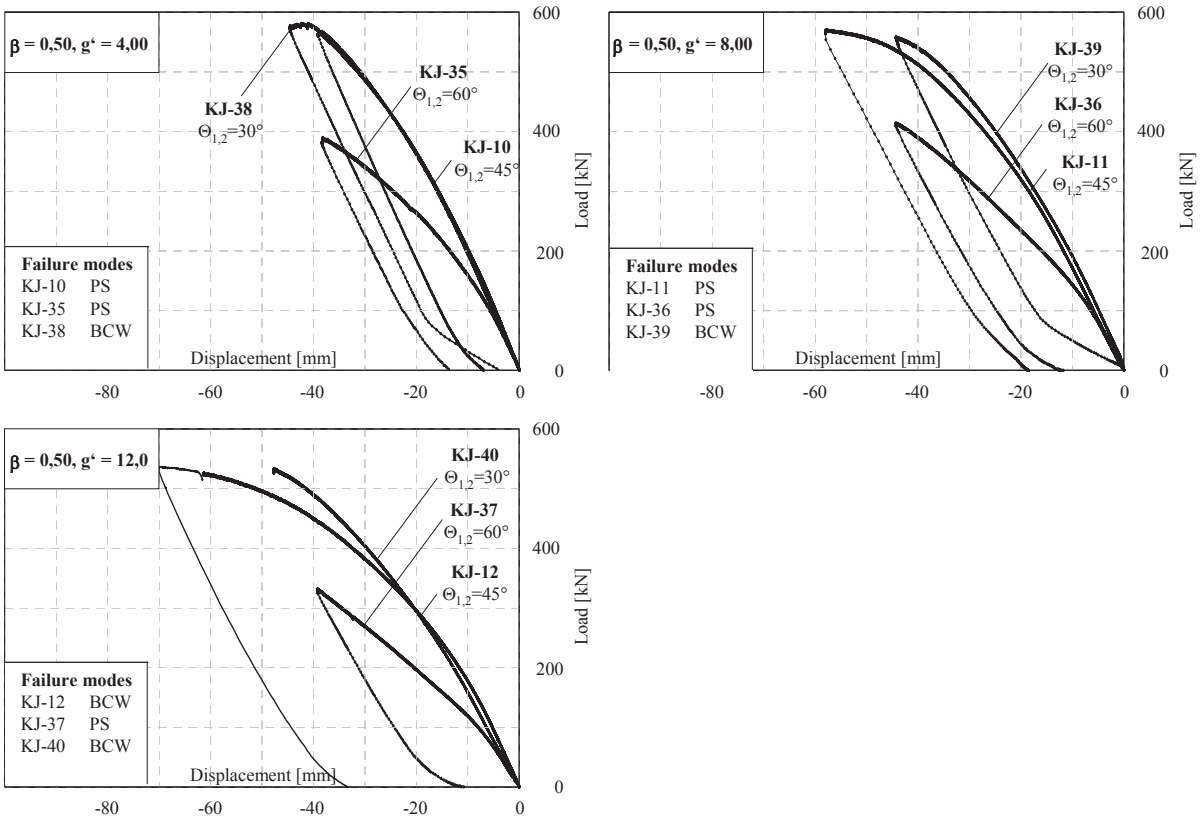

Figure 5-10. Influence of the brace inclinations for β = 0.50 and varying gap sizes g'.

Failure Modes

PS	punching shear failure
BCW	buckling of chord web failure

5.6.4 Influence of material properties on the load carrying behaviour

To determine the influence of the mechanical properties on the load carrying behaviour, the following tests are carried out.

Table 5-5. Similar tests with different mechanical properties.

Tests with steel grade S355		Corresponding tests with steel grade 460		Chord section	Brace sections	Comparison
No.	F_u^{355} [kN]	No.	F_u^{460} [kN]	$b_0 \times h_0 \times t_0$ [mm]	$b_{12} \times h_{12} \times t_{12}$ [mm]	F_u^{460}/F_u^{355}
KJ-15[3]	236	KJ-41	265	200 x 100 x 4.0	80 x 80 x 3.0	1.12
KJ-19	194	KJ-45[4]	186	200 x 100 x 4.0	80 x 80 x 3.0	0.96
KJ-16[1]	304	KJ-42	222	200 x 100 x 4.0	80 x 80 x 4.0	-
KJ-17	290	KJ-43	303	200 x 100 x 5.0	80 x 80 x 5.0	1.04
KJ-18	338	KJ-44[2]	-	200 x 100 x 6.0	80 x 80 x 6.0	-
KJ-20	241	KJ-46	265	200 x 100 x 5.0	80 x 80 x 3.0	1.10
KJ-21	282	KJ-47[2]	-	200 x 100 x 6.0	80 x 80 x 3.0	-

Notes:
1 preliminary test – not considered for the evaluation
2 incorrect weld execution – not considered for the evaluation
3 two different brace members
4 two different brace thicknesses

Because of incorrect welding on test specimens KJ-44 and KJ-47, the comparable tests KJ-18 and KJ-21 cannot be used for the evaluation to check the influence of the material quality. Additionally, the preliminary test KJ-16 (and therefore test KJ-42) is not used for this comparison. Although KJ-15 and KJ-45 have different brace sections, the comparison is included here, because it is assumed that this will not have a significant influence to the load carrying behaviour.

As can be seen from Figure 5-11, the mechanical properties of the material used have only a negligible influence on the load carrying behaviour. Neither the ratio of the ultimate strengths nor the ratio of the yield strengths is reached in the tests.

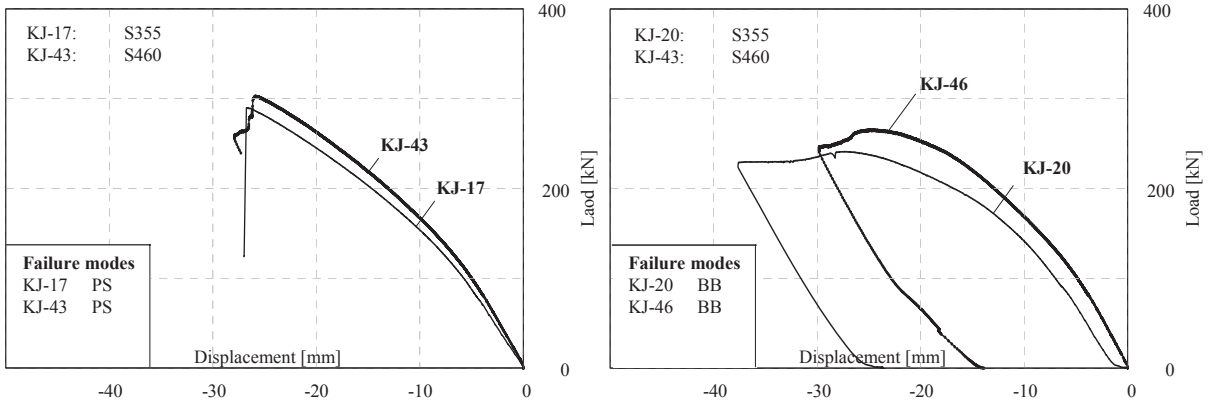

Figure 5-11. Comparison of joints with the same geometrical parameters and different steel grades.

Failure Modes

PS	punching shear failure
BB	buckling of brace failure

$$\frac{F_u^{460}}{F_u^{355}} = \frac{560}{470} = 1.20 \qquad \frac{f_y^{460}}{f_y^{355}} = \frac{460}{355} = 1.30$$

Both tests, KJ-17 and KJ-43, failed by punching shear failure. The crack always runs through the heat affected zone of the welds. It is possible that the mechanical properties of the steel grade S460 are changed by heating caused by welding in this area. The tests KJ-20 and KJ-46 failed by local buckling of the brace. Assuming a strut for the local buckling failure, the reference slenderness can be defined as a function of the characteristic slenderness as follows:

$$\lambda_a = \pi \cdot \sqrt{\frac{E}{f_y}}$$

Additionally the reduction factor κ is dependent upon the buckling curve. For cold formed hollow sections, buckling curve C has to be used. On this basis, there will be an influence of

$$\frac{\overline{\lambda}_{460}}{\overline{\lambda}_{355}} = \frac{\lambda_a^{355}}{\lambda_a^{460}} = \frac{\pi \cdot \sqrt{\frac{E}{f_y^{355}}}}{\pi \cdot \sqrt{\frac{E}{f_y^{460}}}} = \sqrt{\frac{f_y^{460}}{f_y^{355}}} = 1.14$$

in case of buckling of the brace. The observed ratio for the tests KJ-20 and KJ-46 is 1.10.

5.6.5 Influence of imperfections

For some tests (see Table 5-6) the specimens are from the same batch and are therefore well suited for observing the influence of imperfections. Although the specimens have the same geometrical dimensions and the tests are carried out with the same testing conditions, differences of the ultimate loads can be observed. This can be attributed to geometrical imperfections of the sections, imperfections of the test specimens due to inaccurate fabrication and measurement errors, which could not totally be avoided during experimental testing. The effects of imperfections can be seen in the comparison of the load-displacement curves (Figure 5-12).

Table 5-6. Comparison of tests with same geometrical dimensions.

Tests with same geometry parameters					**Chord section**	**Brace sections**	**Gap size**	**Comp-arison**
No.	Material	F_u [kN]	$F_{u,m}$ [kN]	Failure mode	$b_0 \times h_0 \times t_0$ [mm]	$b_{1,2} \times h_{1,2} \times t_{1,2}$ [mm]	g'	$F_u/F_{u,m}$
KJ-25	S355	176	183	BCW	120.2 x 120.2 x 2.8	80.0 x 80.0 x 2.8/2.9	4.00	0.96
KJ-26	S355	201			120.2 x 120.2 x 2.8	80.0 x 80.0 x 2.8/2.9		1.10
KJ-27	S355	165			120.2 x 120.2 x 2.8	80.0 x 80.0 x 2.8/2.9		0.90
KJ-28[1]	S355/S460	190			120.2 x 120.2 x 2.9	80.0 x 80.0 x 2.9/2.9		1.04
KJ-22	S355	222	216	BCW	150.2 x 150.2 x 3.9	80.0 x 80.0 x 3.0/3.0	9.22	1.02
KJ-23	S355	212			150.2 x 150.2 x 3.8	80.0 x 80.0 x 3.0/2.9		0.98
KJ-15[2]	S355/S460	236	215	EW	199.6 x 100.9 x 3.8	80.2 x 80.1 x 3.0/3.0	4.00	1.10
KJ-19	S355	194			199.6 x 100.9 x 3.8	80.0 x 80.0 x 3.0/3.0		0.90
KJ-41	S460	265	226	BB	200.0 x 100.0 x 4.2	80.0 x 80.0 x 3.0/3.0	4.00	1.18
KJ-45[3]	S460	186		EW	199.6 x 99.9 x 4.0	80:3 x 80:3 X 4.0/2.9		0.82

Notes:
[1] two different brace members (compression brace S355, tension brace S460)
[2] two different brace members (compression brace S460, tension brace S355)
[3] two different brace thicknesses (compression brace t = 4mm, tension brace t = 3mm)
BCW buckling of chord web failure
EW brace failure (effective width)
BB buckling of brace failure

In Table 5-6 all relevant parameters of the specimens can be found. The comparison of the results F_u is carried out in reference to the mean values $F_{u,m}$ of the tests with the same geometry. The braces of the

test specimens KJ-15 and KJ-45 and KJ-28 are produced from different charges, as determined by the chemical analysis. The results of these tests should be therefore be interpreted with care.

The difference in ultimate loads for the comparable tests in Table 5-6 is within a range of ±10% for all tests except those which failed by effective width failure of the brace in tension. It is well known that tensile failure is unpredictable due to local variations in material or geometrical properties in the weld region, so that the differences observed between KJ-15 and KJ-19 as well as KJ-41 and KJ-45 are predictable.

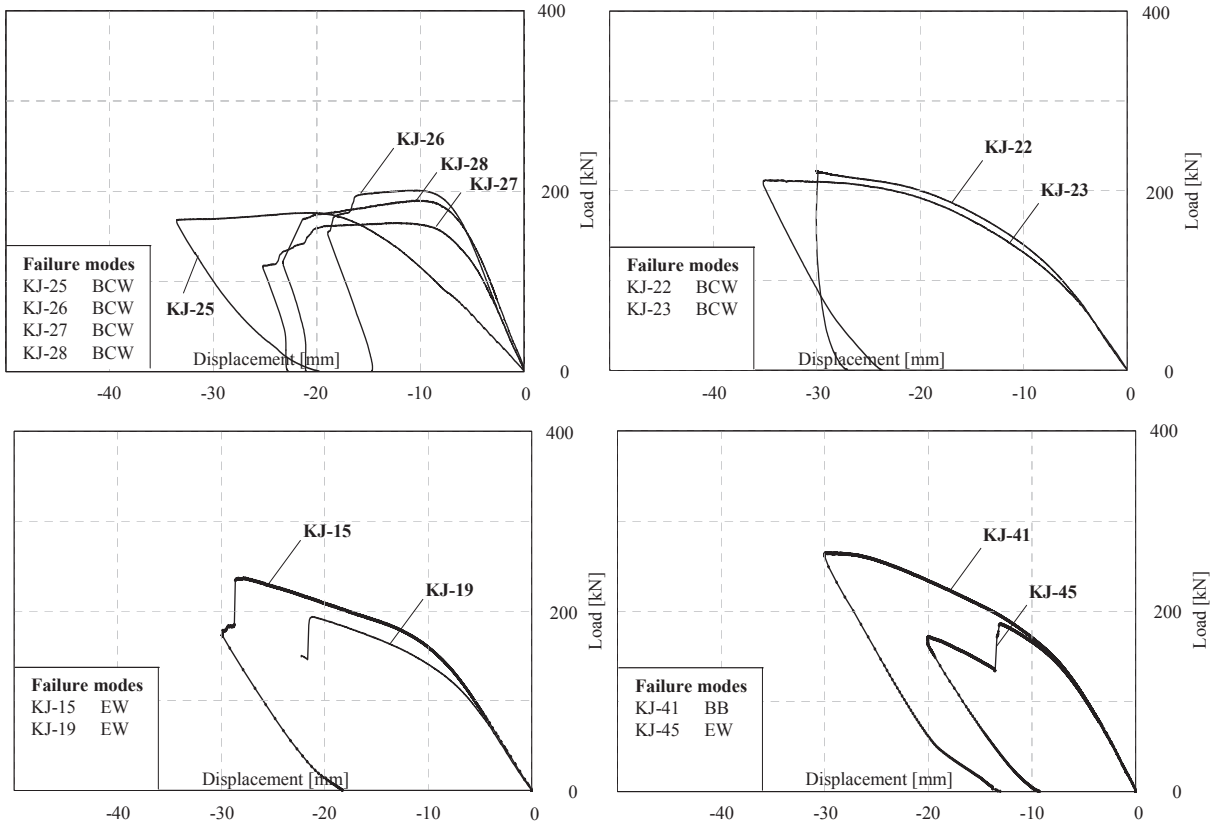

Figure 5-12. Comparison of joints having same geometrical and material properties.

Failure Modes	
EW	brace effective width failure
BCW	buckling of chord web failure
BB	local buckling of brace failure

To gain information of the measurement errors produced by the measuring equipment, an independent measuring method was used. Calibrated callipers with heights of 10, 20, 30 and 40 mm were used to check the precision of the measurements. Additionally, the displacement transducers are labelled with numbers to ensure that every LVDT is used at the same measuring point for all tests. It can be seen from Figure A4-7 that only small deviations between the measured and the correct dimensions exist. Due to a linear dependency of the deviations to the measured lengths (correlation factor r = 1.00 for all transducers), these deviations do not have an influence on the relative deflections between 2 measuring points.

5.6.6 Annotation to some test results

By the tests and the chemical analysis of the test specimens the following general observations could be made:

- The braces of test specimen KJ-15 are out of two different steel grades. The compression brace consist of steel grade S460, whereas the tension brace of steel grade S355. The same observation

was made for KJ-28 where the tension brace of steel grade S460 and the compression brace of S355.

- The test specimen KJ-45 possesses braces with two different wall thicknesses. For the compression brace a section with a thickness of 4 mm, for the tension brace one with 3 mm, was used.
- The chords of test KJ-44 and KJ-47 are composed of two pieces which are welded together with a angle of 45°. The weld is arranged exactly in the middle of the gap. Both specimens failed by brittle fracture at the weld.

5.7 Calculation of welded connections between rectangular hollow sections according to prEN1993-1-8

The following modes of failure (Figure 5-13) could occur for welded connections between rectangular hollow sections. The modes of failure observed from the tests can be seen sin Figure 5-14.

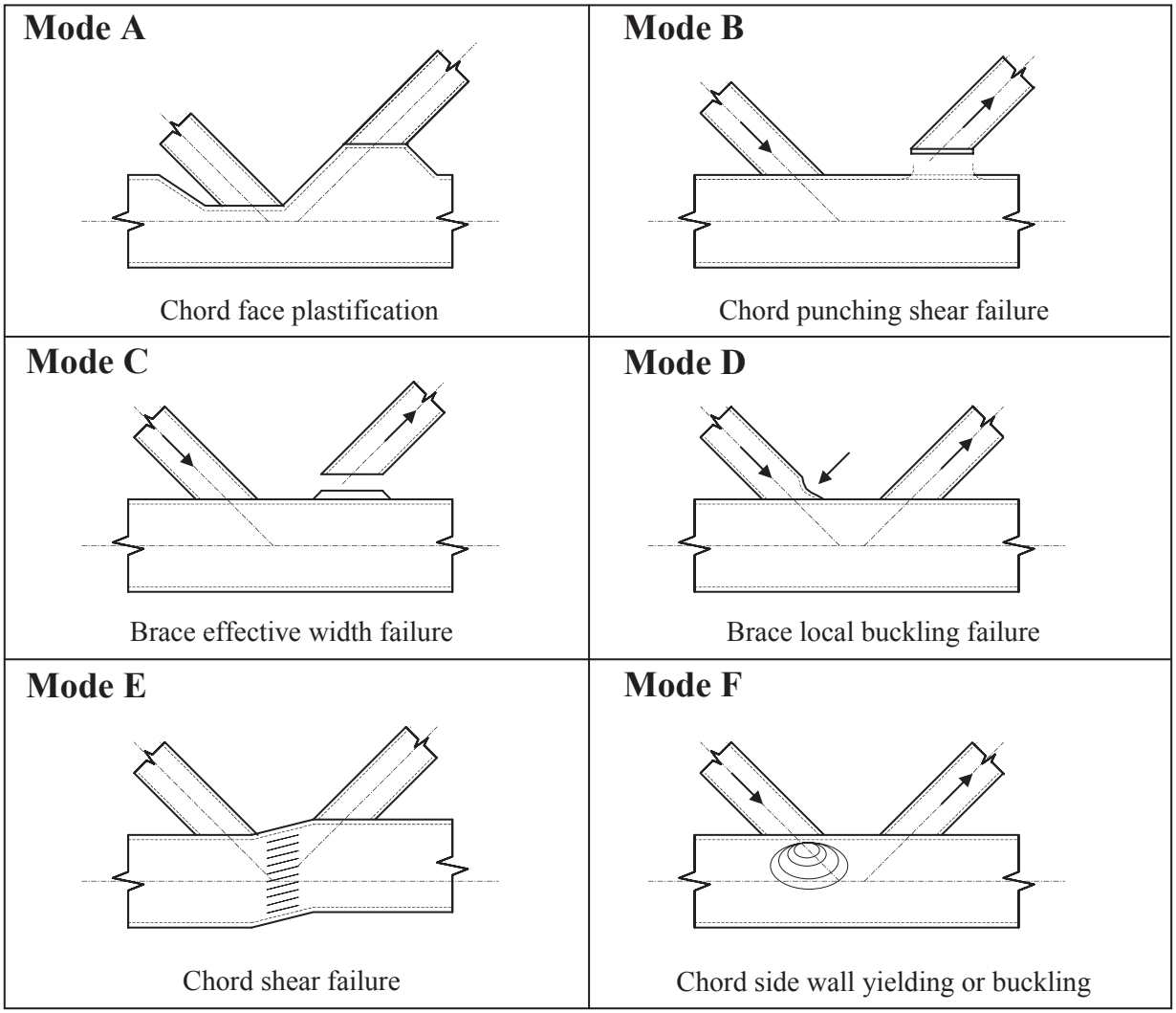

Figure 5-13. Failure modes of hollow section joints.

Figure 5-14a. reduced punching shear failure (KJ-04).

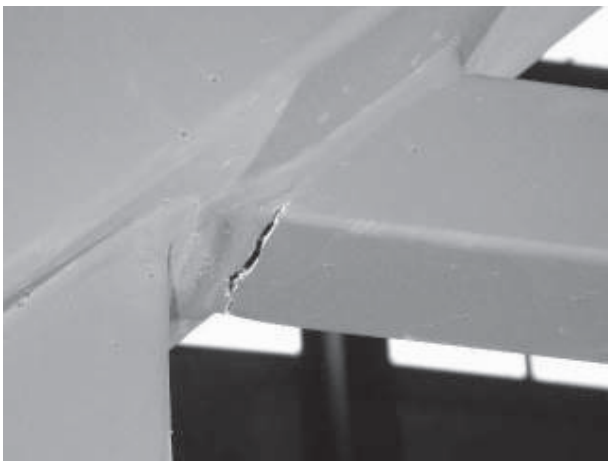

Figure 5-14b. reduced effective width failure (KJ-19).

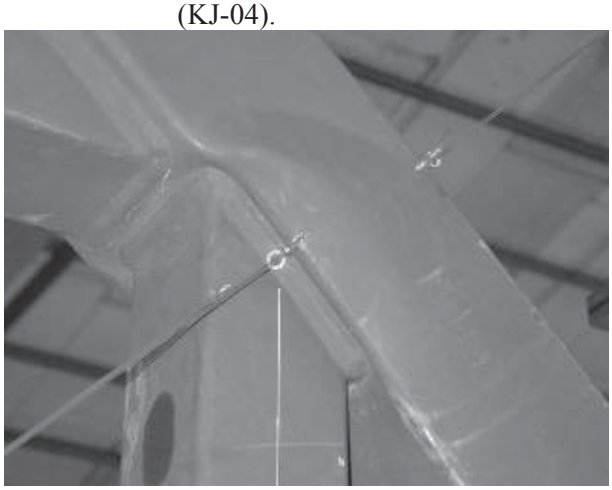

Figure 5-14c. Buckling of chord webs (KJ-25).

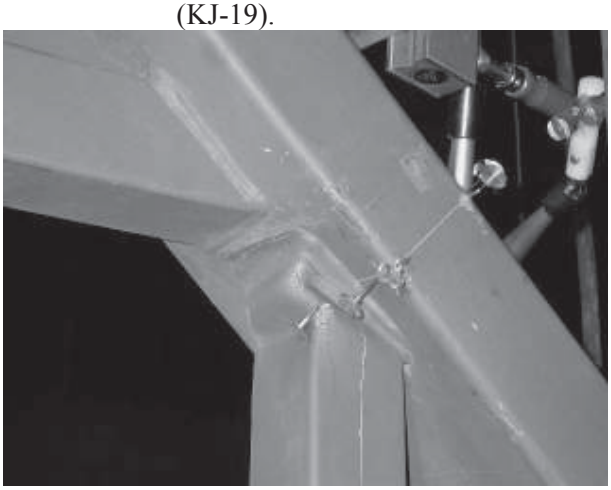

Figure 5-14d. Buckling of compression brace (KJ-20).

In Table 5-7, the ultimate test loads, the failure modes observed and the design loads according to Eurocode 3 [5-1] calculated with measured values (in Table A3-1 calculated with nominal values are presented). Because buckling of the chord webs was observed as a failure mode and no rule to calculate design loads for chord web buckling exist, the design loads according to Eurocode 3 [5-1] for T- and Y-Joints are used for the comparison. Furthermore punching shear had been determined using the following modified formula using a reduced effective length $l_{e,p}$.

The design formulae given in prEN1993-1-8 85-1[5-1] for K-joints can be found in Appendix 3, Table A3-3, the design formulae for buckling of the chord webs for T- and Y- joints used for the evaluation is shown in Table A3-4.

5.7.1 Modified analytical model for (reduced) punching shear failure

Form the test results, it can be seen that the effective length for punching shear failure decreases with the gap size. Use of the formula in Eurocode 3 [5-1] overestimates the effective length and therefore the design loads. Therefore new models have to be developed for small gap sizes. Based on the observations during the tests, the following assumption for the reduced effective punching shear length $l_{e.p.red}$ can be made as a lower bound in case of small gap sizes:

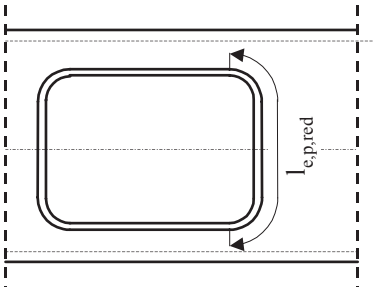

$$l_{e,p,red} = b_{1,2} + r_a \cdot (\pi - 2)$$

for

$$g < 0.5 \cdot \left(1 - \frac{b_{1,2}}{b_0}\right) \cdot 2\gamma$$

Figure 5-15 Reduced effective punching shear length for small gap sizes.

This assumption considers the reduced effective length for small gaps, which is caused by the increased stiffness of the gap region and implies that the load is dissipated only by the transition radii and the width of the brace in the gap region. With this reduced effective length $l_{e,p,red}$ the design load for punching shear failure $N_{1,Rd,red}^{PS}$ can be determined to be:

$$N_{1.d.red}^{PS} = \tau_{R.d} \cdot t_0 \cdot l_{e.p.red} = \frac{f_{y0}}{\sqrt{3}} \cdot t_0 \cdot \left[b_{1.2} + r_{1.2}^{o} \cdot (\pi - 2)\right] \tag{5-4}$$

5.8 Comparison of test results with calculation results according to prEN1993-1-8

The calculated loads according to Eurocode 3 [6-1] based on nominal and measured dimensions and The calculated loads according to Eurocode 3 [5-1] based on measured dimensions and material properties can be found Table 5-7. Additionally the calculated chord side wall failure load using the formula for T- and Y-joints and the reduced punching shear load can be found in Table 5-7.

Comparison of the ultimate loads obtained from the tests with calculations using measured values is given in Figure 5-15. Furthermore the failure modes of the tests are given here.

Loads

$N_{d,CF}$ design resistance load for chord face failure, with measured dimensions
$N_{d,CS}$ design resistance load for chord shear failure, with measured dimensions
$N_{d,EW}$ design resistance load for effective width failure, with measured dimensions
$N_{d,PS}$ design resistance load for punching shear failure assuming a reduced effective punching shear length for small gaps, with measured dimensions
$N_{d,BCW}$ design resistance load for buckling of chord web failure calculated with formulae for T- and Y-joints, with measured dimensions
$N_{1,Rd,nom}$ governing value of design resistance from the above 5 values

Failure Modes

CF chord face failure
CS chord shear failure
EW brace effective width failure
PS punching shear failure
BCW buckling of chord web failure
BB local buckling of brace failure

Table 5-7. Evaluation of test results (measured dimensions)

Nos.	Mat.	Cross sections			Failure mode		Resistance according to prEN1993-1-8					
		Chord $b_0 \times h_0 \times t_0$ [mm]	Brace $b_{1,2} \times h_{1,2} \times t_{1,2}$ [mm]	Radius $r_{0,chord}$ [mm]		F_u^{test} [kN]	$N_{u,CT}$ [kN]	$N_{u,CS}$ [kN]	$N_{u,EW}$ [kN]	$N_{u,PS}$ [kN]	$N_{u,EWC}$ [kN]	$\frac{F_u^{test}}{N_{1,Rd,min}}$
KJ-01	S355	299.6 x 200.6 x 6.0	100.2 x 100.2 x 5.7	14.8	PS[1]	452	341	945	683	**180**	279	2.50
KJ-02	S355	300.0 x 200.3 x 6.0	149.9 x 100.0 x 5.8	14.9	BCW	529	426	944	1038	**257**	280	2.06
KJ-03	S355	300.1 x 199.9 x 6.0	199.9 x 100.1 x 5.7	14.9	BCW	538	511	942	1147	336	**281**	1.91
KJ-04	S355	299.9 x 200.3 x 6.1	100.2 x 100.2 x 5.7	14.3	PS	463	350	1042	685	**183**	294	2.52
KJ-05	S355	299.9 x 200.4 x 5.9	100.2 x 100.2 x 5.7	14.4	PS	421	333	941	682	**177**	266	2.37
KJ-06	S355	299.6 x 200.2 x 6.1	100.2 x 100.2 x 5.7	13.8	PS[1]	456	349	948	685	**183**	295	2.49
KJ-07	S355	300.1 x 200.3 x 5.8	149.9 x 100.0 x 5.8	14.9	PS	530	405	991	1045	**248**	253	2.14
KJ-08	S355	300.0 x 200.4 x 5.8	149.9 x 100.0 x 5.9	15.0	BCW	522	404	925	1044	**248**	253	2.10
KJ-09	S355	299.7 x 200.3 x 6.1	149.9 x 100.0 x 5.8	15.1	BCW	513	436	948	1049	**261**	294	1.97
KJ-10	S355	299.6 x 199.9 x 6.2	199.9 x 100.1 x 5.8	14.1	PS[1]	565	536	1058	1164	347	**310**	1.82
KJ-11	S355	299.7 x 199.9 x 5.7	199.9 x 100.1 x 5.8	14.0	BCW[1]	570	473	907	1151	319	**241**	2.36
KJ-12	S355	299.5 x 200.4 x 6.2	199.9 x 100.1 x 5.8	14.8	BCW[1]	537	536	964	1170	347	**308**	1.74
KJ-13	S355	200.1 x 299.6 x 6.1	100.2 x 100.2 x 5.8	14.6	PS	553	428	1441	725	183	**139**	3.98
KJ-14	S355	199.7 x 299.5 x 6.2	149.9 x 100.0 x 6.0	14.4	[1]	n.A.	547	1464	1109	265	**146**	*n.A.*
KJ-15[1]	*S355*	199.6 x 100.9 x 3.8	*n.A.*	*n.A.*	EW	*n.A.*	*n.A.*	*n.A.*	*n.A.*	*n.A.*	*n.A.*	*n.A.*
KJ-16	S355	199.6 x 100.9 x 4.1	80.2 x 80.1 x 4.1	8.0	*PS*	*304*	169	330	415	**86**	247	3.54
KJ-17	S355	199.6 x 100.1 x 4.8	80.1 x 80.0 x 5.0	11.2	PS	290	257	461	557	**124**	397	2.34
KJ-18	S355	199.9 x 100.1 x 5.8	80.1 x 80.2 x 5.7	13.3	PS	338	335	548	587	**151**	627	2.24
KJ-19	S355	199.6 x 100.9 x 3.8	80.0 x 80.0 x 3.0	8.0	EW	194	149	303	310	**76**	195	2.54
KJ-20	S355	199.6 x 100.1 x 4.8	80.0 x 80.0 x 3.2	11.2	BB	241	253	457	342	**116**	389	2.08
KJ-21	S355	199.9 x 100.1 x 5.8	80.0 x 80.0 x 3.0	13.4	BB	282	336	549	355	**140**	629	2.02
KJ-22	S355	150.2 x 150.2 x 3.9	80.0 x 80.0 x 3.0	7.4	BCW	222	202	479	328	**89**	104	2.50
KJ-23	S355	150.2 x 150.2 x 3.8	80.0 x 80.0 x 3.0	7.4	BCW	212	198	473	323	**88**	100	2.42
KJ-24[7]	*S355*	*150.2 x 150.2 x 3.8*	*n.A.*	*n.A.*	*n.A*	*n.A.*	*n.A.*	*n.A.*	*n.A.*	*n.A.*	*n.A.*	*n.A.*

Nos.	Mat.	Cross sections			Failure mode		Resistance according to prEN1993-1-8					
		Chord $b_0 \times h_0 \times t_0$ [mm]	Brace $b_{1,2} \times h_{1,2} \times t_{1,2}$ [mm]	Radius $r_{0,chord}$ [mm]		F_u^{test} [kN]	$N_{u,CT}$ [kN]	$N_{u,CS}$ [kN]	$N_{u,EW}$ [kN]	$N_{u,PS}$ [kN]	$N_{u,EWC}$ [kN]	$\frac{N_u^{test}}{N_{1,Rd,min}}$
KJ-25	S355	120.2 x 120.2 x 2.8	80.0 x 80.0 x 2.9	7.4	BCW	176	131	260	300	**60**	62	2.92
KJ-26	S355	120.2 x 120.2 x 2.8	80.0 x 80.0 x 2.8	6.5	BCW	201	132	262	302	**61**	63	3.31
KJ-27	S355	120.2 x 120.2 x 2.8	80.0 x 80.0 x 2.8	6.5	BCW	165	132	262	303	**61**	63	2.72
KJ-28[4]	*S355*	120.2 x 120.2 x 2.9	*n.A.*	*n.A.*	*BCW*	*n.A.*	*n.A.*	*n.A.*	*n.A.*	*n.A.*	*n.A.*	*n.A.*
KJ-29	S355	299.9 x 199.9 x 6.1	100.2 x 100.2 x 5.6	14.4	PS	392	285	850	675	**183**	242	2.14
KJ-30	S355	299.8 x 199.8 x 6.1	100.2 x 100.2 x 5.7	14.4	PS	343	285	792	675	**183**	242	1.87
KJ-31	S355	299.8 x 200.2 x 6.2	100.2 x 100.2 x 5.9	14.4	PS	365	292	787	683	**186**	253	1.96
KJ-32	S355	299.5 x 200.5 x 6.3	100.2 x 100.2 x 5.8	14.4	EW[1]	550	519	1524	697	**189**	455	2.91
KJ-33	S355	299.6 x 200.0 x 6.1	100.2 x 100.2 x 5.8	14.6	EW[1]	550	494	1373	690	**183**	415	3.00
KJ-34	S355	299.7 x 200.2 x 6.2	149.9 x 100.0 x 5.9	14.5	EW	519	506	1362	690	**186**	435	2.79
KJ-35	S355	300.5 x 199.8 x 6.1	149.9 x 100.0 x 6.0	14.6	PS[1]	390	392	850	1068	260	**242**	1.61
KJ-36	S355	300.5 x 199.8 x 6.2	149.9 x 100.0 x 5.9	14.3	PS[1]	414	402	805	1109	265	**254**	1.63
KJ-37	S355	299.7 x 199.8 x 6.2	149.9 x 100.0 x 5.8	14.7	PS[1]	414	401	785	1124	265	**254**	1.63
KJ-38	S355	299.6 x 200.0 x 6.2	100.2 x 100.2 x 5.6	14.4	BCW[1]	581	695	1496	1045	**265**	435	2.19
KJ-39	S355	299.7 x 200.2 x 6.0	149.9 x 100.0 x 5.8	14.5	BCW[1]	558	662	1352	1038	**256**	393	2.18
KJ-40	S355	200.5 x 199.8 x 6.1	149.9 x 100.0 x 5.8	14.4	BCW[1]	533	679	1338	1034	**260**	415	2.05
KJ-41	S460	199.6 x 99.9 x 4.2	80.3 x 80.3 x 2.9	8.9	BB	265	219	419	383	**107**	280	2.48
KJ-42	S460	199.6 x 99.9 x 4.1	80.3 x 80.3 x 3.9	8.9	EW	222	208	405	479	**103**	255	2.15
KJ-43	S460	199.7 x 100.2 x 4.8	80.3 x 80.3 x 3.9	11,2	PS	303	284	510	489	**136**	408	2.22
KJ-44[6]	*S460*	*199.7 x 100.2 x 5.9*	*n.A.*	*n.A.*	*CG*	*258*	*n.A.*	*n.A.*	*n.A.*	*n.A.*	*n.A.*	*n.A.*
KJ-45[5]	*S460*	*199.6 x 99.9x 4.0*	*n.A.*	*n.A.*	*EW*	186	*n.A.*	*n.A.*	*n.A.*	*n.A.*	*n.A.*	*n.A.*
KJ-46	S460	199.7 x 100.2 x 4.8	80.3 x 80.3 x 3.0	11.2	BB	265	289	516	404	**131**	419	2.02
KJ-47[6]	*S460*	*199.7 x 100.2 x 5.9*	*n.A.*	*n.A.*	*CG*	*207*	*n.A.*	*n.A.*	*n.A.*	*n.A.*	*n.A.*	*n.A.*

Notes:

[1] test stopped before failure, failure mode assumed (see Appendix 3 for details)
[2] only strain measurements made and tested only in elastic region
[3] different steel grade for the compression brace (S460) and the tension brace (S355)
[4] different steel grade for the compression brace (S355) and the tension brace (S460)
[5] different wall thickness of compression brace (t1 = 3 mm) and tension brace (t = 4mm)
[6] chord welded in mid of the gap
[7] KJ-24 not tested until failure (strain measurement)
the radius specifies the corner radius measured with a radius gauge

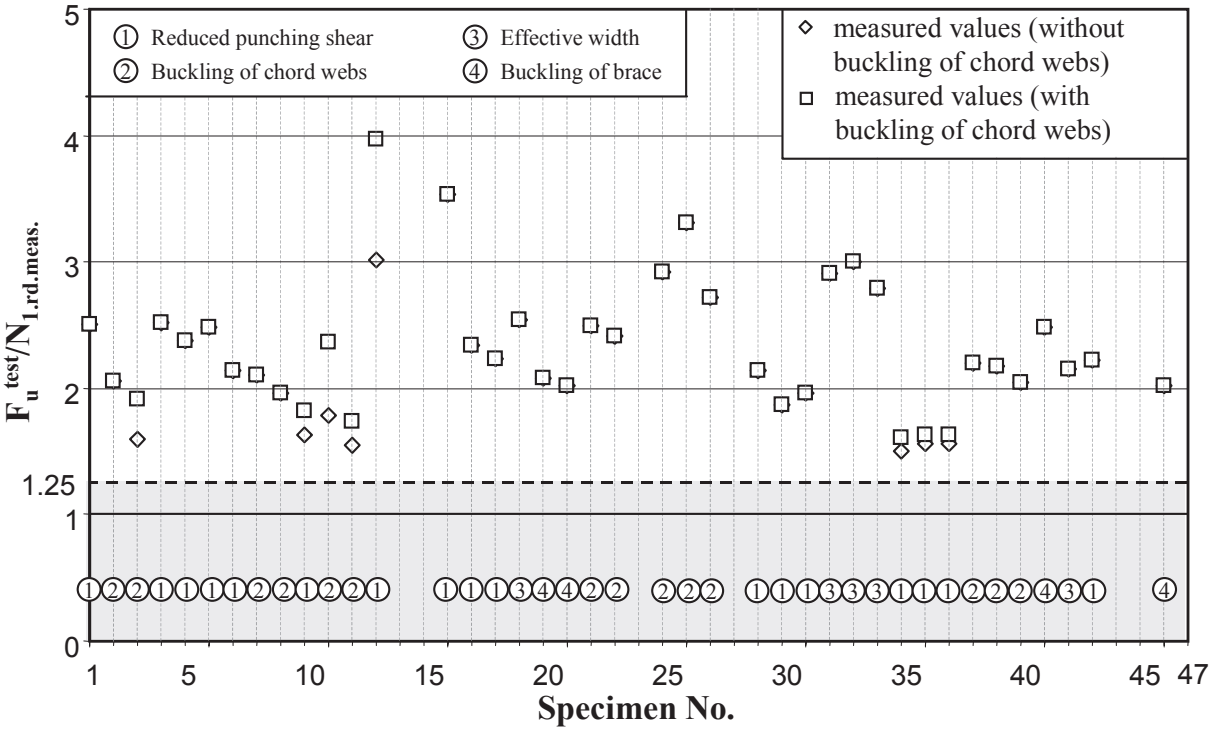

Figure 5-15. Comparison of design resistance calculated with measured dimensions and material properties with and without considering buckling of the chord webs.

The following observations can be made from Figure 5-15:

- Loads calculated with measured values using the formulae given in Eurocode 3 [5-1] and extended for buckling of chord webs (using the formulae for Y- and T-joints) and using a modified punching shear formula give margins of safety higher than 1.25 for all tests.
- For high width ratios ($\beta = 0.50$), buckling of the chord webs is the predominant failure mode (KJ-03 and KJ-10 to KJ-12). For small gaps and middle to small width ratios ($\beta = 0.33$ and $\beta = 0{,}42$) reduced punching shear failure is the predominant failure mode. Note that K-joint β is given by $\beta = (b_{1,2}+h_{1,2})/(2 \cdot h_0)$ so that for example rectangular hollow sections with $b_{1,2} = 200$, $h_{1,2} = 100$ mm (brace) and $b_0 = 300$, $h_0 = 200$ mm (chord) the β value is 0.5, although $b_{1,2}/b_0 = 0.75$.
- Regarding the tests series with the same width ratios (KJ-01, KJ-04 to KJ-06 with $\beta = 0.33$; KJ-02, KJ-07 to KJ-09 with $\beta = 0.42$ and KJ-03, KJ-10 to KJ-12 with $\beta = 0.50$) it can be seen that increasing width ratios give decreasing margins of safety whereas varying gap sizes do not significantly influence the margin of safety.
- Increasing brace inclinations and width ratios give decreasing margins of safety (KJ-29 to KJ-40 and KJ-01, KJ-02 and KJ-04 to KJ-09). From these tests it can also be seen that the gap size does not influence the margin of safety significantly.

5.9 Conclusions

In the framework of this research project 47, tests on K-joints with gap and with slenderness as well as gap sizes outside the range given in Eurocode 3 [5-1] are carried out at the University of Karlsruhe. The ultimate load and the load deformation behaviour had been determined. The results given here are based on the test results only. To develop analytical models which predict the design loads of such joints more accurately than the existing ones, a numerical parameter study using Finite Element analysis needs to be carried out.

For high slenderness 2γ and high width ratios β, buckling of the chord webs could be observed from the tests in case of gap sizes permissible in Eurocode 3 [5-1]. Because this failure mode has not to be considered for K-joints, the formula for T- and Y-joints for chord web failure is used for the design load

prediction. For very small gap sizes, down to the minimum requirements for welding, either punching shear failure or brace effective width failure can be observed. For both failure modes, the influence of a reduced effective length could be observed in the tests. Another failure mode observed in the tests is the buckling of the compression brace, which appears if the width ratio $\tau < 1.00$.

The following conclusions can therefore be drawn for K-joints with slender chord members ($35 \leq 2\gamma \leq 50$) and gap sizes below the lower bound given in Eurocode 3 [5-1]:

- The design resistance for K-joints can be determined by using the formulae according to prEN1993-1-8 but the punching shear resistance should be calculated using a reduced effective length, if the gap size is below the lower bound given in Eurocode 3 [5-1]. This reduced effective punching shear length can be calculated using the proposal given in this report.
- Additionally, buckling of the chord webs should be checked. The formula for T- and Y-joints given in Eurocode 3 [5-1] can be used here.
- The thickness ratio should be restricted to $\tau = 1.0$ for $b_0/t_0 > 35$ and small gap sizes, in order to avoid brace failure. The existing models for brace failure (buckling of brace and effective width failure) should be modified to include the slenderness range and the reduced gap size.
- Only few reliable results of tests for steel grade S460 exist. Although all results obtained by the tests give margins of safety above 1.25, it is proposed to limit the slenderness and the gap size to the values given in Eurocode 3 [5-1] until additional investigations are available.

To develop more precise proposals for chord web buckling failure (for example a reduction factor as given for X-joints already), reduced punching shear failure, reduced effective width failure and local buckling of the brace failure , additional FE analyses have to be carried out.

5.10 Numerical investigations

In the framework of a dissertation, finite elements analysis based on the experimental investigations presented in this report, are carried out at Karlsruhe University. The results of this experimental work and the numerical investigations will be used to modify the existing design rules to include slender chord sections and small gap sizes. Some results are already published in [5-7].

6 Effect of welding in cold formed areas

6.1 Introduction and aims

In the following the main results, conclusions and design recommendations found in the scope of Working Package 4 (WP4) are presented.

According to DIN 17014, Part 1, Edition 1988 (6-1), ageing is a change of the properties of a material at or close to room temperature by movement of interstitial dissolved elements. The literature distinguishes between natural ageing and artificial ageing (increased temperature and reduced influencing time).

The ageing of unalloyed steel requires freely moveable nitrogen and carbon atoms in the crystal structure. Depending on how these atoms lose their mobility, the process is called quench-age hardening or strain ageing, respectively. In relation to welding in cold-formed areas, strain ageing is relevant.

Essentially, the process of strain ageing is based on an influence of a larger number of displacements in the crystal structure caused by cold-forming. Nitrogen and carbon atoms are deposited with a time and temperature dependant diffusion into braced lattice regions, which can also be affected by the heat input during welding. If the concentration of nitrogen and carbon atoms is sufficient, these depositions cause a yield hindrance. This is called ageing and embrittlement of steel (see Ruge [6-2 and 6-3]).

In addition to the preceding cold-forming, strain ageing causes an increase in the yield strength, tensile strength and hardness, together with a decrease of strain, the reduction of area and the Charpy V notch impact energy (Houdremont [6-4]).

Through the addition of, for example, aluminium in steel manufacturing, Nitrogen can be converted to aluminium nitrate, whereby a far-reaching resistance to ageing of the steel can be achieved.

In the last few decades such restrictions have been formulated not only in DIN standards and Eurocode 3, but also in AD Merkblätter (codes of practice for the fabrication and testing of pressure vessels), Technische Regeln Druckbehälter TRD (Technical rules for pressure vessels/ fabrication), VGB codes of practice for the fabrication and the supervision of high performance steam boilers, in the rules of the "Germanischer Lloyd" for shipbuilding/ -hull structures and in the code of practice for railway bridges and other building structures of the Deutsche Bahn AG (DS804). The comparison of these restrictions shows that for the same issue of "*dangerous strain ageing*", the resulting restrictions are very different.

So, for example in AD Merkblätter the main criterions are the cast analysis and the wall thickness. In dependence of both a heat treatment after welding has to be carried out. Regarding the regulations of the Deutsche Bahn AG (DS 804) the influence of fully killed steel is not taken into account and for wall thickness $t > 8$ mm a post weld heat treatment has to be carried out for the relevant cases. The same conditions are given in a National Application Document for steel bridges (DIN Fachbericht 103) based on Eurocode 3.

Preferably, the sensitivity to ageing of steel is assessed by the Charpy V notch impact energy temperature curve.

In the course of the present research programme, only the influence of strain ageing adjacent to the weld seam is to be investigated. Notch effects and geometrical influences such as single-layer welding are to be excluded or minimised in order to prevent any dominating influence of such conditions on the test process. A multi-layer weld would e.g. cause a normalising effect that would cover the ageing. On this basis, the bead-on-plate weld has been removed afterwards, so that only the influence of the thermal effect of the weld bead in the cold-formed area of the specimen – the strain ageing caused by welding – remains as an influencing parameter. The bead-on-plate weld is only regarded as an "expedient" for the generation of the ageing area typical for a weld seam.

The present research programme investigates the shift of the transition temperature caused by welding (ageing effects) using Charpy V notch test (CVN tests) and cold-formed structural hollow sections. For the hollow sections, the condition "*removed weld seam*" is mainly to be checked. A real weld would not lead to a stricter condition for the determination of the ageing effect.

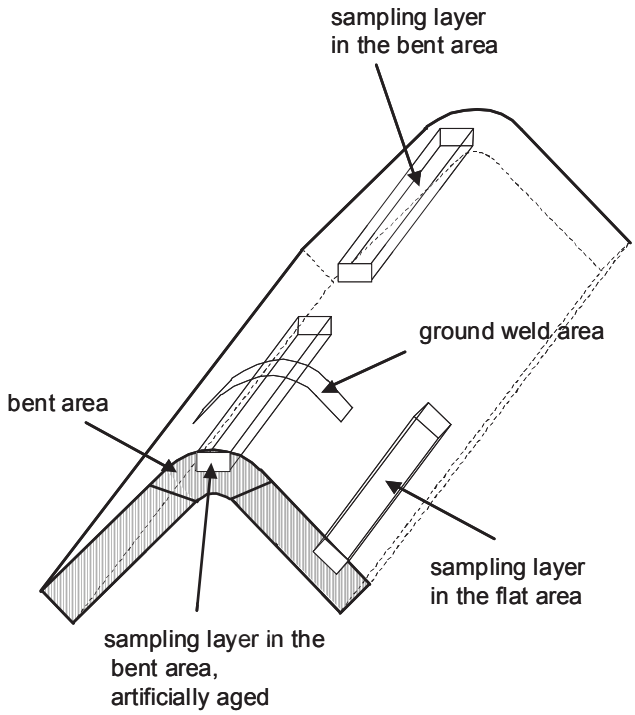

Figure 6-1. Positions of sampling layers.

For the evaluation of brittle fracture, the notch was prepared in the zone reheated by welding (see *Figure 6-1*). It was to be investigated, whether this reheating (ageing) influences the brittle fracture temperature. An extensive material analysis was carried out, in which transition temperatures at 27 J of the following material conditions were to be determined:

- base material (sampling location in flat area)
- base material (sampling location in curved area)
- base material (sampling location in curved area, artificially aged)

For each material condition, about 18 tests are carried out to obtain sufficient data for statistical analysis.

Welding in cold-formed areas is not only an open question for statically loaded sections (brittle fracture) but also for dynamically loaded structures (fatigue resistance).

Especially for structural joints made of hollow sections with large width-ratios b_1/b_0, it is often necessary to weld in the areas close to the edges. A lot of these structures are subjected to dynamic loading. Because there is nearly no information given about the influence of the weld in cold-formed areas on the fatigue resistance of modern steels, welding in this areas is not acceptable.

In the scope of this research project, the fatigue behaviour of welded (notched) and non-welded (un-notched) test specimens made of different steel grades and wall thicknesses are compared directly with each other to determine, whether a weld notch influences the fatigue behaviour in cold-formed regions of hollow sections and if so, to what extent.

It is important to point out that the intention of all tests was to find out, whether there is a difference in the fatigue behaviour of artificial aged specimens and non-aged specimens. It was not the intention to get an absolutely correct fatigue curve for square hollow sections under unusual loading conditions as they have been used during the tests.

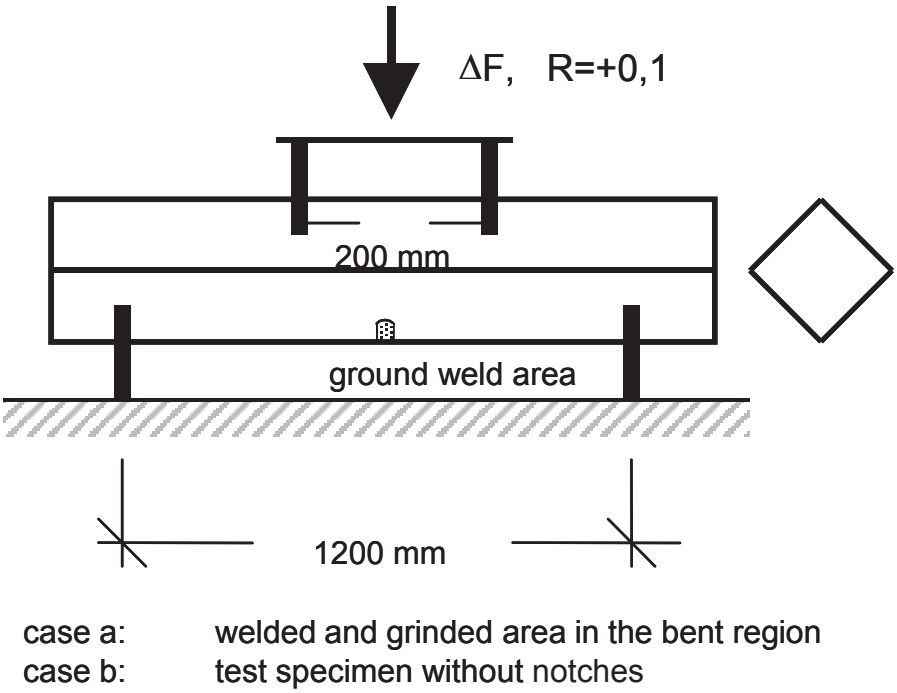

Figure 6-2. Test set-up for 4-point-bending fatigue tests.

The fatigue tests were carried out as 4-point-bending-tests, both on welded and un-welded specimens for comparison (see *Figure 6-2*). The weld seam was removed before the tests by grinding.

For all the tests, CVN and fatigue tests, the specimens have been prepared from the same sections. Also, the weld notches were prepared and documented in the same manner.

With this work, detailed fundamental information is made available about the basics of the material and the weld, as well as the fatigue behaviour of the cold-formed material investigated under notched and un-notched conditions. Finally, conclusions will be made on the influence of welding in the bent area of cold-formed hollow sections on fatigue behaviour. Detailed information about all results are given in Document 4341/WP4/4006 Version 02: WP4 Welding Procedures – Final Technical Report [6-5].

6.2 Test specimens

6.2.1 Hollow sections

For the investigations, the following steel grades have been chosen:

S275J2H as per EN 10219 (1997) (6-6) with the following restrictions:
Content of Al ≥ 0.20 %, S ≤ 0.012 %, P ≤ 0.025 %

S355J2H as per EN 10219 (1997) (6-6) with the following restrictions:
Content of Al ≥ 0.20 %, S ≤ 0.008 %, P ≤ 0.025 %

S460MLH as per EN 10219 (1997) (6-6) with the following restrictions:
Content of Al ≥ 0.20 %, S ≤ 0.008 %, P ≤ 0.025 %

The wall thicknesses of the hollow sections investigated were:

5 mm, 8 mm, 10 mm, 12 mm and 12.5 mm.

From the above mentioned 15 possible steel grade to wall thickness combinations, 3 material batches were investigated in the course of this research programme combined mainly with 5, 8 and 10 mm wall thickness.

The test specimens chosen were cold-formed structural hollow sections (CFSHS). Depending on availability, the dimensions of the specimens tested had two different sizes (100 x 100, 150 x 150). The main interest concentrates on dimension 100 x 100 mm with different wall thickness as given in Table 6-1.

Table 6-1. Dimensions of test specimens.

b x h x t [mm]	b x h x t [mm]
100 x 100 x 5	150 x 150 x 5
100 x 100 x 8	150 x 150 x 8
100 x 100 x 10	150 x 150 x 10
-	150 x 150 x 12.5

For comparison, some reference tests with stress relieved sections have been carried out also.

The geometrical data for all specimens have been measured. In detail, the height h, the width b, and at the four corners the wall thickness t as well as the inner and outer corner radii have been recorded. In addition, using the mean values of the measured dimensions, the non-dimensional parameters $2\gamma = b/t$, r_o/t_m and r_i/t_m have been determined.

6.2.2 Mechanical-technological data

For all sections delivered the main geometrical data have been measured. In detail, the following sizes have been determined: width b, height h, wall thickness t at all four sides of the sections, inner corner radii r_i at all corners and outer corner radii r_o at all corners.

Based on the means of the measured dimensions (denoted by index m) the main geometrical parameters were calculated, which are $2\gamma = b_m/t_m$, outer corner radii related to wall thickness $r_{o,m}/t_m$ and inner corner radii related to wall thickness $r_{i,m}/t_m$. All results are presented in *Table 6-2*. In addition to that, the minimum ratios r/t according prEN1993-1-8, Table 4.2 (6-7), are given. In some cases the measured ratio $r_{i,m}/t_m$ ranges outside the minimum range. Those sections are highlighted in this table.

The determination of the mechanical-technological data has been carried out by the producers within the scope of the usual quality control. In addition to that, the contraction at fracture Z was determined at Karlsruhe University for three different profiles and wall thicknesses. The results for the flat areas, the corner areas without ageing and the corner areas with ageing are given together with all the other data in the Final Technical Report to WP4 [6-1].

Table 6-2. Geometrical data of the sections investigated.

specimen	b_m [mm]	t_m [mm]	$r_{o,m}$ [mm]	$r_{i,m}$ [mm]	2γ	$r_{o,m}/t_m$	$r_{i,m}/t_m$	min. r/t
A0211	149,95	5,03	12,00	8,00	29,80	2,38	1,59	1,0
A0221	150,47	7,97	21,00	13,38	18,89	2,64	1,68	1,5
A0241	150,53	12,68	37,75	25,00	11,87	2,98		3,0
A12	100,64	5,02	12,00	7,50	20,05	2,39	1,49	1,0
A22	100,45	8,09	21,88	12,63	12,42	2,71	1,56	1,5
A32	99,79	10,12	32,50	23,00	9,86	3,21	2,27	2,0
B0111	149,88	4,72	11,13	6,38	31,75	2,36		1,0
B0121	150,04	7,70	20,88	12,00	19,50	2,71	1,56	1,5
B0211	149,85	4,75	11,00	6,25	31,55	2,32	1,32	1,0
B0221	149,94	7,76	19,88	11,88	19,32	2,56	1,53	1,5
B0261	150,12	9,91	25,50	14,88	15,15	2,57	1,50	1,5
B0311	150,10	4,85	10,00	6,13	30,96	2,06	1,26	1,0
B0321	150,48	7,83	19,75	12,63	19,23	2,52	1,61	1,5
B11	99,94	4,61	10,00	5,00	21,70	2,17	1,09	1,0
B12	99,95	4,64	11,00	6,25	21,56	2,37	1,35	1,0
B13	99,94	4,82	10,63	4,88	20,75	2,21	1,01	1,0
B21	99,82	7,65	20,00	11,75	13,06	2,62	1,54	1,5
B22	99,95	7,73	22,00	10,00	12,93	2,85		1,5
B23	100,07	7,81	18,00	12,00	12,82	2,31	1,54	1,5
B32	100,39	9,93	24,63	12,00	10,11	2,48		1,5
D0211	151,01	4,93	9,75	5,25	30,65	1,98	1,07	1,0
D0211N	150,77	4,88	9,88	5,00	30,93	2,03	1,03	1,0
D0212	150,52	4,98	9,63	7,00	30,24	1,93	1,41	1,0
D0221	150,78	8,05	18,00	10,88	18,72	2,24	1,35	1,5
D0221N	150,59	7,97	18,25	10,00	18,91	2,29	1,26	1,5
D0222	150,18	8,06	19,63	10,13	18,64	2,44	1,26	1,5
D0231	149,97	12,14	29,00	15,50	12,36	2,39	1,28	3,0
D0232	150,21	12,27	29,25	15,38	12,24	2,38	1,25	3,0

6.2.3 Chemical analysis

A complete chemical analysis of the following elements has been carried out and recorded: Carbon, Manganese, Silicium, Sulphur, Phosphorous, Aluminium, Nickel, Vanadium, Titanium, Niobium, Boron, Copper, Chromium, Molybdenium, Tungsten, Cobalt and Nitrogen.

6.2.4 Welding

For all test specimens the MAG weld procedure was chosen. The gas applied was Argon with 18% carbon dioxide as shielding gas (M21 according to EN 440 (6-8)). As electrodes, both Thyssen UNION K56 (G4Si1 according to EN 440 (6-8)) and Griduct S-V 4 (G3Si1 according to EN 440) have been used. Both wire electrodes match the corresponding steel grades. The yield strength of the weld metal corresponds approximately with the yield strength of the base material.

The welding was carried out as bead-to-plate weld over the bent corner, perpendicular to the longitudinal direction, without preparing a groove.

The heat input was as high as possible (about 10 kJ/cm) to cause ageing effects.

Welding specifications for all test specimens prepared are given in *Table 6-3* and in *Table 6-4*.

Table 6-3. Welding procedures for sizes 100 x 100 x t.

test series	dimensions [mm]	steel grade	welding current [A]	welding voltage [V]	welding rod feed rate [m/min]	welding speed [cm/min]	wire diameter [mm]
B11 N	100x100x5	S275	210	23.8	6.7	30 – 35	1.2
B21 N	100x100x8	S275	240	25.0	7.6	30 – 35	1.2
B12 N	100x100x5	S355	210	23.8	6.7	30 – 35	1.2
B22 N	100x100x8	S355	280	31.0	8.8	30 – 35	1.2
B32 N	100x100x10	S355	240	25.0	7.6	30 – 35	1.2
B13 N	100x100x5	S460	210	23.8	6.7	30 – 35	1.2
B23 N	100x100x8	S460	280	31.0	8.8	30 – 35	1.0
A12 N	100x100x5	S355	210	24.0	6.7	30 – 35	1.2
A22 N	100x100x8	S355	240	25.0	7.6	30 – 35	1.2
A32 N	100x100x10	S355	240	25.0	7.6	30 – 35	1.2

gas: Argon with 18% CO_2 (M21) wire: Thyssen UNION K56, G4Si1 (acc. EN 440)

Table 6-4. Welding procedures for sizes 150 x 150 x t.

test series	dimensions [mm]	steel grade	welding current [A]	welding voltage [V]	welding rod feed rate [m/min]	welding speed [cm/min]	wire diameter [mm]
D0211 N	150x150x5	S355	225	25.7	4,6	30 – 35	1.6
D0221 N	150x150x8	S355	315	25.7	4,5	30 – 35	1.6
B0111 N	150x150x8	S275	260	28.0	8,5	35	1.2
B0121 N	150x150x8	S275	260	28.0	8,5	35	1.2
A0211 N	150x150x5	S355	220	25.4	8,8	30 – 35	1.0
B0211 N	150x150x5	S355	220	25.4	8,8	30 – 35	1.0
A0221 N	150x150x8	S355	260	28.6	8,5	35	1.2
B0221 N	150x150x8	S355	260	28.6	8,5	35	1.2
A0241 N	150x150x12.5	S355	260	28.6	8,5	35	1.2
B0261 N	150x150x10	S355	260	28.6	8,5	35	1.2
B0311 N	150x150x5	S460	220	25.4	8,8	30 – 35	1.0
B0321 N	150x150x8	S460	260	28.6	8,5	35	1.2
D0212 N	150x150x5	S355	220	25.4	8,8	30 – 35	1.0
D0222 N	150x150x8	S355	260	28.6	8,5	35	1.2
D0231 N	150x150x12	S355	260	28.6	8,5	35	1.2
D0232 N	150x150x12	S355	260	28.6	8,5	35	1.2

gas: Argon with 18% CO_2 (M21) wire: Griduct S-V 4, G3Si1 (acc. EN 440)

To differentiate between un-notched and welded (notched) specimens, an additional „N“ was added to the designation numbers of the notched specimens.

Examples for macro sections are shown in *Figures 6-3 to 6-5*. As the macro sections show, the heat affected zone is very small for the planned CVN tests.

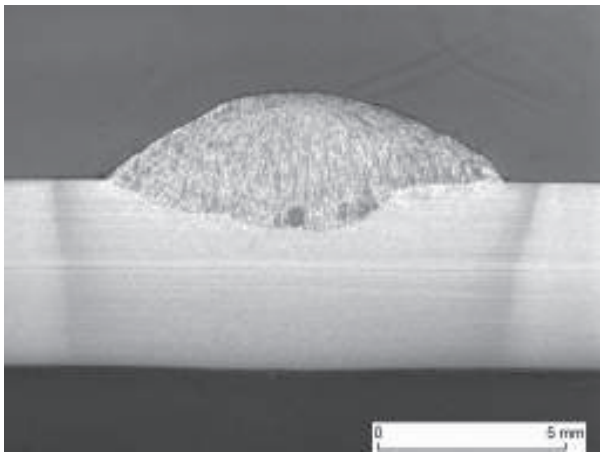

Figure 6-3. SHS 150x150x5 (t=5 mm).

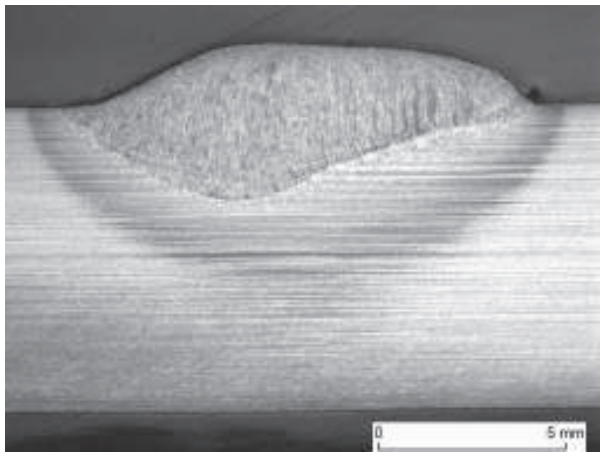

Figure 6-4. SHS 150x150x8 (t=8 mm).

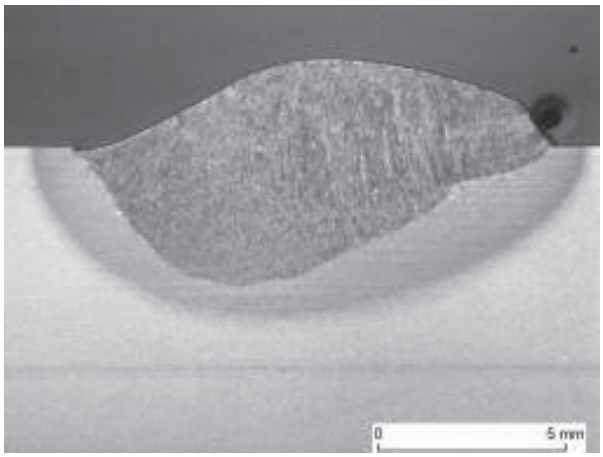

Figure 6-5. SHS 150x150x12 (t=12 mm).

6.2.5 Metallography

To localise the heat affected zone (HAZ), macro sections in the welded corners were made for all specimens prepared for the impact tests.

To get more information of the condition of the corner area, micro sections have been prepared of cracked specimens after the fatigue tests as well as of un-tested specimens. The single steps of the preparation of the micro sections, the positions of the micro sections and the designation are given in the Final Technical Report to WP4 [6-1].

In total, 8 specimens have been prepared and etched. In detail, micro sections of all specimens listed in *Table 6-5* have been made at the outer corner radii as well as at the inner corner radii to find out whether there are special crack initial points at the corners. As in chapter 6.5 will be described no indication for typical crack initial points was found.

Table 6-5. List of micro sections prepared.

specimen	size	steel grade	fatigue test
D0211N-8	150 x 150 x 5	S355J2H	tested
D0211-5	150 x 150 x 5	S355J2H	tested
B0211-3	150 x 150 x 5	S355J2H	tested
B0211-1	150 x 150 x 5	S355J2H	tested
A0211	150 x 150 x 5	S355J2H	un-tested
B0211	150 x 150 x 5	S275J2H	un-tested
D0211	150 x 150 x 5	S355J2H	un-tested
B23	150 x 150 x 8	S460MLH	un-tested

6.3 Charpy V notch impact (CVN) tests

In agreement with project partners, the work was concentrated on the most common profile sizes, which means profiles with wall thickness of 8 and 10 mm. This also includes different grades of transformation. According to *Table 6-2* the ratio for the outer radius $r_{o,m}/t_m$ ranges between 2.06 (specimen B0311) and 3.21 (specimen A32). The ratio for the inner radius $r_{i,m}/t_m$ ranges between 1.21 (specimen B32) and 2.27 (specimen A32). The steel grades of the selected specimens were S355J2H and S460MLH.

For positioning the notch exactly in the HAZ macro sections of all specimens have been prepared. In *Figure 6-6* the exact position of the notch is shown. The base of the notch is crossing the end of the HAZ in the middle of the test specimens. This position was chosen in accordance with wide experiences with specimens taken from un-bent areas.

top view

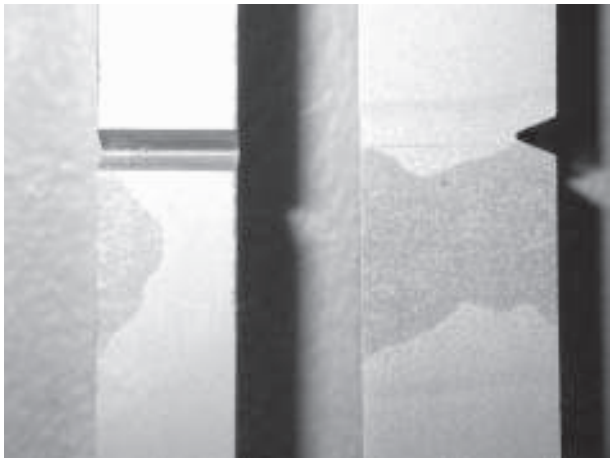

side view

Figure 6-6. Position of the notch crossing the HAZ in the middle of the specimen.

The steps of preparing the Charpy V test specimens are well documented. Big care was taken to eliminate mix-ups. The specimens have been marked with numbers, different colours and were also sorted into different baskets. *Table 6-6* gives an overview, which profiles were prepared for the CVN tests.

Table 6-6. CVN tested specimens.

specimen	size	steel grade
A22	100 x 100 x 8	S355J2H
B23	100 x 100 x 8	S460MLH
A32	100 x 100 x 10	S355J2H
B32	100 x 100 x 10	S355J2H
A0221	150 x 150 x 8	S355J2H
B0121	150 x 150 x 8	S275J2H
B0261	150 x 150 x 10	S355J2H
B0321	150 x 150 x 8	S460MLH

According to *Figure 6-1* and to EN 10045 [6-9] the specimens were worked out of the plane areas, the bent areas and the bent aged areas of the hollow sections. The test specimens from the bent areas are taken as near as possible to the surface: Notch position S (normal to the surface).

In total, about 400 CVN tests have been carried out for eight specimens to have a sufficient statistical reliability. The range of temperature was between room temperature and –80° C, depending on the results found.

Using the test results from CVN tests, the temperature transition curves are drawn up for the Charpy V notch impact energy.

Charpy-V-tests **A32**

Dimensions profile b x h x t [mm] S355J2H

100x100x10

Dimensions specimen l x b x h [mm]

55x10x8

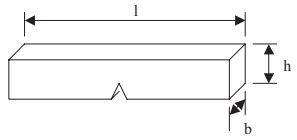

Results related to notch area A = 1.0 cm²

Plane area 1			Bent area 2			Bent area aged 3		
Test No.	Temp. [°C]	KV [J]	Test No.	Temp. [°C]	KV [J]	Test No.	Temp. [°C]	KV [J]
1	-60	16	1	-60	11	1	-60	170
2	-60	9	2	-60	11	2	-60	181
3	-60	13	3	-60	13	3	-60	25
4	-40	170	4	-40	255	4	-40	194
5	-40	28	5	-40	269	5	-40	258
6	-40	28	6	-40	275	6	-40	247
7	-20	284	7	-20	289	7	-20	225
8	-20	227	8	-20	278	8	-20	267
9	-20	291	9	-20	289	9	-20	267
10	-50	13	10	-50	31	10	-80	17
11	-50	11	11	-50	216	11	-60	164
12	-50	92	12	-50	219	12	-80	17
13	-30	275	13	-30	263	13		
14	-30	253	14	-30	283	14		
15	-30	238	15	-30	275	15		
16	-30	197	16	-50	16	16		
17			17	-50	272	17		
18			18	-50	20	18		

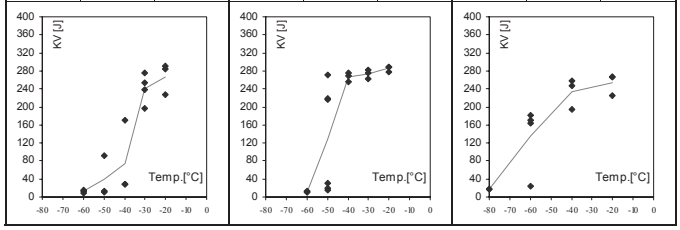

Figure 6-7. CVN tests data sheet.

All data are given in data sheets on which the numerical and graphical results for each section can be compared directly to each other (see *Figure 6-7*). For this reason all results have been related to a notch area of A = 1.00 cm². Also, the results for the tests of specimens prepared of the plane area, the bent area and the bent and aged area are listed in parallel on the same page. For each position the 27 J transition curve is plotted.

The results can be summarised as follows:

Plane area
The notch impact energy KV in the upper shelf is higher than 180 J – 200 J for all cases. The highest transition temperature where the material changes from ductile to brittle fracture ranges between –30° C and –40° C, in two cases no transition could be found in the investigated temperature range down to –80° C.

Bent area
Compared to the behaviour of the specimens prepared out of the plane area, only minor differences can be found. Generally, the same transition curves for both specimens were found.

Bent area aged
Compared to the both cases above the behaviour of the specimens made out of the bent aged area is a little bit different. The notch impact energy KV in the upper shelf is higher than 200 J/cm² for all cases. In six of eight cases no decrease of the notch impact energy KV was found. The temperature ranges between room temperature and –80° C.

In one case (specimen A32) the 27 J transition temperature was found between –70° C and –80° C. In another case (specimen B0261) the transition between upper and lower shelf ranges between 0° C and –40° C. Regarding all tests carried out, the minimum for the lower shelf was found at –60° C with 26,7 J/cm².

For all other cases, a similar or better ductile behaviour was found than for the plane or for the bent area without ageing. It is assumed that the welding in the bent area causes some kind of normalising effect.

Comparing both steel grades (S355J3H and S460MLH) no remarkable differences concerning the notch impact energy have been found.

Influence of HAZ
As in *Figure 6-6* clearly can be seen all notches have been positioned in a manner that the notch is located exactly at the toe of the weld and the beginning of the heat affected zone (HAZ). Later on and due to the results of the Charpy V tests the influence of the position of the notch and with this the influence of the HAZ was investigated.

For two specimens, B0261 (t = 10 mm, S355J2H) and B0321 (t = 8 mm, S460MLH), the distance of the notches from the toe of the weld was varied between 1 and 5 mm. For specimen B0261 the temperature for all tests was kept constant at –20° C. The reason for choosing this temperature was, that at this temperature a change in the notch impact energy was found in the previous tests. For specimen B0321 the testing temperature was kept constant at –50° C.

As the transition curves show, a wide scatter of the notch impact energy can be found nearby the toe of the weld. Compared with the results given in the data sheets for specimen B0261 and specimen B0321 a reasonable agreement with the results given there for a distance d = 1 mm was found. In this distance (d = 1 mm) the notches of all specimens tested before have been positioned. Comparing the results in a distance d = 4 mm to the toe of the weld, the impression can be received that the notch impact energy is lower than in the tests done before at the same temperature. *Table 6-7* summarises this effect.

With consideration of the wide scatter found in the transition of the HAZ to the un-notched area these results prove that the position of the notches as shown in *Figure 6-6* was alright.

Table 6-7. Comparison of notch impact energy in different distances d from the weld toe.

specimen	size	Steel grade	mean KV [J] at d = 1 mm	mean KV [J] at d = 4 mm
B0261	150 x 150 x 10	S355J2H	43	25
B0321	150 x 150 x 8	S460MLH	145	48

Comparison with results found by others

In a recent publication by Packer (6-10) the measured Charpy V notch toughness for cold-formed hollow sections produced in different parts of the world is compared. The specimens have been prepared from the flat areas as well as from the exterior and interior corners. The influence of welding was not considered in this paper.

The hollow sections tested have been produced by companies from North America, South America, Japan and Europe. The cold-formed sections coming from Europe had been delivered by the same producers as the sections investigated in the scope of this programme. In addition to that, hot-rolled sections have been tested for reference.

The highest Charpy V notch toughness was found for the hot-rolled specimens, as it was expected. The results for the cold-formed sections are comparable to the results for non-aged specimens found in this project. Whereas the Charpy V transition curves found for profiles made for example in North America are not meeting the requirements for steel products in Europe. Thus, the consideration of the influence of welding in cold-formed areas is lapsed for these sections.

The main reasons for the differences in the Charpy V notch toughness for sections investigated in the present ECSC project and other sections made in Europe and in other parts of the world are mainly seen in the differences of the chemical compositions of the steels.

6.4 Fatigue tests

The evaluation is done using the nominal stress (Woehler) method. For each test series, a minimum of 3 fatigue tests was carried out, normally 6 tests have been performed. The statistical evaluation is done according to EN 1993-1-1 using computer software developed for this purpose at University of Karlsruhe. The probability of survival is taken into account with 95 % at a confidence level of 75 %.

For comparison, notched and un-notched hollow sections made of the same charge have been investigated and compared with each other. As for the CVN tests, all artificially aged (welded) specimens have been prepared without grooves.

Finally, a total of 171 specimen have been investigated, using three machines in parallel (see *Figure 6-8* and *Figure 6-9*).

Fatigue curves have been prepared for all series with sufficient results. The detailed results of all tests are given in data sheets, one sheet per series. In these data sheets, basic information about the test series is given, such as nominal dimensions, steel grades and welding procedure specifications (WPS) according to *Table 6-3* and *Table 6-4*.

Also, the results of the fatigue tests are listed in a table on this data sheet, where stress range S_R, stress ratio R, numbers of failure N_f, failure mode (see *Figure 6-10*), as well as remarks (if any) are given. The S_R-N_f diagram (Woehler diagram) is presented on the lower half of this data sheet. As far as available and in the scope of Working Package 1.1 [6-12], $R_{p0.2}$ for the flat and for the corner area of the sections are given. All data sheets are given in Appendix 5 of the Final Technical Report to WP4 [6-1].

Figure 6-8. On the left: Test specimen during a test in the 200 kN Schenk machine. On the right: Test specimen during a test in the 200 kN Losenhausen machine.

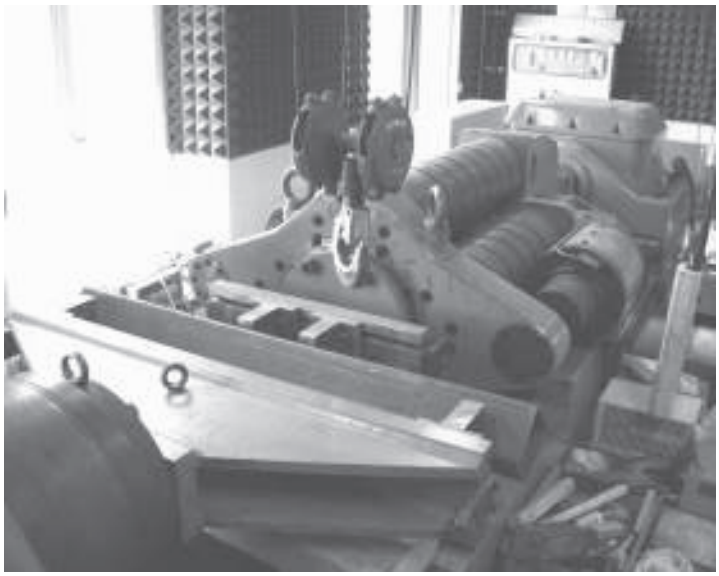

Figure 6-9. Test specimen ready for testing in the 600 kN Schenk machine.

The results of the fatigue tests show different types and locations of failure, which are schematically described in *Figure 6-10*.

Due to the ovalization effects of the hollow sections under bending and as the FE investigations have shown, the stress levels in areas H1 and H2 are nearly the same for un-notched and for artificially aged specimens (see Document 4341/WP4/4005 [6-11]). This explains the different locations of the cracks.

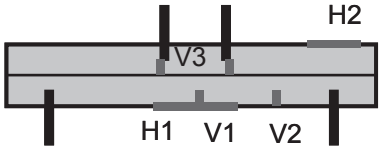

Failure type	Description of failure
H1	Longitudinal crack starting in the middle of the specimen
H2	Longitudinal crack starting in the corner opposite to a support
V1	Vertical crack starting in the middle of the specimen
V2	Vertical crack starting in the middle between support and load introduction
V3	Two v ertical cracks starting parallel at the load introduction

Figure 6-10. Failure modes.

The occurrence of longitudinal cracks, normally vertical cracks are to be expected, could not be explained with the FE analysis alone. To get more evidence on this point, additional macro and micro sections have been carried out. With this, the first assumption that a sporadic occurrence of micro cracks was the reason for that failure mode was not confirmed.

Finally, it is assumed that the degree of bending and the corner radii influence this behaviour. This assumption was confirmed when the measured geometrical data are compared to the minimum r/t ratios given in Eurocode 3, Part 1-8, Table 4.2 (6-7). In *Table 6-2* the sections outside the given range are highlighted. Comparing the sections with the failure mode ”longitudinal crack” with this table, it can be found, that these sections are all highlighted.

For evaluating the fatigue test results, the stresses in the bent areas have to be known. The theoretical calculation has been done using the nominal dimensions and nominal sections modules of the test specimens acc. EN 10219-2 (6-6) as well as the measured geometrical data (mean values). The stresses for both cases, nominal dimensions ($S_{theo.,nom.}$) and measured dimensions ($S_{theo,real}$), have been calculated for a reference load F = 10 kN. In addition, strain gauge measurements as well as finite element calculations have been carried out to verify the results.

Using these results, it can be stated that the real longitudinal stresses are about 10% to 20% lower compared to the theoretical longitudinal stresses. This effect can be ascribed to the ovalisation effect of the hollow sections. The influence of the ovalisation is strongly depending on the width to wall thickness ratio of the sections.

At this point, the aim of the fatigue tests is to be recapitulated. The intention of all tests was to find out, whether there is a difference in the fatigue behaviour of artificial aged specimens and non-aged specimens. It was not the intention to get an absolutely correct fatigue curve for those profiles under unusual loading conditions as they have been used during the tests.

As preliminary tests had shown, for the chosen 4 point bending test set-up fatigue cracks only could be achieved for $N_f < 2$ Million load cycles when an extremely high S_R was implied. As mentioned, S_R was theoretically calculated only for longitudinal stresses in the outer fibres of the edges of the profiles. This results in some cases in calculation stress ranges S_R which are nearly as high as R_m.

Another result is, that in some cases S_D at 2 Million load cycles seems to be very high compared to the nominal yield stress of the profiles. Regarding the mechanical data of the sections tested it can be seen that for the most sections the investigated $R_{p,0.2}$ was remarkable higher than the minimum guaranteed stress (nominal stress).

Taking all these points into account, it was found that S_D (50% mean) was not exceeding about 80% of the real R_m.

In the following, all fatigue results are related to nominal dimensions of the profiles and to the theoretical calculated stresses.

A combined evaluation of the fatigue results of all series presented is given in Appendix 7 of (6-1). For each dimension (100x100x5, 100 x100 x 8.0, 100 x 100 x 10.0, 150 x 150 x 5.0 and 150 x150 x 8.0) a separate fatigue curve is given there, combining results of specimens of different producers with and without ageing effect as well as results for different steel grades.

In a first comparison all fatigue test results for profiles 100x100x5 and for all steel grades are compared, separated into sections with ageing effect and without ageing effect. The same has been done for profiles 100x100x8. Due to the fact that no test results below $5x10^5$ load cycles are available no reliable fatigue curve could be given.

The same diagrams for 100x100x10 have been plotted also. Regarding the diagrams it can be seen, that in all three cases the scatter band of aged specimens is smaller than in the case of non-aged specimens. The fatigue resistance for aged and non-aged specimens at 2 Million load cycles calculated for both, t = 5 mm and t = 8 mm, is about 10% higher for t = 5 mm than for t = 8 mm. Compared to t = 10 mm, both are clearly lower. A remarkable difference occurs in the calculated slope of the curves, which is m = 6.4 for t = 10 mm, m = 5.1 for t = 8 mm and m = 8.0 for t = 5 mm.

Regarding the influence of the ageing effect, this effect decreases the lower bound of the fatigue resistance scatter band for t = 5 mm (287.3 N/mm² compared to 313.1 N/mm²). For t = 8 mm the converse effect occurs (305.8 N/mm² compared to 254.1 N/mm² without ageing effect). Finally, for t = 10 mm nearly the same results have been found (312.3 N/mm² and 313.3 N/mm²).

It is clear, that these results are strongly influenced by the wide scatter band of the non-aged specimens. So, a comparison of 50% mean line at 2 Million load cycles can give more evidence (*Table 6-8*). It is to be noted, that in this contemplation the slopes of the fatigue curves are differing.

Table 6-8. Fatigue resistance at 2 Mio. load cycles for aged and non-aged specimens (50 % mean).

size	**S_R at 2 Mio. load cycles [N/mm²]**		**relation aged/ non-aged**
	aged	**non-aged**	
100 x 100 x 5	332.2	383.8	0.87
100 x 100 x 8	358.1	398.5	0.90
100 x 100 x 10	384.1	448.4	0.86

In *Figure 6-11* this effect is made visible in a S_R-N_f diagram for sections 100x100x10 comparing the mean lines for aged and non-aged specimens, all made of steel S355J2H.

Further on, two diagrams for steel grade S355J2H have been plotted, sections size 100x100 mm including wall thickness 5 mm, 8 mm and 10 mm separated into profiles made by producer A and producer B (see *Figure 6-12*). It is interesting to note, that the calculated slopes as well as the lower boundaries are the same for both producers. Differences only could be seen in the width of the scatter band.

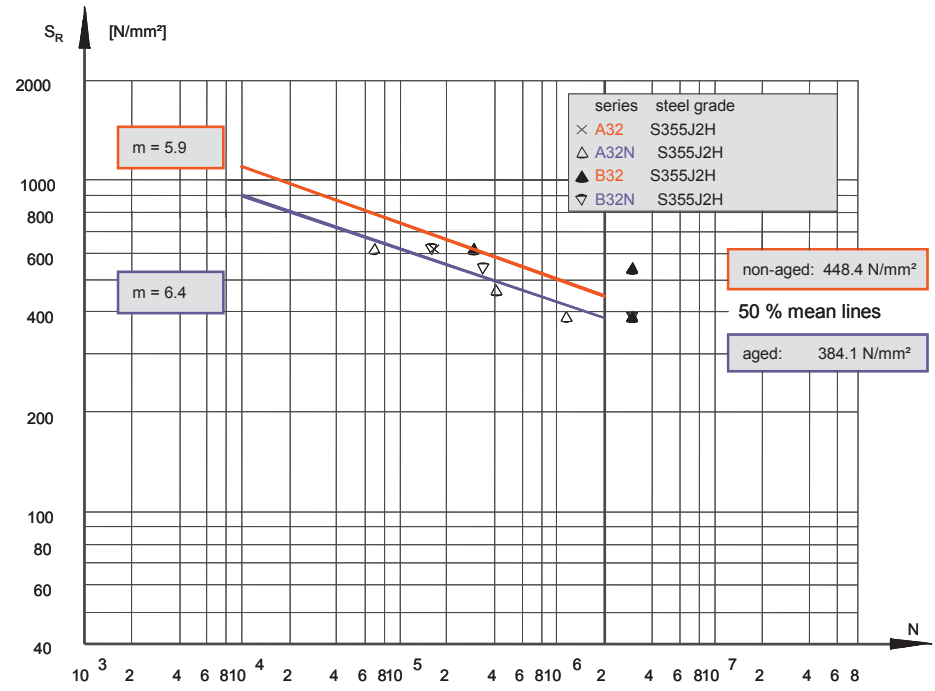

Figure 6-11. Fatigue results series 32 (100 x 100 x 10).

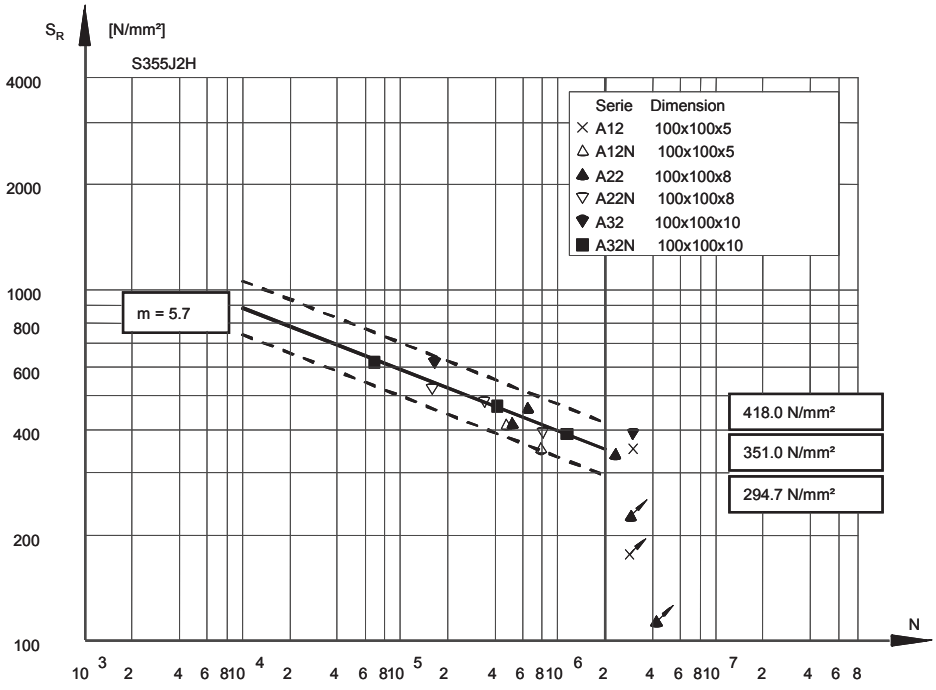

Figure 6-12a. Different sizes (S355J2H) with and without ageing effects (Producer A).

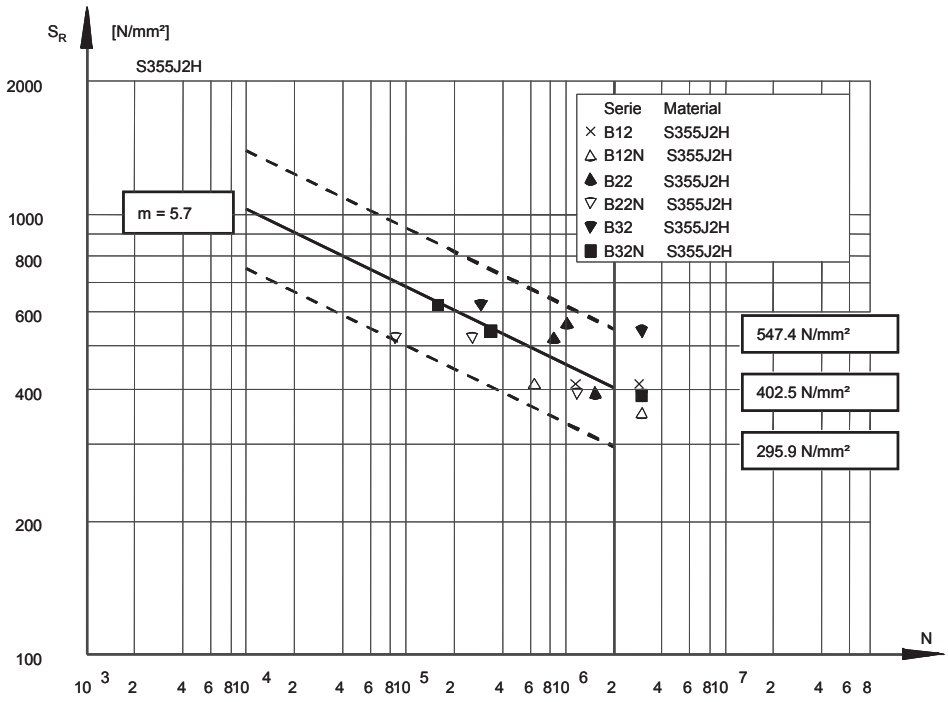

Figure 6-12b. Different sizes (S355J2H) with and without ageing effects (Producer B).

Comparing aged and non-aged sections 100x100x10 made of S355J2H an influence of the ageing effect can be stated for mean lines as well as for lower boundary lines (*Figure 6-13*). On the other hand no influence was found for sections 100x100x8 (S355J2H). This was confirmed by comparing sections 150x150x5 and 150x150x8, all made of S355J2H. Regarding only the lower boundary curves, no clear influence of the ageing effect on the fatigue behaviour could be found.

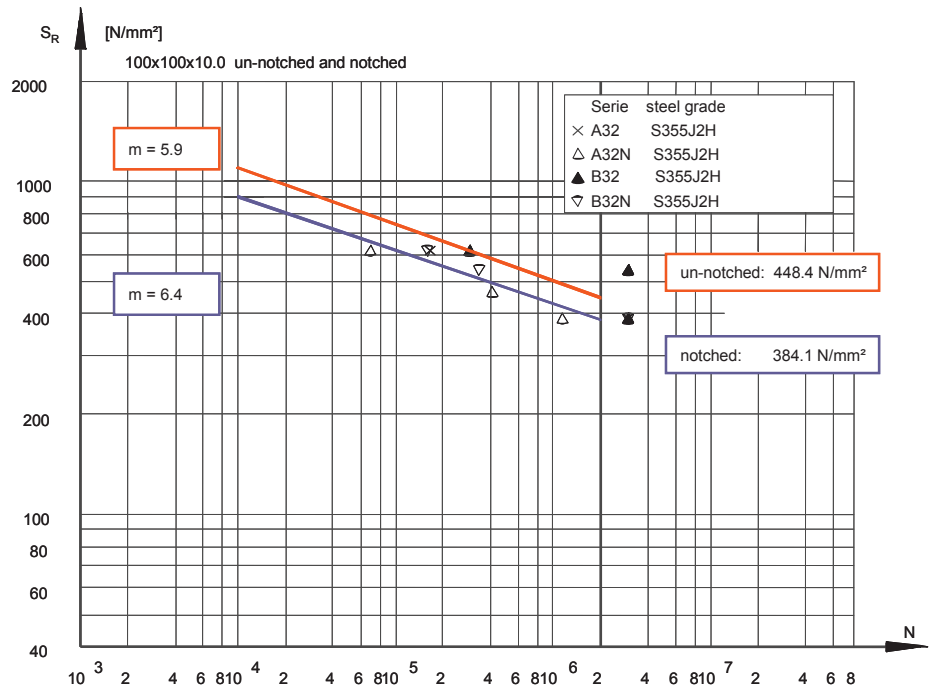

Figure 6-13. Results series 32 (100x100x10),with and without ageing.

To clear the influence of the steel grade two more diagrams have been plotted (see *Figure 6-14*). For a given size of the sections (100x100x8) the fatigue curves (50 % mean) for various steel grades are plotted, separated into specimens with artificial ageing and without ageing effect.

Without ageing, a clear influence of the steel grade used on the slope of the fatigue curve can be seen. Due to that effect, the stress range at 2 Million load cycles varies between S_R = 338 N/mm² and S_R = 500 N/mm².

Taking the ageing effect into account, nearly no difference between the steel grades used in the tests can be found regarding the 50% mean lines. The slope of all lines ranges between m = 6.2 and m = 6.9 with a mean of m = 6.4. The stress range at 2 Million load cycles ranges between S_R = 352 N/mm² and S_R = 370 N/mm².

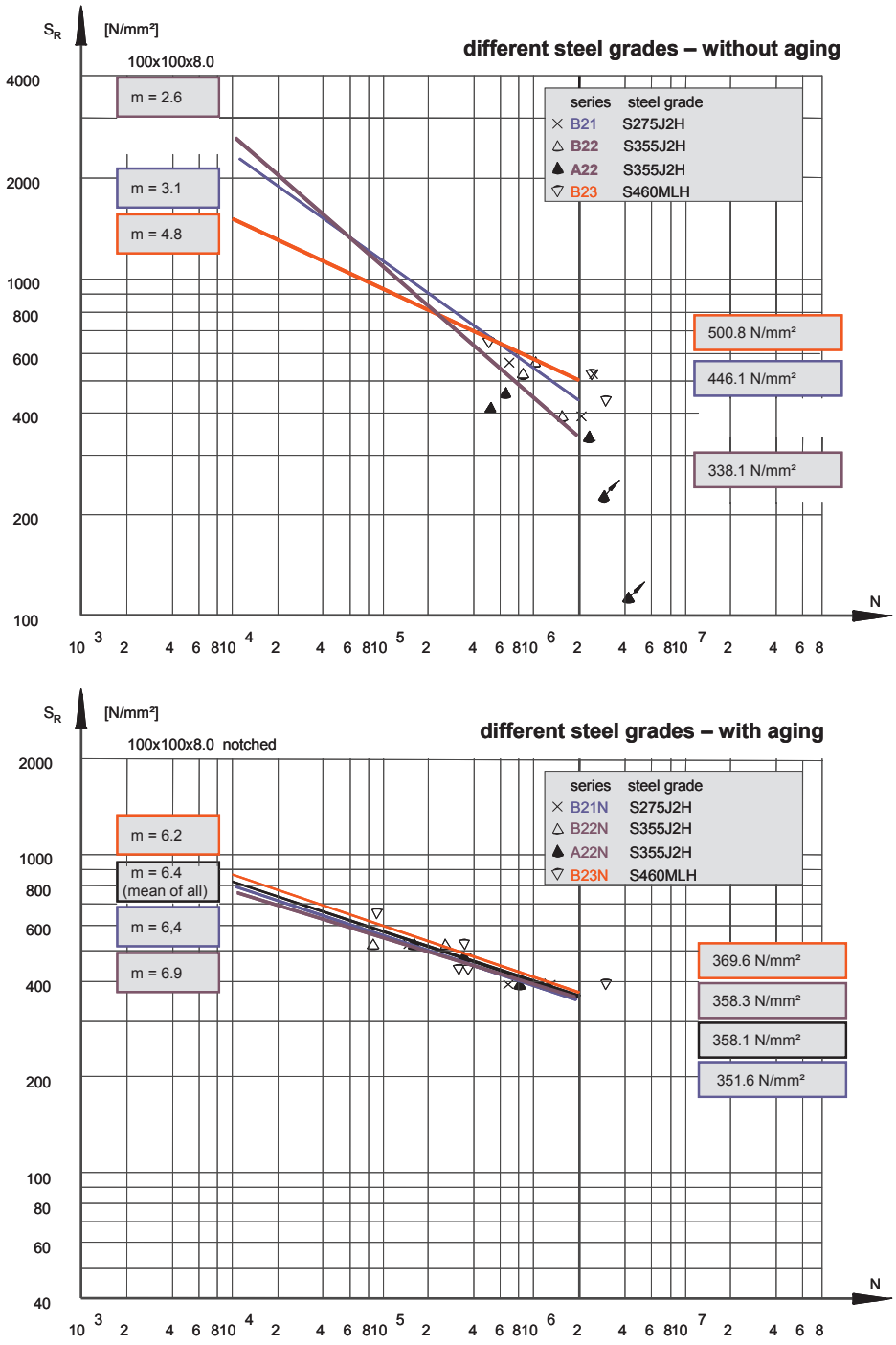

Figure 6-14. Influence of steel grades comparing aged and non-aged sections of size (100x100x8).

The same tendencies can be found for profiles 150x150x5 and 150x150x8. The comparable diagrams for those profiles are given in the Final Technical Report to WP4 (6-1). Regarding the behaviour of stress relieved profiles, for all dimensions investigated (150x150x5, 150x150x8 and 150x150x12) the fatigue results for aged and non-aged specimens are nearly on the same level. Compared to results found for sections without stress relieving no remarkable differences were found (see also *Table 6-9*).

In the next step, the fatigue results have been evaluated with a fixed slope of the Woehler curve. The comparison of the fatigue curves and their free slopes found in the steps before leads to the impression that this fixed slope should be higher than m = 3, the usual slope given in Eurocode 3 Part 1-9 (6-13). For this reason, a fixed slope of m = 5 was assumed in the following, the same slope as given in Table 8.7 of Eurocode 3-1-9 for hollow section joints.

With this assumption the fatigue curves through the lowest values of each series (lower boundary curves) have been plotted. Examples of the resulting diagrams are given in *Figure 6-15* to *Figure 6-18*.

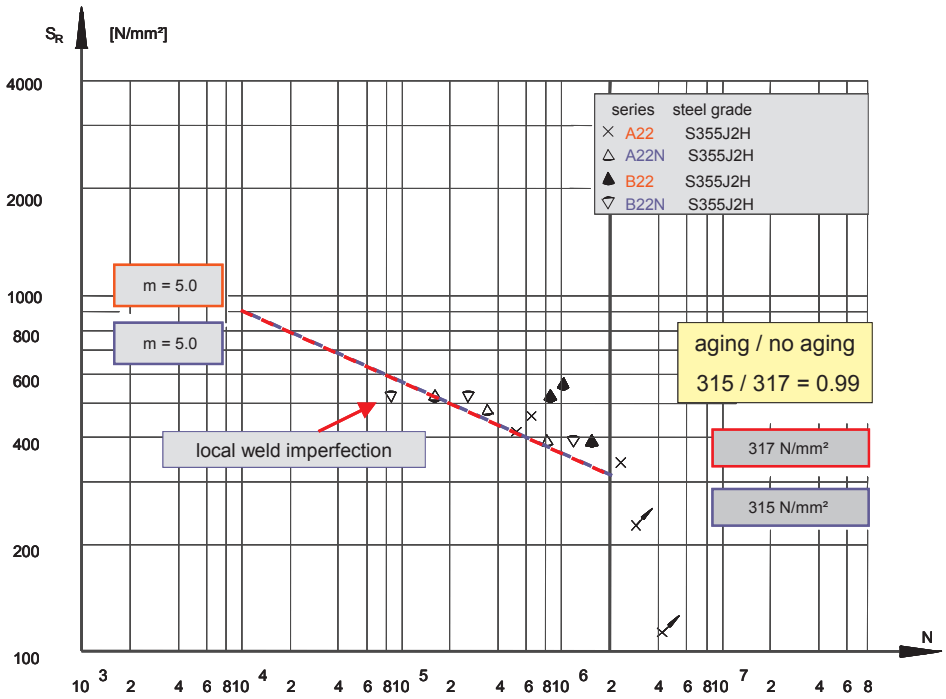

Figure 6-15. Results series 22 (100x100x8), lower boundaries with fixed slope m = 5.

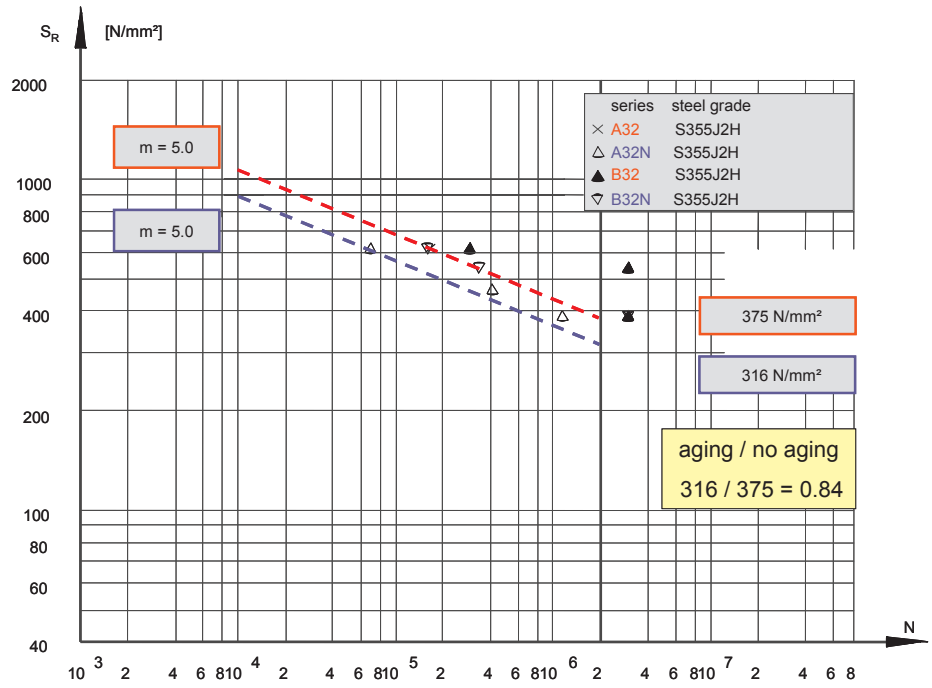

Figure 6-16. Results series 32 (100x100x10), lower boundaries with fixed slope m = 5.

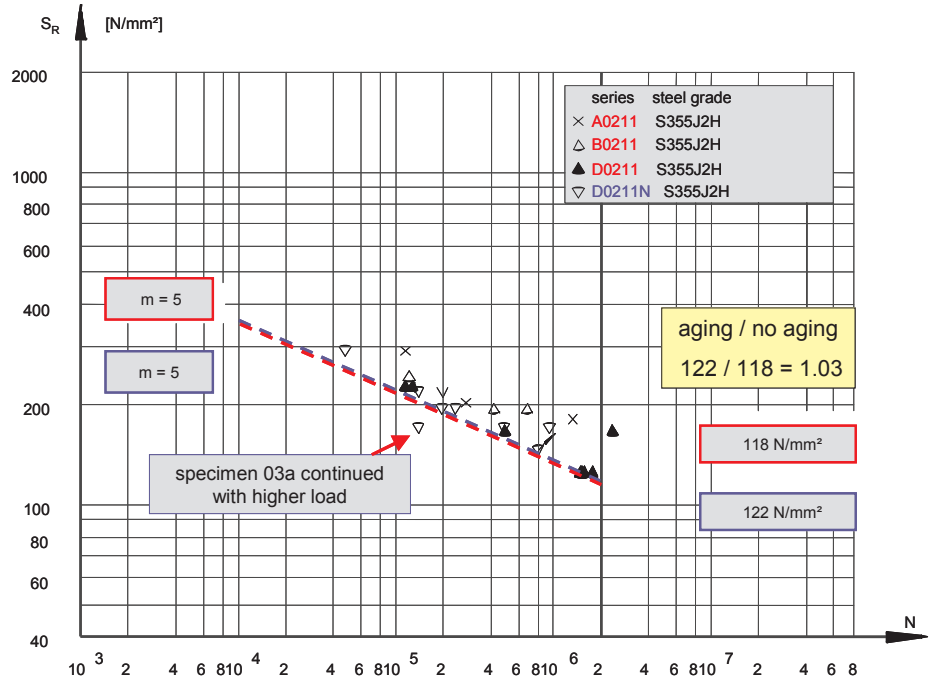

Figure 6-17. Results series 0211 (150x150x5), lower boundaries with fixed slope m = 5.

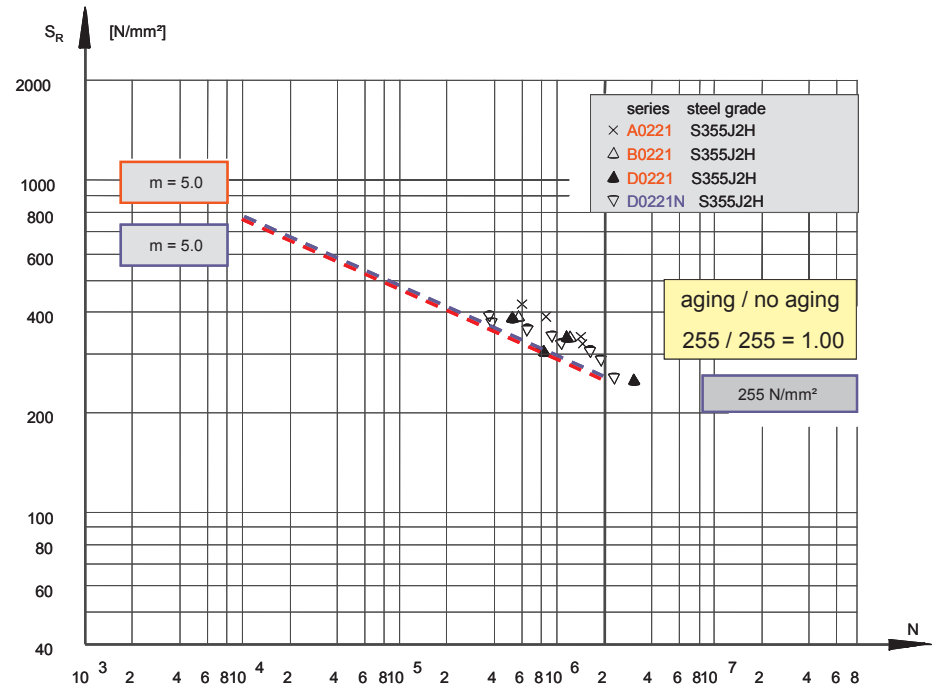

Figure 6-18. Results series 0221 (150x150x8), lower boundaries with fixed slope m = 5.

With the same condition (fixed slope m = 5) a comparison of different steel grades with and without ageing effect was carried out. The relevant diagrams are given in *Figure 6-19* and *Figure 6-20*. In both diagrams the 50% mean line was plotted. *Table 6-9* summarises all results concerning the evaluation with a given slope of m = 5.

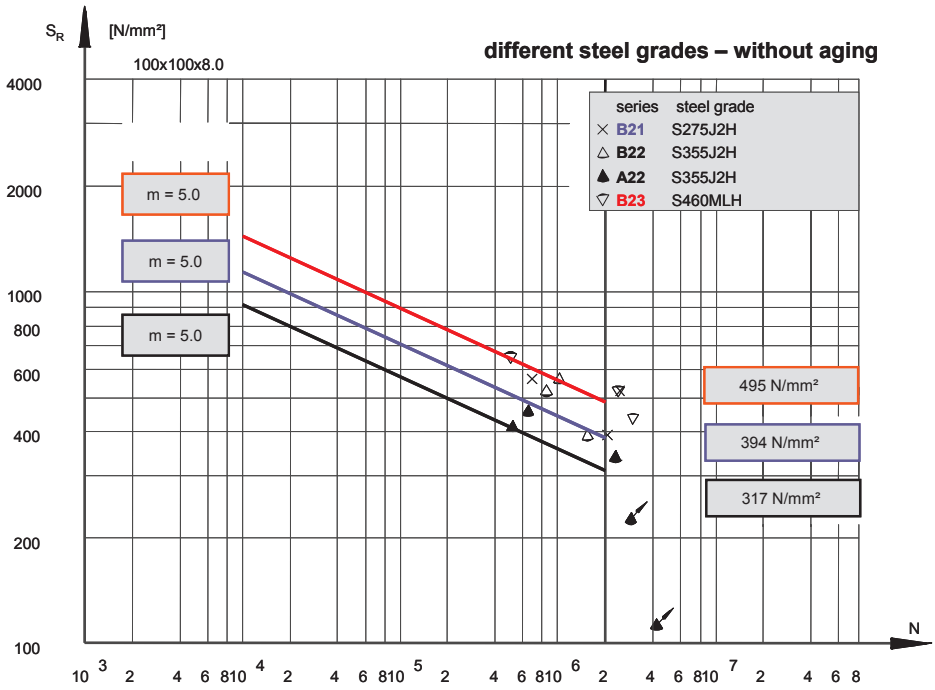

Figure 6-19. Fatigue curves for different steel grades (100x100x8) without ageing, mean lines with fixed slope m = 5.

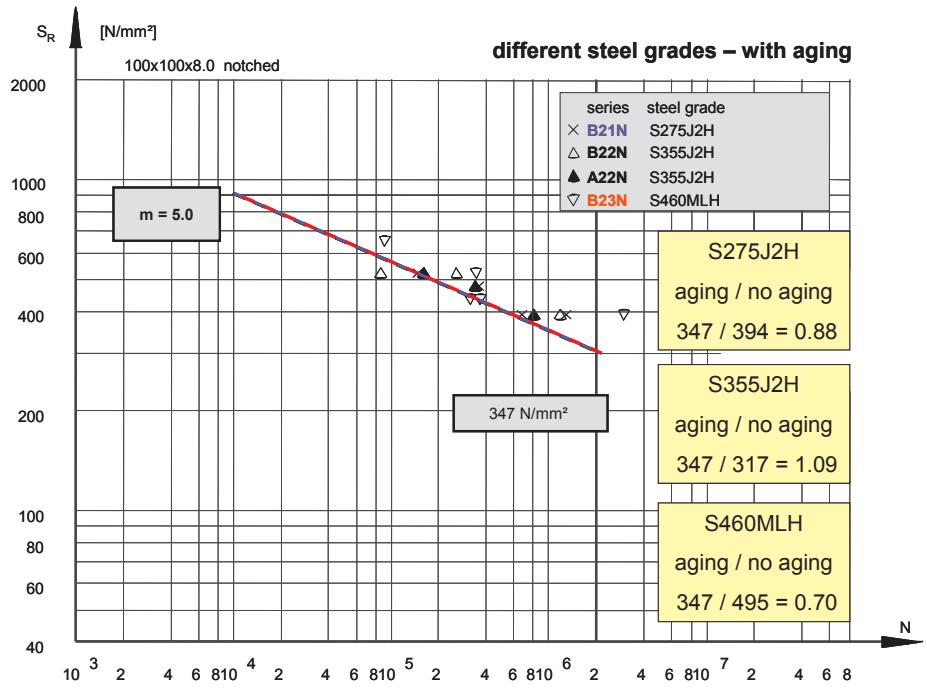

Figure 6-20. Fatigue curves for different steel grades (100x100x8) with artificial ageing, mean lines with fixed slope m = 5.

Table 6-10. Comparison of $\Delta\sigma_c$ (= S_R at 2 Million load cycles) for aged and non-aged sections 100x100xt, slope fixed to m= 5.

wall thickness t [mm]	*steel grade*	*$\Delta\sigma_c$ mean [N/mm²]*			*$\Delta\sigma_c$ lower boundary [N/mm²]*		
		aged	*non-aged*	*aged / non-aged*	*aged*	*non-aged*	*aged / non-aged*
8	*S275J2H*	*347*	*394*	*0.88*	*347*	*394*	*0.88*
8	*S355J2H*	*347*	*317*	*1.09*	*255*	*255*	*1.00*
8	*S460MLH*	*347*	*495*	*0.70*	*315*	*317*	*0.99*
10	*S355J2H*	*346*	*440*	*0.79*	*316*	*375*	*0.84*
12	*S355J2H stress relieved*	*347*	*347*	*1.00*	*321*	*321*	*1.00*

Summarising the effect of welding in the cold-formed areas of the hollow sections investigated the relation between $\Delta\sigma_c$ aged to $\Delta\sigma_c$ non-aged varies between 0.86 and 0.90 (free slope, 50 % mean lines), between 0.70 and 1.09 (slope = 5, 50% mean lines) and between 0.84 and 1.00 (slope = 5, lower boundary).

Regarding all fatigue tests carried out in the scope of this project the results and conclusions can be summarised as follows:

- The occurrence of longitudinal cracks is influenced by the degree of freedom and the corner radii. Normally, vertical cracks are to be expected.

- The calculated slopes of the fatigue lines are ranging between m = 3 and m = 8.
- Regarding the lower bounds of the scatter bands only small differences between aged and non-aged specimens have found.
- Aged specimens show higher values of m than non-aged specimens.
- Regarding the mean lines the relation of S_R between aged and non-aged specimens at 2 Million load cycles ranges between 0.87 and 0.90 for all sections.
- The scatter band of aged specimens is remarkable smaller than for non-aged specimens.
- Different steel grades are resulting in different slopes and different stress ranges at 2 Million load cycles for non-aged specimens.
- Aged specimens lead to nearly the same slope and the same fatigue resistance for all steel grades S275J2H, S355J2H and S460MLH.
- Using a given slope of m = 5 and using the mean lines of the fatigue results the relation aged specimens to non-aged specimens ranges between 0.70 and 1.09.
- Using a given slope of m = 5 and using the lower boundary of the fatigue results the relation aged specimens to non-aged specimens ranges between 0.84 and 1.00.

6.5 Recommendations and Future work

The intention of WP 4 of the present research programme was to investigate the influence of welding in the cold-formed areas of structural hollow sections, regarding mainly the fatigue behaviour. This aim was to be reached by analysing and evaluating the influence of ageing by welding only. Geometrical notches due to the weld geometry were not parts of the investigations.

Due to the fact that only sections made by European producers with high quality standards were tested in the scope of the project, the results found can not be generalised for all profiles available on the European and overseas market. In chapter 6.3 it was stated that the Charpy notch toughness mainly is depending on the chemical composition of the sections and the degree of bending in the corners of the sections. Both parameters can strongly vary, even if all recommendations of the relevant codes are fulfilled.

Keeping this in mind, the following recommendation in respect of welding in cold-formed areas of hollow sections subjected to fatigue load can be given:

1. If the wall thickness of the section is higher than given in Table 4.2 of prEN 1993-1-8:2003, CVN tests in the bent areas are to be made. A minimum energy of 27 J at –20°C must be guaranteed.

2. The detail category acc. prEN 1993-1-9:2003 must be 45 or higher. If that condition is fulfilled, the fatigue detail category of cold-formed sections is to be reduced by two categories.

As example, a K-joint with gap according prEN 1993-1-9:2003, Table 8.7 can be categorised in class 71 for $t_0/t_1 \geq 2.0$. If cold-formed profiles are to be used and welding in the cold-formed areas is necessary, the fatigue detail category is to be reduced to class 56. In addition to that, the Charpy V notch toughness acc. condition 1.) has to be checked.

The restrictions of this recommendation are mainly based on the fact that only the ageing-by-welding effect was investigated in this programme. Geometrical notches have not been examined in the present project. On the other hand it is clear that real structures also have geometrical notches which can

superpose the effect of the ageing-by-welding. This point should be clarified in a sequencing programme.

The verification of the necessary notch toughness acc. condition 1.) is very costly and needs a lot of time. For this verification a new and more economic method should be developed, potentially a relation between notch toughness and chemical composition might be helpful. Also hollow sections with other chemical compositions than the profiles examined in the present project can be included in this evaluation process then.

7 General conclusions

The research work in the *Design rules for cold formed structural hollow section project* was started in July 2000 and was finished formally in the end of year 2003. The project belonged to Steel RTD Programme and was initially accepted by the European Coal and Steel Community (ECSC), but monitored by Research Fund for Coal and Steel (RFCS).

Project consortium comprised of following partners:

VTT Technical Research Centre of Finland, co-ordinator (VTT) (Finland)
Lappeenranta University of Technology (Finland)
Rautaruukki (Finland)
University of Karlsruhe (Germany)
Voest Alpine Krems (Austria)
LABEIN (Spain)
University of Navarra (Spain) and
University of Pisa (Italy).

The overall objective of the project was ***to obtain reliable and economical design rules for cold formed structural hollow sections (CFSHS).*** To obtain this objective most important research items were chosen and more detailed objectives were defined for them. The work to achieve these was divided into five different work packages and tasks within them which were shared between all involved partners. The brief overview of the work and conclusions of work in each work package is summarised in following:

WP1 Mechanical and toughness properties of CFSHS
Objective: Determine mechanical and toughness properties of finished cold formed structural hollow section (CFSHS) (VTT, Rautaruukki, Lappeenranta University of Technology).

The actual characteristics of mechanical and toughness properties of cold formed structural hollow sections (CFSHS) at European market were determined. Mechanical properties around section were determined with tensile coupon tests and toughness properties from flat face were determined with Charpy V Notch tests. The whole test programme contained 51 sections and 15 different section sizes. Most of the sections were from steel grade S355 but some section from high strength steel S460 and hot formed were included for comparison. Requirements set in product standard EN 10219 for steel grade S355 and in Eurocode 3, Part 1.1 for the ductility of steel material were verified. Changes on the property distribution around CFSHS perimeter were studied. Effect low temperature and welding on the mechanical properties was also considered.

Cold forming to hollow sections alters the stress-strain relationship compared to traditional steel material with clear yield plateau. The stress strain relationship becomes curves shape with no clear yield strength but proportional stress level. Special characteristics related to more cold formed corners are:

- Both proof stress $R_{p0.2}$ and tensile strength R_m levels are increased. Elongation values are decreased. Uniform elongation before reaching the maximum force, where necking localises, is significantly lower in cold formed corners than in the faces. Elongation at fracture are also lower, thus the localised elongation at necking before fracture seems be of same order. Cold forming has influence on the properties of the flat face near the corner, but this region is equal to 1-2 times material thickness.

The test sections were verified against requirements set in product standard EN 10219:

- The overall dimensions of sections fulfilled tolerance in the product standard EN 10219 thus the validation of corner radius dimension is not rational. Properties

determined from faces of sections fulfilled strength requirements according to EN 10219. The elongation requirement was fulfilled in all cases.

- Requirement set in product EN 10219 is for 35 J/cm2 for J0 at 0 C temperatures and for J2 at -20 degrees temperature. EATT (energy absorption) transition temperature fulfils these criteria clearly, when the CVN specimen are chosen from plane element with though thickness crack position.

Eurocode 3, Part 1.1 sets following requirements for the ductility of structural steel in section 3.2.2 *Ductility requirements*: 1. requirement for the ratio f_u/f_y, 2. requirement for the elongation at failure and 3. requirement for the ultimate strain ε_u.

- The properties from flat faces B and H of section fulfil all three ductility requirements. Values for elongation after fracture are clearly larger than required 15%.

- The longitudinal seam weld has to be normalised after welding to fulfil elongation requirements in ductility.

- The requirement for uniform elongation at maximum for corners of section is not fulfilled. The changes in characteristic of stress-strain relationship due to high cold forming rate decrease the uniform elongation.

WP2 Applicability of plastic design for CFSHS members and structures
Objective: Determine rotation capacity and limits for cross-section classification required in plastic analysis for CFSHS (LABEIN; University of Navarra, University of Pisa).

Applicability of present section classification limits for CFSHS in Eurocode 3, Part 1.3 was studied. A more demanding limit was proposed based on accounting for interaction between the flange and web slenderness. Advanced approach, which was based on the concept of available inelastic rotation, was proposed for the global plastic design. The method is an alternative for the use of existing section classification rules based on web and flange slenderness. Required and available inelastic rotations φ at plastic hinge location are compared directly. The required rotation was studied with FE simulation for beams and portal frames. The available rotation for CFSHS was verified using different methods: calculation models, FE simulations and experimentally. Test results from literature were collected as test database, which was extended with 20 bending tests in the course of this project.

Following conclusions may be drawn

- The available inelastic rotation marked φ_{av} should be used to model the deformation capacity of a cross-section in bending, while it can be considered as a cross-section property that is limited by material property related yielding and geometric dimension related local buckling. Traditionally rotation capacity $R = (\varphi_{rov} - \varphi_{pl})/ \varphi_{pl}$. is used to describe deformation capacity.

- The inelastic rotation capacity of hollow sections depends on the shape of descending part of the moment rotation curve, which is limited by plastic local buckling as failure mode. Material ductility is not the limiting phenomena on the deformation capacity of hollow sections.

- When moment rotation performance of hollow sections is considered the moment resistance and the inelastic rotation up to the moment resistance seems depends essentially on the flange slenderness. The web slenderness seems to have an influence on the

descending part of moment rotation curve after maximum moment has been reached. Available inelastic rotation depends on both web and flange slenderness ratios. There is interaction between web and flange.

- Cold formed and hot-formed sections behave similarly in four point bending tests. The moment resistance level depends on the material strength, which may be larger in cold formed sections due increased strength of corners. The moment-rotation curves have similar shape and available rotation values are of same magnitude though numerical differences may be found. There are no clear differences in moment rotation characteristic that reflect the manufacturing method.

- The current cross-section classification in EN 1993-1-1 seems to be non conservative for hollow sections. The interaction of web and flange in bending is not considered when slenderness limit are given separately. Also the rotation capacity required to form necessary plastic hinge should be clarified. A more demanding proposal for slenderness limits in class 1 is presented though statistical analyses is still required to set the safety level respective to other section shapes.

- Instead of cross-section classification more advanced analysis of structurally required rotation compared to available rotation of hollow section members should be used. The available rotation of structural member may be determined experimentally, numerically with calibrated FE simulation or using verified empirical design provision such as Kecman or Kubo model.

WP3A Applicability of design rules for tubular connection from CFSHS
Objective: Determine reliable design rules for welded tubular connections using CFSHS
(Lappeenranta University of Technology, Rautaruukki, University of Pisa).

Strength and deformation capacity of welded joints was of interest, while cold forming tends to decrease ductility in corner area. Present design provisions at Eurocode 3, Part 1.8 were based on plastic hinge mechanism. Behaviour of CFSHS in welded connections was studied with K-joint and X-joint tests in normal and at low temperatures. The test programme comprised of altogether 41 K-joint test and 32 X-joint tests. Sections from two different manufacturers were included and some hot formed sections were also tested for comparison.

Main conclusions drawn from tests and their analyses that are valid for both K- and X-joints are:

- Tested K- and X-joints fulfilled the “generally accepted” requirements for deformation capacity down to –40°C temperatures and most test cases even down to –60°C.

- Present design rules in Eurocode 3, Part 1.8 to estimate resistance of K- and X-joints are safe and may be used both cold formed and hot formed structural hollow sections.

- Degree of cold forming defined by b/t-ratio seems to be insignificant on the deformation and load carrying capacity of the joints made from CFSHS.

- The manufacturing method of hollow sections (cold- or hot-formed) does not show significant differences in behaviour down to –40°C test temperatures, when the performance of joints were compared.

WP3B Extension of applicability of design rules for tubular connections
Objective: Extend applicability of design rules for welded tubular connections for CFSHS having *b/t > 35* (University of Karlsruhe, Voest Alpine Krems).

Eurocode 3, Part 1.8 Design of joints (EN 1993-1-8) provides design guidelines for rectangular hollow sections joints made of members having b/t ratios smaller than 35. In practice, there is an increasing demand to use more slender sections. The present product ranges of the manufacturers are however much wider, especially for cold-formed sections. New design provisions were developed for slender sections. Altogether 47 K-joint tests were made to verity applicability of new provision.

Main conclusions are:

- The design resistance for K-joints can be determined by using the formulae according to prEN1993-1-8 but the punching shear resistance should be calculated using a reduced effective length, if the gap size is below the lower bound given in Eurocode 3.This reduced effective punching shear length can be calculated using the proposal given in this report.
- Additionally, buckling of the chord webs should be checked. The formula for T- and Y-joints given in Eurocode 3 can be used here.
- The thickness ratio should be restricted to $\tau = 1.0$ for $b_0/t_0 > 35$ and small gap sizes, in order to avoid brace failure. The existing models for brace failure (buckling of brace and effective width failure) should be modified to include the slenderness range and the reduced gap size.
- Only few reliable results of tests for steel grade S460 exist. Although all results obtained by the tests give margins of safety above 1.25, it is proposed to limit the slenderness and the gap size to the values given in Eurocode 3 until additional investigations are available.

WP4 Effect of welding in cold-formed corner area
Objective: Determine requirements for reliable welding of CFSHS connections
(University of Karlsruhe, Voest Alpine Krems, Rautaruukki).

Effect of welding on the cold formed corner area to toughness and fatigue properties were also covered. After cold forming the strength and toughness properties of steel change slowly at room temperature, but the changes accelerate at higher temperatures. This strain ageing of steel is also met in welded steel structures, in which the weld heat input and temperature changes in the weld zones cause local accelerated ageing. The shift of the transition temperature caused by welding (ageing effects) was investigated using Charpy V notch impact specimen. Fatigue behaviour was studied with similar welded section under four point bending.

The main conclusions drawn from Charpy V tests are:

- The cold forming did not have influence on the transition temperature. If the bent area test specimen are compared to the behaviour of the specimens prepared out of the plane area, only minor differences can be found. Generally, the same transition curves for both specimens were found.

- If the bent area aged is compared to the both cases above the behaviour of the specimens made out of the bent aged area is a little bit different. The notch impact energy KV in the upper shelf is higher than for plane area. In six of eight cases no decrease of the notch impact energy KV was found.

For all other cases, a similar or better ductile behaviour was found than for the plane or for the bent area without ageing. It is assumed that the welding in the bent area causes some kind of normalising effect.

Regarding all fatigue tests carried out in the scope of this project the results and conclusions can

be summarised as follows:

- Regarding the lower bounds of the scatter bands only small differences between aged and non-aged specimens have found. Aged specimens show higher values of m than non-aged specimens.

- Regarding the mean lines the relation of S_R between aged and non-aged specimens at 2 Million load cycles ranges between 0.87 and 0.90 for all sections. The scatter band of aged specimens is remarkable smaller than for non-aged specimens.

- Different steel grades are resulting in different slopes and different stress ranges at 2 Million load cycles for non-aged specimens. Aged specimens lead to nearly the same slope and the same fatigue resistance for all steel grades S275J2H, S355J2H and S460MLH.

Following recommendation in respect of welding in cold-formed areas of hollow sections subjected to fatigue load can be given:

1. If the wall thickness of the section is higher than given in Table 4.2 of prEN 1993-1-8:2003, CVN tests in the bent areas are to be made. A minimum energy of 27 J at –20°C must be guaranteed.

2. The detail category acc. prEN 1993-1-9:2003 must be 45 or higher. If that condition is fulfilled, the fatigue detail category of cold-formed sections is to be reduced by two categories.

The restrictions of this recommendation are mainly based on the fact that only the ageing-by-welding effect was investigated in this programme. Geometrical notches have not been examined in the present project. On the other hand it is clear that real structures also have geometrical notches which can superpose the effect of the ageing-by-welding. This point should be clarified in a sequencing programme.

Technical Annex

WP1

Salmi, P. & Ilvonen. R. Mechanical and toughness properties of cold formed structural hollow sections. Project 7210-PR/253 Design Rules for Cold-Formed Structural Hollow Sections - Document 4341/WP1/1009. February 2004. VTT Technical Research Centre of Finland.

Additional test programme

Salmi, P. Additional test programme - Coupon tests results. WP1.1 Material tests. Project 7210-PR/253 Design Rules for Cold-Formed Structural Hollow Sections - Document 4341/WP1/1008. February 2004. VTT Technical Research Centre of Finland.

Bjork, T., Whole sections tests. Project 7210-PR/253 Design Rules for Cold-Formed Structural Hollow Sections - Document 4341/WP3A/8006, Version 01. Lappeenranta University of Technology, Laboratory of Steel Structures, October 2003.

Salmi, P., Björk, T. and Ilvonen, R. Mechanical properties of cold formed hollow sections. Effect of welding and low temperatures. Distribution around section. Project 7210-PR/253 Design Rules for Cold-Formed Structural Hollow Sections - Document 4341/WPAD/1010. February 2004. VTT Technical Research Centre of Finland.

WP2

Espiga, F. Predictive models for ductility evaluation – WP2 (Deformation Capacity). Project 7210-PR/253 Design Rules for Cold-Formed Structural Hollow Sections - Document 4341/WP2/2002. Labein Technological Centre, Version 04, February 2002.

Espiga, F. FE Modelling of benchmarks (ABAQUS) - WP2 Deformation capacity. Project 7210-PR/253 Design Rules for Cold-Formed Structural Hollow Sections - Document 4341/WP2/2003. Labein Technological Centre, September 2001, Version 02.

Espiga, F. Modelling strategy for virtual testing. WP2 Deformation Capacity. Project 7210-PR/253 Design Rules for Cold-Formed Structural Hollow Sections - Document 4341/WP2/2005. Labein Technological Centre, January 2002, Version 02.

Espiga, F. Parametric study. Loading type and moment gradient WP2 Deformation Capacity. Project 7210-PR/253 Design Rules for Cold-Formed Structural Hollow Sections - Document 4341/WP2/2006 Labein Technological Centre, February 2002, Version 01.

Espiga, F. Parametric study. Plate slenderness and aspect ratio WP2 Deformation Capacity. Project 7210-PR/253 Design Rules for Cold-Formed Structural Hollow Sections - Document 4341/WP2/2007 Labein Technological Centre, September 2002, Version 02.

Espiga, F. Modelling Pisa tests. WP2 Deformation Capacity. Project 7210-PR/253 Design Rules for Cold-Formed Structural Hollow Sections - Document 4341/WP2/2008. Labein Technological Centre, September 2002, Version 02.

Bayo, E. Finite Element Modelling of Benchmarks tests using Cosmos. Project 7210-PR/253 Design Rules for Cold-Formed Structural Hollow Sections - Document 4341/WP2/5001 . University of Navarra, February 2001.

Bayo, E. and Goni, R. Establishment and validation of a modelling strategy for virtual testing (Geometrical aspects). Project 7210-PR/253 Design Rules for Cold-Formed Structural Hollow Sections - Document 4341/WP2/5002. University of Navarra, August 2001.

Bayo, E. and Goni, R. Establishment and validation of a modelling strategy for virtual testing (Geometrical aspects). Project 7210-PR/253 Design Rules for Cold-Formed Structural Hollow Sections - Document 4341/WP2/5003. University of Navarra, February 2002.

Bayo, E. and Goni, R. Parametrical study to evaluate the influence of lateral restraints. Project 7210-PR/253 Design Rules for Cold-Formed Structural Hollow Sections - Document 4341/WP2/5004. University of Navarra, September 2002. .

Bayo, E. and Goni, R. Evaluation of the Required Rotational Capacity at the Structural Level. Project 7210-PR/253 Design Rules for Cold-Formed Structural Hollow Sections - Document 4341/WP2/5005. University of Navarra, February 2003.

Croce, P. Contribution to Common Final Report - Experimental investigations. WP2 Deformation Capacity. Project 7210-PR/253 Design Rules for Cold-Formed Structural Hollow Sections - Document 4341/WP2/3012. University of Pisa. March 2004.

Croce, P. Final Report. WP2 Deformation Capacity. Project 7210-PR/253 Design Rules for Cold-Formed Structural Hollow Sections - Document 4341/WP2/3014. University of Pisa. March 2005

WP3A

Björk. T. WP3A, Tubular Connections, K-joint Tests. Design Rules for Cold-Formed Structural Hollow Sections. Document 4341/WP3A/8007. Version 01. March 3004

Björk. T. WP3A, Tubular Connections, X-joint Tests carried out in LUT. Design Rules for Cold-Formed Structural Hollow Sections. Document 4341/WP3A/8006. Version 02. March 3004.

Croce, P. Contribution to Common Final Report. WP3 Tubular Connections - WP3.A Project 7210-PR/253 Design Rules for Cold-Formed Structural Hollow Sections - Document 4341/WP3A/3012. University of Pisa. March 2004

WP3B

Fleischer, O. WP3.3 b/t > 35, Draft Final Report. Project 7210-PR/253 Design Rules for Cold-Formed Structural Hollow Sections - Document 4341/WP3B/DraftFinal. University of Karlsruhe, Research Centre of Steel, Timber and Masonry, February 2003.

Croce, P. Contribution to Common Final Report. WP3 Tubular Connections - WP3.B Project 7210-PR/253 Design Rules for Cold-Formed Structural Hollow Sections - Document 4341/WP3A/3013. University of Pisa. March 2004

WP4

Herion, S. WP4 Welding procedures – FE investigation for optimising the test set-up. Project 7210-PR/253 Design Rules for Cold-Formed Structural Hollow Sections - Document 4341/WP4/4005 University of Karlsruhe, Research Centre of Steel, Timber and Masonry, February 2002.

Herion, S. WP4: Final Technical Report. Project 7210-PR/253 Design Rules for Cold-Formed Structural Hollow Sections - Document 4341/WP4/4006 University of Karlsruhe, Research Centre of Steel, Timber and Masonry, February 2002.

REFERENCES

Chapter 1:

[1-1] EN 10219-1. Cold formed welded structural hollow sections of non-alloy and fine grain steels. Part 1: Technical delivery requirements.

[1-2] EN 10210 (1994). Hot finished structural hollow sections of non-alloy and fine grain structural steels, 1994.

[1-3] Soininen, R. (1996) Fracture behaviour and assessment of design requirements against fracture in welded steel structures made of cold formed rectangular hollow sections, PhD Thesis, Lappeenranta University of Technology, 238p.

[1-4] Soininen, R. (1998) Design requirements of high strength cold formed RHS to be used in welded steel structures at low temperatures. Journal of Constructional Steel Research, Vol 46: 1-3, Paper No. 232.

[1-5] prEN 1993-1-1 (2003) Eurocode 3, Design of steel structures Part 1.1, General rules and rules for buildings. European Committee for Standardisation, Final Draft, December 2003.

[1-6] prEN 1993-1-8. (2003) Eurocode 3, Design of steel structures. Part 1.8, Design of joints. European Committee for Standardisation, Final Draft, December 2003.

Chapter 2:

[2-1] EN 10219-1. Cold formed welded structural hollow sections of non-alloy and fine grain steels. Part 1: Technical delivery requirements. (Kylmämuovatut hitsatut seostamattomat rakenne- ja hienoraerakenneteräsputkipalkit. Osa 1: Tekniset toimitusehdot). 20 p.

[2-2] EN 10219-2. Cold formed welded structural hollow sections of non-alloy and fine grain steels. Part 2: Tolerances. dimensions and sectional properties. (Kylmämuovatut hitsatut seostamattomat rakenne- ja hienoraerakenneteräsputkipalkit. Osa 2: Toleranssit. mitat ja poikkileikkaussuureet.) 16 p.

[2-3] prEN 1993-1-1 Eurocode 3: Design of Steel Structures - Part 1.1: General rules and rules for buildings. Final Draft - December 2003

[2-4] EN 10002-1. Metallic materials. Tensile testing. Part 1: Method of test (at ambient temperature) (Metallien vetokoe. Osa 1: Menetelmä.). 16 p.

[2-5] EN 1990 Eurocode: Basis of structural design. Brussels, European standard, European Committee for Standardization. 2002. 89 p.

[2-6] Probabilistic model code, 12th draft 2001. Joint committee of Structural Safety (JCSS). http://www.jcss.ethz.ch/

[2-7] EN 10045-1. Metallic materials. Charpy impact test. Part 1: Test method. (Metallien iskukoe. Charpyn V- ja U- koe. Osa 1: Menetelmä). 10 p.

Chapter 3:

[3-1] prEN 1993-1-1 Eurocode 3: Design of Steel Structures - Part 1.1: General rules and rules for buildings. Final Draft - December 2003

[3-2] Wilkinson, T. (1999), Plastic Behaviour of Cold-Formed Rectangular Hollow Sections, PhD Thesis, Department of Civil Engineering, the University of Sydney, Sydney, Australia

[3-3] Wilkinson T., Hancock G. J., Tests for the compact web slenderness of cold-formed rectangular hollow sections, Research Report, June 1997. Centre for Advanced Structural Engineering, Department of Civil Engineering, The Univeristy of Sydney, 31 p.

[3-4] Wilkinson, T. and Hancock, G.J. Tests to examine compact web slenderness of CFRHS. J.Struct.Eng. Vol. 124 No10, Oct. 1998.

[3-5] Report EUR 18366 EN: Promotion of plastic design for steel and composite cross-sections)

[3-6] Sedlacek and Feldmann (1995)Background document 5.09 for chapter 5 of EN 1993-1-1 on b/t ratios.

[3-7] ENV 1993-1-1 (1993) Eurocode 3: Design of steel structures, Part 1.1:

[3-8] Sedlacek, G, Dahl, W., Stranghöner, N and Kalinowski, B. Investigation of the rotation behaviour of hollow section beams. EUR 17994 EN. 1998. Final report of project No 7210-SA/ -119.

[3-9] Zhao, X. L. and Hancock, G. J. Tests to determine plate slenderness limits for cold formed RHS of grade C450. Steel Constr. Vol.25 No4, 1991.

[3-10] Kecman, D. (1979) Bending Collapse of Rectangular Section tubes in Relation to the Bus Roll Over Problem, Ph.D Thesis., Cranfield Institute of Technology, 1979

[3-11] Kecman, D. (1983) Bending Collapse of Rectangular and Square Section Tubes. Int. J. Mech. Sci. Vol.25, No.9-10, pp 623-636, 1983

[3-12] Kubo, M and Ogawa, H. (1991) A simple method for evaluating ultimate strength of thin-walled steel beams" , J. Struct. Eng., ASCE, Vol.114, No.ST4, 841-855, 1991 (in Japanese)

Chapter 4:

[4-1] SFS-ENV 1993-1-1. Eurocode 3 Design of steel structures. Part 1-1: general rules and rules for buildings. SFS 1993.

[4-2] Björk. T. Document 4341/WP3A/8007. Version 01. Design Rules for cold-Formed Structural Hollow Sections. WP3A, Tubular Connections, K-joint Tests. March 3004

[4-3] Björk. T. Document 4341/WP3A/8006. Version 02. Design Rules for cold-Formed Structural Hollow Sections. WP3A, Tubular Connections, X-joint Tests carried out in LUT. March 3004.

Chapter 5:

[5-1] prEN1993-1-8 (05.2003), „Design of steel structures – Design of joints”, European Committee for Standardisation, May 2003

[5-2] EN 10210 (1994). Hot finished structural hollow sections of non-alloy and fine grain structural steels, 1994.

[5-3] EN 10219 (1997). Cold formed welded structural hollow sections of non-alloy and fine grain steels, 1997

[5-4] EN 10204 (01.08.1995), ”Metallic Products – Types of Inspection Documents”, European Committee for Standardisation, August 1995

[5-5] EN 10002 (01.12.2001), ” Metallic Materials - Tensile Testing”, European Committee for Standardisation, December 2001

[5-6] EN 10045 (01.01.1993), ”Impact Test on Metallic Materials”, European Committee for Standardisation, January 1993

[5-7] Packer J. A., Henderson J. E., (1997), „Hollow Structural Section – Connections and Trusses – A Design Guide”, Canadian Institute of Steel Construction, Universal Offset Limited, Alliston, Ontario, Canada, ISBN 0-88811-086-3

[5-8] Packer J. A., Wardenier J., Kurobane Y., Dutta D., Yeomans N., (1993), “Design Guide for rectangular hollow sections (RHS) under predominantly static loading“, Cidect, Verlag TÜV Rheinland, Köln, Deutschland

[5-9] Puthli R.S., (1998), „Hohlprofilkonstruktionen aus Stahl nach DIN V ENV 1993 (EC3) und DIN 18800 (11.90)“, Werner Verlag GmbH & Co. KG, Düsseldorf, Deutschland, ISBN 3-8041-2975-7

[5-10] Puthli R.S., (2002), „Hohlprofilkonstruktionen im Geschossbau – Ausblick auf die europäische Normung“, im Stahlbau Kalender, Ernst&Sohn Verlag, Düsseldorf, Deutschland, Berlin, Deutschland, ISBN 3-433-01594-5

[5-11] Wardenier J., (1982) „Hollow section joints“, Delft University Press, Delft, The Netherlands, ISBN 90.6275.084.2

[5-12] Wardenier J. (2000), „Hollow sections in structural applications“, CIDECT

Chapter 6:

[6-1] Document WP4-4006 v02:
Improvement and extension of design rules for cold-formed structural hollow sections. WP4: Final Technical Report.

[6-2] DIN 17014-1, 01-Aug-1988
Wärmebehandlung von Eisenwerkstoffen - Begriffe (Tempering of iron materials – Terms)

[6-3] Ruge, J.:
Handbuch der Schweißtechnik - Band 1: Werkstoffe (Guide of welding technology – Volume 1: Materials)
2. Auflage, Springer-Verlag Berlin Heidelberg, New York 1980

[6-4] Ruge, J. und H. Wösle:
Schweißen an kaltverformten Teilen - Entwicklung und Beurteilung aus heutiger Sicht (Welding on cold-formed sections - Development and assessment from present view),
Der Stahlbau 46 (1977), Vol. 9, p. 266 – 277 and Vol. 11, p. 353 - 359

[6-5] Houdremont, E.:
Handbuch der Sonderstahlkunde (Guide of special steels)
3. Auflage, Bd. 1, Springer-Verlag Berlin / Göttingen / Heidelberg
Verlag Stahleisen mbH, Düsseldorf 1956

[6-6] EN 10219, 01-Nov-1997
Cold formed welded structural hollow sections of non-alloy and fine grain steels - Part 1: Technical delivery requirements; German version EN 10219-1:1997
Cold formed welded structural hollow sections of non-alloy and fine grain steels - Part 2: Tolerances, dimensions and sectional properties; German version EN 10219-2:1997

[6-7] prEN 1993-1-8
Design of steel structures, Part 1-8: Design of joints; German version prEN 1993-1-8:2003

[6-8] EN 440, 01-Nov-1994
Welding consumables - Wire electrodes and deposits for gas-shielded metal arc welding of non-alloy and fine grain steels - Classification; German version EN 440:1994

[6-9] EN 10045-1, 01-Apr-1991
Charpy impact test on metallic materials; part 1: test method; german version EN 10045-1:1990

[6-10] Packer, J.A.:
Whither tubular structures research?, published in Tubular Structures X, editors Jaurietta, Alonso & Chica, Sweets& Zeitlinger B.V., Netherlands 2003, p. 3 -11

[6-11] Document WP4-4005 v01:
Improvement and extension of design rules for cold-formed structural hollow sections. WP4: FE investigation for optimising the test set-up.

[6-12] Document WP1-1009 v01:
Improvement and extension of design rules for cold-formed structural hollow sections. WP1 Collection of test results, WP1.1 Material tests.

[6-13] prEN 1993-1-9
Design of steel structures, Part 1-9: Fatigue; German version prEN 1993-1-9:2003

European Commission

EUR 21973 — Steel products and applications for building, construction and industry
Design rules for cold-formed structural hollow sections

P. Salmi, J. Kouhi, R. Puthli, S. Herion and O. Fleischer, F. Espiga, P. Croce, E. Bayo, R. Goñi, T. Björk, R. Ilvonen, W. Suppan

Luxembourg: Office for Official Publications of the European Communities

2006 — 150 pp. — 21 × 29.7 cm

Technical steel research series

ISBN 92-79-01088-3

Price (excluding VAT) in Luxembourg: EUR 25